

**Autogenous Deformation  
and  
Internal Curing of Concrete**

Cover illustration by Johannes Lura

# **Autogenous Deformation and Internal Curing of Concrete**

Proefschrift

ter verkrijging van de graad van doctor  
aan de Technische Universiteit Delft,  
op gezag van de Rector Magnificus prof.dr.ir. J.T. Fokkema  
voorzitter van het College voor Promoties,  
in het openbaar te verdedigen op maandag 14 april 2003 om 16:00 uur  
door  
Pietro LURA  
Ingegnere civile (Università degli Studi di Brescia)  
geboren te Desenzano (Italië)

Dit proefschrift is goedgekeurd door de promotor:  
Prof.dr.ir. K. van Breugel

*Samenstelling Promotiecommissie*

Rector Magnificus	voorzitter
Prof.dr.ir. K. van Breugel	Technische Universiteit Delft, promotor
Prof.dr.ir. J. Walraven	Technische Universiteit Delft
em.Prof.Dr.-Ing.habil.Dr.-Ing.E.h. F.S. Rostásy	Technische Universität Braunschweig, Deutschland
Prof.dr. O.M. Jensen	Aalborg Universitet, Danmark
Prof.dr.ir. G. De Schutter	Universiteit Gent, België
Dr.ir. E.A.B. Koenders	Technische Universiteit Delft
Dr.ir. E. Schlangen	Intron BV, Nederland
Prof.dr.ir. J.M.J.M. Bijen	Technische Universiteit Delft, reservelid

*Published and distributed by:* DUP Science

DUP Science is an imprint of  
Delft University Press  
P.O. Box 98  
2600 MG Delft  
The Netherlands  
Telephone: +31 15 27 85 678  
Telefax: +31 15 27 85 706  
E-mail: [info@Library.TUdelft.NL](mailto:info@Library.TUdelft.NL)

ISBN 90-407-2404-0

Keywords: high strength concrete, internal curing, autogenous shrinkage

Copyright © 2003 by Pietro Lura.

All rights reserved. No part of the material protected by this copyright notice may be reproduced or utilized in any form or by any means, electronic or mechanical, including photocopying, recording or by any information storage and retrieval system, without written permission from the publisher: Delft University Press.

Printed in the Netherlands

...fatti non foste a viver come bruti,  
ma per seguir virtute e canoscenza.

*Dante Alighieri, La Divina Commedia, Inferno, Canto XXVI*

Chi troppo studia, matto diventa.

*Annunciata Malvezzi*

*per Yvonne e Piera*



# Table of contents

---

List of symbols	xi
List of abbreviations	xv

## **PROLOGUE**

---

<b>Chapter One: Introduction</b>	<b>3</b>
1.1 Introduction	3
1.2 Scope of this thesis	3
1.3 Terminology: autogenous phenomena and internal curing	5
1.4 Objectives of this thesis	8
<b>Chapter Two: From hydration to autogenous deformation</b>	<b>11</b>
2.1 Introduction	11
2.2 Hydration and formation of microstructure	11
2.3 Driving forces of autogenous shrinkage	15
2.4 Macroscopic expansion	18
2.5 Blast furnace slag cement	21
2.6 Silica fume	25
2.7 Internal curing	25
2.8 Measurements of autogenous deformation	28
2.9 Conclusions	34

## **PART I: CEMENT PASTE**

---

<b>Chapter Three: Paste measurements at room temperature</b>	<b>37</b>
3.1 Introduction	37
3.2 Materials	37
3.3 Methods	38
3.4 Results and discussion	42
3.5 Conclusions	50
<b>Chapter Four: Paste measurements at different temperatures</b>	<b>51</b>
4.1 Introduction	51
4.2 Materials	52
4.3 Methods	52
4.4 Results and discussion	54
4.5 Conclusions	60
<b>Chapter Five: Modeling of self-desiccation shrinkage</b>	<b>63</b>
5.1 Introduction	63

5.2	Modeling of self-desiccation shrinkage	63
5.3	Self-desiccation shrinkage of a Portland cement paste	65
5.4	Self-desiccation shrinkage of a BFS cement paste	71
5.5	Conclusions	75

---

**PART II: NORMAL WEIGHT CONCRETE**

---

<b>Chapter Six: Measurements on NWC</b>		<b>79</b>
6.1	Introduction	79
6.2	Materials	79
6.3	Methods	80
6.4	Results	82
6.5	Discussion	89
6.6	Conclusions	91
<b>Chapter Seven: Modeling of shrinkage of NWC</b>		<b>93</b>
7.1	Introduction	93
7.2	Materials	93
7.3	Calculation of concrete shrinkage	94
7.4	Results	96
7.5	Discussion	97
7.6	Conclusions	100

---

**PART III: LIGHTWEIGHT AGGREGATE CONCRETE**

---

<b>Chapter Eight: LWAC with Liapor aggregates</b>		<b>103</b>
8.1	Introduction	103
8.2	Properties of LWA	104
8.3	Experiments on LWAC	108
8.4	Modeling of internal curing	119
8.5	Conclusions	124
<b>Chapter Nine: Pumice aggregates and lightweight mortar</b>		<b>127</b>
9.1	Introduction	127
9.2	Materials	127
9.3	Absorption-desorption isotherms of pumice aggregates	128
9.4	Low Temperature Calorimetry study of pumice aggregates	132
9.5	X-ray absorption test and chemical shrinkage	134
9.6	SEM observation of the interface between pumice and cement paste	141
9.7	Mortars with different pumice content	145
9.8	Conclusions	152



**EPILOGUE**

---

<b>Chapter Ten: Conclusions and further research</b>	<b>155</b>
10.1 Conclusions	155
10.3 Recommendations	156
10.4 Future research	156
<b>References</b>	<b>159</b>
<b>Appendix A: Derivation of Raoult and Kelvin laws</b>	<b>171</b>
<b>Appendix B: Powers' model</b>	<b>175</b>
<b>Appendix C: Amount of entrained water</b>	<b>177</b>

Summary

Samenvatting

Acknowledgements

Curriculum vitae



# List of symbols

---

$a_i$	activity of component $i$	[-]
$c$	actual concentration of growing phase in solution	[mol/l]
$c_s$	solubility in state of equilibrium	[mol/l]
$c_{LT}, d_{LT}, g_{LT}$	parameters dependent of particle size distribution of aggregates	
$dp_i$	infinitesimal change of pressure acting on phase $i$	[MPa]
$l$	length`	[m]
$k$	parameter in Powers' model for silica fume modified cement paste	[-]
$n_w$	number of moles of water consumed during reactions (for 1 mol solid)	[-]
$p$	parameter in Powers' model for Portland cement paste	[-]
$p^0$	atmospheric pressure	[MPa]
$p_g$	gas pressure	[MPa]
$p_{sat}$	saturation pressure	[MPa]
$r$	radius of meniscus	[m]
$s/c$	silica fume/cement ratio by weight	[kg silica fume / kg cement]
$t$	time	[s, h, d]
$t_{SH}$	thickness of influence shell	[m]
$w/b$	water/binder ratio by weight	[kg water / kg binder]
$w/c$	water/cement ratio by weight	[kg water / kg cement]
$(w/c)_e$	entrained water/cement ratio by weight	[kg water / kg cement]
$C_{anhyd}$	number of pixels of anhydrous cement	[-]
$C_f$	cement content of concrete mix	[kg/m <sup>3</sup> ]
$CH$	number of pixels of calcium hydroxide	[-]
$CS$	chemical shrinkage	[kg water/kg cement hydrated]
$CSH$	number of pixels of calcium silicate hydrates	[-]
$E_A$	elastic modulus of aggregates	[MPa]
$E_C$	elastic modulus of concrete	[MPa]
$E_{LWA}$	elastic modulus of lightweight aggregates	[MPa]
$E_{LWAC}$	elastic modulus of lightweight aggregate concrete	[MPa]
$E_{LWAC,EF}$	effective stiffness of lightweight aggregate concrete	[MPa]
$E_M$	elastic modulus of matrix	[MPa]
$E_{MOR}$	elastic modulus of mortar	[MPa]
$E_S$	elastic modulus of sand	[MPa]
$E_P$	elastic modulus of cement paste	[MPa]
$G_i$	Gibbs free energy of component $i$	[J/mol]
$G_i^0$	Gibbs free energy of component $i$ in standard conditions	[J/mol]
$G_A$	shear modulus of aggregates	[MPa]
$G_P$	shear modulus of cement paste	[MPa]

---

$K_P$	bulk modulus of cement paste	[MPa]
$K_S$	bulk modulus of solid material	[MPa]
$M_l$	molar mass of liquid	[kg/mol]
$P$	crystallization pressure	[MPa]
$P_W$	vapor pressures of water at given temperature	[MPa]
$P'_W$	vapor pressure of hydrated substance at given temperature	[MPa]
$Q(t)$	heat of hydration developed at time $t$	[kJ/kg]
$Q_{pot}$	potential heat of hydration	[kJ/kg]
$R$	ideal gas constant	8.314 J/(mol·K)
$R(t)$	percentage of stress that has been relaxed at time $t$	[%]
$RH$	relative humidity	[-] or [%]
$RH_S$	relative humidity due to dissolved salts	[-] or [%]
$RH_K$	relative humidity due to menisci	[-] or [%]
$S$	saturation fraction	[m <sup>3</sup> water / m <sup>3</sup> pore-]
$T$	absolute temperature	[K]
$V_W$	molar volume of water	[m <sup>3</sup> /mol]
$V_0$	molar volume of original substance	[m <sup>3</sup> /mol]
$V_{cs}$	chemical shrinkage	[m <sup>3</sup> /m <sup>3</sup> ]
$V_{cw}$	capillary water	[m <sup>3</sup> /m <sup>3</sup> ]
$V_e$	volume of entrained water	[m <sup>3</sup> /m <sup>3</sup> ]
$V_{ew}$	evaporable water content	[m <sup>3</sup> /m <sup>3</sup> ]
$V_{gw}$	gel water	[m <sup>3</sup> /m <sup>3</sup> ]
$V_b$	molar volume of hydrated substance	[m <sup>3</sup> /mol]
$V_i$	volume of phase $i$	[m <sup>3</sup> /mol]
$V_{iw}$	initial water content	[m <sup>3</sup> /m <sup>3</sup> ]
$V_{new}$	non-evaporable water content	[m <sup>3</sup> /m <sup>3</sup> ]
$V_p$	pore volume	[m <sup>3</sup> /m <sup>3</sup> ]
$V_S$	molar volume of solid phase	[m <sup>3</sup> /mol]
$V_{SH}$	volume of influence shells	[m <sup>3</sup> /m <sup>3</sup> ]
$W_n$	non-evaporable water content per gram of cement	[g water / g cement]
$X_0$	molar fraction pure water	[-]
$X_l$	molar fraction of water in pore fluid	[-]
$Z$	atomic number	[-]
$\alpha$	degree of hydration	[-]
$\alpha_{max}$	maximum achievable degree of hydration	[-]
$\alpha_P$	parameter in Pickett's model	[-]
$\gamma$	surface tension of the pore fluid	[N/m]
$\epsilon_A$	strain of aggregates	[m/m]
$\epsilon_C$	strain of concrete	[m/m]
$\epsilon_{LIN}$	elastic strain of cement paste under internal stress	[m/m]
$\epsilon_{LWAC}$	strain of lightweight aggregate concrete	[m/m]

$\varepsilon_{MOR}$	strain of mortar	[m/m]
$\varepsilon_P$	strain of cement paste	[m/m]
$\varepsilon_{PEAK}$	peak expansion strain of lightweight aggregate concrete	[m/m]
$\theta$	contact angle between water and solids	[-]
$\lambda$	coefficient of proportionality	[s <sup>2</sup> /kg]
$\nu$	volume ratio of reaction products and anhydrous cement	[-]
$\nu_A$	Poisson's ratio of aggregates	[-]
$\nu_C$	Poisson's ratio of concrete	[-]
$\nu_P$	Poisson's ratio of cement paste	[-]
$\rho_{LT}$	number of lightweight aggregates per unit volume	[-]
$\rho_C$	density of cement	[kg/m <sup>3</sup> ]
$\rho_l$	density of liquid	[kg/m <sup>3</sup> ]
$\rho_S$	density of silica fume	[kg/m <sup>3</sup> ]
$\rho_{Sol}$	density of solids	[kg/m <sup>3</sup> ]
$\rho_W$	density of water	[kg/m <sup>3</sup> ]
$\sigma_{cap}$	stress in the pore fluid	[MPa]
$\sigma_{C,el}(t)$	elastic stress in concrete at time $t$	[MPa]
$\sigma_{PEAK}$	measured peak compressive stress	[MPa]
$\sigma_{TSTM}(t)$	measured stress at time $t$	[MPa]
$\phi_A$	volume fraction of aggregates	[m <sup>3</sup> /m <sup>3</sup> ]
$\phi_{LWA}$	volume fraction of lightweight aggregates	[m <sup>3</sup> /m <sup>3</sup> ]
$\phi_S$	volume fraction of sand in mortar	[m <sup>3</sup> /m <sup>3</sup> ]
$\Delta l$	length change	[m]
$\Delta\gamma$	change in surface tension of solid particles	[N/m]
$\Delta\sigma_{C,el}$	elastic stress increment	[MPa]
$\Sigma$	internal surface of porous body	[m <sup>2</sup> /kg]
$\partial\varepsilon_C/\partial\varepsilon_P$	ratio between shrinkage of concrete and shrinkage of paste	[-]



# List of abbreviations

---

ACI	American Concrete Institute
ADTM	Autogenous Deformation Testing Machine
ASTM	American Society for Testing and Materials
BE	Backscattered Electrons
BFS	Blast Furnace Slag
C <sub>2</sub> S	Dicalcium Silicate
C <sub>3</sub> A	Tricalcium Aluminate
C <sub>3</sub> S	Tricalcium Silicate
C <sub>4</sub> AF	Tetracalcium Aluminoferrite
CCRL	Cement and Concrete Research Laboratory at NIST
CH	Calcium Hydroxide
CSH	Calcium Silicate Hydrate
DSC	Differential Scanning Calorimeter
FE	Finite Elements
HCSS	Hard-Core Soft-Shell
HPC	High Performance Concrete
HVC	Hydraulic Valve Controller
IDT	Inductive Displacement Transducers
ITZ	Interfacial Transition Zone
LDPE	Low Density Polyethylene plastic
LTC	Low Temperature Calorimetry
LVDT	Linear Variable Differential Transformers
LWA	Lightweight Aggregate(s)
LWAC	Lightweight Aggregate Concrete
MIP	Mercury Intrusion Porosimetry
NIST	National Institute of Standards and Technologies
NMR	Nuclear Magnetic Resonance
NWA	Normal Weight Aggregate(s)
NWC	Normal Weight Concrete
PSD	Particle Size Distribution
RH	Relative Humidity
RILEM	Réunion Internationale des Laboratoires d'Essais et de recherche sur les Matériaux et les Constructions
SAP	Super Absorbent Polymers
SEM	Scanning Electron Microscope
TSTM	Thermal-Stress Testing Machine





# Prologue

---



# Chapter One

## Introduction

---

### 1.1 Introduction

In this chapter the scope of this thesis will be presented, followed by a terminology section where autogenous phenomena and internal curing are defined. Finally, the main objects and goals of this research will be addressed.

### 1.2 Scope of this thesis

#### 1.2.1 Early-age cracking of high-performance concrete

High-performance concrete (HPC) is generally characterized by low porosity and discontinuous capillary pore structure of the cement paste. This is mostly obtained by employing a low water/cement ratio with the aid of superplasticizers and by adding silica fume to the mixture. Modern concretes generally possess some highly advantageous properties compared to traditional concrete, for example good workability in the fresh state, high strength, and low permeability. However, these types of concretes have also shown to be more sensitive to early-age cracking than traditional concrete [RILEM TC 181-EAS 2002]. According to Aïtcin et al. [2002], the paradox is that “with HPC we can end up with the most impervious concrete in between cracks if it is not properly cured”. Such cracks constitute a serious problem with regard to strength, durability and aesthetics.

Early-age cracking of HPC occurs due to the fact that the deformations are restrained. Restraint can be external, e.g. caused by adjoining structures, or internal to the concrete member, caused by the reinforcement [Sule 2003] or by the non-shrinking aggregates [Dela 2000]. External restraint may cause through cracking of a concrete member (Figure 1.1), while internal restraint may result in microcracking. Early-age volume changes are caused by thermal dilation, a consequence of the development of hydration heat, autogenous deformation, and drying shrinkage due to the loss of moisture to the ambient.

While drying shrinkage can be avoided or limited by proper curing, the first two phenomena are difficult to overcome and occur simultaneously in the first days of hardening.

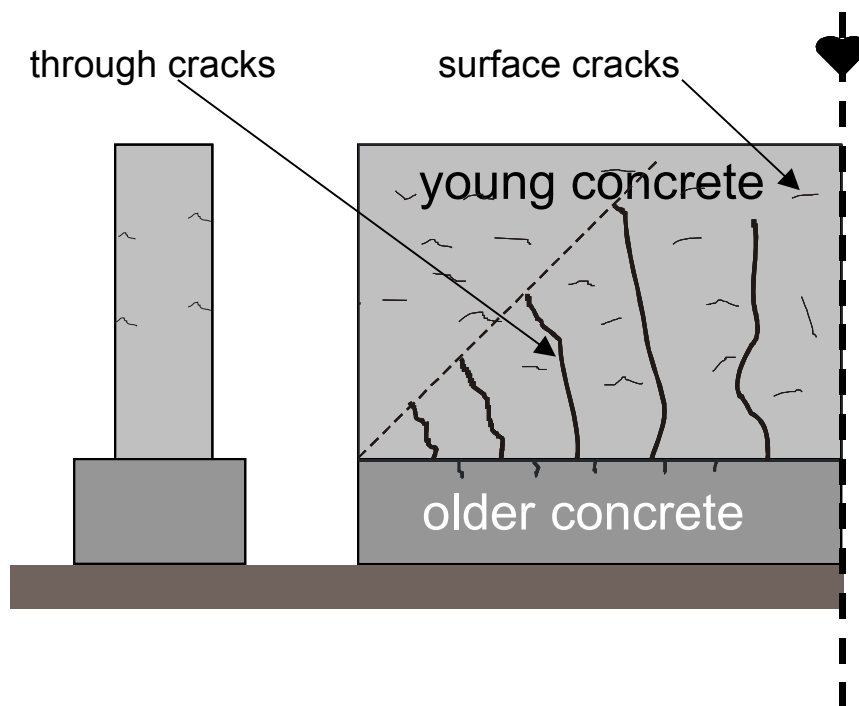


Figure 1.1 – Schematic representation of early-age cracking in a concrete wall, after [Bernander 1982]

The reaction of cement with water is exothermic and results in a temperature rise of tens of degrees K in massive concrete members [Bjøntegaard 1999]. When the structure cools down, the concrete contracts and may crack if restrained. The high cement content of HPC results in a higher temperature rise compared to traditional concrete and possibly in increased cracking risk.

### 1.2.2 Autogenous deformation

Autogenous deformation is the self-created deformation of a cement paste, mortar or concrete during hardening. In traditional concretes autogenous deformation is negligible if compared i.e. to drying shrinkage [Davis 1940]. On the contrary, in HPC the low water/binder ratio and the addition of silica fume cause a significant drop of the internal relative humidity (RH) in the cement paste during sealed hydration [Jensen & Hansen 1996]. A phenomenon closely related to autogenous RH change is autogenous shrinkage. In concrete, autogenous shrinkage results in tensile stresses in the cement paste due to aggregate restraint [Dela 2000]. Autogenous shrinkage should be limited since it may induce micro- or macro-cracking and may impair the concrete quality [Paillere et al. 1989].

Autogenous shrinkage is a phenomenon known from the beginning of the 20<sup>th</sup> century [Neville & Jones 1928, Lynam 1934], but its practical importance has only been recognized in recent years [Paillere et al. 1989, Tazawa & Miyazawa 1995]. Despite the growing interest in autogenous deformation, no consensus has yet been reached in the scientific community on standard test methods and on the terminology, although some attempts have been made in this direction [JCI 1999]. In this thesis, the terminology proposed by Jensen & Hansen [2001b] will be adopted (see sec. 1.3).

### 1.2.3 Internal curing

Conventional curing procedures of water ponding, as used for drying shrinkage, are not effective in the case of autogenous shrinkage. They may eliminate the autogenous shrinkage in small cross-sections only, because the penetration of water from the external surface is limited. Moreover, external curing might be difficult to apply to some surfaces. In view of this limitation, different strategies have been developed in recent years, based on the use of internal water reservoirs [RILEM TC-ICC 2002]. One strategy, which has been investigated more extensively, is based on the use of lightweight aggregates (LWA) [Hammer 1992], while the other is based on the use of water absorbing polymers [Jensen & Hansen 2001a]. Both water-saturated porous aggregates and water-saturated polymers are able to act as internal reservoirs, providing a source of curing water to the paste volume in their vicinity. This process of internal curing should offset self-desiccation and help avoiding self-desiccation shrinkage.

## 1.3 Terminology: autogenous phenomena and internal curing

### 1.3.1 Terminology for autogenous phenomena

#### *Definitions*

The following terminology is adopted, with minor modifications, from Jensen & Hansen [2001b], the only complete review article on the subject of autogenous deformation and autogenous relative humidity change. Another terminology was proposed by the Japan Concrete Institute committee [JCI 1999].

Consider a homogeneous, isotropic cementitious system. Homogeneous and isotropic are here meant at different scales: millimeters in cement paste and centimeters in concrete, depending on the maximum aggregate size. The following definitions hold:

- 1) Chemical shrinkage: *Absolute* volume reduction associated with the hydration reactions in a cementitious material.
- 2) Autogenous deformation: The bulk deformation of a closed, isothermal, cementitious material system not subjected to external forces.

- 3) Autogenous relative humidity change: The change of internal relative humidity in a closed, isothermal, cementitious material system not subjected to external forces.
- 4) Self-desiccation shrinkage: Autogenous deformation of a cementitious material system after setting, caused by chemical shrinkage.
- 5) Self-desiccation: Autogenous relative humidity change of a cementitious material system after setting, caused by chemical shrinkage.

### *Examples of autogenous phenomena*

Autogenous deformation: self-desiccation shrinkage, expansion due to salts or ettringite.

Autogenous RH change: self-desiccation, RH change due to dissolved salts.

### *Comments to the definitions*

Definition 1): The original definition by Jensen & Hansen [2001b] has *internal* in place of *absolute*. The internal chemical shrinkage after setting is much larger than the bulk shrinkage, but the latter is not negligible. Moreover, when the system is not set, the internal shrinkage is converted into external by collapse of the paste. Before setting, the word *internal* has no clear meaning. Therefore the original definition by Le Chatelier [1900], which distinguishes between *absolute* volume and *apparent* volume, has been utilized.

Definition 2): Chemical shrinkage before setting may be completely converted into a bulk deformation of the system, so-called setting shrinkage. According to the definitions, this is a part of autogenous deformation.

Definition 2): Autogenous deformation might be divided into autogenous shrinkage and autogenous expansion. In this thesis, autogenous shrinkage will be considered and plotted as negative autogenous deformation and autogenous expansion as positive.

Definitions 2) and 3): If the temperature is not constant or the system exchanges matter, e.g. water or gas, with the surroundings, the phenomena that cause deformation and relative humidity change will still occur but cannot be defined as autogenous. They will be superimposed to, and modified by, external factors.

Definitions 2) and 3): Bleeding is considered in Jensen & Hansen [2001b] as non-autogenous phenomenon since the definitions concern a homogeneous and isotropic material. This is true for cement paste and for concrete in the case of external bleeding. If internal bleeding were present, as hypothesized by Bjøntegaard [1999] to explain early-age expansion, this definition would face problems.

Definitions 2) and 3): Settlement occurs in every cementitious system, due to gravity. This will make the material inhomogeneous. Rotation of the sample helps avoiding settlement, but is not always possible or practical (see sec. 2.4.4).

Definition 3): External forces, e.g. changes in pressure, produce minor changes, but not negligible, on the internal RH.

For a more thorough discussion of the definitions, and an historical overview of autogenous deformation, reference is made to Jensen & Hansen [2001b].

### 1.3.2 Terminology for internal curing

#### *Definitions*

The following definitions have been adapted from a document in preparation for the RILEM Technical Committee “Internal Curing of Concrete” [RILEM TC-ICC 2003].

Internal Curing: The term *internal curing* implies the introduction of a component into the concrete mixture that serves as a curing agent. Internal curing, as well as normal curing, can be classified into two categories:

- 1) *Internal water curing* (sometimes called water-entrainment), when the curing agent performs as a water reservoir, which gradually releases water.
- 2) *Internal sealing*, when the curing agent is intended to delay or prevent loss of water from the hardening concrete.

For curing of HPC, internal water curing is preferable, since internal sealing is unable to prevent self-desiccation. As the internal curing agent is part of the system and is finely dispersed, it can overcome the problem of low permeability of a low w/b ratio cementitious system, which harmfully affects the efficiency of traditional external curing. Internal water supply can be considered the most effective method to reduce autogenous shrinkage, since it straightforwardly affects self-desiccation.

Internal water curing using presaturated lightweight aggregate: The idea that self-desiccation can be counteracted by use of saturated LWA was conceived by several authors [Philleo 1991, Vaysburd 1996, Weber & Reinhardt 1996]. This method was named *autogenous curing* [Weber & Reinhardt 1997]. Later on it was suggested that if self-desiccation could be diminished or even prevented by this method, self-desiccation shrinkage would also be affected. The autogenous deformation of Lightweight Aggregate Concrete (LWAC) made with pre-soaked LWA and concrete made with normal weight aggregate (NWA), which was partly replaced by saturated LWA, were investigated. The experiments showed that high-strength concrete without autogenous shrinkage could be obtained by this method.

Internal water curing using super-absorbent polymer: A new method for prevention of self-desiccation by using super-absorbent polymer (SAP) particles as a concrete admixture was proposed recently [Jensen & Hansen 2001a]. During concrete mixing, the SAP particles absorb water and form macroinclusions containing free water. This free water is consumed during cement hydration providing internal curing to the surrounding paste matrix and preventing self-desiccation. This concept is analogous to the air entrainment, used for frost protection of concrete, and thus is called *water entrainment*.

Internal sealing: A method of curing concrete, which does not need an externally applied curing, but is not based on adding water to the concrete, was suggested recently [Dhir et al. 1994]. This concept involves adding to the concrete during mixing a water-soluble chemical, which will reduce water evaporation when the concrete is exposed to

air-drying and also water loss to subjacent concrete. Water-soluble polymers, having hydroxyl (-OH) and ether (-O-) functional groups, satisfied the requirements set out for a “self-cure chemical”, i.e. they enhanced water retention in the concrete and increased the degree of hydration. Hydrogen bonding occurring between these functional groups reduced water pressure and decreased evaporation [Dhir et al. 1994]. The concept of concrete that does not need any externally applied curing was called *self-curing* in these studies.

### *Conventions in this thesis*

In this thesis the term *internal curing* will be generally employed with reference to the use of water containing LWA to counteract self-desiccation. This term seems to be more neutral and widespread than *autogenous curing*.

## 1.4 Objectives of this thesis

This thesis deals with autogenous deformation of cementitious materials and internal curing as a means to reduce early-age shrinkage and self-induced stresses. The main aim of this study was to reach a better comprehension of autogenous shrinkage in order to be able to model it and possibly reduce it. Once the important role of self-desiccation shrinkage in autogenous shrinkage is shown, the benefices of avoiding self-desiccation through internal curing become apparent.

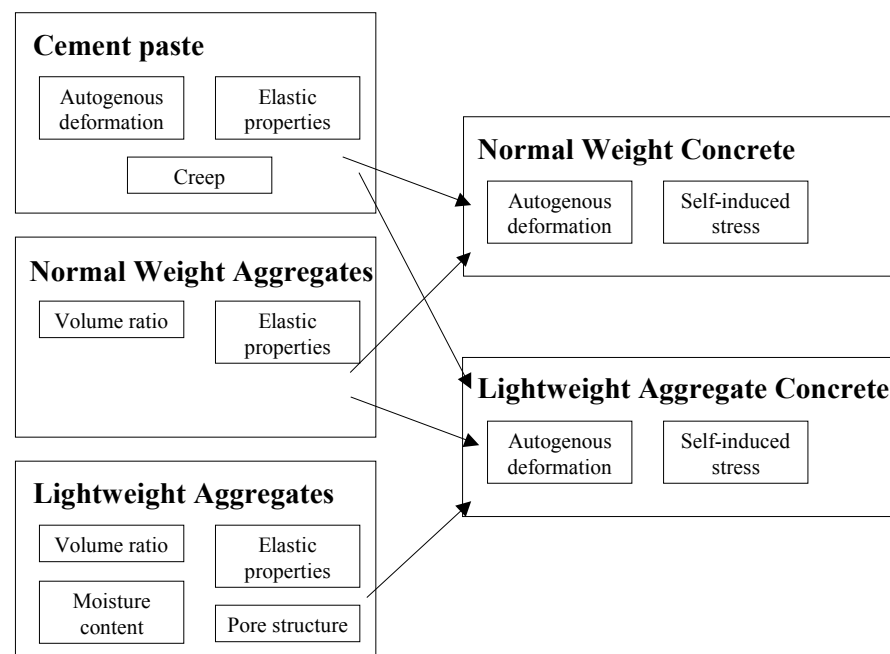


Figure 1.2 – Outline of this thesis



This thesis is divided in three main parts, corresponding to studies on cement paste (Part I), Normal Weight Concrete (Part II) and Lightweight Aggregate Concrete (Part III). The leading thread of this thesis proceeds from autogenous deformation of cement paste to autogenous deformation of concrete and finally to comprehension of internal curing and mitigation of autogenous shrinkage in LWAC. Within each part, other specific problems, relevant both for the theory and for the practical implications, have been addressed and investigated. In Figure 1.2 a schematic outline of this thesis is shown.

#### **1.4.1 Part I: Cement Paste**

The autogenous deformations of Portland and of blast furnace slag (BFS) cement pastes have been measured at different temperatures (Chapters 3 & 4). BFS cement is widely used in the Netherlands (sec. 2.5) both for economical and technical reasons, but its autogenous deformation was poorly investigated so far. The effect of different constant temperatures on autogenous deformation was object of previous studies [Jensen & Hansen 1999] but an unsystematic temperature dependency was found by some authors [Bjøntegaard 1999] and the issue remains controversial [Hedlund & Jonasson 2000]. The self-desiccation shrinkage of cement paste was modeled as a function of the internal RH change, which had been decomposed in one term due to menisci formation and one due to salts dissolved in the pore solution (Chapter 5). This shows that calculation of self-desiccation shrinkage with the capillary tension approach (Chapter 2) is feasible and convenient, as already found by other authors [Hua et al. 1995]. The importance of creep on the early-age deformations is pointed out once again.

#### **1.4.2 Part II: Normal Weight Concrete**

Autogenous deformation of concretes made with Portland and BFS cement was measured at different curing temperatures and development of self-induced stresses was measured in the case of internal restraint (Chapter 6). The relationship between autogenous deformation of cement paste and concrete was calculated with simple composite models, originally developed for drying shrinkage, which were in good agreement with the experiments (Chapter 7).

#### **1.4.3 Part III: Lightweight Aggregate Concrete**

Expansion of LWAC was measured as a function of the degree of saturation of the LWA and of the dimension of the LWA (Chapter 8). Early-age expansion of LWAC was calculated with composite models on the basis of expansion of water-cured cement pastes. The quantity of entrained water needed to avoid self-desiccation was calculated based on Powers' model [Powers & Brownyard 1948] in Chapters 8 and 9. The properties of LWA that influence internal curing, i.e. water absorption/desorption, porosity, and pore structure, were studied for different types of LWA (Chapters 8 & 9). Measurements of water transport from LWA to cement paste were performed with x-ray absorption and the implications for internal curing discussed (Chapter 9).



# Chapter Two

## From hydration to autogenous deformation

---

### 2.1 Introduction

In this chapter hydration and microstructure formation of Portland cement paste will be briefly discussed, in order to form a theoretical background for the comprehension of self-desiccation, autogenous shrinkage, and early-age expansion. Hydration and pozzolanic reactions of BFS and of silica fume will be also addressed, because of their importance in modern concretes in general and in the mixes studied in this thesis in particular.

Self-desiccation can be limited or avoided by internal curing of the paste with water reservoirs, for example saturated LWA or SAP. The theoretical background of water-entrainment is discussed together with results found in the literature.

In the last part of this chapter, experimental techniques to measure autogenous deformation of cement paste and concrete will be presented. Advantages and drawbacks of both the volumetric and the linear technique will be addressed.

### 2.2 Hydration and formation of microstructure

#### 2.2.1 Stages of hydration

The hydration of Portland cement can be divided into three stages [Jennings et al. 1981]: early period, middle period and late period (Figure 2.1).

Early period: On contact with water cement grains start to react. This early reaction period lasts only a few minutes and is called the pre-induction period [Skalny & Young 1980]. It corresponds to the first peak of heat liberation measured with an isothermal calorimeter. This peak is mainly due to the reaction of calcium aluminate,  $C_3A$ , with gypsum,  $CaSO_4 \cdot 2H_2O$ , (interground with Portland cement to avoid flash set) and water to form ettringite. A period of several hours with little hydration follows, called dormant

stage. One of the explanations of the dormant stage is the formation of a protective layer around the cement grains that prevents further hydration.

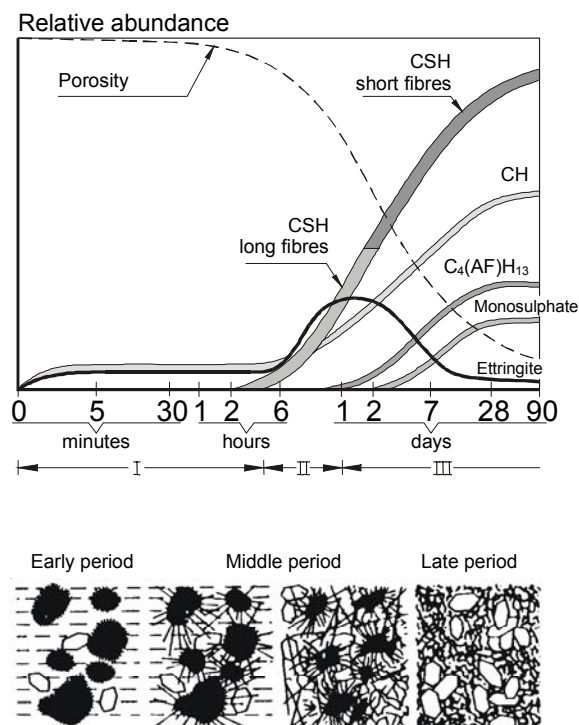


Figure 2.1 – Three stages of hydration [Locher et al. 1976]

**Middle period:** The layer breaks open and the anhydrous cement continues to hydrate. The principal components of Portland cement, tricalcium silicate,  $C_3S$ , and dicalcium silicate,  $C_2S$ , react with water and form amorphous calcium silicate hydrate, CSH, and crystalline calcium hydroxide, CH. Aluminates also react in this period forming ettringite that is later converted into monosulphate. The early hydration products are mostly in the form of long fibers that grow into the pore space and form bridges between the cement particles. In calorimeter curves the middle period is characterized by a second peak, lower but wider than the first peak.

**Late period:** In the late period the hydration products form a dense layer around the original particles that acts as a barrier for the diffusion of ions, slowing down the rate of reaction. Thus, the hydration process becomes controlled by the rate of diffusion of the ions through the layer of hydrates. The rate of heat liberation slows down accordingly.

## 2.2.2 Degree of hydration

The degree of hydration,  $\alpha$  [-], is defined as the amount of cement reacted divided by the original amount of cement [van Breugel 1991]:

$$\alpha = \frac{\text{amount of hydrated cement}}{\text{initial amount of cement}} \quad (2.1)$$

Reaction of cement with water involves liberation of heat and chemical and physical binding of water. Both the liberated heat and the bound water, relative to the maxima of these quantities when all the cement has reacted, may be used as indicators of degree of hydration [Parrot et al. 1990, van Breugel 1991]. According to Powers & Brownnyard [1948], the stoichiometric amount of water to obtain full hydration in a closed system corresponds to w/c ratio of 0.42. With lower w/c ratio, hydration stops due to lack of water and a considerable amount of anhydrous cement remains in the hardened cement paste. If water is allowed to penetrate into the hardening cement paste (open system), the w/c ratio needed to obtain full hydration is reduced to 0.36. In Figure 2.2, a backscattered electron (BE) micrograph of a 14-days old cement paste with w/c ratio 0.3 is shown. A substantial amount of unreacted cement (white color) is visible.

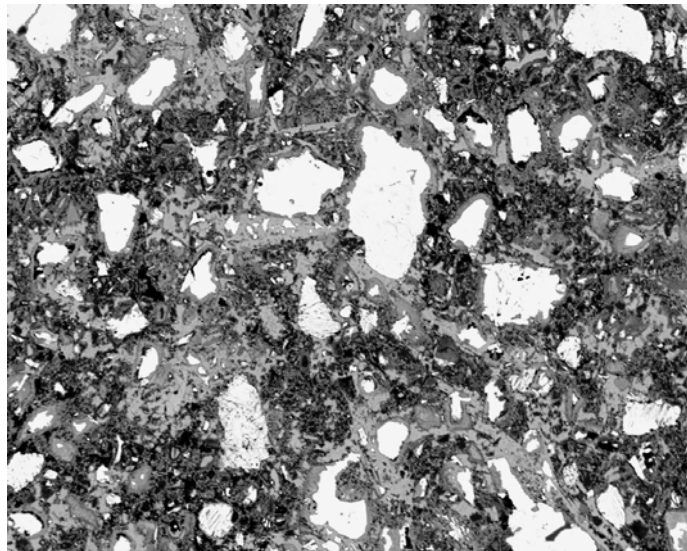


Figure 2.2 – BE image of a 2-weeks old Portland cement paste with w/c ratio 0.3 (160  $\mu\text{m}$   $\times$  200  $\mu\text{m}$ )

### 2.2.3 State of water

In a hydrating water/cement system, water can be roughly classified into three different forms, i.e. chemically bound water, physically bound water and capillary (free) water. The differences between the types of water are not pronounced since their energy levels partially overlap. At complete hydration of cement, an amount of water of about 22-23% of the weight of the anhydrous cement is chemically bound [Powers & Brownnyard 1948]. The amount of physically bound or adsorbed water depends on the RH of the pore system. The thickness of the adsorption layer goes from 1 monomolecular water layer (about 2.76 Å) at 20% RH to about 6 monomolecular layers at 100% RH [Hagymassy et al. 1969, Setzer 1977, Badmann et al. 1981], as shown in Figure 2.3.

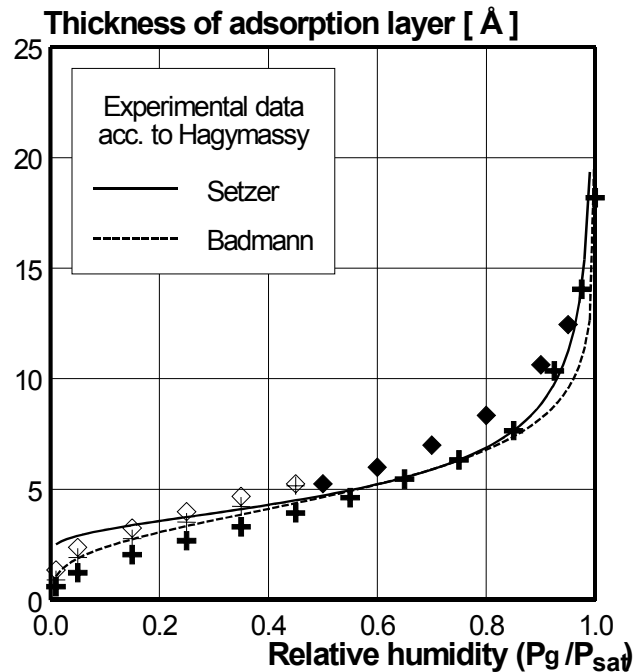


Figure 2.3 – Thickness of adsorption layer as a function of relative humidity [Koenders 1997]

#### 2.2.4 Microstructure and porosity

As a consequence of formation of hydrates, cement particles become interconnected and a solid skeleton is formed. The water/cement system evolves from a colloidal suspension in water to a porous solid partially saturated. This transition is called setting.

In the set cement paste, three types of pores are present [Bažant & Wittmann 1982]: gel pores, with typical diameter  $18 \text{ \AA}$ , macro pores (capillary), from about  $1000 \text{ \AA}$  to  $10 \text{ \mu m}$ , and mesopores, between the two. Larger than the capillary pores are the air voids. During sealed hydration, the capillary pores are gradually emptying (Figure 2.4), as will be described in detail in the next sections.

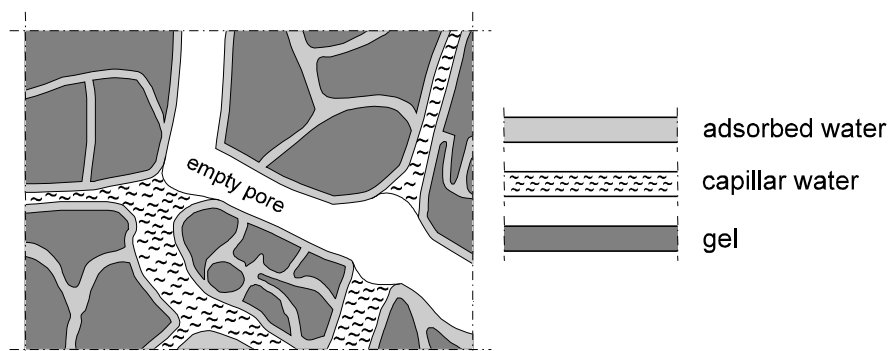


Figure 2.4 – Schematic view of state of water in the pore system of a cement paste [van Breugel 1991]

### 2.2.5 Chemical shrinkage

Hydration of Portland cement is accompanied by a chemical shrinkage. The chemical shrinkage amounts typically to 6-7 ml / 100 g of cement reacted [Powers & Brownard 1948]. Not only hydration of the main clinker minerals, but also the secondary reactions, including formation of ettringite, result in chemical shrinkage [Jensen 1993b, Barcelo 2002].

The global reduction of the volume in cement hydration goes at the expense of the water, while the solid volume increases. The volume of the hydrates is about 2.2 times the volume of the original cement [Powers & Brownard 1948]. Some authors [Bentur et al. 1979] have found that the porosity at the same degree of hydration changes with the curing temperature, with higher porosity corresponding to higher curing temperature. This may be an indication that the density of the cement gel is a function of temperature.

## 2.3 Driving forces of autogenous shrinkage

### 2.3.1 General

The mechanisms leading to autogenous shrinkage are poorly understood. While there is general agreement about the existence of a relationship between autogenous shrinkage and RH changes in the pores of the hardening cement paste, the actual mechanisms are still under discussion. Changes in the surface tension of the solid gel particles, disjoining pressure, and tension in capillary water are the principal mechanisms that have been debated [van Breugel 2001]. For each of these approaches, knowledge of the development of the pore volume and pore size distribution, of the state of water in the capillary pores (free or adsorbed), and of the mechanical properties of the solid skeleton as hydration proceeds is needed.

### 2.3.2 Self-desiccation

As long as the cement paste is fluid, the chemical shrinkage may be totally converted into an external volume change. In other words, the fluid paste is not able to sustain the internal voids created by chemical shrinkage and contracts. When the hydrates percolate and the first solid paths are formed in the hardening paste, the stiffness increases and gas bubbles start to nucleate and grow in the bigger pores (Figure 2.5). Water-air menisci form and the RH drops (Kelvin's law). The presence of menisci also causes hydrostatic tensile stresses in the pore fluid (Laplace's law). The RH drop results in a change in the thickness of the water layer adsorbed on the solid surfaces [Hagymassy et al. 1969]. This is accompanied by changes both in the surface tension of the solids and in the disjoining pressure of adsorbed water between solid surfaces. At this early stage of hydration, the stiffness of the paste is so low and the viscous behavior so pronounced that the slightest stress acting on the system results in a large deformation.

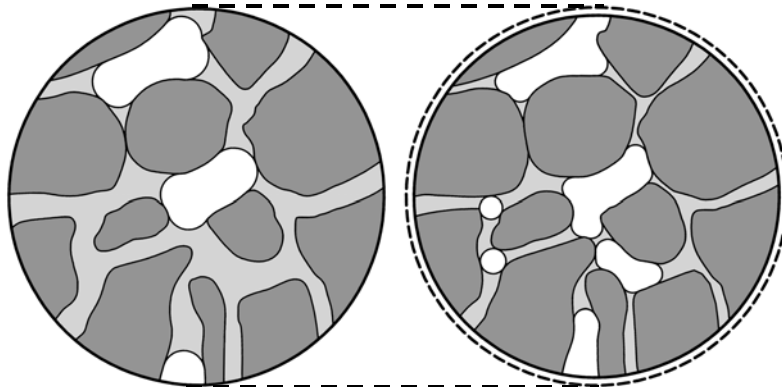


Figure 2.5 – Schematic representation of a cross-section of hydrating cement paste [Jensen & Hansen 2001b]. Left: low degree of hydration. Right: high degree of hydration. Solid matter (hydrates and anhydrous cement) is shown dark gray, pore water is light gray and empty pore volume is white. The figure illustrates the formation of empty pore volume due to chemical shrinkage, which results in a decrease of the radius of curvature of the menisci and in bulk shrinkage due to increased tensile stresses in the pore water, i.e., self-desiccation shrinkage

### 2.3.3 Surface tension

According to the surface tension approach, bulk shrinkage and expansion of the cement paste are results of changes in the surface tension of the solid gel particles. Adsorption of water lowers the surface tension of the cement gel particles and results in expansion. Conversely, removal of adsorbed water causes shrinkage.

Bangham [Bangham & Fakhoury 1931] proposed an equation that relates swelling of coal to changes in the surface tension:

$$\frac{\Delta l}{l} = \lambda \cdot \Delta \gamma \quad (2.1)$$

where  $l$  [m] is the length,  $\Delta l$  [m] the length change,  $\Delta \gamma$  [N/m] the change in surface tension of the solid particles, and  $\lambda$  [s<sup>2</sup>/kg] a coefficient of proportionality.

According to Hiller [1964] the constant depends only on the internal surface of the porous body, on the density of the solid and on the elastic modulus of the porous material:

$$\lambda = \frac{\Sigma \cdot \rho_{Sol}}{3 \cdot E} \quad (2.2)$$

where  $\Sigma$  [m<sup>2</sup>/kg] is the internal surface of the porous body,  $\rho_{Sol}$  [kg/m<sup>3</sup>] the density of the solids, and  $E$  [MPa] the elastic modulus of the porous material.

Wittmann [1977] used a similar relationship to model the swelling of a hardened cement paste upon wetting and Koenders [1997] to model autogenous shrinkage of a hardening cement paste. However, according to Wittmann [1976], this linear relationship



between deformation and changes in the surface tension must be considered semi-phenomenological. The surface tension mechanism can account only for a small part of the total shrinkage, since it acts on the solids alone, and only indirectly on the whole porous body [Powers 1965]. Moreover, the changes in the surface tension of the solids due to adsorption of water molecules are of significance for the first three adsorbed layers only. The outer layers are bound by weak forces and their influence on the surface tension of the adsorbent is almost negligible. Therefore, the relative importance of the surface tension is higher the lower the RH. This mechanism may not play a major role in autogenous deformation, where normally the RH does not drop under 75% [Jensen 1995].

### 2.3.4 Disjoining pressure

The disjoining pressure is active in areas of hindered adsorption, i.e. where the distances between the solid surfaces are smaller than two times the thickness of the free adsorbed water layer (Figure 2.6). This effect should be important also at high RH, since the change in the number of adsorbed water layers is very steep in this region [Hagymassy et al. 1969], as evident in Figure 2.4.

The disjoining pressure between the solid particles is the result of van der Waals forces, double layer repulsion and structural forces [Ferraris & Wittmann 1987]. The disjoining pressure varies with the RH and with the concentration of  $\text{Ca}^{2+}$  ions in the pore fluid [Beltzung et al. 2001]. When the RH drops, the disjoining pressure is reduced, causing shrinkage.

Nielsen [1991] proposed a relationship between RH changes and disjoining pressure in hardened cement pastes. In order to quantify the effect of the change of disjoining pressure on the deformation of the cement paste, not only its magnitude but also its area of influence as a function of RH should be known. To this end, Nielsen proposed to determine the pore size distribution of the hardened cement paste through water-vapor sorption isotherms. This approach is fundamentally correct, but an extension to hardening cement paste is extremely difficult. A first problem is the rapid change in the properties of the cement paste due to the progress of hydration. A second problem is the very weak structure of the cement paste that might be damaged by drying.

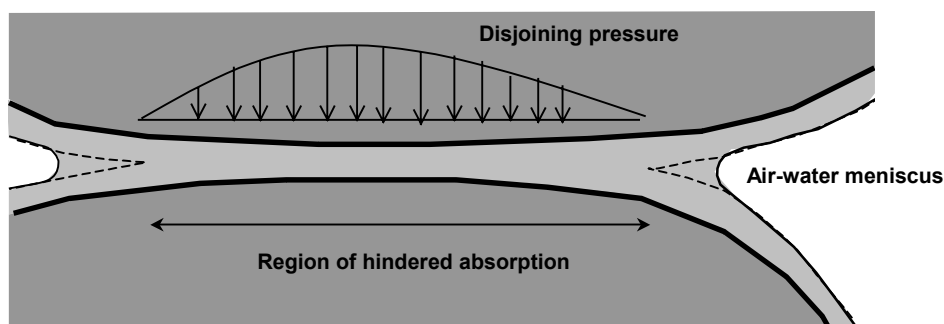


Figure 2.6 – Surfaces of hindered adsorption and distribution of disjoining pressure. Based on Soroka [1979].

### 2.3.5 Capillary tension

The capillary tension in the pore fluid is related to the water-air menisci in the partly empty pores. Its effect should be present in the upper RH range, above about 45% RH [Soroka 1979].

Hua et al. [1995] applied this mechanism to calculate autogenous shrinkage of cement paste. Experimentally, they used mercury intrusion porosimetry (MIP) to indirectly determine the capillary tension of the pore water. Some difficulties are connected with this technique. For example, the drying of the paste before the MIP measurements take place may modify the pore structure, especially in the first days of hydration. Also, big internal pores that are accessible only through small entries are identified as smaller ones due to the so-called inkbottle effect [Diamond 2000].

A more direct approach is to calculate the capillary depression from an internal state parameter of the hardening cement paste, such as the internal RH. Jensen [1993b] calculated the slope of the autogenous shrinkage a few days after casting with the capillary tension approach, using RH measurements to calculate the capillary depression. A good agreement with experimental results was obtained.

An advantage of the capillary tension approach compared with the other mechanisms discussed above is that, once the capillary tension of the pore water is calculated, one only needs to know the degree of saturation and the deformability of the paste to estimate the autogenous deformation [Bentz et al. 1998]. Thus, if one derives the capillary depression from internal RH measurements, no information on the internal surface area or on the pore size distribution of the hardening cement paste is needed to calculate self-desiccation shrinkage.

The capillary tension approach will be used in Chapter 5 to calculate self-desiccation shrinkage of Portland and BFS cement paste.

## 2.4 Macroscopic expansion

### 2.4.1 General

If a cement paste hydrates in saturated conditions, it will show an outer expansion, as observed already by Le Chatelier [1900]. According to Neville [1995], values of 1000-2000  $\mu$ strain are measured for cement pastes cured under water, where the pore system of high w/c cement pastes is supposed to remain saturated throughout hydration. L'Hermite [1960] measured 1300  $\mu$ strain at 100 days and 2200  $\mu$ strain at 2000 days, starting to measure at 24 hours. Swelling of concrete cured under water was smaller, 100-150  $\mu$ strain reached 6 to 12 months after casting for a mix with cement content 300 kg/m<sup>3</sup>.

It must be pointed out that the observed expansion cannot be due to capillary forces or lowering of the surface tension, which might be the case for cement pastes that are first dried and then immersed in water. In the case of a cement paste hydrating with free access

to water, the pores remain permanently saturated and no effect due to drying or re-wetting plays a role on the deformations. If this is the case, the origin of the macroscopic expansion must be found elsewhere.

### 2.4.2 Mechanism causing expansion

Already Le Chatelier [1900] noticed that, besides the internal contraction measured in the chemical shrinkage test, an apparent swelling was observed, which produced rupture of the encasing glass tubes at 1-6 months. He concluded that hydration is accompanied by a decrease of the absolute volume and an increase of the apparent volume. According to Powers [1935] the expansion is due to the fact that in a hardening paste cured in saturated conditions no capillary pressure develops to oppose the expansion of the solid phases.

A series of different mechanisms causing expansion can be invoked. Even if the reaction products have a lower volume (about 7% less) than the reagents, due to their shape they form a spatial network. Growth of further reaction products inside the network generates an internal pressure that may cause moderate swelling of the system [Bažant & Wittmann 1982]. In particular, according to Wittmann [1992] the mechanism of disjoining pressure might be responsible for the expansion. In fact, since the reaction products have a total surface that is much greater than the reactants, the repulsive forces between the solid particles will act on a growing area and will produce an expansion.

On the other hand, Schmidt-Döhl & Rostásy [1995] indicate the cause of the expansion in the pressure of a growing solid phase. According to them, the pressure produced by the growth of a solid phase can be described by the following equation:

$$P = \frac{n_w RT}{V_b - V_0} \cdot \ln \frac{P_w}{P'_w} \quad (2.3)$$

where  $n_w$  [-] is the number of moles of water consumed during the reactions (related to 1 mol solid),  $R$  the ideal gas constant, 8.314 J/(mol·K),  $T$  [K] the absolute temperature,  $V_b$  and  $V_0$  [m<sup>3</sup>/mol] the molar volumes of the hydrated and the original substance,  $P_w$  and  $P'_w$  [MPa] the vapor pressures of water and the hydrated substance at the given temperature.

Eq. (2.3) can be applied for instance to the formation of ettringite, which is considered as a principal cause of early-age expansion [Tezuka et al. 1986], but also to the portlandite (CH) crystals [Vernet & Cadoret 1992].

Jensen [1993a] calculated with the following formula [Correns 1949], the crystallization pressure of ettringite:

$$P = \frac{RT}{V_s} \cdot \ln \frac{c}{c_s} \quad (2.4)$$

where  $V_s$  [m<sup>3</sup>/mol] is the molar volume of the solid phase,  $c$  [mol/l] the actual concentration of the growing phase in the solution,  $c_s$  [mol/l] the solubility in the state of equilibrium.

Assuming  $c/c_s = 100$ , which is an upper value for the supersaturation of most salt solutions [Winkler 1973], a value of about 16 MPa is found at 20°C. It is noticed that this value is high enough to cause a relevant expansion in a hardening cement paste. According to Schmidt-Döhl & Rostásy [1995], however, Eq. 2.4 is approximate and the calculated values for the crystallization pressure differ sensibly from the measured ones.

Budnikov & Strelkov [1966] proposed a different mechanism to explain early-age expansion. During hydration, a cement particle is converted in a number of much smaller hydrated particles through topochemical reactions. These smaller reaction products tend to occupy a larger volume than the unhydrated particle, generating an internal pressure that produces macroscopic swelling.

Barcelo [1997] observed that the outer hydration products are localized in a volume previously occupied by the pore fluid and the volume balance of the reaction will be a contraction. In the case of the inner product, on the other hand, the volume they can occupy is fixed and corresponds to the anhydrous cement that is consumed. Thus the hydrates that form inside the boundary of the original cement grain might either cause the densification of the outer product or push it out, causing an expansion to occur. This fact can have an impact especially on low w/c ratio pastes. For a discussion of mechanisms causing early-age expansion, see also Garcia Boivin [2001].

### **2.4.3 Superposition of expansion and autogenous shrinkage**

If the cement paste is cured in sealed conditions, empty pores are formed after setting and air-water menisci will appear. The RH will drop according to the Kelvin equation and shrinkage will occur. Thus, the previously described expansive mechanisms act simultaneously with forces causing shrinkage. For the sake of simplicity, it is possible to suppose a linear superposition of shrinkage and expansion, but most likely there will be an interaction of the different mechanisms. For instance, the concentration of dissolved salts in the pore solution will influence the capillary stresses (changing the surface tension of the pore fluid, Chapter 5), the disjoining pressure [Beltzung et al. 2001], and the coefficient of supersaturation (Eq. 2.4).

The measured deformation will in general be caused by many forces of different origin interacting during hydration. Microcracking and viscous flow will also influence the measured deformations [Wittmann 2001, Hua et al. 1995].

### **2.4.4 Bleeding**

According to Bjøntegaard [1999], the principal cause of concrete swelling at early age is to be found in re-absorption of bleeding water. Experimental evidence produced by the author showed that a paste with ‘natural’ bleeding experienced early-age expansion (converted subsequently into shrinkage), while the expansion was substantially reduced (but not eliminated) if the bleeding water was removed. Additionally, if extra water was added on a bleeding sample, the measured expansion was greater and lasted longer. The

author adds that if no obvious external bleeding is visible, the same mechanism might occur due to internal bleeding of the concrete.

The fact that bleeding and re-absorption of bleeding water influence the early-age deformations of the concrete does not need to be questioned, since bleeding alters the moisture state of the concrete. However, the reason of the expansion is not to be found in the water absorption itself, since the system remains saturated until all the water on top is sucked into the paste or removed. In other words, the expansion of the concrete is not related to changes in the internal RH. The causes of the expansion are to be found in the mechanisms described in sec. 2.4.2, or in others not yet identified, but acting in saturated conditions. The presence of bleeding water or its removal has the only influence of postponing or accelerating the occurrence of self-desiccation and self-desiccation shrinkage, which will eventually override the continuing expansion.

If the paste is rotated during hardening to avoid bleeding, the resulting cementitious system will be different. The paste with bleeding will have in fact a reduced porosity (lower w/c ratio) compared to the rotated paste and will hydrate as an open system, with free access to water until all the bleeding water is consumed. The rotated paste will maintain the original w/c ratio and will hydrate in autogenous conditions. Both the shrinkage and, in a lesser extent, the mechanical properties of the two pastes will differ.

As a conclusion, bleeding and re-absorption of bleeding water are by no means the cause of early-age expansion of cement pastes and concrete. The expansion is actually evident in the case of a saturated sample because self-desiccation shrinkage does not occur. Bleeding will change the properties of the resulting cement paste and the course of hydration. However, removing the bleeding water will interfere with the system, which cannot be called autogenous any longer. Rotation will maintain the original w/c ratio (and autogenous conditions) but will interfere with the microstructure build up and postpone setting, if prolonged in time.

## 2.5 Blast furnace slag cement

### 2.5.1 General

Ground granulated blast-furnace slag (BFS) is a waste product in the manufacture of pig iron, about 300 kg of slag being produced for each ton of pig iron. It is a mixture of lime, silica, and alumina, the same oxides that make up Portland cement but not in the same proportions. BFS varies greatly in composition and physical structure depending on the processes used and on the method of cooling of the slag. Average composition is 40-50% lime, 30-40% silica, 8-18% alumina and 0-8% magnesia. Magnesia is not in crystalline form and therefore does not lead to harmful expansion. The specific density is about 2.9, lower than Portland cement (3.15). For use in the manufacture of BFS cement, the slag has to be quenched so that it solidifies as glass, crystallization being largely prevented. This rapid cooling by water results also in fragmentation of the material into a granulated form.

Figure 2.7 shows microscope images of the BFS cement and of the Portland cement that have been used in this thesis (see Chapter 3). Notice the large angular slag particles in the BFS cement.

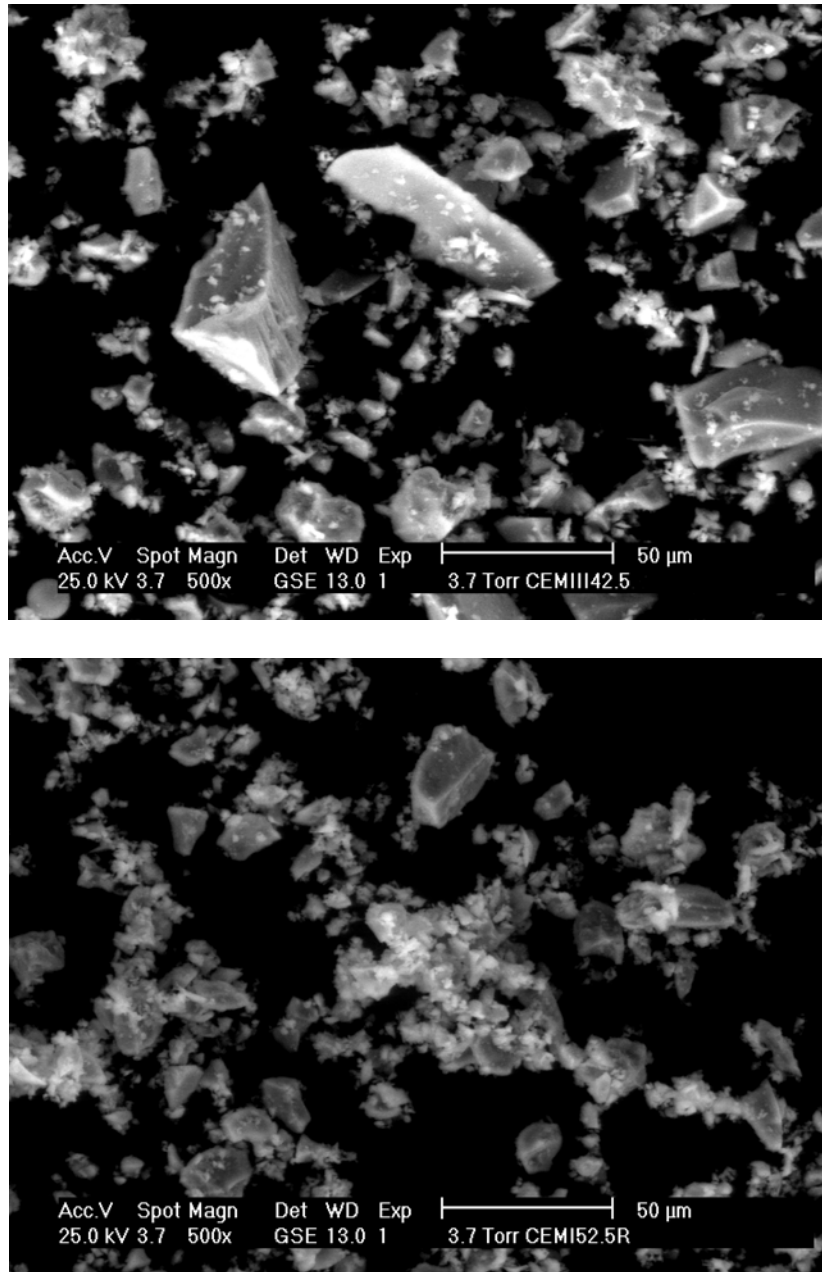


Figure 2.7 – Scanning electron microscope photographs of a BFS cement (CEM III 42.5 containing 76% slag), above, and of a rapid hardening Portland cement (CEM I 52.5 R), below

Slag can be used together with limestone as a raw material for the manufacture of Portland cement. Secondly, if ground to the appropriate fineness, it can be used on its own, in the presence of an alkali activator or starter. The third and major use of granulated BFS is in the Portland-BFS cement, which is produced either by intergrinding Portland cement clinker and dry granulated BFS (together with gypsum) or by dry blending of Portland cement powder and granulated BFS [Neville 1995].

When Portland-Blastfurnace cement is mixed with water, the Portland cement component begins to hydrate first, although there is also a small amount of immediate reaction of granulated BFS that releases calcium and aluminum ions into solution [ACI 1995]. The granulated BFS then reacts with alkali hydroxide; this is followed by reaction with calcium hydroxide released by Portland cement, CSH being formed [ACI 1995].

The European standard ENV 197-1: 1992 recognizes three classes of Portland Blastfurnace cement, called Blastfurnace cement III/A, III/B, and III/C. All of them are allowed to contain up to 5% of filler, but differ for the granulated BFS content: A 36-65%, B 66-80%, and C 81-95%.

Cements with a high content of BFS can be used as low heat cements in mass concrete. This implies also a slow gain of strength, which might be a problem if the ambient temperature is low [Bijen 1996]. The apparent activation energy of slag is higher than the one of Portland cement, which implies a higher sensitivity to temperature. Cements containing BFS are beneficial from the standpoint of resistance to chemical attack. Hydraulic activity of BFS is conditioned by its fineness.

### **2.5.2 Blast furnace slag cements in the Netherlands**

Blast furnace slag cement has market share of 60% in the construction industry of the Netherlands [Bijen 1996]. It consists of a mixture of Portland cement with 60-70% BFS, which contributes to decrease the costs. This cement performs outstandingly in hostile environment, such as in marine structures.

### **2.5.3 Effects on self-desiccation and autogenous shrinkage**

There are some indications in the literature that BFS cement paste might have lower internal RH and greater autogenous shrinkage than Portland cement paste [Hanehara et al 1999]. Possible causes of this behavior are:

- 1) Greater chemical shrinkage of the BFS cement if compared to Portland cement, leading to faster and greater self-desiccation. Figures by Bentz [2002] suggest a chemical shrinkage of 0.26 ml/g slag reacted vs. about 0.06 ml/g Portland cement reacted. In terms of chemical shrinkage, the slag would be quite similar to silica fume, 0.22 ml/g silica fume reacted [Jensen 1993b].
- 2) Finer pore structure of BFS cement pastes. Researchers have found a lower permeability of BFS cement pastes [Roy & Idorn 1982] and also MIP measurements have confirmed this fact [Xu et al. 2001]. This finer pore structure should be the product of the dissolution of the calcium hydroxide

crystals and the precipitation of pozzolanic CSH. The volume of gel pores is higher in BFS cement and the volume of capillary pores is lower, as confirmed also by low-temperature calorimetry [Lura & Bentz 2002]. Finer pores result in a lower RH according to the Kelvin equation (see Chapter 5).

- 3) Ca, Si and Al contained in the slag tend to migrate outside the original particle and precipitate forming an Al-rich CSH gel and so-called AFm phase ( $3\text{CaO}\cdot\text{Al}_2\text{O}_3\cdot\text{CaSO}_4\cdot 12\text{H}_2\text{O}$ ) [Feng & Glasser 1990, Bijen 1996]. Possibly some of the porosity is concentrated in larger isolated pores inside the original particles [Bentz 2002a], and the rest of the microstructure is filled with hydration products (Figure 2.8). This morphology of the hydration products would produce both a lower permeability and a lower RH [Bakker 1983, Feng & Glasser 1990].

The initial expansion observed in BFS cement pastes and concrete [Hanehara et al. 1998, Schackinger 2002] is possibly due to ettringite needles formed inside the solid skeleton of the cement paste, which is at this stage extremely weak. Later conversion of this ettringite into monosulphate could induce additional shrinkage.

An additional source of shrinkage is the pozzolanic reaction, which consumes calcium hydroxide crystals, inducing shrinkage due to removal of restraints in the paste. The pozzolanic reaction and related shrinkage proceed also at later stages, steadily for years [Roy & Idorn 1982] and also at reduced RH [Jensen 1993b].

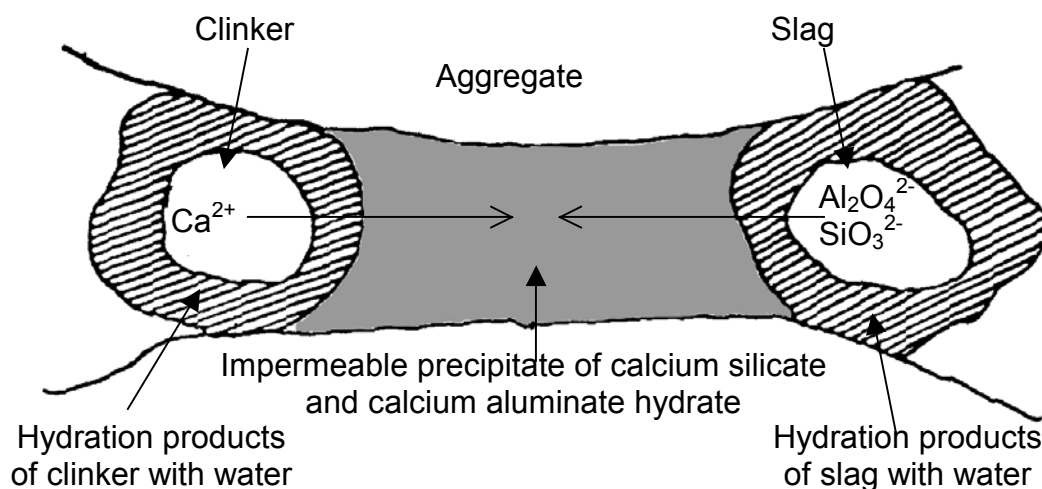


Figure 2.8 – Hydrates between adjacent particles in BFS cement paste and mechanism of pore blocking [Bakker 1983]



## 2.6 Silica fume

The principal effects of silica-fume on microstructure of concrete are due to the pozzolanic reaction and to the filler-effect due to particle dimension, being the average silica-fume particle size (0.1  $\mu\text{m}$ ) one order of magnitude smaller than the cement particle size. By adding silica-fume to the fresh mix, it is also possible to improve the workability and decrease or avoid bleeding [Neville 1995, Aïtcin 1998].

The actual mechanisms by which silica fume improves the concrete behavior are still under discussion. Certainly an improvement of the microstructure, i.e. pore refinement, leads to an increase of the concrete strength. If silica fume is added to the cement paste both the total porosity is reduced [Khan et al. 2000] and the pore structure as measured by MIP is refined [Li et al. 1996]. Another very important effect of silica fume, that was found experimentally [Scrivener et al. 1988] and confirmed by numerical simulation [Bentz & Garboczi 1991], is the improvement of the interfacial transition zone (ITZ) between aggregates and cement paste.

Some problems are connected to the use of silica fume as an admixture. The reaction of silica fume with calcium hydroxide has a high chemical shrinkage, about 0.22 ml/g of silica fume reacted [Jensen & Hansen 2001a]. Silica fume modified cement pastes show much greater self-desiccation and autogenous shrinkage than Portland cement pastes [Jensen & Hansen 1996]. This fact leads both to greater bulk shrinkage of silica fume concrete [Paillere et al. 1989] and to microcracking of the cement paste restrained by the aggregates [Dela 2000].

## 2.7 Internal curing

In the literature, two principal methods of internal curing with the purpose of reducing autogenous shrinkage are present, differing in the nature of the water reservoirs: LWA and SAP. The first has been used for about 10 years [Hammer 1992], the second is much more recent [Jensen & Hansen 2001a]. In the following a brief literature review of the two techniques will be presented, focused mainly on the studies that aimed at reducing autogenous shrinkage.

### 2.7.1 Lightweight Aggregate Concrete

Already in the 60ies, Aroni & Polivka [1967] stated "...some degree of internal curing can be achieved through the use of saturated porous aggregate such as certain types of lightweight aggregates. The pores of a lightweight aggregate can constitute a reservoir of water available for internal curing of the concrete. Such internal curing can significantly affect the rate and magnitude of expansion". Internal curing was also mentioned by Holm [1980] as one possible cause of absence of microcracking and improved durability of LWAC exposed to aggressive environments, such as bridge decks or concrete ships. The benefits of using LWA in concrete to help reduce cracking in slabs and bridge decks had

been intuitively known for decades by the LWA industry but the reasons were not examined [Hoff 2002]. It was generally believed that the improved properties of LWAC were due to elastic compatibility between LWA and matrix [Bremner & Holm 1986] and to improved ITZ [Zhang & Gjorv 1990, Wasserman & Bentur 1996].

At the beginning of the 90ies, Philleo [1991] suggested incorporating saturated lightweight fine aggregate into the concrete mixture to provide an internal source of water to replace that consumed by chemical shrinkage during hydration of the paste. His suggestion opened the way to extensive research in the field. Several studies have dealt with the experimental evaluation of the presence of LWA on autogenous shrinkage. Most of them assessed the use of coarse aggregates, evaluating the influence of their amount and degree of saturation. Recently, the use of fine LWA has been explored [Bentur & van Breugel 2002].

Hammer [1992] demonstrated that autogenous shrinkage was practically eliminated by the use of wet LWA and showed that the compressive strength did not suffer significantly from internal or external drying when a sufficient replacement of NWA with pre-wetted LWA was used [Hammer 1993]. Hammer used expanded clay LWA, Liapor and Leca, 4-12 mm. Their content was about 600 kg/m<sup>3</sup> and the absorbed water exceeded 40 kg/m<sup>3</sup> when soaked. The LWA were employed in three different states: oven-dried, moist (as delivered), and water-impregnated. In concrete with w/b ratio of 0.3, autogenous shrinkage was eliminated even in the case of dry LWA, suggesting that LWA can absorb part of the mixing water and release it afterwards to the self-desiccating matrix.

Weber & Reinhardt [1996] suggested replacing part of the coarse aggregates by LWA of similar size as a means for providing internal curing in HPC to optimize for strength. They named this method *autogenous curing*. The concrete obtained had improved mechanical properties regardless of the curing conditions. Continuous hydration for months after casting was observed with x-ray diffraction [Weber & Reinhardt 1997]. In [Weber & Reinhardt 1999] a mechanism of water transport from the LWA to the hydrating cement paste based on capillary suction was proposed. However, the issue of early-age deformations was not addressed.

The influence of the percentage of replacement of *coarse* NWA with saturated LWA (10, 17.5, and 25% Liapor by volume of coarse aggregates) on the autogenous deformation from setting time was studied by van Breugel & de Vries [1999]. With 25% replacement, the autogenous shrinkage was about half of the reference mix. When all the coarse aggregates were substituted with Liapor or Lytag, early-age expansion was measured when the saturation of the LWA was 100% or 60%, while some shrinkage followed by expansion was measured when the saturation was 30% [Takada et al. 1999].

Bentur et al. [2001] observed that with 25% replacement by volume of the *total* aggregate content with Leca 4.5-9 mm, autogenous shrinkage was avoided and expansion occurred.

Sickert et al. [1999] measured expansion on LWAC with different amounts of LWA until more than 1 year after casting; measurements started at 24 hours. The mixtures

contained from 500 to 800 kg/m<sup>3</sup> of Liapor 9.5 that was moisturized with 1/3 of the mixing water for 45 s prior to mixing.

Kohno et al. [1999] obtained expansion for several days or reduced shrinkage by substituting NWA with LWA of different type and moisture content.

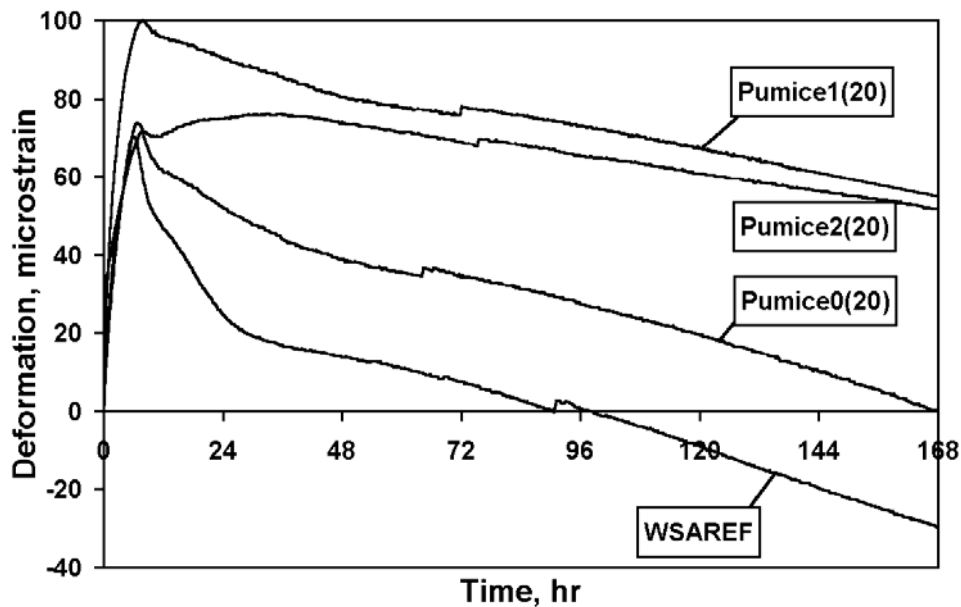


Figure 2.9 – Effect of grain size on free shrinkage of mixes with  $w/b$  ratio 0.33 containing saturated pumice sand [Zhutovsky et al. 2003]

Zhutovsky et al. [2001a, 2001b, 2002, 2003] studied the effect of replacing a small part of the NWA by saturated LWA, mainly pumice sand of different size fractions. Expansion was measured in the first hours, followed by some shrinkage in the first week of hydration (Figure 2.9). The use of pumice sand of different fractions led to different shrinkage reductions, with the largest grains being more effective. This was attributed to the different pore structure of the different sizes.

According to Bentz & Snyder [1999], the spatial distribution of the ‘water reservoirs’ in the mixture is of primary importance in the internal curing process. The distance of the saturated LWA from the point in the cement paste where the RH-drop takes place determines the efficiency of the internal curing. They estimated the maximum transport distance of water, as a consequence of the depercolation of the pores in a low  $w/c$  ratio paste, as few hundreds of micrometers. If the water-reservoirs are well distributed within the matrix, shorter distances have to be covered and the efficiency of the internal-curing process is increased. These considerations lead to the choice of small LWA. Bentz & Snyder [1999] calculated the percentage of cured paste with analytical formulas and numerical simulation as a function of the distance of water penetration and of the particle size distribution of the LWA.

### 2.7.2 Concrete with Super Absorbent Polymers

Water entrainment is a new technique for mitigation of self-desiccation shrinkage in HPC. The concept is based on embedment of a separate water phase in the hardening cement paste matrix [Jensen & Hansen 2001a]. This water phase is created through absorption of water into SAP. The dry SAP are added to the raw materials and absorb water during mixing of the concrete, forming macroinclusions of controlled dimension. Water entrained in the SAP is released when the paste self-desiccates, leaving a system of pores that can also be used in place of air entrainment. With 0.6% addition of SAP by weight of cement, corresponding to an entrained w/c of 0.075, self-desiccation in a w/c 0.3 cement paste was totally avoided, as shown by RH measurements [Jensen & Hansen 2002]. On the cement paste an expansion of about 800  $\mu$ strain was measured, mostly occurring in the first day of hardening.

## 2.8 Measurements of autogenous deformation

Autogenous deformation of cement paste and concrete varies enormously in magnitude and even in sign between different publications [Hammer et al. 2002]. Barcelo et al [1999] have demonstrated how difficult it is to interpret results based on different techniques. Since concrete is the material which is used in practical application, the principal aim of autogenous deformation measurements on cement paste is to understand and possibly predict autogenous deformation of concrete made with the same paste. However, this approach suffers of a series of drawbacks (see also Chapter 7), of which one of the most serious lies in the measuring methods.

### 2.8.1 Cement paste

Measurements of autogenous deformation on cement pastes have been performed in two fundamentally different ways, viz. measurement of volumetric deformation and measurement of linear deformation. The following discussion of the measuring methods is based on a paper by Jensen & Hansen [2001b].

Volumetric measurement of autogenous deformation is frequently performed by placing the fresh cement paste in a tight rubber balloon immersed in water. The change in volume of the cement paste is measured by the amount of water displaced by the immersed sample, for example, by measuring the weight change of the immersed sample (buoyancy) [Yamazaki et al. 1976], see Figure 2.10.

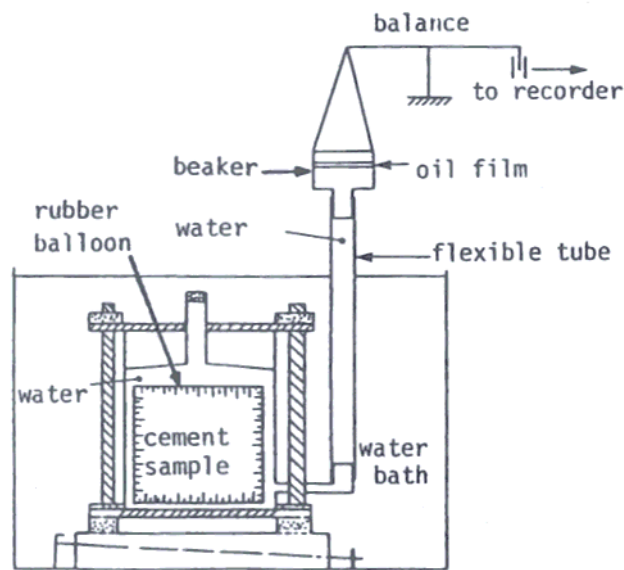


Figure 2.10 – Apparatus for measurements of volumetric autogenous deformation of cement paste [Setter & Roy 1978]

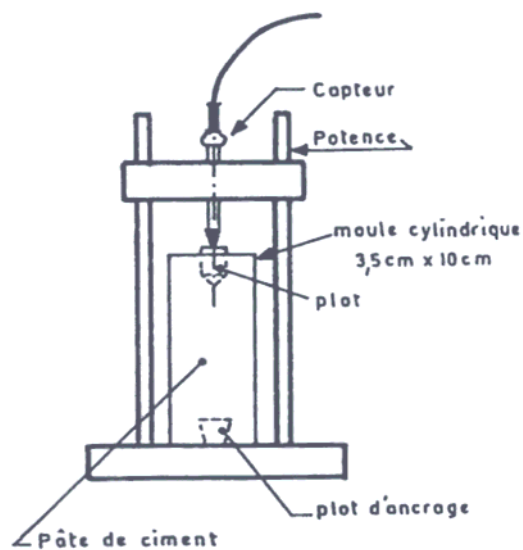


Figure 2.11 – Apparatus for measurements of linear autogenous deformation of cement paste [Buil 1979]

Linear measurement of autogenous deformation is frequently performed by placing the cement paste in a rigid mould with low friction. The length change of the cement paste is recorded by a displacement transducer at the end of the specimen, see Figure 2.11.

Both experimental methods have been extensively used in parallel for more than 50 years [Davis 1940, Wuerpel 1946]. The two methods should give identical results, but this is not at all the case since the volumetric method typically gives, after transforming the volumetric strain into linear strain, up to 5 times higher shrinkage than the linear technique [Barcelo et al. 1999]. Surprisingly, few researchers have tried to find the reason for this disagreement; a good debate with an attempt to clarify this problem can only be found in a few papers [Baron & Buil 1979, Barcelo 1999, van Breugel 2001, Hammer et al. 2002].

Both methods of measurement have advantages and drawbacks. One advantage of the volumetric method is the possibility of starting the measurements immediately after casting. Before setting, measurements have to be volume-based since the plastic state prevents an unambiguous definition of length. In contrast, the lack of a steady contact between the rubber balloon and the cement paste is a considerable disadvantage of the volumetric method. A film of water, e.g. due to bleeding, or entrapped air at the surface of the cement paste may interfere with this contact. During the hydration process the water or entrapped air will be sucked back into the cement paste as a consequence of chemical shrinkage. In this way the internal volume reduction may also be erroneously measured as an outer deformation. In fact, the volume of the rubber balloon is the combined volume of the cement paste and the volume of the surface water or entrapped air. Since the chemical shrinkage is considerably larger (up to 10 times) than the autogenous deformation, this may lead to a substantial error. In addition, Buil [1979] mentions that the pressure caused by a tight rubber balloon could damage the weak structure during setting. Another source of error might be osmosis through the latex membrane (condom) used in volumetric measurements [Marciniak 2002]. Furthermore, volumetric measurement results of autogenous deformation seem to be associated with large scatter.

One advantage of the linear method is the firm anchorage of the measuring points to the set cement paste. This greatly reduces the above-mentioned problems. At the same time, this is a disadvantage since the measurements cannot be carried out before the cement paste has set. The linear method has an additional problem: the risk of restraining the cement paste. In the very first hours after setting, the cement paste is too weak to overcome the friction against a rigid mould [Barcelo et al. 1999]. However, lubricating the mould can greatly reduce the friction. Bleeding may also influence the linear measurement of autogenous deformation. After setting, the bleed water may be reabsorbed by the cement paste and reduce the autogenous deformation or even cause expansion [Hammer et al. 2002]. However, for both the volumetric and the linear technique, sample rotation eliminates the bleeding problem.

Despite the number of difficulties, which have been identified and solved, a significant difference between the results from the two measuring techniques still persists. Even under carefully controlled conditions the volumetric method may give 3-5 times higher measuring results than the linear technique [Barcelo et al. 1999], depending on the type of cement paste and on the experimental conditions.

The deformation in the vertical direction is expected, at least before setting and due to settlement of cement, to be different from the deformation in the horizontal directions. Some authors [Barcelo et al. 1999, Garcia Boivin 2001] suppose that autogenous deformation might not be isotropic even after setting, and this might explain a part of the differences in the results of the two techniques. However Charron et al. [2001] measured shrinkage after setting in three directions on cubes and found no difference.

Jensen & Hansen [1995] developed a special, corrugated mould system, which combines the advantages of linear and volumetric measurement of autogenous deformation. Before set, the corrugated mould transforms the volumetric deformation into a linear deformation, and after set a normal, linear deformation is measured. In this way, it is possible to commence linear measurements directly after casting.

In this thesis the technique developed by Jensen & Hansen [1995] has been used in Chapter 3 to measure autogenous deformation of Portland and BFS cement pastes. In Chapter 4 a more traditional linear measurement method has been used [Koenders 1997]. For details about the measurements, reference is made to Chapter 3 and 4.

## 2.8.2 Concrete

The volumetric method cannot be used for concrete since the aggregates would damage the condom. Different linear methods have been used to measure autogenous deformation of concrete on beams, slabs or cylinders (Figures 2.12-16):

- 1) Cast-in nails through a hole in the middle of the end plates with the nail heads embedded in a concrete beam (Figure 2.12).
- 2) Moveable endplates with plugs in a concrete beam (Figure 2.13).
- 3) Horizontal transverse cast-in bars through a concrete beam (Figure 2.14), the system used in this thesis, see Chapter 7.
- 4) Vertical cast-in bars in a concrete slab (Figure 2.15).
- 5) Cast-in strain gage [Hanehara et al. 1999].
- 6) Metal plates placed on top of cylinders (Figure 2.16).

The movement has been measured using inductive displacement transducers (IDT) or linear variable differential transformers (LVDT). Also non-contact transducers like reflection of electronic pulses or laser against a metal chip have been used.

For all the measuring systems presented, the main problems to overcome are ensuring a good contact between the measuring points and the concrete, minimizing restraint and moisture loss and keeping the temperature constant. The systems presented in Figures 2.11-14, solve these problems in a similar way: embedment of rods or bars in the fresh cast, to which later the measuring points are fixed; reduction of friction on the lower face with low-friction foils; moisture loss is reduced by a plastic or aluminum foil on the upper face after casting; constant temperature is obtained with temperature-controlled baths or by circulation of cooling liquid in the mould. These issues will be dealt with in detail in sec. 4.3.2. The system in Figure 2.16, on the other hand, presents different solutions and is analogous to the one designed for cement paste (sec. 3.3.4).

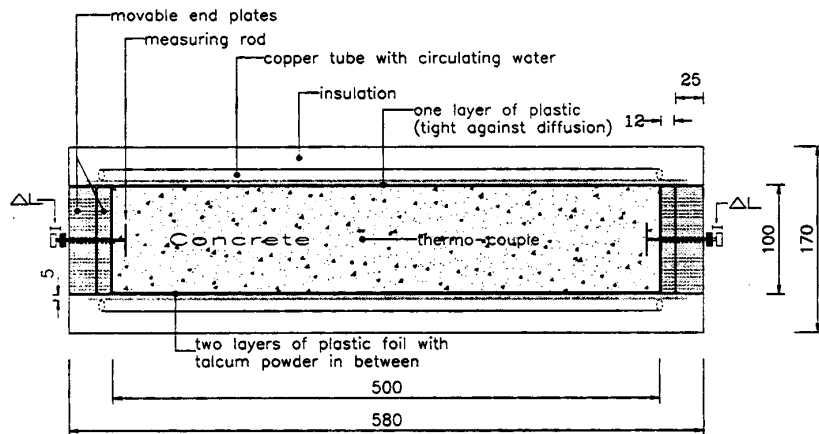


Figure 2.12 – Measuring system with cast-in nails [Bjontegaard 1999]

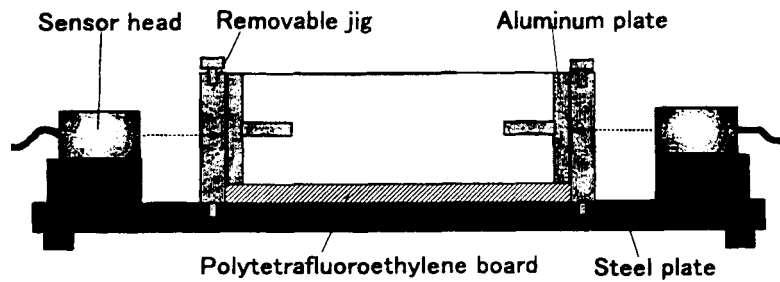


Figure 2.13 – Measuring system with moveable end plates in a  $40 \times 40 \times 160 \text{ mm}^3$  beam [Morioka et al. 1999]

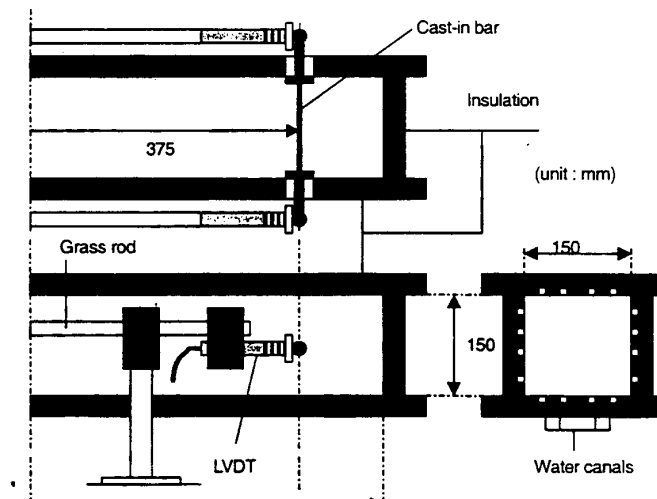


Figure 2.14 – Measuring system with horizontal cast-in bars in a  $150 \times 150 \times 1000 \text{ mm}^3$  beam [Lokhorst 1998]



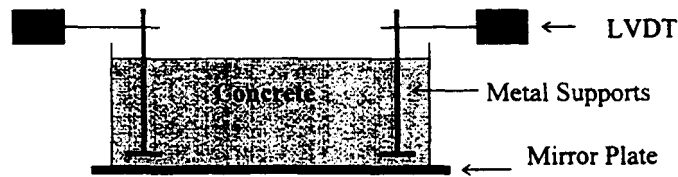


Figure 2.15 – Measuring system with vertical cast-in bars in a  $270 \times 270 \times 100 \text{ mm}^3$  slab [Holt & Leivo 1999]

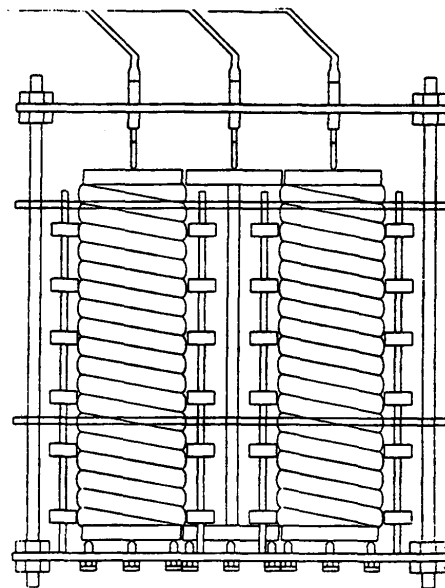


Figure 2.16 – Measuring system with flexible tubes (diameter 100 mm, length 375 mm) and vertical length measurement [Hansen & Jensen 1997].

As pointed out in the previous section about cement paste, linear measurements of autogenous deformation on a concrete mix before setting are not only associated with a large scatter, but are also intrinsically ambiguous, since the length is not defined in a fluid system. Start of the measurement should coincide with setting, but exact determination of the fluid-solid transition is difficult and subjective. A possible approach, which was followed in the measurements presented in Chapter 6, is to start measuring before setting and to register at the same time the self-induced stress of a restrained specimen. The deformations are then zeroed at the moment when a stress is recorded in the restrained specimen. This ensures that only the deformations measured on a solid system, which is able to exert an external stress, are taken into account.

## 2.9 Conclusions

In this chapter some issues have been outlined that will be dealt with in detail further on.

Understanding the differences between Portland and BFS cement pastes, both the hydration mechanisms and the microstructure, is essential to explain the measured autogenous deformation and internal RH of the pastes (Chapter 3). Measurements of internal RH, which depends on the hydration kinetics and on the microstructure formed, allow calculating self-desiccation shrinkage (Chapter 5) based on the capillary tension approach that was outlined in this chapter. Possible explanations for early age expansion were also suggested and discussed.

A brief introduction to internal curing with LWA or SAP to limit self-desiccation was presented. Previous studies reported somewhat contrasting results in the early-age deformations of similar mixes. A more thorough investigation of the internal curing process, especially of the water transport from the aggregates to the hardening matrix, is required.

A main source of controversy in the field of autogenous deformation lies in the measuring techniques, which have not been standardized so far. The volumetric and the linear technique yield very different results for the same cement paste, a fact that must be due to some fundamental differences between the techniques and probably also to experimental error. The measuring techniques used in this thesis (see Chapter 3, 4 and 6), all based on the linear method, were presented.

# **Part I**

## **Cement paste**

---



# Chapter Three

## Paste measurements at room temperature

---

### 3.1 Introduction

In this chapter, measurements of autogenous deformation, internal RH, non-evaporable water content, chemical shrinkage, elastic modulus, pore solution composition, and surface tension of pore solution are presented and discussed. Two cement pastes with w/c ratio 0.37 and 5% silica fume addition were cured at 20°C for at least one week. The two cement pastes differed in the kind of cement: Portland cement or BFS cement.

The objective of this investigation was twofold:

- 1) To investigate early-age properties of Portland cement and BFS cement pastes. The differences between the cement pastes are mainly due to the reaction kinetics and to the microstructure formed, with the BFS cement paste having a slower reaction but also a finer pore structure (Chapter 2).
- 2) To providing data for modeling of the self-desiccation shrinkage as a function of the internal RH, as will be shown in Chapter 5.

### 3.2 Materials

Portland cement (CEM I 52.5 R) and BFS cement (CEM III/B 42.5 LH HS) were used. The Portland cement had Blaine fineness 530 m<sup>2</sup>/kg and calculated Bogue composition of C<sub>3</sub>S 53.6%, C<sub>2</sub>S 20.1%, C<sub>3</sub>A 8.2%, and C<sub>4</sub>AF 9.1%. The BFS cement contained 76% slag and 24% Portland cement and had Blaine fineness of 390 m<sup>2</sup>/kg. Two cement pastes were studied, one with Portland cement and one with BFS cement. In both cases, the w/c ratio of the pastes was 0.37. Silica fume with a BET surface area of 19 m<sup>2</sup>/g was added in slurry form, 5.2% by cement weight. For both pastes, a liquid lignosulphonate-based water-reducing agent (0.2% by cement weight) and a liquid naphthalene-sulphonate-based superplasticizer (1.7% by cement weight) were also added to the mix.

1.5 l of cement paste were mixed in a 5 l epicyclic Hobart mixer. Demineralized water was mixed with the admixtures and added in two steps to ensure homogeneity. Total mixing time from first water addition was 5 minutes. To avoid bleeding, the BFS cement paste was slowly rotated (4 rev./min). Rotation was stopped a few hours after casting, when no further bleeding was observed.

### 3.3 Methods

#### 3.3.1 Non-evaporable water content

About 10 g of fresh cement paste were placed in a plastic vial. The height of the cement paste sample was about 5 mm. The vials were either capped to maintain sealed curing conditions, or about 1 ml of water was added on top of the cement paste to maintain saturated curing conditions throughout the experiment. The samples were stored at 20°C until their evaluation. After achieving the required age, samples for the determination of non-evaporable water content,  $W_n$  [g water / g cementitious material], were ground to powder in a mortar and flushed with methanol to stop hydration, using a porous ceramic filter and vacuum. The powder was divided approximately in half and placed in two crucibles of known mass, which were left overnight (for about 20 h) in an oven at 105°C. When removed from the oven, the crucibles and samples were weighed before placing them in a furnace at 1000°C for at least 4 h. The non-evaporable water content was calculated as the average difference between the 105°C and 1000°C mass measurements for the two crucibles, corrected for the loss on ignition of the cement powder itself, which was assessed in a separate measurement.

#### 3.3.2 Chemical shrinkage

Chemical shrinkage was measured using the method described in [Geiker 1983]. About 5 g of freshly mixed cement paste were cast in the bottom of a small glass jar, with diameter 25 mm and height 60 mm. The thickness of the cement paste sample was about 5 mm. After the cement paste was covered with 1 ml of water, the jar was filled with hydraulic oil. The jar was sealed with a rubber stopper encasing a pipette graduated in 10  $\mu$ l increments and placed in a constant-temperature water bath at 20°C. The oil level within the pipette was measured to the nearest 2.5  $\mu$ l over time, for a period of 7 days. The chemical shrinkage per gram of initial cement and silica fume was determined by normalizing the change in volume to the mass of solids in the sample. For each measurement, two specimens were tested.

#### 3.3.3 Internal relative humidity

About 10 g of fresh cement paste were cast into the measuring chambers of two Rotronic hygroscope DT stations equipped with WA-14TH and WA-40TH measuring cells (Figure

3.1). Each station was equipped with a Pt-100 temperature sensor and a DMS-100H RH sensor. The RH sensors contain an electrolyte whose electrical impedance depends on the ambient RH. The RH stations were placed in a thermostatically controlled room at  $20 \pm 0.1^\circ\text{C}$ . The RH in the samples and the temperature were measured every 15 minutes for a period of about 1 week after water addition. Before and after the measurements, calibration of the stations was carried out with four saturated salt solutions ( $\text{K}_2\text{SO}_4$ ,  $\text{KNO}_3$ ,  $\text{KCl}$ ,  $\text{NaCl}$ ) with known constant RH in the range 75-100% RH. The whole calibration procedure took about 24 hours. It is noticed that even for a high-quality sensor the drift may exceed 1% RH per month. In the present case calibration before and after the measurements showed a maximum 0.1% difference in the measured values. This calibration procedure yields a global measuring accuracy of about  $\pm 1\%$  RH.

Besides calibration and sensor drift, there are further possible sources of error in the measurements:

- 1) Lack of thermal equilibrium between sensor and sample. The temperature gradients may be due to insufficient thermostatic control or to development of heat of hydration in the paste.
- 2) Condensation on the sensor may occur if the sample has a higher temperature than the sensor itself. If condensation takes place, the RH readings may be affected for the rest of the measurement, until all water evaporates. To avoid this problem, the sensor is locally heated to approximately  $+0.5^\circ\text{C}$ , but in special cases (such as samples developing significant heat of hydration) this precaution may not be enough.
- 3) The sensor needs some time to reach moisture equilibrium with the cement paste. This fact influences the RH measurements in the first hours after casting.



Figure 3.1 – Rotronic station for RH measurement

### 3.3.4 Autogenous Deformation

The cement paste was cast under vibration into tight plastic molds (low density polyethylene plastic, LDPE), which were corrugated to minimize restraint on the paste. The length of the samples was approximately 300 mm and the diameter 25 mm. The specimens were placed in a dilatometer and immersed into a temperature controlled glycol bath at  $20 \pm 0.1^\circ\text{C}$ . Two samples were tested simultaneously in the dilatometer, with a measuring accuracy of  $\pm 5 \mu\text{strain}$ . Linear measurements every 15 minutes were started about half an hour after casting for the Portland cement paste and after about 4 hours of rotation for the BFS cement paste.

A top view of the dilatometer is shown in Figure 3.2. The dilatometer frame consisted of two steel plates joined rigidly by four solid invar rods (diameter 20 mm). Each specimen was longitudinally supported by two parallel rods attached to the steel plates. The specimens were gripped by coil springs at one end, while the rest could slide freely on the rods, which were lubricated by the glycol bath. The longitudinal deformation was measured at the free end by a TRANS-TEK 350-000 displacement transducer. A detailed description of the dilatometer is provided in [Jensen & Hansen 1995].

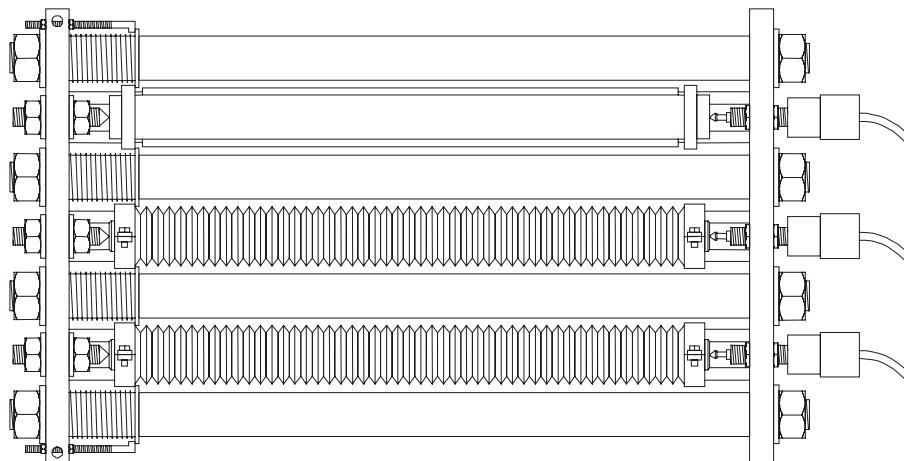


Figure 3.2 – Dilatometer for autogenous deformation measurements [Jensen & Hansen 1995]

The corrugated mould (Figure 3.3) transformed volumetric deformations into linear deformations when the paste was in a fluid state, due to a greater stiffness in the radial than in the longitudinal direction of the mold. The ratio between the length and volume change was found to be 1.85 mm/ml [Jensen 1996]. Length changes occurring before set should be divided by 2.53 if isotropic deformation is used as a reference. The corrugated moulds were specially designed to minimize restraint on the paste. A maximum restraint force of 0.5 N (corresponding to a stress of 0.001 MPa) on the paste was measured [Jensen 1996] for a deformation of 10,000  $\mu\text{strain}$ . For a comparison, it is noticed that the forces acting on the paste before setting are of the magnitude of the atmospheric pressure, about 0.1 MPa. The moulds were watertight: water loss from a tube filled with water kept



at 20°C and RH close to 0% for one week was about 0.04 g, corresponding to 0.03% of the water content [Jensen 1996].

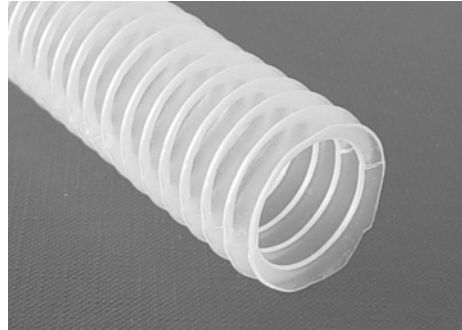


Figure 3.3 – Special corrugated plastic mould for autogenous deformation measurements

### 3.3.5 Elastic Modulus

The elastic modulus in compression (secant modulus at 30% of the compressive strength) was measured after 1, 3, and 7 days of sealed hardening on cement paste prisms, 50×50×200 mm<sup>3</sup>. The prisms were cast into temperature-controlled steel moulds and cured at 20°C.

### 3.3.6 Pore solution analysis

Ion chromatographic analysis of pore solution extracted from the hydrating cement pastes was performed. For early ages on the order of a few hours, the pore solution was obtained by filtering about 150 g of hydrating cement paste. For later ages, it was necessary to express the pore solution from the hardened cement paste using a special die and a universal testing machine, based on the methodology developed in [Longuet et al. 1973]. For three replicates analyzed by ion chromatography, the maximum standard deviation in the determined concentrations was less than 4 mmol/l.

### 3.3.7 Surface tension

The surface tension of pore solutions filtered from the cement pastes after 1 h of hydration was measured with a DuNouy tensiometer at 23°C (Figure 3.4, left). This method of measuring the surface tension of a liquid is based on the interaction of a platinum ring with the liquid surface being tested. The ring is submerged below the interface and subsequently raised. As the ring moves upwards it raises menisci of the liquid (Figure 3.4, right). Eventually the menisci tear apart from the ring and return to their original position. Prior to this event, the force exerted by the menisci reaches a maximum, from which the surface or interfacial tension is calculated.

Synthetic pore solutions, representing the measured composition of the pore solutions, and solutions of the water-reducing agent and of the superplasticizer were prepared and measured as well. Demineralized water was used as a reference.

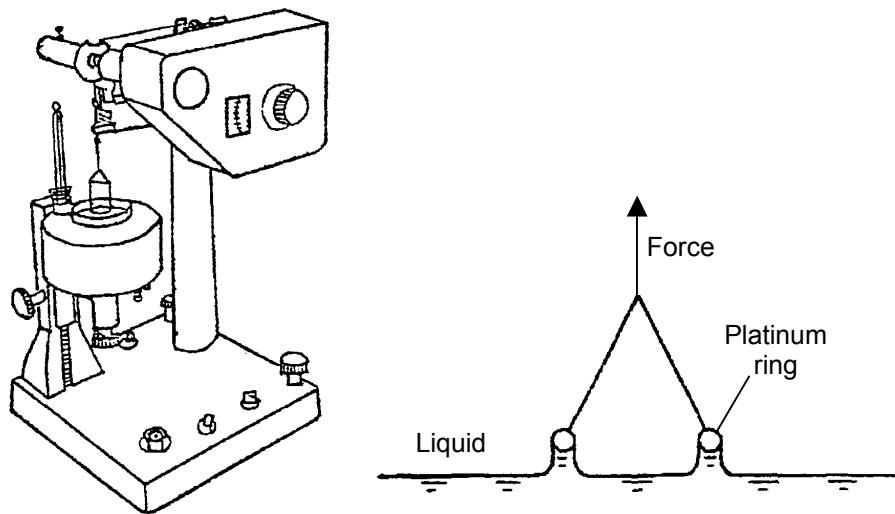


Figure 3.4 – View of a Du Nouy tensiometer (left) and measuring principle of the tensiometer (right)

### 3.4 Results and discussion

#### 3.4.1 Non-evaporable water content

In Figure 3.5, the non-evaporable water content as a function of age for the two cement pastes is shown.

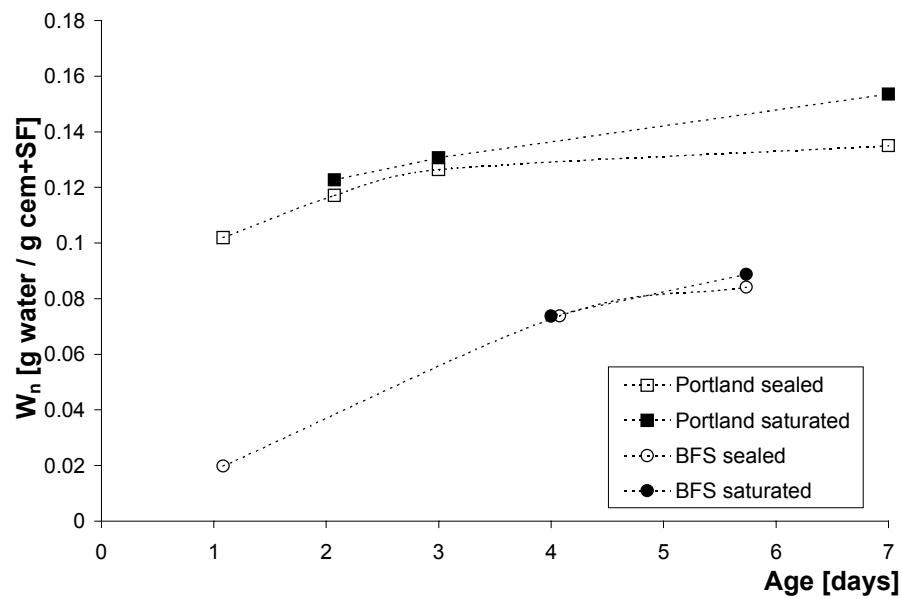


Figure 3.5 – Non-evaporable water content as a function of age

The non-evaporable water content of the BFS cement paste is much lower than the one of the Portland cement paste. As a reference, Harrison et al. [1987], measured a non-evaporable water content of 0.173 g H<sub>2</sub>O / g solids on a 14-month old 0.5 w/b ratio paste with 60% Portland cement and 40% BFS. This fact indicates that the quantity of water bound by slag should be somewhat lower than the water bound by Portland cement, which amounts to about 0.22 g H<sub>2</sub>O / g cement [Powers & Brownyard 1948].

Additional information in Figure 3.5 is that the values of non-evaporable water for sealed and saturated samples diverge after 2 days for the Portland cement paste, and after 4 days for the BFS cement paste. This may indicate the occurrence of self-desiccation in the pastes, which decreases the rate of hydration.

### 3.4.2 Chemical shrinkage

Figure 3.6 shows the chemical shrinkage of the two cement pastes.

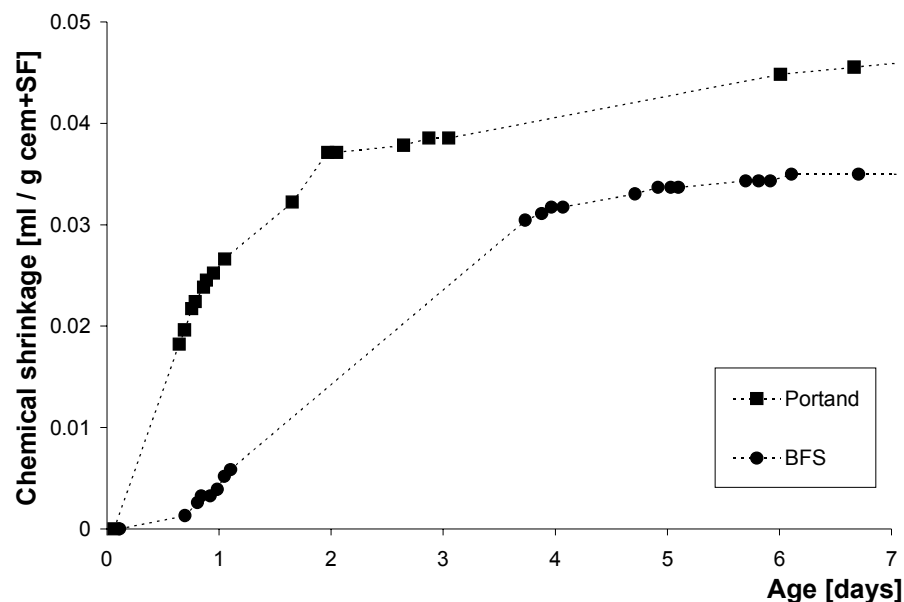


Figure 3.6 – Chemical shrinkage as a function of age

Chemical shrinkage of the BFS cement paste develops later and is lower in the first week. Notice that for the BFS cement paste almost no chemical shrinkage is measured in the first day. The plateau of the curve for the BFS cement paste after 3.5 days hydration may be a measuring artifact due to depercolation of the water-filled capillary porosity in the hardening cement paste [Geiker 1983]. Roy & Idorn [1982] also measured lower chemical shrinkage in the first day of hydration for a BFS cement paste (50% slag) with w/b ratio 0.375 compared to a Portland cement paste. However, this result was obtained measuring bulk shrinkage with the weighing method (see Chapter 2); therefore it is reliable only in

the first hours of hydration, until setting takes place. After setting, the bulk shrinkage and the chemical shrinkage diverge, as described in Chapter 1 and 2.

### 3.4.3 Internal relative humidity

Internal RH of the cement pastes was measured on two independent samples for a period of at least 6 days. The development of internal RH with hydration time is provided in Figure 3.7. After equilibrium between the sensors and the paste was reached, the RH decreased with hydration time.

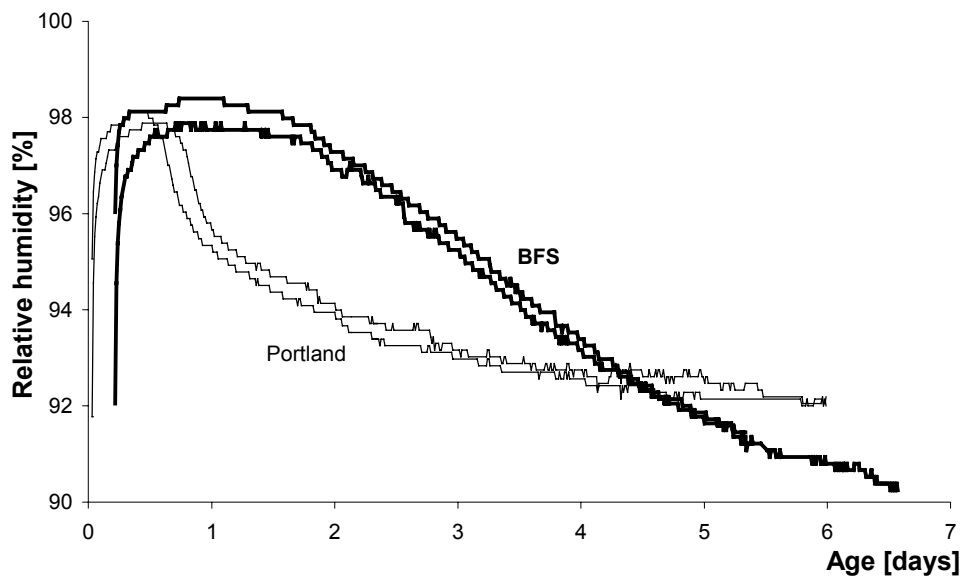


Figure 3.7 – Internal RH vs. age for the two cement pastes

Besides the initial moisture equilibration of the RH-sensors (see the first hours in Figure 3.7), a lack of thermal equilibrium between the sensor and the sample may occur during the test, due to insufficient thermostatic control or to development of heat of hydration in the paste. This may lead to a significant measuring error: for example, near saturation at 20°C a temperature difference of 1°C may lead to an error of about 6% RH [Jensen & Hansen 1999]. The BFS cement paste develops less heat of hydration and slower than the Portland cement paste [Lura et al. 2002a]; therefore the temperature, also due to the small dimensions of the sample, is closer to isothermal and the measured RH should be more reliable. In fact, the temperature measured inside the Rotronic stations was always lower than 21°C in the case of the Portland cement paste, while for the BFS cement paste the temperature remained practically constant.

Figure 3.7 shows that the initial RH is similar in the two pastes, about 98%. Initial RH values around 97-98% were measured on a number of Portland cement pastes [Jensen & Hansen 1996, Bentz et al. 2001]. The internal RH in the Portland cement paste reached a plateau 4 days after mixing, at a value around 92% RH. In the BFS cement paste, on the

other hand, the internal RH was 90% at 6.5 days of hydration and was still decreasing by that time (Figure 3.7). Also in [Hanehara et al. 1999] BFS cement pastes reached lower internal RH than Portland cement pastes.

Different mechanisms might contribute to the higher RH drop in BFS cement pastes:

- 1) A higher chemical shrinkage of the BFS cement compared to Portland cement might lead to greater self-desiccation (Chapter 2). This is in contrast with the results shown in Figure 3.6, where the BFS cement paste had lower chemical shrinkage than the Portland cement paste. However, a great part of the chemical shrinkage may have not been detected due to depercolation of the capillary porosity after about 3.5 days hydration.
- 2) BFS cement pastes have a finer pore structure than Portland cement pastes (Chapter 2). This finer pore structure should be the result of CH-crystals dissolution and precipitation of CSH produced by the pozzolanic reaction. Finer pores result in a lower RH according to the Kelvin equation (see also Chapter 5).
- 3) The reaction of BFS might also be less affected by a RH-drop than Portland cement hydration. In fact, it was found that the pozzolanic reaction of silica fume and calcium hydroxide was only slightly affected by a RH drop: nuclear magnetic resonance (NMR) measurements [Jensen 1993a] on a cement paste with w/c 0.25 and 10% silica fume addition showed that the degree of reaction of silica fume still increased after the hydration of C<sub>3</sub>S and C<sub>2</sub>S had stopped, at RH lower than 80%. If the slag has the same behavior, the ongoing pozzolanic reaction will result in a progressive RH decrease due to refinement of the porosity and water absorption on the CSH gel formed.
- 4) Finally, a different composition of the pore water in Portland cement and in BFS cement paste could influence the RH depression due to dissolved salts. This issue will be dealt with in Chapter 5.

#### 3.4.4 Autogenous deformation

The measured autogenous deformations for the two mixtures are provided in Figure 3.8. Deformations were recorded for about 6 days in the case of the Portland cement paste and 9.5 days in the case of the BFS cement paste. The deformations were zeroed at the moment of setting, which occurred 7 hours and 15 hours after mixing for the Portland cement and the BFS cement paste, respectively. The initial deformation of the two pastes in Figure 3.8, until setting, was due to chemical shrinkage. At setting, a self-supporting skeleton formed and, thereafter, chemical shrinkage resulted mainly in internal voids. Setting was identified by a change in the slope of the deformations, in the case of the Portland cement paste, or by the occurrence of expansion, in the case of the BFS cement paste.

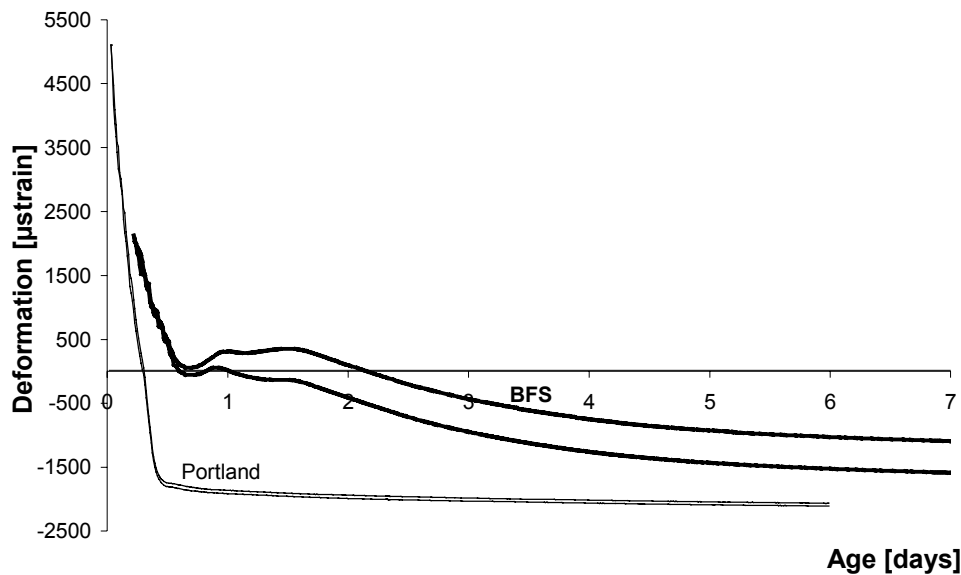


Figure 3.8 – Autogenous deformation vs. age of Portland and BFS cement pastes

Expansion in the BFS cement paste was different in the two samples, while both the initial deformations due to chemical shrinkage and the shrinkage after 36 hours of hydration were the same. Since the pastes were rotated for 4 hours, the expansion did not come from re-absorption of bleeding water and should be considered as an autogenous phenomenon, perhaps caused by formation of ettringite. According to [Roy & Idorn 1982, Hill & Sharp 2002] ettringite is in fact also formed in BFS cement pastes. Since this reaction occurs with a chemical shrinkage [Jensen 1993b], expansion can only take place if the reaction products form within a solid skeleton (Chapter 2), in a situation of constraint.

Possible explanations of the large scatter in the expansion of the BFS cement pastes:

- 1) The forces producing expansion (i.e. crystallization pressure of ettringite or other hydrates, see Chapter 2), acting in a very weak cement paste, are influenced by very small differences in the samples, for example due to differences in the temperature regime or inhomogeneities within the sample. According to [Scherer 1999], the magnitude of the stress that a crystal exerts against the pore walls depends on the pore radius. The pore radius where ettringite is first nucleated would in this case govern the expansion; nucleation of ettringite would be different in pastes cured in slightly different conditions.
- 2) Since bleeding began already at mixing, the single samples might have had a slightly different w/c ratio, depending on the way of pouring them into the moulds. However, inhomogeneities between the samples do not explain why they experienced the same shrinkage after the expansion phase ended.

### 3.4.5 Elastic modulus

Figure 3.9 shows the elastic modulus as a function of age for the two cement pastes. The average value of two samples is reported. The BFS cement paste had a later development of stiffness and reached lower values after one week. This is a consequence of the slower reaction of the slag compared to Portland cement.

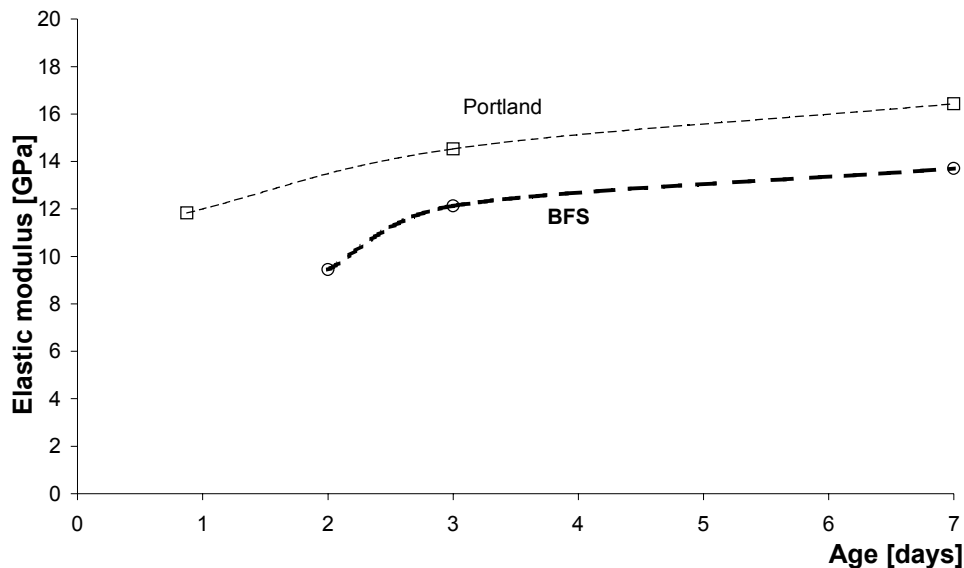


Figure 3.9 – Elastic modulus as a function of age measured on Portland and on BFS cement paste

### 3.4.6 Pore solution composition

In Table 3.1, the concentrations of  $\text{Na}^+$ ,  $\text{K}^+$ , and  $\text{Ca}^{++}$  ions in the pore solution measured at different ages are shown. The quantity of pore solution that could be extracted from the Portland cement paste at 6 days was not enough for the chromatographic detection.

Table 3.1 – Ion concentration in the pore solution of cement pastes measured at different ages

	Age [days]	$\text{Na}^+$ [mmol/l]	$\text{K}^+$ [mmol/l]	$\text{Ca}^{++}$ [mmol/l]
<b>Portland</b>	1/24	239	317	0.056
	2	1037	763	0.316
<b>BFS</b>	3/24	126	111	0.012
	2	184	183	-
	6	200	183	-

The alkali concentration in the pore solution of the Portland cement paste is much higher than in the BFS cement paste, and is increasing in time. It is noticed that the alkali content of the Portland cement was:  $\text{K}_2\text{O}$  1.23% and  $\text{Na}_2\text{O}$  0.30%. The alkali content of the BFS cement was:  $\text{K}_2\text{O}$  1.17% and  $\text{Na}_2\text{O}$  0.22%. Lower alkali content in pore solution of BFS

cement pastes compared to Portland cement pastes were observed also by Roy et al. [2000]. Roy & Idorn [1982] supposed that this fact might be due to incorporation of alkali into the CSH gel of BFS cement pastes, which is different from the one of Portland cement, having a lower Ca/Si ratio.

### 3.4.7 Surface tension

The surface tension of pore solutions, extracted by filtering the paste after 1-h hydration, measured 0.065 N/m for both cement pastes. Demineralized water yielded 0.075 N/m, somewhat higher than the theoretical value, 0.072 N/m. Synthetic pore solutions were realized by mixing demineralized water with NaOH and KOH corresponding to the concentrations reported in Table 3.1. Their surface tension was about 0.078 N/m. Solutions of the superplasticizer, naphthalene sulphonate, in the same concentration as in the cement paste, yielded values similar to demineralized water. However, the water-reducing agent, lignosulphonate, reduced the surface tension to 0.050 N/m. It is suggested that the decrease in the surface tension of the pore solution is due mainly to the lignosulphonate.

### 3.4.8 Autogenous deformation as a function of relative humidity

In Figure 3.10 the autogenous deformation of the Portland cement paste is plotted vs. the internal RH, starting from about 11 hours after mixing with water. The RH drop is a measure of the tension state in the pore water, due to increasing capillary depression and changes in the disjoining pressure (Chapter 2).

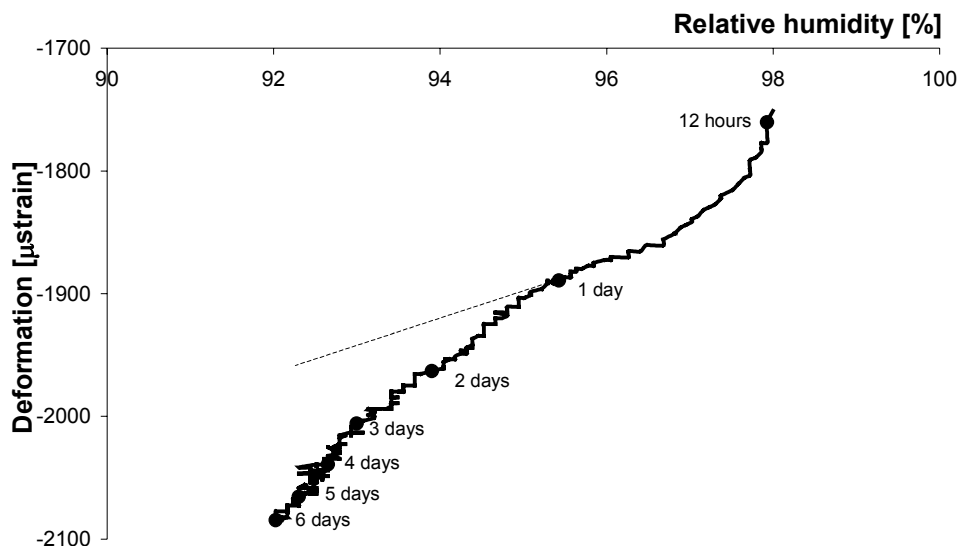


Figure 3.10 – Autogenous deformation of Portland cement paste as a function of internal relative humidity



In the first 24 hours the steepness of the curve decreased, corresponding to an increase of the elastic modulus of the cement paste. Afterwards, the RH change decelerated (Figure 3.7) and the deformation per % RH increased. This fact could be due to the onset of the pozzolanic reaction of silica fume that consumed the CH crystals. Internal restraints in the paste were removed and a further shrinkage took place [Jensen & Hansen 1996]. Creep of the cement paste could be an additional reason. In fact, the effect of creep became evident because in the second part of the curve the deformations were occurring during a longer time (as shown by the dots in Figure 3.10). Creep in the first hours was probably very fast and was measured as a quasi-instantaneous deformation. This behavior can be modeled with a reduction of the elastic modulus of the paste [Jensen 1993b] that indirectly takes the effect of creep into account. It is noticed that the measured increase in the slope of the shrinkage-RH curve after 1-day hydration cannot be related to temperature changes due to heat of hydration, because these occurred only in the first hours after mixing with water.

In Figure 3.11 the autogenous deformation of the BFS cement paste is plotted vs. the internal RH. The deformations were zeroed 36 hours after mixing with water, coinciding with the end of the expansion period. As for the Portland cement paste (Figure 3.10), the decreasing slope of the shrinkage-RH curve in the first hours was probably due to the increase of the elastic modulus of the cement paste. It is noticed that in the case of drying shrinkage measurements on hardened Portland cement pastes, where the elastic modulus is constant during the test, the measured slope of the shrinkage-RH curve was almost constant in the RH range 90-40% [Baroghel-Bouny et al. 1999].

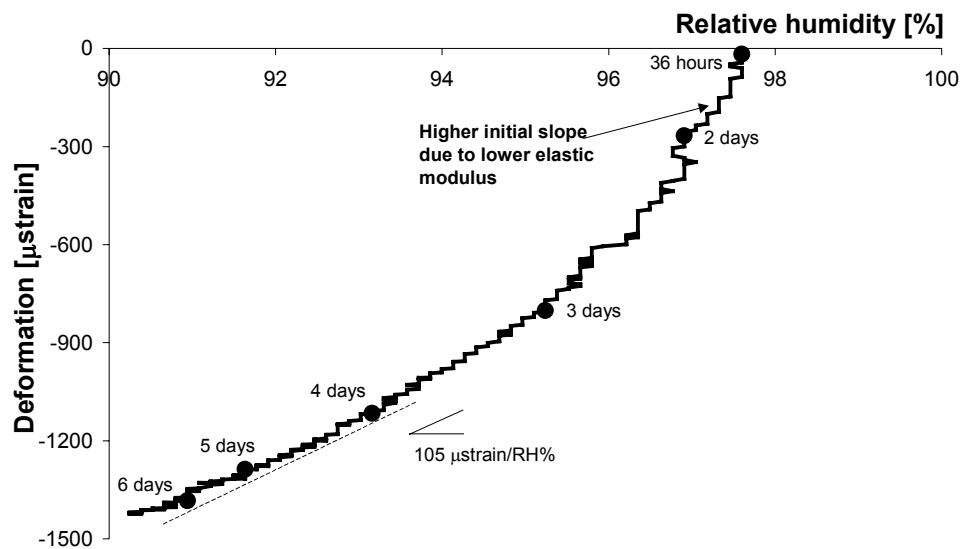


Figure 3.11 – Autogenous deformation of Blast Furnace Slag cement paste plotted as a function of internal relative humidity

From the third day after casting, the rate of the RH drop in the BFS cement paste decreased and the deformation showed an almost constant slope, about  $105 \mu\text{strain}/\%RH$ . For a comparison, Jensen [1993b] found a value of  $80 \mu\text{strain}/\%RH$  for a Portland cement paste with w/c 0.4 and 10% silica fume addition. In the case of the BFS cement paste no increase in the slope of the deformation at a later age was found, as in the case of Portland cement paste (Figure 3.10). One possible reason is that the RH was still decreasing after one week, when the measurements were stopped. This continuous increase of the shrinkage-inducing internal stress possibly masked the effect of creep.

### 3.5 Conclusions

From the analysis of the experimental results regarding cement pastes with Portland or BFS cement and 5% silica fume addition cured at  $20^\circ\text{C}$ , the following conclusions can be drawn:

- 1) Non-evaporable water content of the BFS cement paste increased slowly and was much lower after one week than for the Portland cement paste.
- 2) Chemical shrinkage of the Portland cement paste was higher. However, this may be an artifact of the measurements caused by depercolation of capillary porosity in the BFS cement paste.
- 3) Self-desiccation occurred earlier for the Portland cement paste than for the BFS cement paste. In time, the internal RH of the BFS paste decreased at a higher rate and eventually became lower than in the Portland cement paste.
- 4) Most of the autogenous deformation of the Portland cement paste occurred before and around setting and did not correspond to a RH drop, but was due to chemical shrinkage. On the other hand, the BFS cement paste expanded after setting. A substantial shrinkage followed, accompanied by a drop of the RH.
- 5) The elastic modulus of the Portland cement paste was higher and developed earlier than the one of the BFS cement paste.
- 6) The alkali ions concentration in the pore solution of the Portland cement paste was much higher than in the BFS cement paste.
- 7) The surface tension of the pore solution in the first hours of hydration was about  $0.065 \text{ N/m}$  for both cement pastes. This low value, compared with pure water, was probably mainly due to the water-reducing agent.
- 8) Plots of shrinkage vs. RH for the Portland cement paste showed a decreasing slope in the first days, corresponding to a stiffness gain of the paste. A further increase in the deformation rate followed. In the case of the BFS cement paste, only a decreasing slope was observed. Globally, the BFS cement paste showed higher shrinkage per unit RH decrease, due to lower elastic modulus and possibly greater creep, and greater self-desiccation shrinkage than Portland cement pastes.

# Chapter Four

## Paste measurements at different temperatures

---

### 4.1 Introduction

In Chapter 3 experimental data was presented about autogenous deformation, internal RH and other early-age properties of Portland and BFS cement pastes cured at 20°C. The main objective of this Chapter is to assess the influence of different temperature regimes on the development of autogenous deformation. Both for the theory and for practical applications, the goal is to measure autogenous deformation of cement paste at one given curing temperature and to calculate it at any temperature regime, for example with a maturity transformation [Hansen & Pedersen 1977].

Jensen & Hansen [1999] demonstrated that a rigorous application of the maturity principle to autogenous deformation is not feasible. The maturity principle will only be applicable to autogenous deformation if it is monotonously dependent on the degree of hydration. This is not the case, since the surface tension of the pore water is temperature-dependent and the internal RH change, which is linked to self-desiccation shrinkage (see Chapter 5), is function of both the degree of hydration and the curing temperature.

Moreover, experimental evidence [Bentur et al. 1979] suggests that the pore structure of a cement paste depends on the curing temperature. A coarser structure is formed at higher temperatures, due to a higher density of the gel. According to Thomas & Jennings [2001], coarsening of the pore structure at higher temperature would also be produced by polymerization of the CSH gel, which would cause expulsion of water and increase the capillary porosity. A coarse pore structure of the hardening cement paste would result in lower self-desiccation and consequently lower self-desiccation shrinkage (see Chapter 5).

However, for practical applications and only within a limited temperature range, it might still be possible to apply a modified maturity concept to autogenous deformation. This has been done for example using a further temperature-correcting coefficient

[Hedlund & Jonasson 2000] or multiple activation energies for silica-fume modified cement pastes [Jensen & Hansen 1999].

In this chapter, measurements of autogenous deformation and heat of hydration are presented and discussed. Three cement pastes with water/cement ratio 0.37 and 5% silica fume addition were cured at 10, 20, 30, and 40°C for about one week. The three cement pastes differed in the kind of cement: Portland cement, BFS cement or a blend of the two.

## 4.2 Materials

Two of the cement pastes investigated in this study (Portland cement paste and BFS cement paste) were already described in section 3.2. Additionally, a cement paste with blended cement, half CEM I 52.5 R and half CEM III/B 42.5 LH HS, was mixed. The w/c ratio of the pastes was 0.37, with 5.2% addition of silica fume by cement weight. The cement pastes were mixed in a 5 l epicyclic Hobart mixer for 5 minutes before casting.

## 4.3 Methods

### 4.3.1 Rate of heat evolution and isothermal heat of hydration

The rate of heat evolution of the cement pastes was measured with an isothermal calorimeter (3114/3236 TAM Air Isothermal Calorimeter by Thermometric AB). The specimens of cement paste weighted 10 g. The cement pastes were cast into capped glass vials and the vials were inserted in the calorimeter. For this reason it was not possible to register the first hydration peak, which occurs immediately after water addition (Chapter 2). The test was performed on 2 parallel samples at 20, 30, and 40°C. It was not possible to measure at 10°C because of formation of condensation inside the calorimeter, which was kept in a room at 20°C. The isothermal heat of hydration was derived by integration of the rate of heat evolution.

### 4.3.2 Autogenous deformation

Measurements of the autogenous deformations were performed with an Autogenous Deformation Testing Machine (ADTM) [Koenders 1997]. The cement pastes were cast in a prismatic mould, 150 mm wide and 1000 mm long, made with thin steel plates provided with an external insulating material. The mould was 40 mm high. A side view and a cross-section of the ADTM are shown in Figure 4.1. Figure 4.2 shows a picture of the device.

A foil was folded into the mould to prevent leakage of water from the fresh material and drying of the hardening material. A felt placed beneath the foil reduced the friction between the mould and the specimen. After casting, the top surface was covered with a plastic foil and with a tight cover in order to avoid moisture loss to the environment. A wooden frame supported the mould during casting and setting of the cement paste. The

mould was cooled or heated by a system of tubes located between the plates and the insulation. This system was meant to guarantee almost isothermal conditions throughout the experiment. For the Portland cement paste, however, deviations from the target curing temperature occurred during the hydration peak. Length changes were measured between two steel bars embedded in the cement paste, 750 mm apart. The bars passed through the mould and at their ends LVDT registered the deformations (Figures 2.14 and 4.2). The temperature of the specimen was measured at 3 points along the cross section of the specimen. Readings of displacements and temperature were taken for at least 5 days after casting.

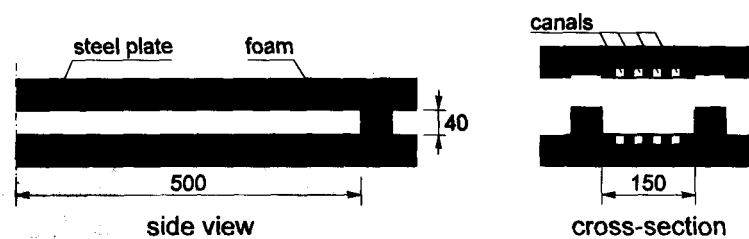


Figure 4.1 – Side view and cross-section of the Autogenous Deformation Testing Machine (ADTM)

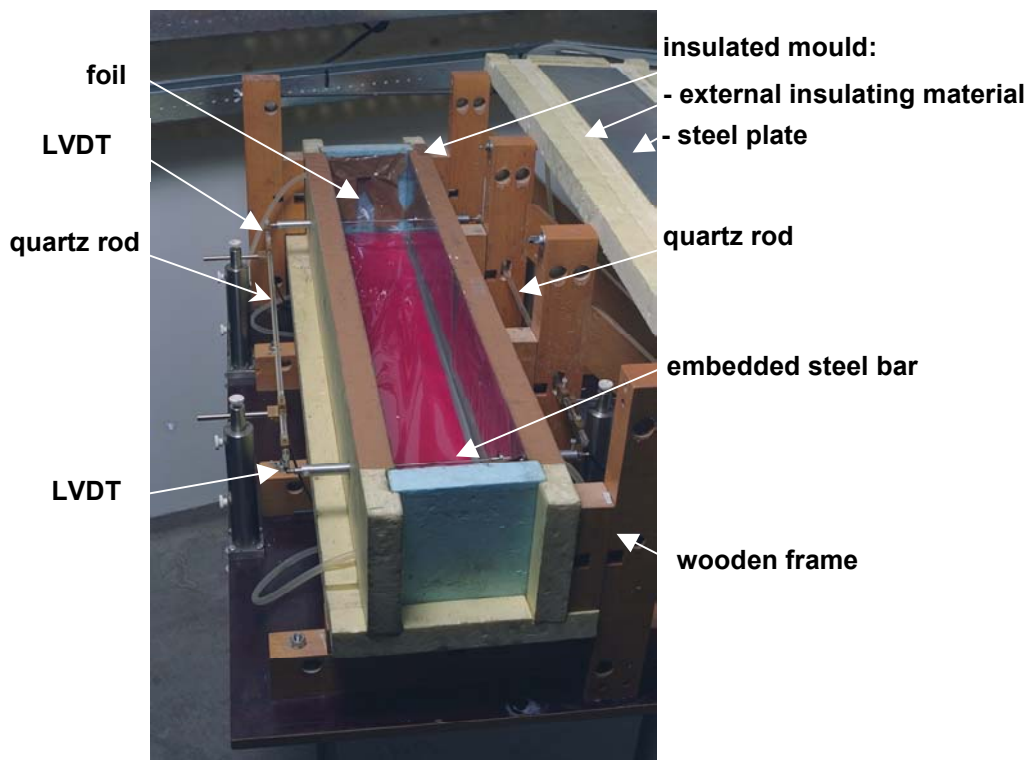


Figure 4.2 – Picture of the Autogenous Deformation Testing Machine (ADTM)

The ADTM allows starting measurements of autogenous deformation around setting, when the cement paste has reached a sufficient strength to sustain the measuring bars. An advantage of this machine is its flexibility. Thanks to the temperature controlled steel mould, a temperature history may be imposed to the cement paste. On the other hand, by varying the thickness of the mould, cement pastes or concrete can be tested with the same machine (Chapters 6 & 8). However, the ADTM possesses some major drawbacks:

- 1) The weight loss of the specimen cannot be monitored during the experiment or after its end. This is also due to the fact that the fresh cementitious material is poured directly into the mould and its exact weight cannot be measured in the fresh state. For this reason, moisture loss from the sample during the experiment cannot be excluded.
- 2) The measuring system is rather cumbersome, involving four LVDT, two imbedded steel bars, and two external quartz rods (Figure 4.2). Every problem occurring with one single LVDT will invalidate the whole measurement. On the contrary, for the dilatometer shown in Figure 3.2 only one LVDT is sufficient to register the deformation of the sample.
- 3) Friction between the cement paste and the mould is reduced by an interposed felt, but will probably still be relevant at very early age, when the cement paste has a low stiffness.
- 4) The dimensions of the specimen make keeping isothermal conditions difficult when cement paste is tested, rapid Portland cement is used, and the curing temperature is high.

## 4.4 Results and discussion

### 4.4.1 Rate of heat evolution and isothermal heat of hydration

Figure 4.3 shows the rate of heat evolution of the cement pastes in the first 48 hours of hydration at 20, 30, and 40°C. Figures 4.4-4.6 show the isothermal heat of hydration of the three cement pastes at 20, 30, and 40°C. The heat of hydration was obtained by integration of the rate of heat evolution. The Portland cement paste shows the highest reaction peaks at all temperatures, with narrower peaks corresponding to higher temperatures. The BFS cement paste hydrates later and shows a first peak and a shoulder of almost the same height at the lower curing temperatures. The blended cement paste shows an intermediate behavior, with shoulders visible at 20°C and 30°C but not at 40°C.

The heat of hydration was highest for the Portland cement paste (Figure 4.4), especially at higher temperatures, and lowest for the BFS cement pastes (Figure 4.5). The blended cement paste had an intermediate behavior (Figure 4.6).

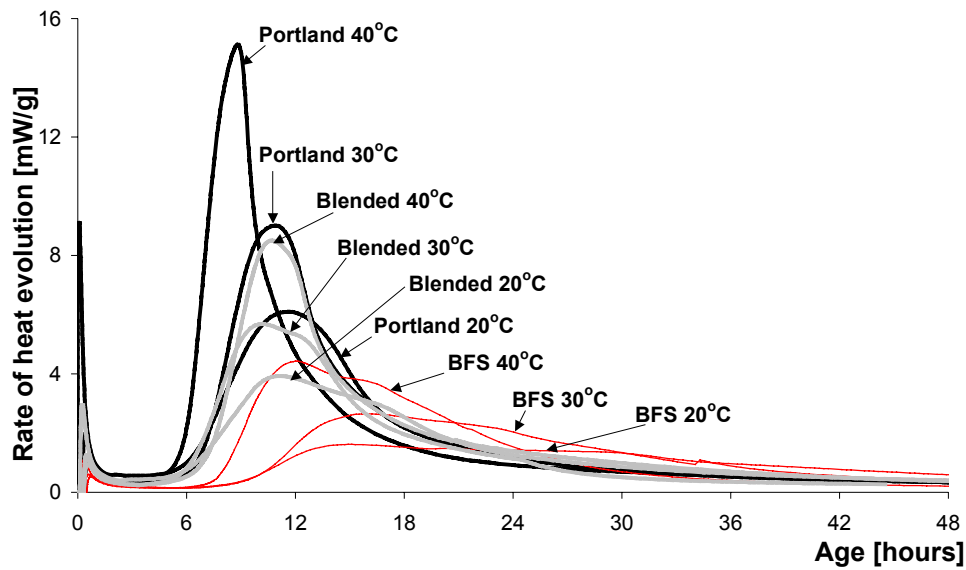


Figure 4.3 – Rate of heat evolution in the first 48 hours after mixing of 3 cement pastes cured at different temperatures

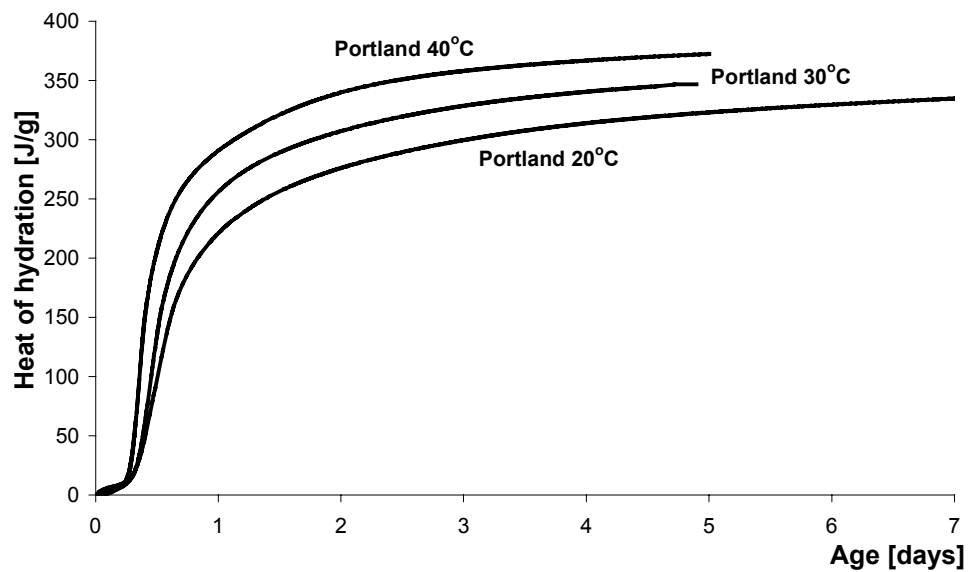


Figure 4.4 – Isothermal heat of hydration of Portland cement paste as a function of temperature

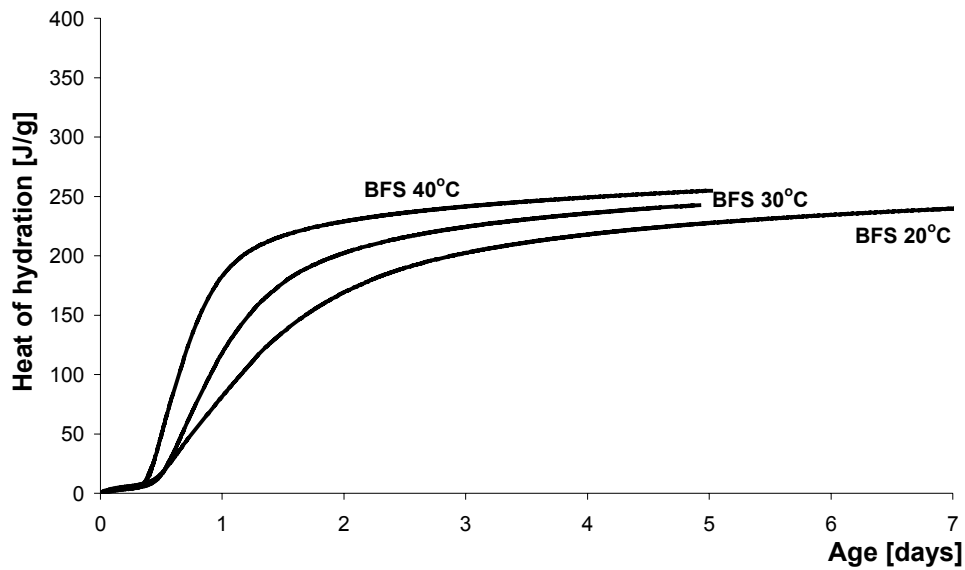


Figure 4.5 – Isothermal heat of hydration of BFS cement paste as a function of temperature

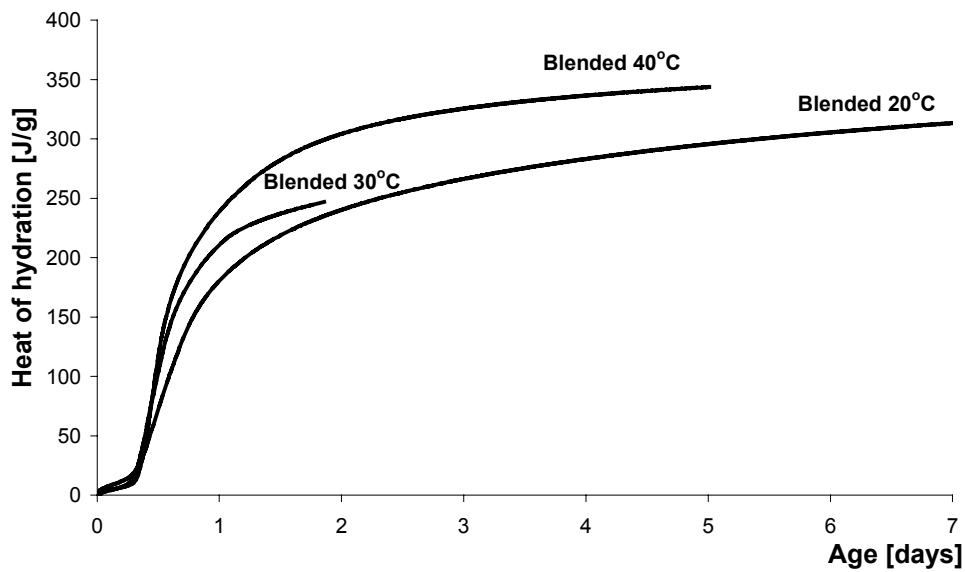


Figure 4.6 – Isothermal heat of hydration of blended cement paste as a function of temperature

#### 4.4.2 Autogenous deformation

In Figures 4.7-4.9 the autogenous deformations of the cement pastes are shown as a function of age for different curing temperatures. Each curve represents the average of at least 2 tests.



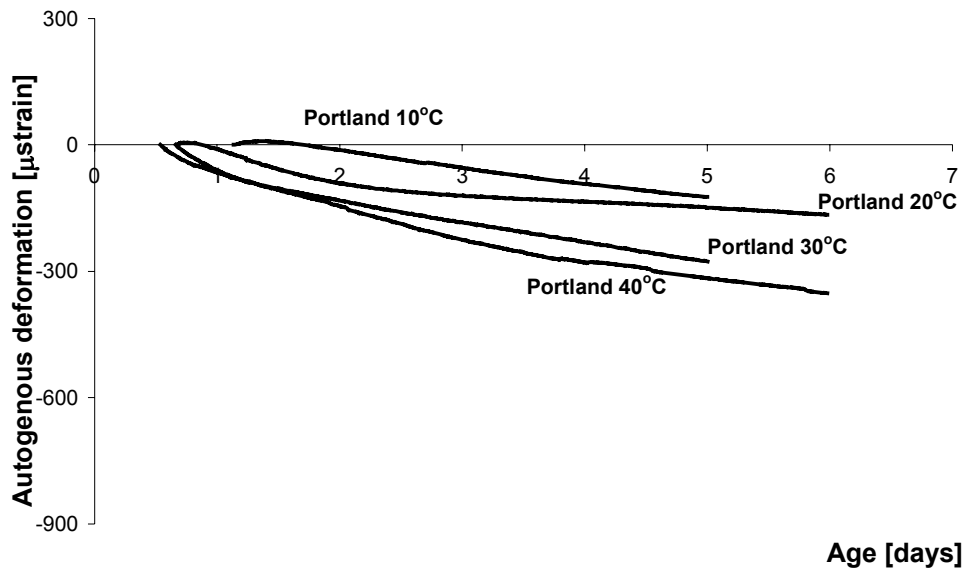


Figure 4.7 – Autogenous deformation of Portland cement paste cured at different temperatures

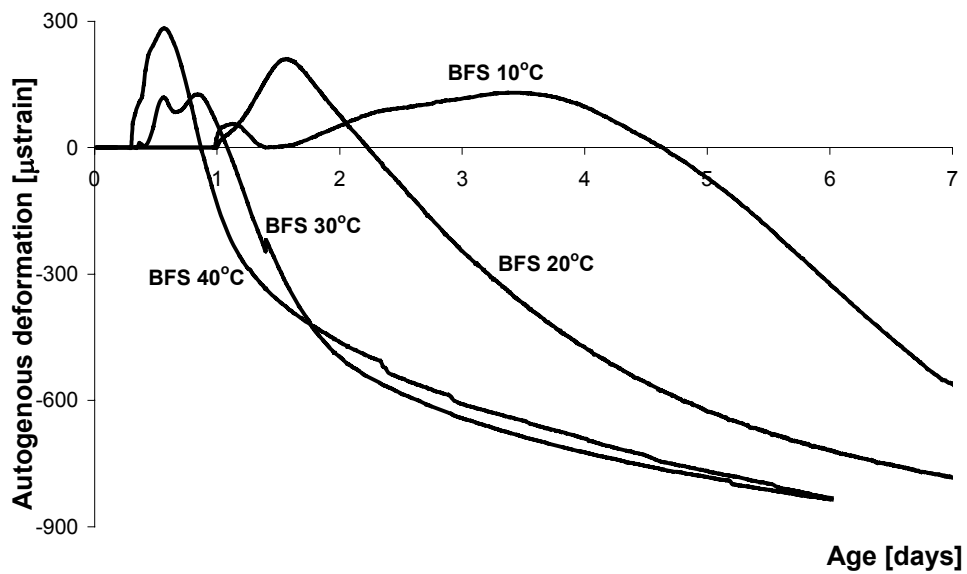


Figure 4.8 – Autogenous deformation of BFS cement paste cured at different temperatures

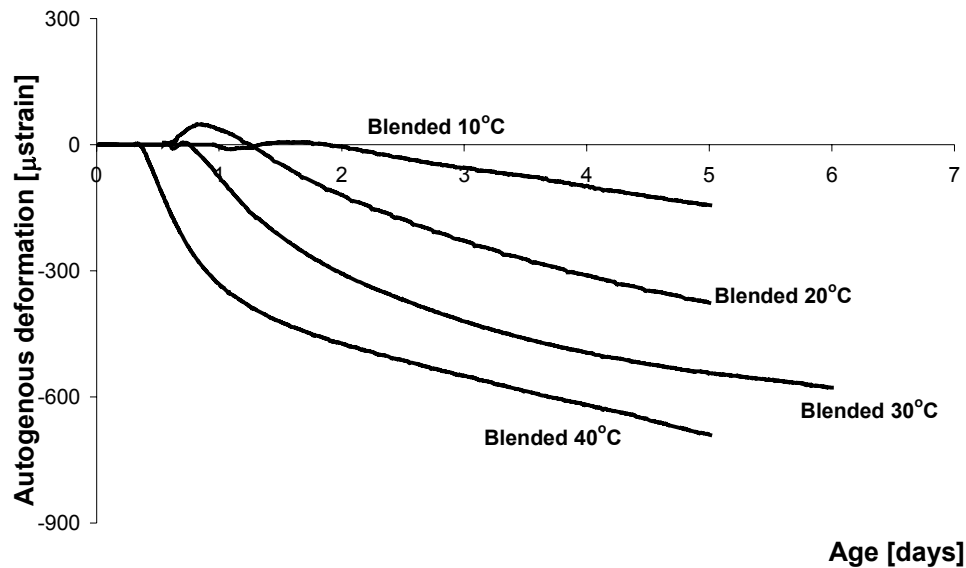


Figure 4.9 – Autogenous deformation of blended cement paste cured at different temperatures

The deformations in Figures 4.7 and 4.9 were zeroed when the temperature in the sample was constant, which generally happened a few hours after the hydration peak registered in the calorimeter (Figure 4.3). The actual measured deformation for the Portland cement pastes was bilinear, similar to the one shown in Figure 3.8. As already discussed in Chapter 3, the first large deformation of the Portland cement paste happens around setting and is due to chemical shrinkage. After setting, the slope of the deformations suddenly decreases. This second shrinkage is related to self-desiccation (Chapter 3).

In the case of the measurements performed with the ADTM on the Portland and on the blended cement paste, a substantial increase of the temperature was registered, which reached values up to  $\Delta T=10^{\circ}\text{C}$  in the case of the Portland cement paste cured at  $40^{\circ}\text{C}$ . For this reason it was decided to zero the deformation when thermal equilibrium was reached. Another additional reason is that the measurements with the ADTM in the plastic stage were connected with a large scatter, probably due to some friction between the mould and the sample or to the fact that the weak cement paste could not sustain the measuring points (Figure 4.2). After setting, when the temperature of the sample had equilibrated, the autogenous deformations measured with the ADTM showed good repeatability. For a comparison, measurements of autogenous deformation performed with the dilatometer (Figure 3.8) showed good repeatability also in the plastic phase, where duplicate samples behaved almost identically.

The BFS cement paste, on the other hand, due to a lower development of heat of hydration, remained at almost constant temperature throughout the test, with a maximum difference of about  $\Delta T=1^{\circ}\text{C}$  for curing at  $40^{\circ}\text{C}$ . Moreover the BFS cement paste showed expansion from the moment of setting, confirming the measurements performed with the dilatometer on the same paste (Figure 3.8). Since no important deviation from thermal

equilibrium was registered in these cases, all the deformations measured on the BFS cement paste are shown in Figure 4.8.

For all cement pastes, a higher curing temperature accelerates the development of shrinkage, while the magnitude of the shrinkage after some days is similar for all curing temperatures. The BFS cement paste showed expansion at the beginning of the measurements, lasting for a couple of days at the lower temperatures. A possible cause is the crystallization pressure due to formation of ettringite, occurring before self-desiccation takes place. It is noticed that the shrinkage of BFS cement paste, even if occurring at a later time, was much higher than the one of Portland cement paste, as already observed for the measurements at room temperature (Chapter 3). This fact can be attributed to the finer pore structure of the BFS paste, which enhances self-desiccation and self-desiccation shrinkage. The shrinkage of the blended cement paste (Figure 4.9) was intermediate between the other pastes, following a minor initial expansion.

#### 4.4.3 Autogenous deformation as a function of heat of hydration

In Figure 4.10 the autogenous deformations of the three cement pastes cured at 20, 30, and 40°C have been plotted against the heat of hydration. In the figure, crosses indicate curing at 20°C, full dots curing at 30°C, and empty squares curing at 40°C. The deformations of the Portland cement paste are a function of the heat of hydration and seem to be almost independent of the curing temperature. As a consequence it should be possible to apply the maturity concept to the autogenous deformation of this paste. Indeed, Jensen & Hansen [1999] found that it was possible to apply a modified maturity transformation to autogenous deformation of Portland cement pastes with w/c ratio 0.30 and 20% silica fume addition.

In the case of the BFS cement paste, the initial expansion was different for each curing temperature, while the subsequent shrinkage followed the same pattern, especially evident for curing at 30 and 40°C. A possible explanation of this fact is that expansion occurs at the same time as self-desiccation shrinkage [Hammer 2002]; both phenomena depend on the curing temperature (see Chapter 2 and 5) but in a different way. In fact, the stresses caused by crystals growing in pores are temperature dependent [Scherer 1999]. Furthermore, it has been reported in literature [Chartschenko et al. 1996] that the magnitude of the expansion caused by expansive cements, used for example to compensate autogenous shrinkage, is very sensitive to the curing temperature. These expansive reactions are often based on formation of ettringite [Nagataki & Gomi 1998]. Superposition of shrinkage due to self-desiccation and expansion due to ettringite formation could explain why the expansion measured for the BFS cement paste (Figure 4.8) did not show a clear dependence on the curing temperature. An additional reason for the unsystematic expansion behavior might be that the outer expansion of the sample depends also on the stiffness of the paste and not only on the internal stresses.

Also the deformations of the blended cement paste do not fall on a master curve when plotted as a function of the heat of hydration. However, the value of the shrinkage at the hydration plateau was similar for the three curing temperatures. Also in this case,

this could be explained by shrinkage due to self-desiccation and expansion due to salts occurring simultaneously.

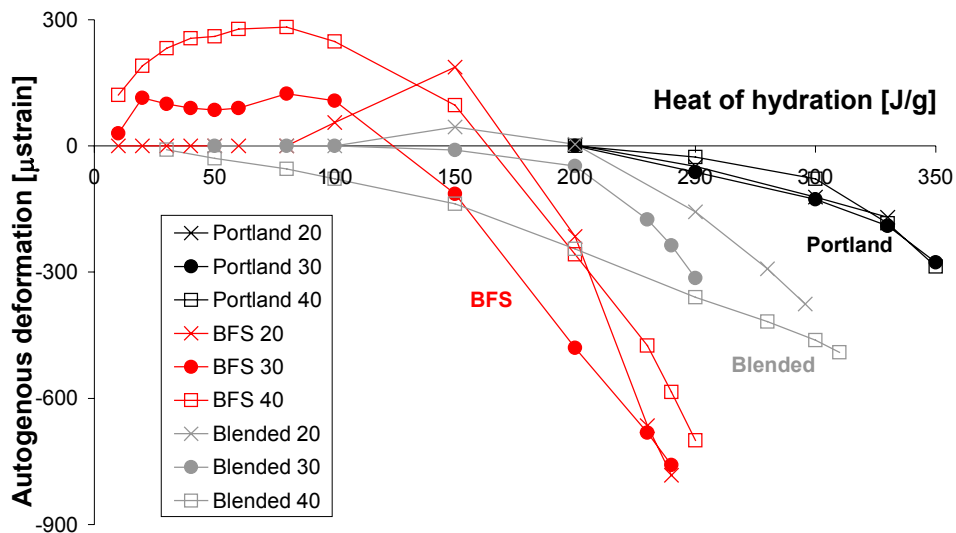


Figure 4.10 – Autogenous deformation vs. heat of hydration for three cement pastes

## 4.5 Conclusions

Measurements of autogenous deformations of cement pastes at different temperatures were performed. The most relevant conclusions of this study are:

- 1) The magnitude of the shrinkage after a few days hydration is not significantly influenced by the curing temperature. Higher curing temperatures accelerate the autogenous shrinkage but do not substantially modify its value in the first week of hydration.
- 2) Portland cement pastes show substantial shrinkage around setting at all curing temperatures. The shrinkage then shows a knee point after which the rate of deformation is strongly reduced.
- 3) Pastes containing BFS show expansion at all curing temperatures. The expansion is very variable from test to test. Intensive shrinkage follows, much higher than in Portland cement pastes.
- 4) Autogenous shrinkage can be normalized to isothermal heat of hydration, showing the dependence of the shrinkage on the degree of hydration. However, the early-age expansion does not show a clear dependence on the degree of hydration.

Results of this study show that the autogenous shrinkage after setting of a Portland cement paste with 5% silica-fume addition cured at different temperatures in the range 10-

40°C could be normalized to the heat of hydration. This could potentially allow prediction of shrinkage at different temperatures knowing the shrinkage at one temperature and the development of the hydration at the other temperatures. In the case of pastes containing BFS, on the other hand, initial expansion occurred and the total deformations measured were not only a function of the heat of hydration. A possible explanation of this fact is that both expansion and self-desiccation shrinkage occur simultaneously and both are a function of the temperature.



# Chapter Five

## Modeling of self-desiccation shrinkage

---

### 5.1 Introduction

In this chapter, measurement of early-age properties of cement pastes, presented in Chapter 3, are used as input data for the calculation of self-desiccation shrinkage of a Portland and of a BFS cement paste. The capillary tension approach is advantageous when compared to other modeling strategies (Chapter 2), since it has a sound mechanical and thermodynamical basis. Furthermore, it is possible to employ it in a numerical model when dealing with a continuously changing microstructure. Since a part of the RH drop in the cement paste is due to dissolved salts in the pore solution, a method is suggested to separate this effect from self-desiccation and to calculate the actual stress in the pore fluid associated with menisci formation.

### 5.2 Modeling of self-desiccation shrinkage

#### 5.2.1 Autogenous relative humidity change

The initial value of the internal RH of the cement pastes measured in Chapter 3 was about 98%. Similar values were found by other researchers [Jensen & Hansen 1996, Bentz et al. 2001]. The initial RH drop can be attributed to dissolved salts in the pore fluid. The  $RH_s$  [-] due to dissolved salts can be estimated with Raoult's law [Jensen 1993]:

$$RH_s = X_l \tag{6.1}$$

where  $X_l$  [mol water / mol pore fluid] is the molar fraction of water in the pore fluid.

Based on expressed pore fluid compositions and Raoult's law, the RH drop in a cement paste due to dissolved salts may amount to several percents. For example, for a composition of the pore fluid of a two-month old cement paste with w/c ratio 0.45 [Page & Vennesland 1983], a value of 96.7% RH is calculated. This 3.3% RH drop is mainly due

to the alkali and not to the  $\text{Ca}^{2+}$  ions, whose solubility is depressed by the presence of the former.

As a consequence of hydration, a solid skeleton forms in the cement paste. From the formation of the solid skeleton, the chemical shrinkage is only partly transformed into an external volume change. If the water supply is restricted, empty pores are created inside the paste and air-water menisci occur. The air bubbles in the cement paste are formed in the bigger pores (Figure 2.5), which for thermodynamic reasons empty first. Simultaneously, a drop of the RH occurs. The RH due to menisci formation in a circular cylindrical pore can be calculated according to Kelvin's equation:

$$RH_K = \exp\left(-\frac{2\gamma \cdot V_w \cdot \cos\theta}{r \cdot RT}\right) \quad (5.2)$$

where  $\gamma$  is the surface tension of the pore fluid, 0.073 N/m for pure water,  $V_w$  the molar volume of water,  $18.02 \cdot 10^{-6} \text{ m}^3/\text{mol}$ ,  $\theta$  [-] the contact angle between water and solids,  $r$  [m] the radius of the meniscus,  $R$  the ideal gas constant,  $8.314 \text{ J}/(\text{mol}\cdot\text{K})$ , and  $T$  [K] the absolute temperature, in this chapter 293.15 K.

Assuming perfect wetting, the contact angle between water and solids is zero and thus  $\cos\theta = 1$ . In any case, for small values of  $\theta$ ,  $\cos\theta \cong 1$ . With this assumption the radius of the largest capillary pore filled with water can be calculated by rearranging Eq. 5.2:

$$r = -\frac{2\gamma \cdot V_w}{\ln RH_K \cdot RT} \quad (5.3)$$

If we take into account both the RH related to menisci formation and to dissolution of salts, the total RH can be approximated according to the following formula [Jensen 1993a]:

$$RH = RH_s \cdot RH_K = X_l \cdot \exp\left(-\frac{2\gamma \cdot V_w}{r \cdot RT}\right) \quad (5.4)$$

Note that the presence of the dissolved salts influences the total RH also indirectly through  $RH_K$ , since dissolved salts lower the surface tension. As an example, for a pore fluid about 0.055 N/m was measured with a du Noüy tensiometer [Jensen 1993b]. The derivation of Eq. 5.4, as well as of Raoult's law (Eq. 5.1) and Kelvin's law (Eq. 5.2) is discussed in Appendix A.

## 5.2.2 Kelvin radius and tensile stress in the pore fluid

To calculate the radius of the largest capillary pore filled with water directly from the RH measurements, the influence of the dissolved salts has also to be considered by combining Eq. 5.3 and Eq. 5.4:



$$r = -\frac{2\gamma \cdot V_w}{\ln \frac{RH}{RH_s} \cdot RT} \quad (5.5)$$

When the Kelvin radius is known, the tensile stress in the pore fluid can be calculated with the Laplace law, for circular cylindrical pores (assuming perfect wetting):

$$\sigma_{cap} = -\frac{2\gamma}{r} \quad (5.6)$$

### 5.2.3 Deformation of the cement paste

The deformation of the cement paste is calculated according to the following equation [Bentz et al. 1998]:

$$\varepsilon_{LIN} = \frac{S \cdot \sigma_{cap}}{3} \cdot \left( \frac{1}{K_p} - \frac{1}{K_s} \right) \quad (5.7)$$

where  $S$  [m<sup>3</sup> water / m<sup>3</sup> pore] is the saturation fraction,  $\sigma_{cap}$  [MPa] the stress in the pore fluid,  $K_p$  [MPa] the bulk modulus of the whole porous body, in this case the cement paste, and  $K_s$  [MPa] the bulk modulus of the solid material.

This equation is strictly speaking only valid for a fully saturated linear elastic material. It is only approximate at partial saturation and creep is not taken into account.

The saturation fraction can be calculated as the ratio between the evaporable water content in the hardening paste,  $V_{ew}$  [m<sup>3</sup> water / m<sup>3</sup> paste], and the total pore volume of the paste,  $V_p$  [m<sup>3</sup> pore / m<sup>3</sup> paste], which are both functions of the w/c ratio and of the degree of hydration:

$$S = \frac{V_{ew}(\alpha)}{V_p(\alpha)} \quad (5.8)$$

## 5.3 Self-desiccation shrinkage of a Portland cement paste

In this section, self-desiccation shrinkage of a Portland cement paste (measurements shown in Chapter 3) will be modeled following the approach described above.

### 5.3.1 Separation of different contributions to the internal RH

Assuming that the RH drop measured in the first hours (Figure 3.7), about 2%, is due only to dissolved salts and, further, that this effect remains constant during hydration, it is possible to calculate the RH drop due to menisci formation for the cement paste studied. Measured and calculated RH values are shown in Figure 5.1.

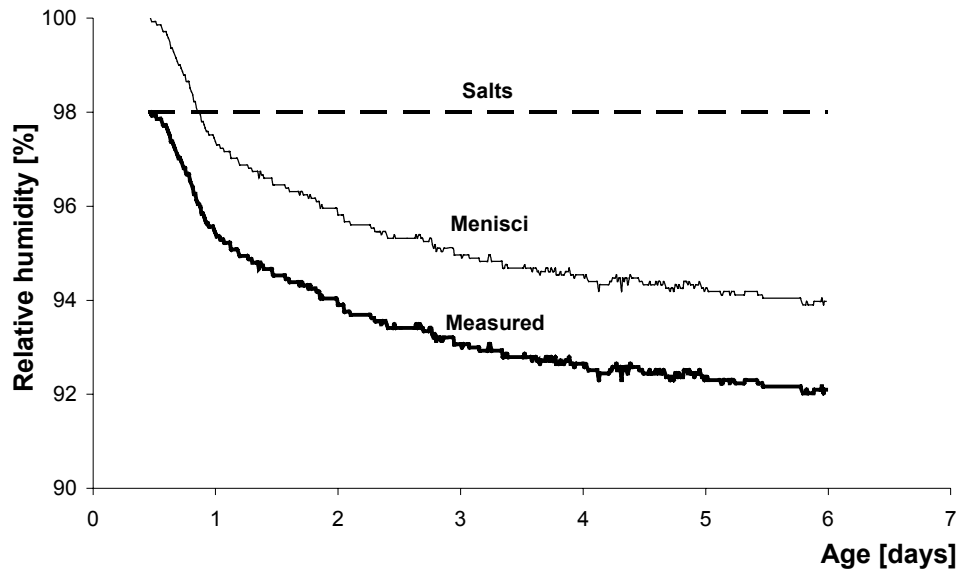


Figure 5.1 – Measured RH, RH due to salts dissolution in the pore fluid and RH due to menisci formation in a Portland cement paste during sealed hardening (Eq. 5.4)

### 5.3.2 Kelvin radius calculation

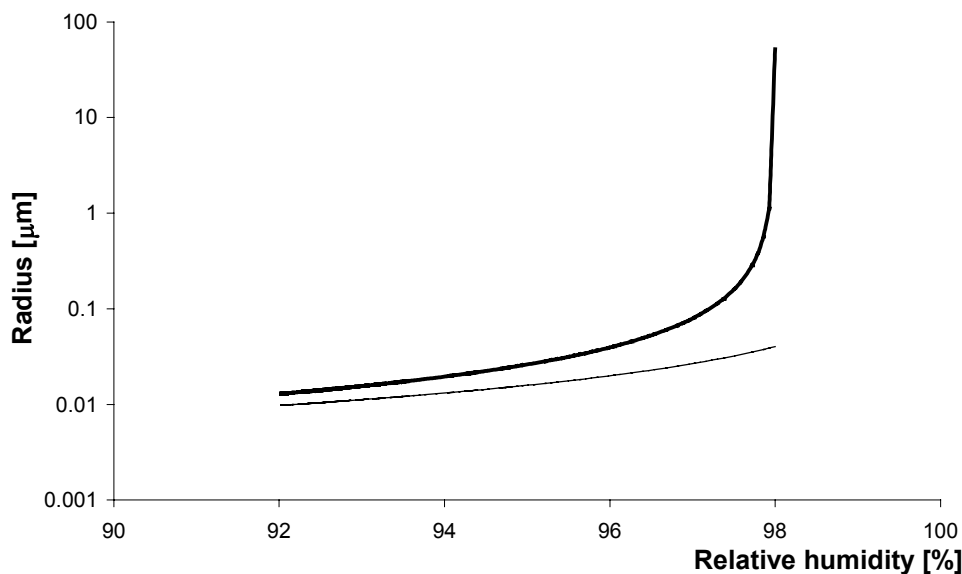


Figure 5.2 – Kelvin's radius calculated with (bold line) and without (thin line) correction for the influence of dissolved salts. The RH drop due to salts (2%) is assumed constant (Figure 5.1).

Once the RH drop due to self-desiccation is separated from the one due to salt dissolution, it is possible to calculate the Kelvin radius from the measured RH with Eq. 5.5. Results are shown in Figure 5.2. The thin line shows the Kelvin radius calculated with Eq. 5.3, assuming a surface tension of 0.065 N/m, as was measured on the pore fluid

(sec. 3.4.7). At 98% RH, Eq. 5.3 predicts that all the pores with a radius greater than 0.05  $\mu\text{m}$  are empty. This obviously cannot be true, since the cement paste, before setting, is still semi-fluid and saturated. On the other hand, according to Eq. 5.5 (bold line in Figure 5.2), at 98% RH all the pores are water-filled. As the RH drops, differences between the two curves presented in Figure 5.2 diminish.

### 5.3.3 Calculation of the degree of saturation

To calculate the degree of saturation, the development of the evaporable water content and of the total porosity of the paste during hydration must be known (Eq. 5.8). These quantities may be calculated with Powers' model [Powers & Brownyard 1948].

*Powers' volumetric model for Portland cement paste*

If we consider a Portland cement paste and apply Powers' model (Appendix B) to calculate the non-evaporable water and the total pore volume, Eq. 5.8 becomes:

$$S = \frac{V_{cw}(\alpha)}{V_p(\alpha)} = \frac{V_{cw}(\alpha) + V_{gw}(\alpha)}{V_{cw}(\alpha) + V_{gw}(\alpha) + V_{cs}(\alpha)} = \frac{p - 0.72 \cdot (1 - p) \cdot \alpha}{p - 0.52 \cdot (1 - p) \cdot \alpha} \quad (5.9)$$

where  $V_{cw}(\alpha)$  [ $\text{m}^3$  capillary water /  $\text{m}^3$  paste] is the capillary water,  $V_{gw}(\alpha)$  [ $\text{m}^3$  gel water /  $\text{m}^3$  paste] the gel water,  $V_{cs}(\alpha)$  [ $\text{m}^3$  chemical shrinkage /  $\text{m}^3$  paste] the chemical shrinkage, and the initial porosity  $p$  [-] is defined as:

$$p = \frac{w/c}{(w/c) + (\rho_w / \rho_c)} \quad (5.10)$$

where  $\rho_w$  [ $\text{kg}/\text{m}^3$ ] is the density of water,  $\rho_c$  [ $\text{kg}/\text{m}^3$ ] the density of the cement, and  $w/c$  [-] the water to cement ratio by weight.

The development of the degree of hydration,  $\alpha(t)$  [-], as a function of age can be estimated by isothermal calorimetry (Chapter 2), according to the following formula:

$$\alpha(t) = \frac{Q(t)}{Q_{pot}} \quad (5.11)$$

where  $Q(t)$  [ $\text{kJ}/\text{kg}$ ] is the heat of hydration developed at time  $t$  and  $Q_{pot}$  [ $\text{kJ}/\text{kg}$ ] is the potential heat of hydration, which is the heat developed by 1 kg of cement at complete hydration ( $\alpha = 1$ ).

The cement paste in this study is assumed to have a potential heat of hydration of 535  $\text{kJ}/\text{kg}$  [van Breugel 1991]. The heat of hydration of the Portland cement paste was measured by isothermal calorimetry (sec. 4.4.1). Figure 5.3 shows the development of the degree of hydration in the paste.

*Powers' volumetric model for silica-fume modified cement paste*

The Portland cement paste also contains 5.2% silica fume (sec. 3.2). Silica fume modifies substantially the properties of the paste, especially the RH change and the autogenous deformation [Jensen & Hansen 1996]. To consider the effect of silica fume, Powers' model modified for silica-fume addition was applied (Appendix B):

$$S = \frac{V_{cw}(\alpha) + V_{gw}(\alpha)}{V_{cw}(\alpha) + V_{gw}(\alpha) + V_{cs}(\alpha)} = \frac{p - 0.72 \cdot k \cdot (1 - p) \cdot \alpha}{p - k \cdot (0.52 - 0.69 \cdot (s/c)) \cdot (1 - p) \cdot \alpha} \quad (5.12)$$

where  $(s/c)$  [-] is the silica fume/cement ratio by weight, and  $p$  [-] and  $k$  [-] are two parameters defined as:

$$p = \frac{w/c}{(w/c) + (\rho_w / \rho_c) + (\rho_w / \rho_s) \cdot (s/c)} \quad (5.13)$$

$$k = \frac{1}{1 + 1.43 \cdot (s/c)} \quad (5.14)$$

where  $\rho_s$  [kg/m<sup>3</sup>] is the density of silica fume.

Figure 5.3 shows the development in time of the saturation fraction, calculated both using Powers' model (Eq. 5.9) and the model modified for silica fume (Eq. 5.12). It has to be noticed that the saturation fraction changes by the addition of 5% silica fume.

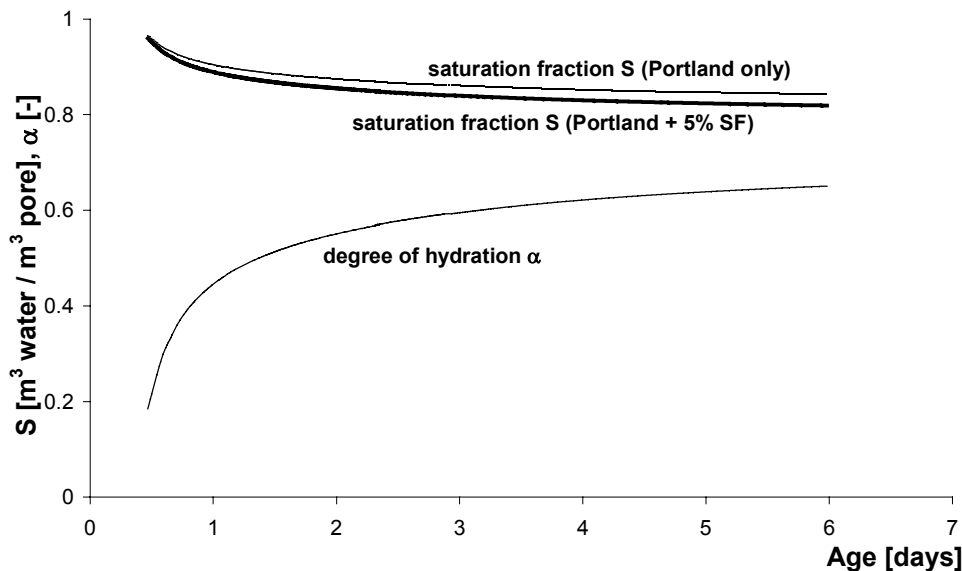


Figure 5.3 – Degree of hydration and saturation fraction of Portland cement paste during sealed hydration as a function of age

### 5.3.4 Stress in the pore solution and stress acting on the porous body

If the tensile stress in the pore solution is multiplied by the saturation fraction  $S$ , the magnitude of the bulk stress acting on the solid skeleton is obtained (Figure 5.4). The stress acting on the porous body is compressive. The absolute value of the bulk stress is lower than the capillary stress as the saturation fraction is always lower than unity. If the model including silica fume is used for the calculation (Eq. 5.12), the calculated internal stress is slightly lower.

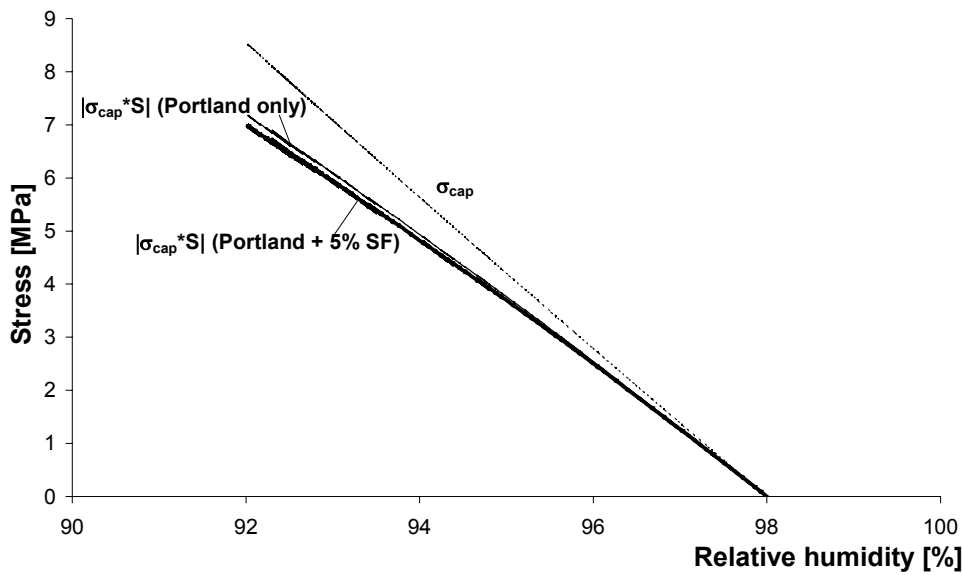


Figure 5.4 – Stresses in the pore fluid ( $\sigma_{cap}$ ) and absolute value of the bulk stress in the unit volume ( $|\sigma_{cap} \cdot S|$ ) as a function of the internal relative humidity

### 5.3.5 Bulk modulus of the cement paste and of the solid material

The bulk modulus  $K_P$  of the cement paste was calculated using the following formula:

$$K_P = \frac{E_P}{3 \cdot (1 - 2\nu_P)} \quad (5.14)$$

where  $E_P$  [MPa] is the elastic modulus and  $\nu_P$  [-] the Poisson's ratio.

The elastic modulus was measured on the Portland cement paste in the first week of hydration. Results are shown in Figure 3.9.

The bulk modulus of the solid material,  $K_S = 44$  GPa, and the Poisson's ratio,  $\nu_S = 0.2$ , were obtained from the literature [Nielsen 1991]. The effect of the choice of  $K_S$  on the calculated shrinkage (Eq. 5.7) is only minor: a variation of  $K_S$  from 40 to 50 GPa leads to a 6% variation in the calculated shrinkage.

### 5.3.6 Calculation of self-desiccation shrinkage

The self-desiccation shrinkage of the cement paste was calculated according to Eq. 5.7, where  $S$  was calculated either with Eq. 5.9 or Eq. 5.12,  $\sigma_{cap}$  with Eq. 5.6 and  $K_P$  and  $K_S$  as explained in section 5.3.5. In Figure 5.5 a flow chart of the whole calculation procedure is shown.

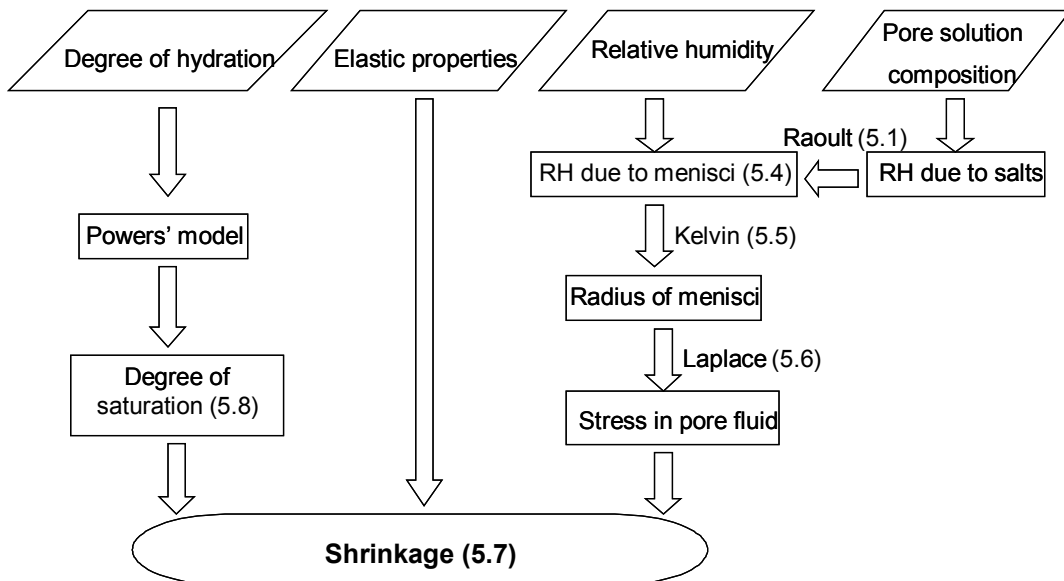


Figure 5.5 – Flow chart of self-desiccation shrinkage calculation

In Figure 5.6, the autogenous deformation is plotted against the internal RH. Only the part of the deformation occurring after the start of the RH drop is shown. The calculated values agree very well with the experimental ones down to a RH of 95%. Then the measured deformation increases while the calculated one remains almost constant, which is due both to the flattening out of the bulk stress in the cement paste (Figure 5.4) and to the increase of the elastic modulus (Figure 3.9). It must be noticed that Eq. 5.7 supposes an elastic behavior of the cement paste. In fact, in the first 24 hours the slope of the measured shrinkage decreases, corresponding to an increase of the elastic modulus of the cement paste. Afterwards, the RH drop slows (Figure 5.1) and the deformation per % RH increases. This fact could be due to the onset of the pozzolanic reaction of silica fume that consumes the calcium hydroxide crystals. Internal restraints in the paste (represented by CH crystals) are removed, inducing additional shrinkage [Jensen & Hansen 1996]. Another possible reason could be creep of the cement paste. Perhaps the effect of creep becomes evident at lower RH because in the second part of the curve the deformations occurred during a longer time span, as shown by the marks in Figure 5.6.

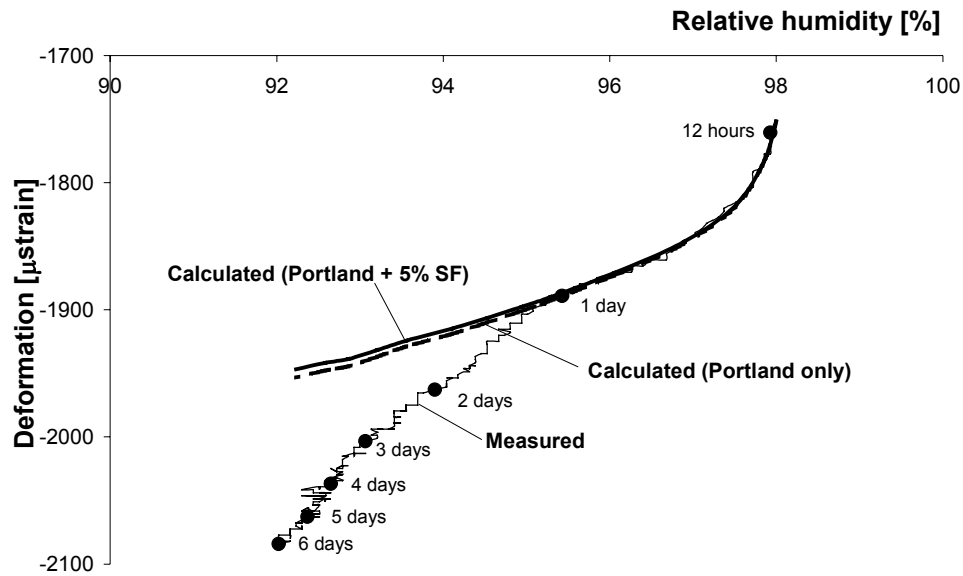


Figure 5.6 – Measured and calculated autogenous deformation of Portland cement paste vs. internal relative humidity

## 5.4 Self-desiccation shrinkage of a BFS cement paste

In this section, self-desiccation shrinkage of the BFS cement paste studied in Chapter 3 will be modeled. Some results relative to the Portland cement paste will be also shown for comparison.

### 5.4.1 Separation of different contributions to the internal RH

In the previous section, it was assumed that the internal RH due to salts remains constant during hydration of the Portland cement paste. This assumption was necessary because the pore solution of the Portland cement paste was analyzed only at 1 hour and 2 days after casting (Table 3.1). Since no data were available for later ages, the development of  $RH_s$  in the first week of hydration could not be calculated with Eq. 5.1.

In the case of the BFS cement paste, the pore solution was analyzed at 3 hours, 2 days and 6 days. This allowed calculating the RH due to salts (Eq. 5.1) in the first week of hydration. The values of  $RH_s$  corresponding to the composition of the pore solution are plotted in Figure 5.7. In the same figure also the results for the Portland cement paste, only during the first 2 days, are shown. The calculations indicate that in the Portland cement paste a major part of the RH depression in the first days is actually due to salts dissolved in the pore solution. On the contrary, most of the RH drop in the BFS cement paste seems to be due to self-desiccation.

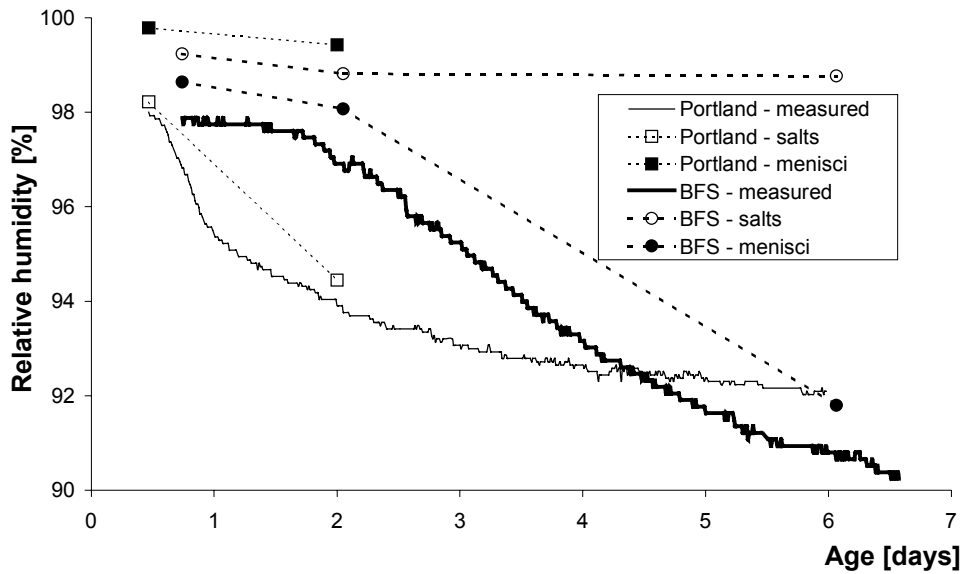


Figure 5.7 – Internal relative humidity as a function of age in Portland and BFS cement pastes

#### 5.4.2 Calculation of the degree of saturation

In Section 5.3,  $S$  was calculated for the Portland cement paste using Powers' model modified for silica fume addition (Appendix B). In theory, it would be possible to modify Powers' model to take into account the presence of BFS; this would require data about the non-evaporable water content and the gel water of the CSH gel formed in the BFS cement paste, and also about the chemical shrinkage produced by slag hydration. While these data were extensively studied for Portland cement pastes [Powers & Brownyard 1948, Geiker 1983], only scant data are available for BFS cement paste [Harrison et al. 1987, Song & Jennings 1999]. However, for the paste examined in this study, it is possible to calculate the saturation fraction  $S$  directly from the non-evaporable water content and the chemical shrinkage measurements (Chapter 3):

$$S = \frac{V_{ew}}{V_p} = \frac{V_{iw} - V_{new}}{V_{iw} - V_{new} + V_{cs}} \quad (5.15)$$

where  $V_{iw}$  [ $\text{m}^3$  water /  $\text{m}^3$  paste] is the initial water content,  $V_{new}$  [ $\text{m}^3$  non-evaporable water /  $\text{m}^3$  paste] the non-evaporable water content, and  $V_{cs}$  [ $\text{m}^3$  chemical shrinkage /  $\text{m}^3$  water] the volume of chemical shrinkage.

In Eq. 5.15 the initial air content of the paste is not considered. Moreover, to derive Eq. 5.15, it is assumed that the density of the evaporable water is equal to the density of bulk water. This is true only for capillary water, whereas the adsorbed layers of water may have higher density [Powers & Brownyard 1948, Wensink et al. 2000].

The degree of saturation of the two pastes is shown in Figure 5.8. For the Portland cement paste there is good agreement between Powers' model (Eq. 5.12) and Eq. 5.15.



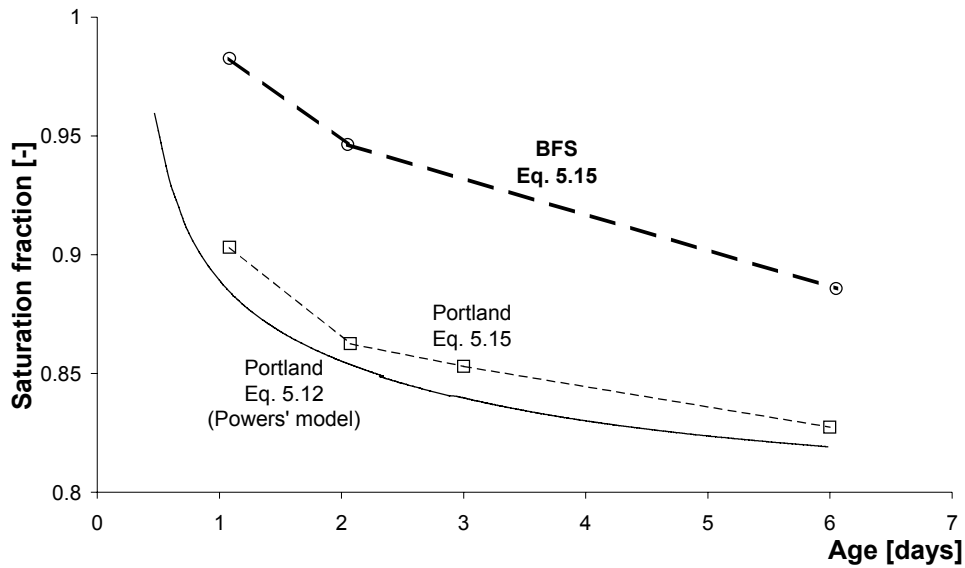


Figure 5.8 – Saturation fraction of BFS and Portland cement pastes as a function of age

### 5.4.3 Internal stress in the paste

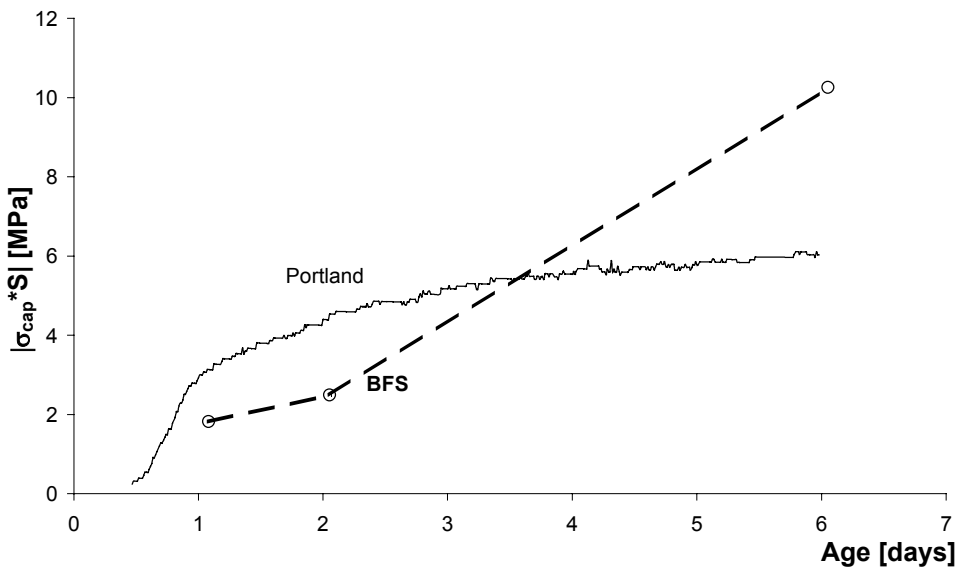


Figure 5.9 – Magnitude of bulk internal compressive stress acting on the solid skeleton as a function of age in Portland and BFS cement pastes

The tensile stress in the pore fluid, calculated with Eq. 5.6, was multiplied by the saturation fraction, obtaining the magnitude of the compressive bulk stress acting on the solid skeleton shown in Figure 5.9. The stress in the Portland cement paste does not increase after 3 days, whereas for the BFS paste a sudden increase of the stress after 2 days

is observed. This is in accordance with the measured deformations, which change from expansion to shrinkage from the second day on (Figure 3.8).

#### 5.4.4 Calculation of self-desiccation shrinkage

Figure 5.10 represents the self-desiccation shrinkage of the BFS cement paste, calculated according to Eq. 5.7, and the measured deformation, which was zeroed at 1 day. If the measured elastic modulus (Figure 3.9) is used in the calculation, the calculated deformations are substantially smaller than the measured ones. Possible explanations of this difference are:

- 1) Eq. 5.7 is valid only for elastic material. To take creep and plastic deformation of the cement paste into account, a reduction of the measured elastic modulus might be considered [Jensen 1993b]. In Figure 5.10 a curve obtained with Eq. 5.7, but considering an effective elastic modulus equal to 1/3 of the measured one, is shown. Measured and calculated shrinkage curves are in this case much closer.
- 2) The BFS cement paste expanded from setting until 2 days. It was assumed that this expansion was caused by ettringite formation (Chapter 3). Part of the following shrinkage may be due to conversion of ettringite into monosulphate (Chapter 2).
- 3) In the BFS paste, the Portland cement fraction, about 24% by weight, hydrates first, as discussed in sec. 4.4.1. Subsequently, pozzolanic reaction of slag and silica fume with calcium hydroxide and hydration of the slag take place. The consumption of the calcium hydroxide crystals may remove internal restraints in the paste, allowing further shrinkage to occur [Jensen & Hansen 1996].

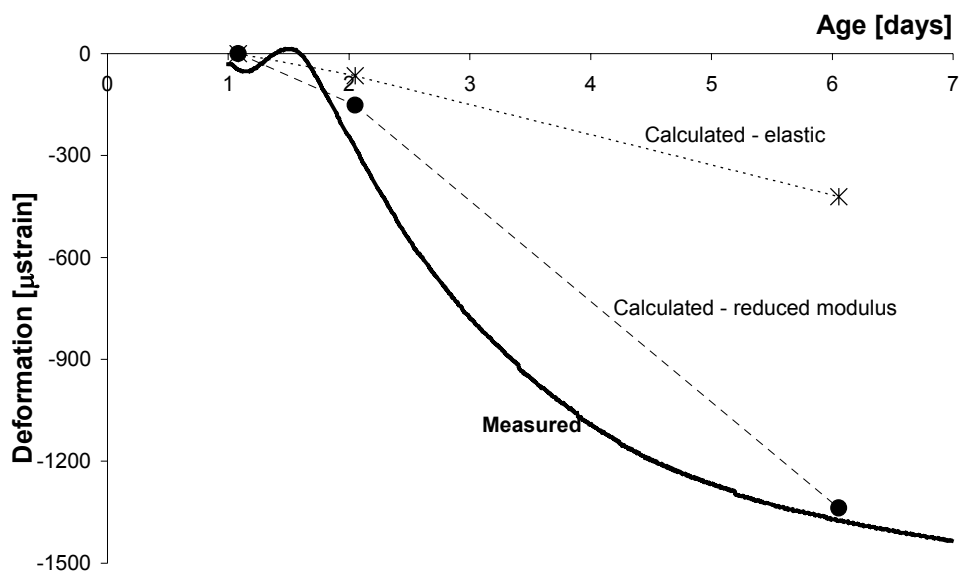


Figure 5.10 – Measured and calculated autogenous deformation of BFS cement paste

## **5.5 Conclusions**

Self-desiccation shrinkage of Portland and BFS cement pastes was modeled with the capillary tension approach. The calculations showed that in the Portland cement paste a major part of the RH depression in the first days was due to salts dissolved in the pore solution. In the case of the BFS cement paste, however, most of the RH drop seems to be due to self-desiccation. Since the chemical shrinkage of the BFS cement paste was smaller, the explanation of this fact may be found in the finer pore structure of the BFS cement paste.

Calculations of self-desiccation shrinkage based on the capillary tension approach could explain only part of the measured shrinkage of both cement pastes. In particular, for the BFS cement paste, the plastic deformations were largely predominant and should be taken into account in the calculation. It is suggested that additional shrinkage may have been caused by creep of the cement paste under internal stress, conversion of ettringite into monosulphate, and consumption of calcium hydroxide crystals.



**Part II**  
**Normal Weight Concrete**

---



# Chapter Six

## Measurements on NWC

---

### 6.1 Introduction

In Part I of this thesis, measurements of autogenous deformation of cement pastes at different curing temperatures and a model for calculating self-desiccation shrinkage have been presented. The main object of Part II, dedicated to Normal Weight Concrete (NWC), is to verify how autogenous deformation and other early-age properties of concrete relate to the properties of the corresponding cement pastes.

In this chapter, the effect of curing temperatures and cement type on autogenous deformation of HPC mixtures is presented and discussed. Four different curing temperatures (10, 20, 30, and 40°C) were imposed. The type of cement was varied: Portland cement, BFS cement, and a blend of the two. For every concrete mixture and curing temperature, the autogenous deformation and also the self-induced stress in the case of total restraint were measured.

### 6.2 Materials

Mixtures with w/c ratio 0.37 and 5% silica fume addition were studied (Table 6.1). The cement pastes in the concrete mixtures were identical to the ones studied in Chapter 4. Portland cement (CEM I 52.5 R) was used in mixture A, BFS cement (CEM III/B 42.5 LH HS) in mixture B, and a blend of the two in mixture C. The aggregate volume ratio of the mixes was 0.66. Data about the performance of mixture C cured at 20°C were obtained in a previous study [van Breugel & de Vries 1999]. For mixture C cured at 20°C, the elastic modulus was not measured.

Table 6.1 – Mixture compositions of concretes with w/c 0.37 and 5% silica fume

	Mix A	Mix B	Mix C
	[kg/m <sup>3</sup> ]	[kg/m <sup>3</sup> ]	[kg/m <sup>3</sup> ]
CEM I 52.5 R (Portland)	475.0	---	238.0
CEM III/B 42.5 LH HS (BFS)	---	475.0	237.0
Water (including water in admixtures)	175.8	175.8	175.8
Crushed aggregate (4-16 mm)	944.2	944.2	944.2
Quartz sand 0-4 mm	772.5	772.5	772.5
Lignosulphonate	0.9	0.9	0.9
Naphtalene sulphonate	8.1	7.1	7.6
Silica fume slurry (50% water)	50.0	50.0	50.0

## 6.3 Methods

### 6.3.1 Autogenous Deformation

Measurements of the autogenous deformation were performed with the ADTM (described in Chapter 4). In the case of measurements on concrete, the mold was 150 mm high, while for the cement pastes the height was 40 mm (sec. 4.3.2). The concrete mold used is also shown in Figure 2.14. Measurement of length changes between two steel bars embedded in the cement paste, 750 mm apart (Figure 4.2), started around setting, when the paste had sufficient strength to sustain the measuring point. However, to remove uncertainties and subjectivity in the choice of the ‘time zero’ for the deformations [Bjøntegaard 1999], the deformations were zeroed at the moment when a measurable stress was recorded on a companion specimen that was fully restrained in the axial direction. This ensured that only the stress-inducing deformations of the hardening concrete were taken into account. The restrained specimen is described in the following section [Lokhorst 1998].

### 6.3.2 Self-induced stresses

The Temperature-Stress Testing Machine (TSTM) is a horizontal steel frame (Figure 6.1) in which hardening concrete specimens can be loaded in compression and in tension under various hardening conditions. Both load-controlled and deformation-controlled experiments can be performed. The TSTM allowed measuring stress development due to restrained deformations but also creep and relaxation behavior in compression and in tension under prescribed thermal conditions. To obtain the prescribed thermal conditions, the specimen was cast in a temperature-controlled mold. To perform experiments in tension, a dovetailed interlock was used between the concrete specimen and the frame. Two steel claws held the dovetailed specimen. One of the claws was fixed to the frame and the other lay on roller bearings and could be moved with a hydraulic actuator. The claws could be pre-stressed to avoid slip of the specimen when the load changed from



compression to tension. Loads were measured with a load-cell (range of 100 kN in compression and in tension; resolution 0.049 kN). The specimen was cast in a mold integrated in the TSTM, which consisted of two parts:

- 1) An insulated temperature-controlled mold, similar to the ADTM mold described in sec. 4.3.2, for the middle section of the specimen.
- 2) The claws that surrounded the ends of the specimen. Attached to the claws was a formwork that formed a smooth, curved transition between the straight insulated mold and the slanting inner sides of the claws.

The TSTM was used in combination with the ADTM mold, with which the load-independent deformations during hardening were measured. The deformations were in general used to control the TSTM specimen: by allowing only a part of the free deformations to take place, different degrees of restraint could be obtained [Lokhorst 1998]. In this research only stresses obtained under total restraint were measured. In this case the deformations of the ADTM were not used to control the TSTM: it was sufficient to impose a constant length of the section, 750 mm long, on which the deformations were measured (Figure 6.1). Since the claws were made of steel, the thermal insulation of the outer ends of the TSTM was rather poor. Although the mold used for the middle part of the TSTM was similar to the ADTM mold, the temperature gradients in longitudinal direction of the ADTM and the TSTM specimen were not identical. To compensate the heat loss at the outer ends, copper pipes connected to a cryostat were cast in the concrete at the dovetails. With these adjustments the temperature gradients in the axial direction of the TSTM were accurately controlled. Maximum temperature differences of  $\Delta T = \pm 1^\circ\text{C}$  in similar positions in the TSTM and in the ADTM were measured.

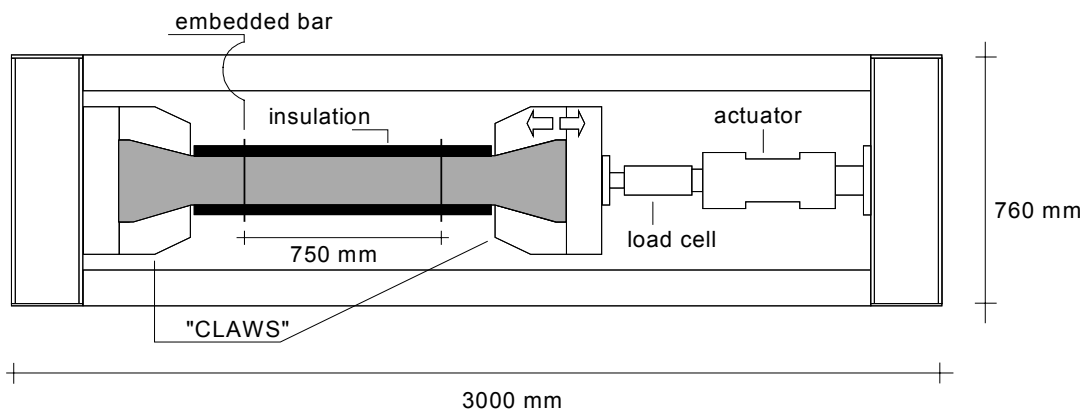


Figure 6.1 – Top view of experimental setup for the determination of stress development in hardening concrete (Temperature-Stress Testing Machine)

Experiments with the TSTM started immediately after casting. However, at that time it was not yet possible to measure the displacement of the fresh concrete with the cast-in steel bars. Therefore, two LVDT were used to control the displacement between the claws during the first hours. Around setting time, the displacement control was switched to the

four LVDT that measured the displacement between the cast-in bars. All experiments were performed in a deformation-controlled mode. With the Hydraulic Valve Controller (HVC) the deformation of the specimen was continuously adjusted. The voltage of the LVDT was used as a feedback signal in the closed loop servo control. During the first hours after casting the distance between the claws was kept constant. In this period hardly any stress development was measured. During the installation of the quartz glass measuring system the HVC was switched to load-control, keeping the load constant to avoid failure of the specimen as result of accidental touching of the LVDT. The installation took about 15 minutes. Then the HVC was switched back to deformation control. Depending on the type of experiment, the deformation control was set to static mode or dynamic mode. In a static experiment all deformations of the specimen were completely restrained. In a dynamic experiment the deformation of the specimen was adjusted with a function generator. Some hours before the stress in the specimen changed from compression to tension the specimen was tightened in the TSTM by pre-stressing the claws. During pre-stressing, the controller was in load-control mode, keeping the load constant. This procedure lasted approximately 5 minutes.

### **6.3.3 Compressive strength and elastic modulus**

Compressive strength and elastic modulus at different ages were measured on sealed specimens. Compressive strength was measured on concrete cubes,  $150 \times 150 \times 150 \text{ mm}^3$ . Elastic modulus in compression was tested on prisms,  $100 \times 100 \times 400 \text{ mm}^3$ . Cubes and prisms were cast in temperature-controlled steel molds and cured at 10, 20, 30, and 40°C. The specimens tested at later ages were removed from the molds after 6 days, sealed with plastic and aluminum foils and stored at constant temperature until testing.

## **6.4 Results**

### **6.4.1 Compressive strength and elastic modulus**

Results of compressive strength and elastic modulus are reported in Tables 6.2 and 6.3. The results represent the average value of 3 specimens. Mixture A, made with Portland cement, shows, as expected, both the fastest strength gain and the highest value at 28 days, followed by mixture C. The strength of mixture B develops slowly, especially at the lower temperatures. Similar trends are found for the elastic modulus.

Table 6.2 – Cube compressive strength of concretes with w/c = 0.37 cured at different temperatures

Mixture	Temperature	Cube compressive strength [MPa]						
		1 day	2 days	3 days	7 days	14 days	28 days	56 days
<b>Mix A (Portland)</b>	10°C	---	57.2	65.8	81.7	91.7	97.7	---
	20°C	53.2	65.1	---	85.9	94.0	99.5	---
	30°C	55.4	68.5	78.6	92.3	100.1	---	---
	40°C	66.5	74.2	86.6	92.5 <sup>1)</sup>	97.0	---	---
<b>Mixture B (BFS)</b>	10°C	---	5.2 <sup>2)</sup>	13.1 <sup>3)</sup>	34.5	51.8	58.9	---
	20°C	4.9	20.4	32.7	53.8	---	65.9	---
	30°C	23.6	44.6	50.6	59.6	64.8	---	---
	40°C	31.8	47.7	53.6	59.4 <sup>1)</sup>	---	---	69.7
<b>Mixture C (blended)</b>	10°C	---	31.1 <sup>2)</sup>	38.1 <sup>3)</sup>	57.4	72.2	82.8	---
	20°C	42.0	52.0	58.0	70.0	---	82.0	---
	30°C	40.7	54.5	63.9	---	84.8	---	---
	40°C	44.9	65.1	71.4	78.8 <sup>1)</sup>	79.2	---	---

<sup>1)</sup> Tested 8 days after casting<sup>2)</sup> Tested 1.5 days after casting<sup>3)</sup> Tested 2.5 days after casting

Table 6.3 – Elastic modulus of concretes with w/c = 0.37 cured at different temperatures

Mixture	Temperature	Elastic modulus [GPa]						
		1 day	2 days	3 days	7 days	14 days	28 days	56 days
<b>Mix A (Portland)</b>	10°C	---	30.1	32.2	---	34.5	35.5	---
	20°C	30.6	33.7	---	---	35.7	38.2	---
	30°C	31.4	33.0	33.9	---	37.4	---	---
	40°C	32.0	35.2	35.7	---	39.7	---	---
<b>Mixture B (BFS)</b>	10°C	---	6.7 <sup>1)</sup>	18.4 <sup>2)</sup>	---	29.3	33.5	---
	20°C	11.7	24.2	27.3	---	---	36.7	---
	30°C	27.4	32.3	32.6	---	35.5	---	---
	40°C	28.3	33.5	33.7	---	---	---	38.7
<b>Mixture C (blended)</b>	10°C	---	24.9 <sup>1)</sup>	26.5 <sup>2)</sup>	32.7	---	37.3	---
	30°C	27.8	32.2	32.2	---	39.5	---	---
	40°C	30.7	34.5	34.2	---	38.0	---	---

<sup>1)</sup> Tested 1.5 days after casting<sup>2)</sup> Tested 2.5 days after casting

#### 6.4.2 Autogenous deformation, self-induced stress, and relaxed stress

In Figures 6.3-6.8 the autogenous deformation and self-induced stress of mixtures A, B, and C are plotted. The autogenous deformation was zeroed at the moment when a stress was first recorded in the TSTM. Therefore, only the stress-inducing deformations are plotted. For mixtures A and C this means that only shrinkage is plotted, since only tensile stresses were measured in the TSTM. For mixture B, shrinkage was preceded by expansion, inducing a small compressive stress in the TSTM. The stress-inducing deformations were preceded by some hours when the concrete deformed without generating any stress in the TSTM. In this plastic phase, all the concrete mixtures

expanded shortly after the beginning of the measurements, with expansion up to 50  $\mu$ strain. For example, Figure 6.2 shows the complete record of the deformations in the first 2 days in the case of curing at 40°C.

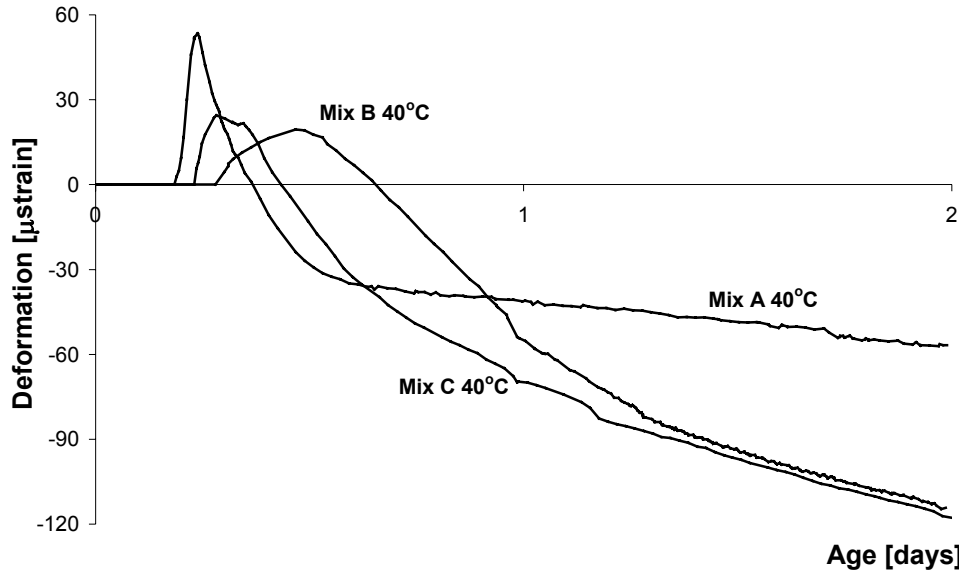


Figure 6.2 – Autogenous deformations of mixtures A, B, and C in the first 2 days, cured at 40°C. All the deformations measured in the Autogenous Deformation Testing Machine are shown

The self-induced stresses measured in the TSTM give an indication about the time when the deformations should be zeroed; besides, they can also be used to estimate the extent of stress relaxation in the hardening concrete. The self-induced elastic stress in a restrained specimen is proportional to the elastic modulus and to the restrained deformation. The difference between the calculated elastic stress and the stress measured in the TSTM can be attributed to relaxation. In Figures 6.4, 6.6, and 6.8 the self-induced stress measured in the TSTM (thick lines) is shown together with the calculated elastic stress (thin lines). The elastic stress,  $\sigma_{C,el}(t)$  [MPa], was calculated according to:

$$\sigma_{C,el}(t_i) = \sigma_{C,el}(t_{i-1}) + \Delta\sigma_{C,el} \quad (6.1)$$

where:

$$\Delta\sigma_{C,el} = \frac{E_C(t_i) + E_C(t_{i-1})}{2} \cdot (\varepsilon_C(t_i) - \varepsilon_C(t_{i-1})) \quad (6.2)$$

where  $E_C(t_i)$  [MPa] is the elastic modulus of concrete at time  $t_i$  and  $\varepsilon_C(t_i)$  [m/m] is the free deformation of the concrete at time  $t_i$ .

In Eq. 6.2 the elastic modulus in tension should be used in the case of shrinkage, which causes tensile stress in the restrained specimen. In the case of expansion, which

causes compression in the TSTM, the elastic modulus in compression should be used. However, according to Gutsch [1998], early age secant elastic moduli in compression and in tension do not differ very much. Therefore, in this research, the elastic modulus in compression measured on prisms (Table 6.3) was used in all cases.

The percentage of relaxed stress,  $R(t)$  [%], was calculated according to:

$$R(t) = \frac{\sigma_{C,el}(t) - \sigma_{TSTM}(t)}{\sigma_{C,el}(t)} \cdot 100\% \quad (6.3)$$

where  $\sigma_{TSTM}(t)$  [MPa] is the stress measured in the TSTM at time  $t$ .

The percentage of relaxed stress is plotted in Table 6.4 as a function of age for the different concrete mixtures and curing temperatures. The highest values were found for the BFS concrete. This fact confirms results obtained in Chapter 5 on BFS cement paste, where it was observed that a major part of the early-age deformation was due to creep and plastic deformations (Figure 5.10).

Table 6.4 – Percentage of relaxed stress of concrete mixtures cured at different temperatures

Mixture	Temperature	Percentage of relaxed stress [%]							
		12 hours	1 day	2 days	3 days	4 days	5 days	6 days	7 days
<b>Mix A (Portland)</b>	10°C	---	---	9	25	26	29	32	35
	20°C	---	13	27	32	35	35	---	---
	30°C	---	19	27	38	43	46	48	---
	40°C	24	29	---	---	---	---	---	---
<b>Mix B (BFS)</b>	10°C	---	---	---	65	59	60	59	59
	20°C	---	---	47	60	59	60	59	---
	30°C	---	37	47	---	---	---	---	---
	40°C	---	35	19	27	36	43	52	---
<b>Mix C (Blended)</b>	10°C	---	69	80	67	62	59	59	57
	30°C	---	---	11	22	---	---	---	---
	40°C	24	48	49	51	52	49	51	---

The results of mixture A, regarding stress-inducing deformations and stress development, are shown in Figure 6.3 and 6.4. The stress-inducing shrinkage developed rather unsystematically with temperature. For example, the specimen cured at 40°C showed a fast shrinkage in the first hours, but then it slowed down. After 1 day the total value was less than for 20°C curing. Shrinkage values after 6 days varied between 130 and 170  $\mu$ strain for the four curing temperatures. The self-induced stresses, however, developed faster at higher curing temperatures. The recording of the stresses at 40°C curing was stopped at about 30 hours after casting, due to technical problems. The other specimens showed maximum stresses between 1.5 and 2 MPa at 6 days. No specimen cracked in the testing period. The percentage of relaxed stresses grew from less than 20%

in the first hours of hydration up to 35-50% after a few days, depending also on the curing temperature (see Table 6.4).

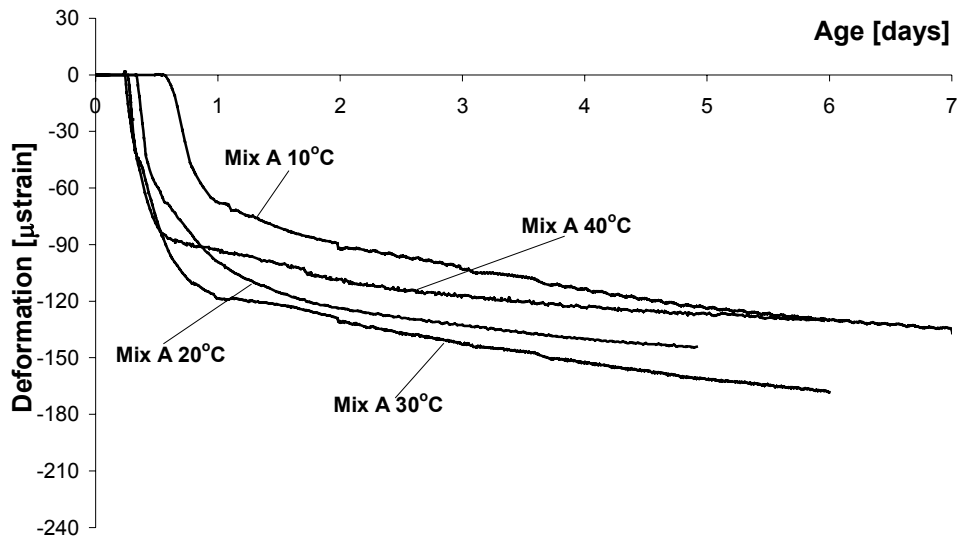


Figure 6.3 – Autogenous deformation of Mix A (Portland cement) cured at different temperatures

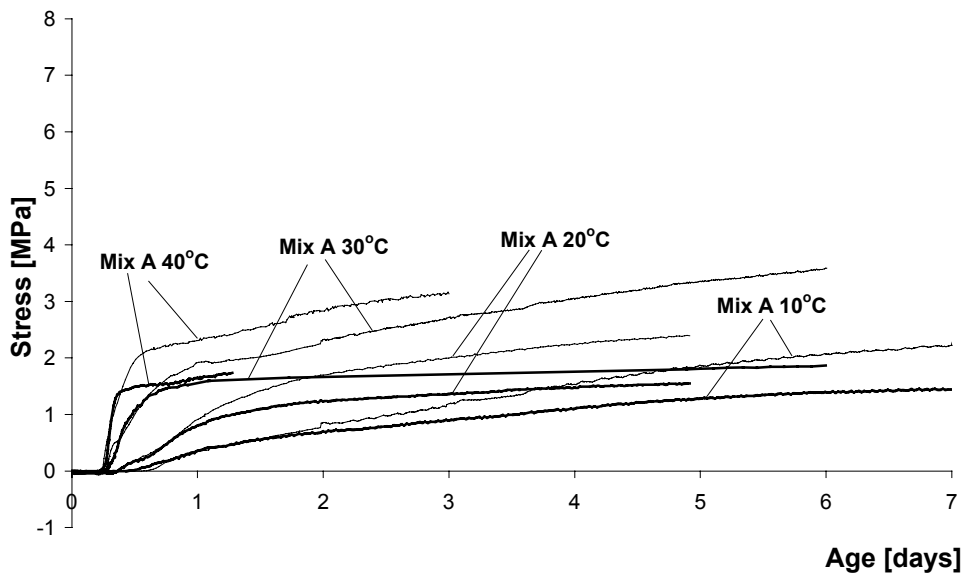


Figure 6.4 – Measured self-induced stress at full restraint (thick lines) and calculated elastic stress (thin lines) of Mix A (Portland cement) cured at different temperatures

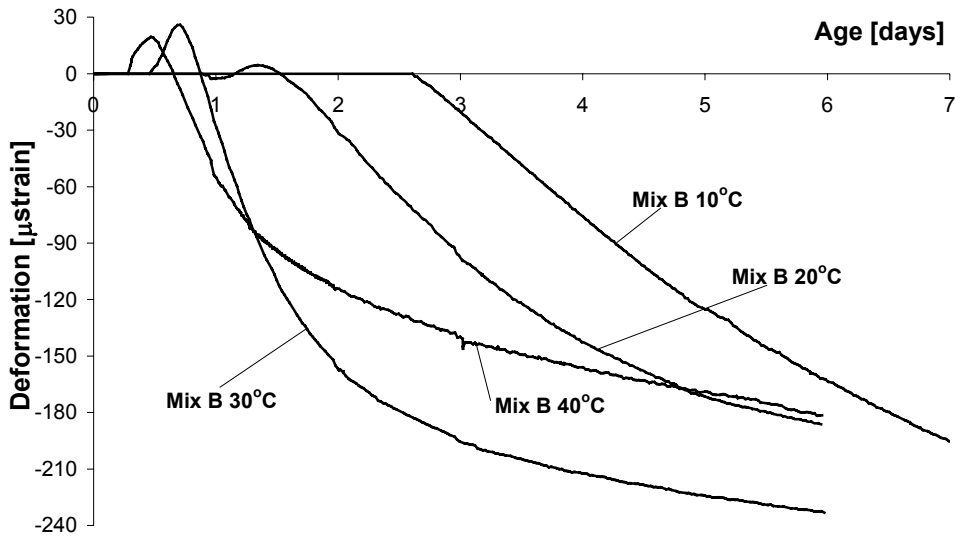


Figure 6.5 – Autogenous deformation of Mix B (BFS cement) cured at different temperatures

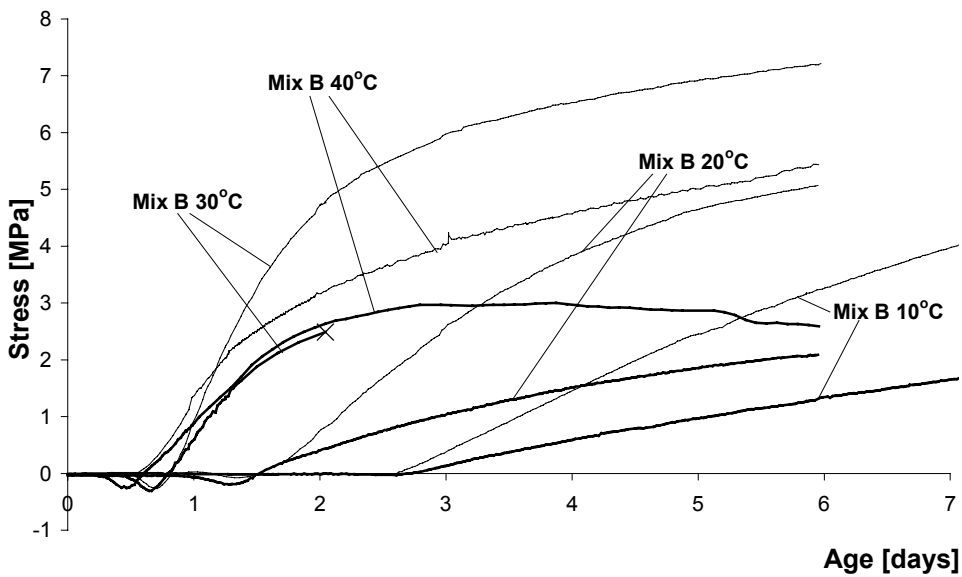


Figure 6.6 – Measured self-induced stress at full restraint (thick lines) and calculated elastic stress (thin lines) of Mix B (BFS cement) cured at different temperatures. A cross indicates failure of the specimen

Figures 6.5 and 6.6 show the results for mixture B, made with BFS cement. Also in this case, the influence of the curing temperature on the autogenous deformation is uncertain. The initial expansion of the specimens cured at 20, 30 and 40°C was stress inducing, with compressive stresses lower than 0.3 MPa. The following shrinkage occurred earlier for the specimen cured at 40°C, but 30 hours after casting the shrinkage of the specimen cured at 30°C became higher. Shrinkage of the specimen cured at 10°C developed slowly, but at

the end of the test it was about the same as in the case of 40°C curing. Shrinkage values after 6 days were about 170-180  $\mu$ strain for curing at 10, 20 or 40°C, and about 230  $\mu$ strain for curing at 30°C. These values are higher than those found for Portland cement mixtures (Figure 6.3). Also in this case the self-induced stress (Figure 6.6) provided a clearer picture, with higher stresses corresponding to higher curing temperatures. The specimen cured at 30°C cracked 2 days after casting, when the measured stress was about 2.5 MPa. The specimen cured at 40°C probably experienced microcracking around that age, evident by the decreasing slope of the stress curve, while the deformations were still increasing. The measured stresses were on average about 30% higher than the ones registered for the Portland cement mix. For the BFS mixture, differences between the calculated and the measured stress were greater than for the Portland cement concrete (Mix A). After a few days, the percentage of relaxed stress was on average 60% (Table 6.4).

Results of tests on mixture C, made with blended cement, are shown in Figures 6.7 and 6.8. Shrinkage was lowest for 10°C and highest for 40°C curing. The specimen cured at 20°C showed faster shrinkage development than the one cured at 30°C. It should be pointed out, however, that the data at 20°C curing had been obtained in a previous study [van Breugel & de Vries 1999] and the materials used might have been slightly different, for example due to variability between different cement batches. Shrinkage values after 6 days were 120  $\mu$ strain for 10°C curing, 140  $\mu$ strain for 30°C and 210  $\mu$ strain for 20 or 40°C. These values lie between the ones found for mixtures A and B.

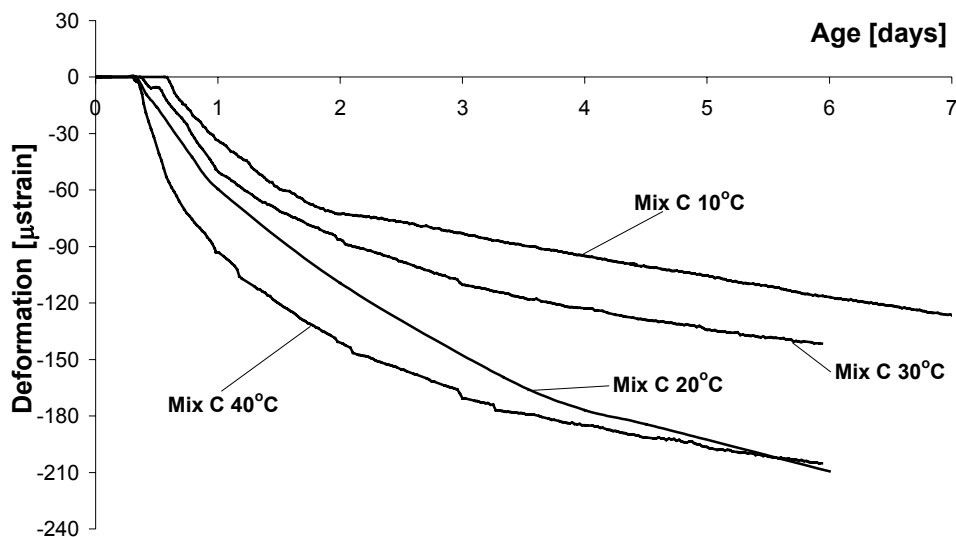


Figure 6.7 – Autogenous deformation of Mix C (blended cement) cured at different temperatures



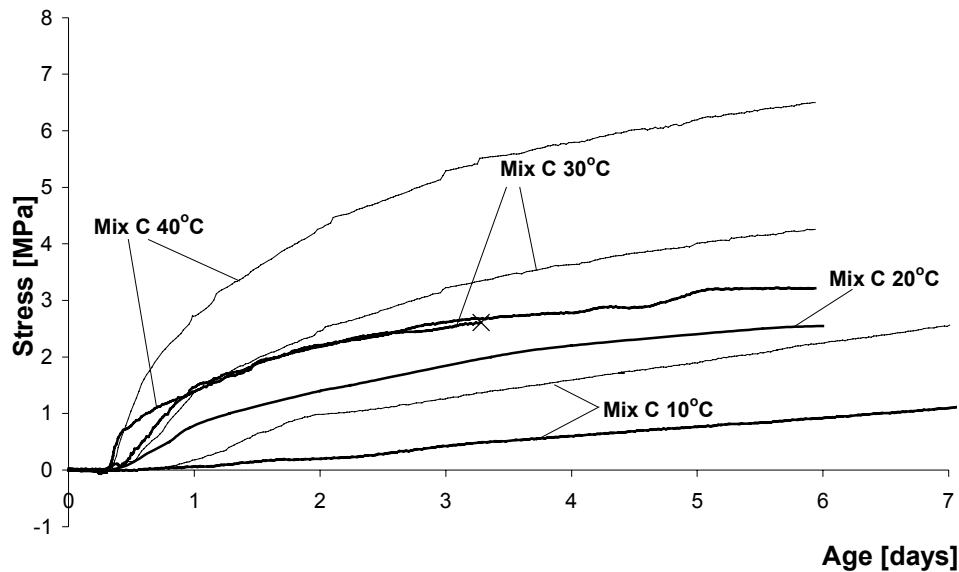


Figure 6.8 – Measured self-induced stress at full restraint (thick lines) and calculated elastic stress (thin lines) of Mix C (blended cement) cured at different temperatures. A cross indicates failure of the specimen

Self-induced stresses (Figure 6.8) were higher for curing at 40 and 30°C. The specimen cured at 30°C cracked 3 days after casting, at a tensile stress around 2.5 MPa. The specimen cured at 40°C did not crack in the testing period, reaching a stress higher than 3 MPa. The stresses of the specimen cured at 10°C were extremely low, below 1 MPa at 6 days. The measured stresses were in between the other two mixtures. It was not possible to calculate the elastic stress in the case of curing at 20°C, since the elastic modulus was not measured at this temperature. The percentage of relaxed stress was about 50%. For mixture C, creep tests in compression with constant load have also been performed [Lura et al. 2002b]. In that study, the relaxation behavior was calculated on the basis of the creep behavior. In the case of loading at 4 days, the percentage of relaxed stresses at 1 week from loading was 50%, confirming the findings presented in this chapter. For earlier loading, the percentage was even higher, more than 70%.

## 6.5 Discussion

### 6.5.1 Compressive strength and elastic modulus

Although higher temperatures improve the initial compressive strength development, the value at a later stage, 14 or 28 days, seems to be penalized, as already measured by other authors [Rakel 1965.]. For example, comparing specimens of mix A and C cured at 30 and 40°C, it can be noticed that specimens cured at higher temperatures show a lower strength at 14 days (Table 6.2).

The elastic modulus development shows a trend similar to the compressive strength but the stiffness increased faster than the strength, as had been already observed [Rostásy et al. 1993].

### 6.5.2 Early-age expansion

The phenomenon of the very early-age expansion is well known in the literature. A series of authors [Bentur et al. 1999, Bjøntegaard 1999, Tazawa et al. 1995] registered early-age expansion on a variety of concretes using different measuring devices, even if the absolute values of expansion differ quite substantially.

In Chapter 3 and 4, early-age expansion, observed in the BFS and in the blended cement paste, was attributed to ettringite formation. This opinion is shared by other authors [Tezuka et al. 1986].

In the literature, re-absorption of bleeding water was also indicated as cause of expansion (Chapter 2). In fact, removing the bleeding water reduces the expansion, but does not eliminate it totally [Bjøntegaard 1999]. The residual expansion could be due to internal bleeding in the mixture. In the present research, no external bleeding was observed, but the occurrence of internal bleeding cannot be excluded *a priori*. On the other hand, expansion of the BFS concrete (Figure 6.5) follows the same pattern as expansion of the BFS cement paste (Figure 3.8), for which no macroscopic bleeding was observed and no internal bleeding should have occurred.

A part of the initial expansion measured in the plastic phase might actually be an artifact due to the measuring method. The force exerted by the LVDT on the fresh concrete might pull apart the cast-in bars (Figure 4.2), causing a displacement of the LVDT that would be interpreted as expansion. Notice that this applies only to the expansion measured in the first hours, before setting (Figure 6.2). The expansion happening in the BFS mixture (Figure 6.5), however, occurred in a set concrete and was actually stress inducing: therefore it cannot be considered as an artifact caused by the measuring method.

### 6.5.3 Autogenous deformation

The effect of a temperature increase on the development of the autogenous deformation is unsystematic and varies for different sorts of cement. Higher curing temperatures accelerated the autogenous shrinkage but did not lead to higher deformations in the tested period. Other authors [Bjøntegaard 1999, Tazawa et al. 1995] obtained similar results. Differences in the shrinkage after 6 days could also be due to experimental scatter in the results. Two tests were run for each temperature, with a difference of about 8%. At all the tested temperatures, BFS cement concretes show higher shrinkage after 6 days than Portland concretes. This fact has already been reported [Hanehara et al. 1999, Zhang et al. 2000]. The phenomenon could be related to the supposed denser structure of the BFS cement paste, which shows smaller pores [Hanehara et al. 1999]. Smaller pores induce

higher capillary forces during the self-desiccation process (Chapter 5), increasing the autogenous shrinkage.

#### 6.5.4 Self-induced stresses and stress relaxation

Higher temperatures caused faster development of shrinkage and self-induced stress. It is noticed that the stress development was more systematic than the autogenous shrinkage, showing always higher stresses for higher curing temperatures. An explanation might be found in the fact that deformation measurements performed with the ADTM are much more difficult and delicate than stress measurements performed with the TSTM. Especially the choice of the zero point of the deformations constitutes a significant source of error. As an example, during a round-robin test performed by several laboratories on the same concrete mixture [Morabito et al. 2001], the measured self-induced stresses showed a much better reproducibility than the autogenous deformations.

The faster development of stresses and the higher stresses observed at high curing temperatures might be due to the fact that the rate of creep (and thus of stress relaxation) has an activation energy lower than the one of the hydration reaction itself. In fact, the development of the elastic modulus and the autogenous deformation are roughly proportional to the hydration process [Jensen & Hansen 1999]. This means that the elastic self-induced stress should have activation energy of 20-60 kJ/mol in the case of Portland cement. On the other hand, according to [Sellevold & Richards 1972], the activation energy of creep corresponds to the one of diffusion of water, about 17 kJ/mol.

These considerations are confirmed by the results shown in Table 6.4. In fact, only a small part (about 20-30%) of the elastic stresses was relaxed in the first days by the specimens cured at 30 or 40°C. On the other hand, tensile stresses in the specimens cured at 10 or 20°C reached their maximum at later ages, when relaxation had had sufficient time to take place.

## 6.6 Conclusions

The effect of a temperature increase on the development of the autogenous deformation in concrete was rather unsystematic and varied for different sorts of cement. Higher temperatures generally accelerated the deformations but did not lead to higher deformations in the tested period. On the other hand, higher temperatures caused faster development of self-induced stresses. This has been attributed to the fact that relaxation of the stress is influenced by temperature to a lesser extent than the build up of the stress.

Another experimental finding is that, at all temperatures, concrete containing BFS cement showed much higher shrinkage and higher self-induced stresses than Portland cement concrete. This occurred in spite of the fact that relaxation of the stresses was higher for BFS concrete, as already observed for BFS cement pastes in Chapter 5.



# Chapter Seven

## Modeling of shrinkage of NWC

---

### 7.1 Introduction

Shrinkage of the cement paste in hardening concrete is restrained by the stiff, non-shrinking aggregates. Measurements of concrete shrinkage presented in Chapter 6 are in fact the result of the interaction between a shrinking cement paste, whose mechanical properties change during hardening, and the inert inclusions. A challenge in the modeling of autogenous shrinkage is to calculate shrinkage of concrete based on shrinkage of the corresponding cement paste. If this would be accomplished, it would save experiments on concrete. In fact, the autogenous deformation of a number of concrete mixtures, varying in the aggregates' properties and in their volume ratios, could be predicted from the autogenous shrinkage of the corresponding cement paste. In the literature, different opinions about the feasibility of this approach are represented. According to Tazawa et al. [2000] autogenous shrinkage of concrete at 28 days could be calculated from autogenous deformation of cement paste with a simple composite model. On the other hand, Hammer et al. [2002b] excluded that shrinkage of a concrete mixture could be calculated from shrinkage of a cement paste using composite models.

In this chapter, autogenous shrinkage of NWC is calculated based on the autogenous shrinkage of cement paste. Models developed by Pickett [1956] and by Hobbs [1969] for drying shrinkage of concrete were applied to autogenous shrinkage. The calculated shrinkage was in fairly good agreement with the measurements. A number of further issues involved in autogenous shrinkage of concrete, such as micro-cracking, creep of cement paste, and presence of the interfacial transition zone (ITZ), are discussed.

### 7.2 Materials

Shrinkage of a cement paste made with Portland cement (CEM I 52.5 R), w/c ratio 0.37 and 5% silica fume addition, cured in sealed condition at 20°C, is shown in Figure 3.8.

Elastic modulus of the paste is shown in Figure 3.9. The autogenous deformation of the concrete made with the same paste, with aggregate volume ratio 0.66, is shown in Figure 6.3. The elastic modulus of the concrete as a function of age is reported in Table 6.3. These data constitute the input for the models that are presented in the next section.

## 7.3 Calculation of concrete shrinkage

### 7.3.1 General

In the following calculations, concrete is assumed to consist of two phases, namely aggregate particles dispersed in a cement paste matrix. If the shrinkage of the paste is greater than the one of the aggregates, the aggregates restrain the shrinkage of the paste. According to this approach, concrete shrinkage is a function of the paste shrinkage, the aggregate shrinkage, the stiffness of the paste and of the aggregate, and the aggregate volume concentration.

Some attempts [Pickett 1956, Hansen & Nielsen 1965, Hobbs 1969] have been made to obtain expressions for the dependence of the concrete shrinkage upon the aggregate volume concentration and the properties of the constituents. However, exact solutions for concrete shrinkage cannot be obtained because of the geometric complexity of concrete and the many interacting particles. In order to obtain a solution, simplifying assumptions have to be made and as a consequence the solutions are only approximate.

Analytical models for concrete shrinkage are discussed in [Hobbs 1973]. Basic assumptions common to the solutions are:

- 1) Concrete consists of two homogenous phases, aggregates and cement paste.
- 2) Aggregate and paste behave elastically.
- 3) Elastic properties are not influenced by shrinkage, i.e. microcracking of the paste, if it occurs, does not reduce the stiffness.
- 4) The total volume occupied by shrinkage cracks is independent of aggregate grading.

In the following, Pickett's model [Pickett 1956] and Hobbs' model [Hobbs 1969] will be discussed and applied to quantify autogenous shrinkage of concrete.

### 7.3.2 Pickett's model

Pickett [1956] derived an expression for the effects of aggregates on concrete shrinkage. The formula is derived by considering the restraining effect of one small spherical aggregate particle embedded in a large body of shrinking concrete. The concrete surrounding the aggregate particle is considered as a homogeneous material and both the particle and the concrete are assumed to be elastic. As further particles are added, the elastic properties and the shrinkage are recalculated, while the body is still considered to remain homogenous. Integration and a number of assumptions lead to the expression:

$$\varepsilon_C = \varepsilon_P \cdot (1 - \phi_A)^{\alpha_P} \quad (7.1)$$

where  $\varepsilon_C$  [m/m] is the shrinkage of concrete,  $\varepsilon_P$  [m/m] the shrinkage of the paste,  $\phi_A$  [m<sup>3</sup>/m<sup>3</sup>] the volume fraction of the aggregates and  $\alpha_P$  [-] is a parameter defined as:

$$\alpha_P = \frac{3 \cdot (1 - \nu_C)}{1 + \nu_C + 2 \cdot (1 - 2\nu_A) \cdot E_C / E_A} \quad (7.2)$$

where  $\nu_C$  and  $\nu_A$  [-] are the Poisson's ratio of the concrete and of the aggregates, respectively, and  $E_C$  and  $E_A$  [MPa] are the elastic moduli of the concrete and of the aggregates, respectively.

According to Eqs. 7.1 and 7.2,  $\varepsilon_C = \varepsilon_P$  only when the ratio  $E_C/E_A \rightarrow \infty$ , i.e.  $E_A \rightarrow 0$ .

The shrinkage of mixture A (Table 6.1) cured at 20°C was calculated from the shrinkage of the corresponding cement paste using Pickett's model. Inputs for the calculation were:

- 1)  $\varepsilon_P$  [m/m], equal to the shrinkage of the cement paste as a function of age, measured with the dilatometer (Figure 3.8).
- 2) The elastic modulus of the concrete as a function of age (Table 6.3) and the Poisson's ratio,  $\nu_C = 0.25$ , measured on mature concrete. Actually, according to de Schutter [1996],  $\nu_C$  has a minimum in the first hours after setting. The evolution in time of the Poisson ratio was not taken into account in the calculation.
- 3) The elastic modulus of the aggregates was varied between  $E_A = 50$  MPa and 70 MPa, corresponding to average values for quartz aggregates [van Mier 1997]. The Poisson's ratio was assumed as  $\nu_A = 0.25$ .
- 4) The volumetric content of the aggregates (Table 6.1) was equal to 66%.

### 7.3.3 Hobbs' model (C&CA model)

Hobbs' model, also called C&CA model [Hobbs 1969 & 1974], was developed for drying shrinkage, where the elastic modulus of the paste is constant. According to the model, the shrinkage of the concrete,  $\varepsilon_C$  [m/m], is equal to:

$$\varepsilon_C = \frac{\varepsilon_P \cdot (1 - \phi_A) \cdot (G_P + G_A) + 2 \cdot \varepsilon_A \cdot \phi_A \cdot G_A}{G_P + G_A + \phi_A \cdot (G_A - G_P)} \quad (7.3)$$

where  $\varepsilon_P$  [m/m] is the shrinkage of the cement paste,  $\varepsilon_A$  [m/m] the shrinkage of the aggregates,  $G_A$  [MPa] the shear modulus of the aggregates, and  $G_P$  [MPa] the shear modulus of the paste.

This model is more general than Pickett's, taking into account also the possible shrinkage of the aggregates upon drying. A further difference is that the elastic modulus of the paste, and not of the concrete, is used in the computation.

Tazawa et al. [2000] applied Eq. 7.3 to autogenous shrinkage of concrete at 28 days, finding a good agreement with the measurements.

The shrinkage of mixture A (Portland cement) at 20°C as a function of age was calculated from the shrinkage of the corresponding cement paste with Eq. 7.3. Values for the shrinkage of the cement paste, elastic properties and volumetric content of the aggregates were already indicated in sec. 7.3.2. In addition, the shrinkage of the aggregates was considered negligible and the shear modulus of the cement paste as a function of age was calculated from the elastic modulus (Figure 3.9), assuming Poisson's ratio  $\nu_p = 0.2$ .

## 7.4 Results

The ratio between shrinkage of concrete and shrinkage of paste as a function of age,  $\partial\epsilon_c/\partial\epsilon_p$  [-], calculated with the two models, is plotted in Figure 7.1.

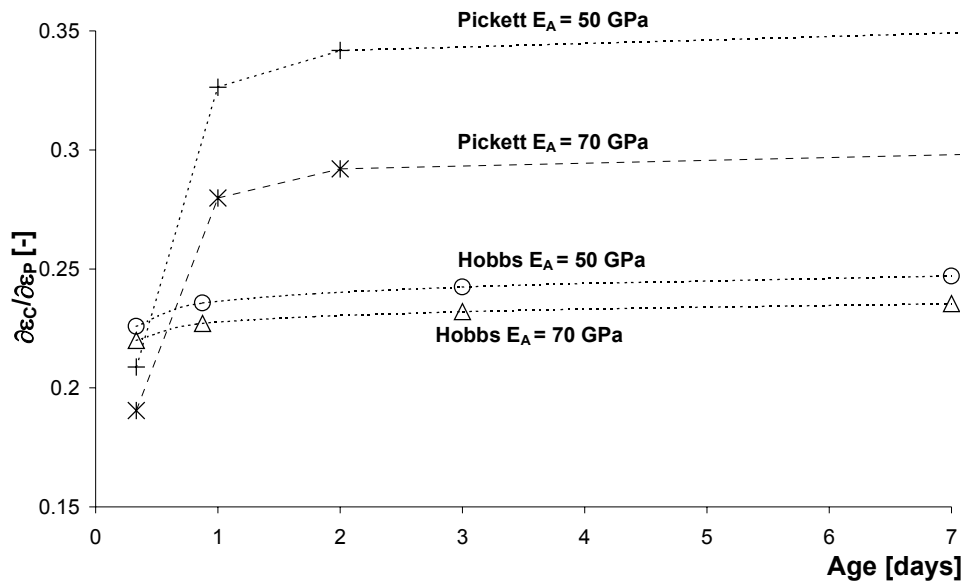


Figure 7.1 – Ratio between shrinkage of concrete and shrinkage of paste as a function of age calculated with Pickett's and with Hobbs' models

Since the ratio between the shrinkage of the concrete and the shrinkage of the cement paste varies in time, the shrinkage of the concrete at time  $t_i$  is calculated, for both models, with an incremental procedure:

$$\epsilon_C(t_i) = \epsilon_C(t_{i-1}) + \frac{\left(\frac{\partial\epsilon_C}{\partial\epsilon_P}\right)_{t_i} + \left(\frac{\partial\epsilon_C}{\partial\epsilon_P}\right)_{t_{i-1}}}{2} \cdot (\epsilon_P(t_i) - \epsilon_P(t_{i-1})) \quad (7.4)$$



where the ratio between the shrinkage of the concrete and the shrinkage of the pastes at different ages is derived from Figure 7.1.

Figure 7.2 shows the calculated shrinkage and the measured autogenous deformation of the concrete (Mix A).

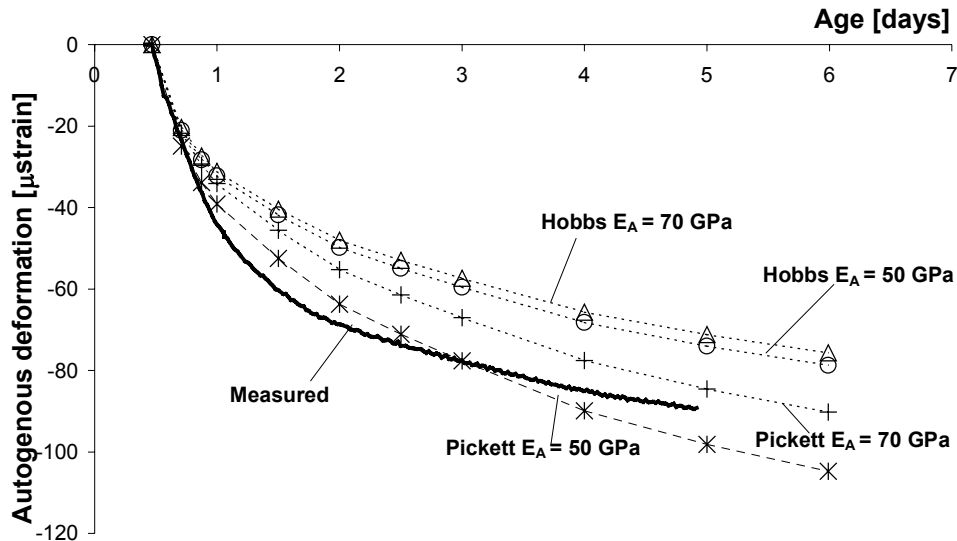


Figure 7.2 – Measured shrinkage of Mix A (Portland cement) at 20°C compared with the shrinkage calculated with Pickett's and with Hobbs' models

## 7.5 Discussion

### 7.5.1 Measured and calculated shrinkage

Figure 7.1 shows that the ratio between shrinkage of concrete and shrinkage of the paste in Pickett's model is very sensitive to the variation in the modulus of elasticity of the concrete, especially when the stiffness of the aggregates is low. On the contrary, Hobbs' model predicts ratios that are rather constant with age and independent of the elastic modulus of the paste; the ratios do not appear to be much influenced by the stiffness of the aggregates either, at least in the explored range. Moreover, Pickett's model provides much larger ratios at later ages.

As a result, the calculated shrinkage, shown in Figure 7.2, is larger for Pickett's model, and varies more with  $E_A$ . Both models seem to fit the experimental results in the first hours. After the first day, Hobbs' model predicts lower shrinkage, while Pickett's model overestimates the shrinkage at later ages. Moreover, while the measured autogenous shrinkage showed a distinct bilinear behavior, with a reduction of the deformation rate

after 1 day, the calculated shrinkage curves, especially with Pickett's model, did not show this feature.

The results indicate that both Pickett's and Hobbs' models may be used for an estimation of autogenous shrinkage of a concrete mixture when the deformation of the corresponding cement paste is known. While Hobbs' model yields in this case a worse prediction, a possible advantage is that no information on the concrete mix is needed for the calculation, while Pickett's model (Eqs. 7.1 & 7.2) requires knowledge of the elastic modulus of the concrete as a function of age. For both models, information about the elastic properties of the aggregates is needed, but Pickett's model is much more sensitive to their variability (Figure 7.1).

### 7.5.2 Microcracking and stress relaxation

The presence of aggregates restrains the deformation of the cement paste. According to the linear elastic solution [Goltermann 1994], the aggregates will be under hydrostatic compression and the paste in radial compression and in tangential tension at the interface. As a consequence of the low tensile strength of the cement paste, radial cracks in the paste around the aggregates may form [Goltermann 1994]. Opening microcracks result in a reduction of the global shrinkage of the concrete, and also of its stiffness.

In [Bisschop et al. 2001], the occurrence of autogenous shrinkage microcracking (crack width  $< 50 \mu\text{m}$ ) was investigated with optical microscopy on  $40 \times 40 \times 160 \text{ mm}^3$  prisms made of cement paste and 6-mm glass spheres. Three cement pastes were investigated (the same as those presented in Chapter 4) and among them the Portland cement paste studied in this Chapter. Previous research [Bisschop 2002] had shown that, in the case of drying shrinkage micro-cracking, a pattern of interconnected cracks formed and it was possible to impregnate it with epoxy from the outer surface of the specimen. In the case of autogenous shrinkage, no such cracks were detected after 1-week hydration. It was concluded that no micro-cracking occurred in the studied composites, nor in the concrete mixes realized with the same pastes. In fact, in [Bisschop 2002] it was observed that much less micro-cracking occurred in composites with graded aggregates than in composites with monosize aggregates.

If cracking does not occur, creep may relax the tensile stresses in the cement paste [Dela 2000]. Early-age creep and relaxation might be taken into account by assuming a reduced elastic modulus for the cement paste (Chapter 5). If we apply the models discussed in sec. 7.2, a lower stiffness of the cement paste would result in a lower concrete shrinkage.

### 7.5.3 Setting time and water adsorbed by the NWA

Cement pastes generally set at later ages than the corresponding concrete [Jensen 1997]. This fact is probably due to absorption of water-reducing agents, superplasticizers, and water on the surface of the finer sand fraction. Another contributing factor is the nucleation of hydration products (especially CH crystals) on the surfaces of the aggregates.

Using aggregates with different moisture conditions may influence shrinkage. Zhutovsky et al. [2001a] showed that autogenous shrinkage of concrete was substantially reduced when saturated-surface dry normal weight aggregates were used instead of dry aggregates.

Based on these considerations, it is not wholly justified to derive the shrinkage of the concrete only from the shrinkage of the corresponding plain cement paste, as pointed out also by Hammer et al. [2002b].

#### 7.5.4 Interfacial transition zone

The interfacial transition zone (ITZ), being porous and initially water-rich, should have different shrinkage from the bulk paste. Moreover, both ITZ and bulk cement paste should differ from the plain paste: the ITZ should be less dense and the bulk paste denser than the plain cement paste. Additionally, also the hydration process of concrete may be different from hydration of plain paste, since the water-rich interface may provide water to the bulk cement paste in the first hours of hydration [Koenders 1997].

To take into account the presence of the ITZ, it is possible to consider a 3-phase composite. This approach is already established for the calculation of the elastic properties of concrete [Nilsen & Monteiro 1993, Lutz & Zimmerman 1996, Ramesh et al. 1996, Yang 1998] and was also applied to autogenous shrinkage [Neubauer et al. 1996, Dela 2000]. The main drawback of this approach is that one needs to know the elastic (or viscoelastic) properties, the shrinkage, and the thickness of the ITZ. These properties are normally assumed or obtained by analytical calculations [Nadeau 2002] or by numerical simulation [Koenders 1997, Stroeven 1999]. An experimental approach to derive the properties of the interface is extremely difficult: micro-hardness measurements in bulk and interface cement paste [Acker 2001] might be an option to calculate the elastic properties and the thickness.

#### 7.5.5 Numerical concrete

An alternative to the analytical calculations discussed in sec. 7.2 is the so-called ‘numerical concrete’ [Roelfstra et al. 1985]. Inclusions with a regular shape are randomly distributed in a 3-dimensional volume following a predetermined particle-size distribution and volume ratio. The generated composite structures are then subdivided into finite elements (FE) to perform the intended numerical analysis. Realistic shaped aggregates are currently being introduced in such models [Garboczi 2002].

Sadouki & Wittmann [2000] studied autogenous shrinkage micro-cracking with the numerical concrete approach. Aggregates were considered linear-elastic, cement paste linear elastic up to the tensile strength, when cracking occurred. A diffuse, randomly oriented micro-crack pattern was found in the first days of hydration.

This approach might be also used to calculate the autogenous shrinkage of concrete. In order to obtain realistic predictions, early age creep of the cement paste should be incorporated into the model (sec. 7.4.2). On the other hand, due to the different orders of

magnitude involved, the explicit description of the ITZ in such FE models does not seem feasible.

## **7.6 Conclusions**

Autogenous shrinkage of NWC was calculated based on the shrinkage of the corresponding cement paste according to 2-phase models developed by Pickett [1956] and Hobbs [1969]. The magnitude of the calculated shrinkage was in fair agreement with the measurements.

Micro-cracking, which might reduce the measured concrete shrinkage, was excluded for the studied concrete based on experimental evidence [Bisshop et al. 2001]. On the other hand, creep of the cement paste, not considered in the models, might have reduced the concrete shrinkage through relaxation of the eigenstresses. The presence of the ITZ should also have influence on the measured shrinkage, but the difficult determination of its properties makes a calculation with a 3-phase material model unreliable.

**Part III**  
**Lightweight Aggregate**  
**Concrete**

---



# Chapter Eight

## LWAC with Liapor aggregates

---

### 8.1 Introduction

In Part I of this thesis, it was shown that a significant part of autogenous deformation, self-desiccation shrinkage, was related to the drop of the internal RH in the cement paste. Shrinkage of the cement paste was caused by tensile stress in the capillary water as a consequence of self-desiccation. In Part II, it was shown how concrete shrinkage results from shrinkage of the cement paste and internal restraint caused by the non-shrinking aggregates. Early-age shrinkage may be harmful for the concrete, causing micro and macro-cracks and potentially jeopardizing the durability. A solution to this problem, which tackles the phenomenon directly and fundamentally, is to avoid or limit self-desiccation by entraining additional water into the concrete in the form of saturated LWA [Philleo 1991]. When the cement paste self-desiccates due to hydration, a RH gradient is generated within the concrete and water migrates out of the LWA into the cement paste. Use of saturated LWA not only reduces the autogenous shrinkage [van Breugel & de Vries 1999], it may even induce early-age expansion [Takada et al. 1999].

The potentiality of water-entrainment by LWA to offset self-desiccation of low water/binder ratio concrete and turn early-age shrinkage into expansion has been known observed for 10 years [Hammer 1992]. However, some fundamental questions regarding the actual mechanisms of internal curing remain unanswered. The mechanisms of water transport from the LWA to the self-desiccating paste have received only scant attention [Weber & Reinhardt 1999] and no attempt was made to quantify how much of the water remains in the pores of the LWA when the internal RH of the concrete is high. The origin of early-age expansion of LWAC was mostly ignored and no attempt was made to relate it to volume changes of paste and aggregates during hardening. In one case the volume stability of the LWA in consequence of moisture loss was investigated [Schmidt-Döhl & Thienel 2000], but with inconclusive results. The quantity of entrained water necessary to avoid self-desiccation was recently studied [Bentz & Snyder 1999, Jensen & Hansen 2001a], but only for Portland cement paste: the influence of additional cementitious

materials, which are becoming increasingly common in modern concretes, was not taken into account. Also systematic studies are missing about the effect of the degree of saturation of the LWA and the dimension of the LWA on the early-age deformation of LWAC.

This chapter addresses the issues outlined above both with experiments and with calculations. Autogenous deformation of LWAC realized with pre-wetted expanded shale (Liapor) aggregates was measured. LWAC showed early-age expansion instead of shrinkage, which was measured on the corresponding NWC mix (Chapter 6). The expansion depended both on the degree of saturation of the LWA and on their dimension. To understand the internal curing process, properties of the LWA (Liapor 8) were investigated. Some issues relevant to the internal curing process, such as the amount of entrained water and the distribution of the water reservoirs in the mixture, are also discussed.

## 8.2 Properties of LWA

### 8.2.1 Density, porosity, and pore structure

According to the producer, the density of Liapor 8 varies between 1450 and 1550 kg/m<sup>3</sup>. With helium picnometry, long-term water absorption and mercury intrusion porosimetry (MIP), Zhang & Gjrv [1991] calculated densities and porosity of Liapor 8. Their results are summarized in Table 8.1.

Table 8.1 – Porosity and density of Liapor 8 [Zhang & Gjrv 1991]

Particle size	Liapor 8	
	4-8 mm	8-16 mm
Open porosity [%]	40.3	34.8
Closed porosity [%]	5.3	4.1
Total porosity [%]	45.6	38.9
Solid density [kg/m <sup>3</sup> ]	2520	2520
Particle density [kg/m <sup>3</sup> ]	1370	1540

In the MIP tests [Zhang & Gjrv 1991], the maximum intruded volume was 0.29 cm<sup>3</sup>/g for the 4-8 mm fraction and 0.215 cm<sup>3</sup>/g for the 8-16 mm fraction. For both fractions, most of the pore volume was intruded when the pressure corresponded to pore necks with diameter between 350 and 70 nm. Weber & Reinhardt [1999] report MIP results on the 4-8 mm fraction. According to their measurements, the peak diameter of the pore size distribution was found at 400 nm. Zhang & Gjrv [1991] observed the pore structure of the LWA with scanning electron microscopy (SEM), noticing a dense outer shell 0.1-0.3 mm thick and a more porous interior. Shapes of the pores were irregular, some spherical and isolated and others elongated and interconnected.



## 8.2.2 Absorption under water

Measurements of water absorption were performed on Liapor 8, fractions 4-8 mm and 8-16 mm. The LWA were first oven dried at 105°C for one night to determine the dry weight and then immersed in water at 20°C. The weight was measured every few days. Results are shown in Figure 8.1. The two fractions show different absorption behaviors. The coarser fraction absorbed about 17% by weight in the first day and then the weight remained almost unchanged. The finer fraction absorbed only slightly more water in the first day, but the absorption proceeded until 2 weeks after immersion, reaching a value of 25% by weight. The absorption after 6 hours was 80-85% of the 1-day value. In the finer fraction of the Liapor 8 aggregates more water can be absorbed. This is confirmed by the lower density of the finer fraction and by its higher porosity (Table 8.1). This fact might be beneficial if one wants to minimize the LWA content and maximize the water content of the mixture. On the other hand, it is unpractical to immerse the LWA in water for such a long time before concrete mixing. In another experiment, performed only on the 4-8 mm fraction, the LWA were vacuum-saturated with water and immersed for 2 hours. The absorption was in this case 26% by weight, very similar to the long-term absorption.

Zhang & Gjrv [1991] measured water absorption of Liapor 8 4-8 mm from 2 minutes to 14 days of immersion. 1-day and 14-day absorptions were lower than the values measured in this thesis (Figure 8.1). After 2 minutes the absorption was already 35% of the 1-day value, and 50% after 30 minutes.

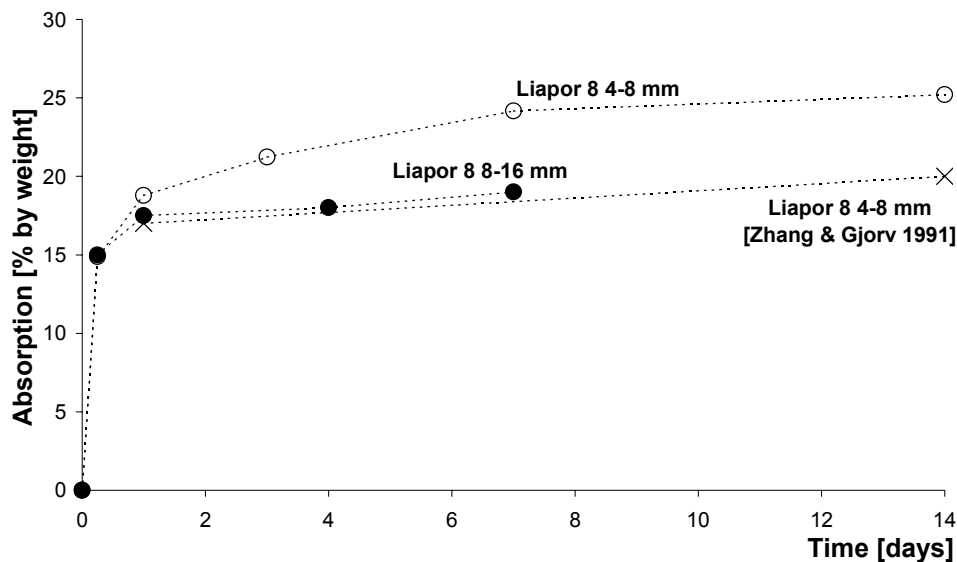


Figure 8.1 – Percent water absorption by weight of Liapor 8, 4-8 mm and 8-16 mm fractions, stored in water at 20°C

### 8.2.3 Desorption

The LWA, Liapor 8 4-8 mm, were first immersed in water for 6 hours and then exposed to decreasing RH levels in a desiccator until moisture equilibrium was reached. The desiccator was kept in a room at  $20\pm 1^\circ\text{C}$ . The different RH levels were obtained by storage above saturated salt solutions, with known equilibrium RH at  $20^\circ\text{C}$ . Three different saturated salt solutions were used:  $\text{KNO}_3$  (94.5% RH),  $\text{KCl}$  (85% RH), and  $\text{NaCl}$  (75.5% RH). The LWA followed a decreasing RH ramp, remaining about 2 weeks at every RH level. The RH in the desiccators took on average 3 days to stabilize. After the 2-week period, the LWA were weighed and moved to another desiccator. After the last step, they were dried in the oven at  $105^\circ\text{C}$  to determine the dry weight.

Results are shown in Figure 8.2. At 94.5% RH a great fraction of the water content, about 13% by weight, was lost. This amount of absorbed water is thus readily available for transport to the paste while it self desiccates, since it is weakly bound by capillary forces to the pores of the LWA. In fact the pores of the LWA are relatively big, having an average radius of  $0.05\text{-}0.2\ \mu\text{m}$  [Zhang & Gjrv 1991]. This pore neck size corresponds to an equilibrium RH of 98 to 99.5%, calculated with Kelvin's law (Eq. 5.2).

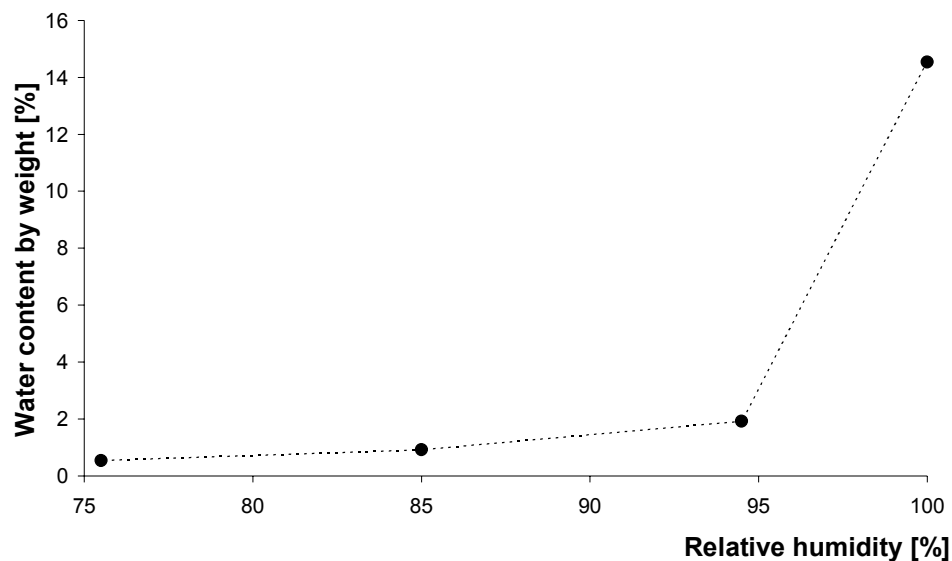


Figure 8.2 – Desorption of Liapor 8 4-8 mm at  $20\pm 1^\circ\text{C}$

### 8.2.4 Volume stability

The volume stability of Liapor 8, 8-16 mm fraction, was tested measuring the diameter changes of single grains subjected to drying. The Liapor grains were immersed in water for 6 hours and then exposed to 50% RH and  $20\pm 1^\circ\text{C}$  for several days. The weight change of 1 aggregate particle was measured. Additionally, LVDT measured continuously the length changes of 3 Liapor grains in the setup shown in Figure 8.3.

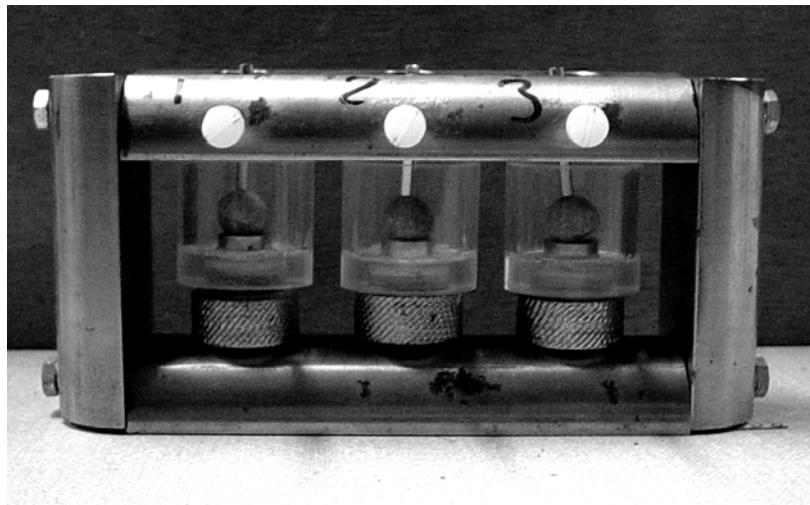


Figure 8.3 – Setup for measurements of length changes of LWA subjected to drying

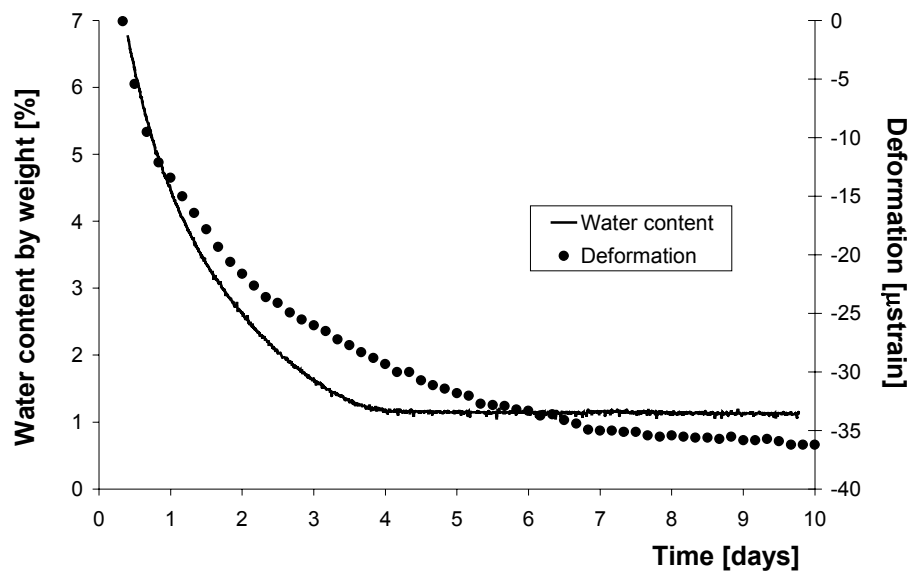


Figure 8.4 – Water content and shrinkage of wet LWA dried at  $20 \pm 1^\circ\text{C}$  and 50% RH

In Figure 8.4 the average result of 3 parallel tests is shown, together with the water content. Strain measurements were zeroed after about 8 hours. The LWA showed substantial shrinkage, about 35  $\mu\text{strain}$ . For the same LWA type, Schmidt-Döhl & Thienel [2000], using a technique based on microscopy observations, observed no clear trend of shrinkage and even some unexplained swelling, in the case of drying from saturated conditions first to 65% and then to 44% RH. The shrinkage shown in Figure 8.4 was measured in the case of almost complete drying of the LWA, down to 50% RH. In the case of a LWAC at early ages, the internal RH in the concrete is expected to remain high, above 95% [Bentz et al. 2002]. From the desorption isotherm shown in Figure 8.2, the

water content by weight of the LWA at 95% RH is about 2%; according to Figure 8.4, this would correspond to a shrinkage of 30  $\mu$ strain, which might be significant for the early-age deformations of the LWAC mixture.

## 8.3 Experiments on LWAC

### 8.3.1 Materials

#### *General*

Mixtures with w/c ratio 0.37 and 5% silica fume addition were studied. The mixtures were identical to Mixture C discussed in Chapter 7 (Table 7.1), except for the LWA. A blend of Portland cement (CEM I 52.5 R) and BFS cement (CEM III/B 42.5 LH HS) was used. Aggregate volume ratio of the mixes was 0.66. The coarse aggregate fraction of the NWC mix, with a volume ratio of about 0.36, was substituted with LWA.

#### *Different degrees of saturation*

Table 8.2 shows the three mixtures with different degrees of saturation of the LWA.

**Table 8.2 – Mixture compositions of LWAC with different degrees of saturation of the LWA**

Saturation of the LWA	LWAC with Liapor 9.5		
	100% (97.7%)	60% (69.3%)	20% (31.2%)
w/b ratio (without entrained water)	0.35	0.35	0.35
w/b ratio (with entrained water)	0.49	0.45	0.40
	[kg/m <sup>3</sup> ]	[kg/m <sup>3</sup> ]	[kg/m <sup>3</sup> ]
CEM I 52.5 R (Portland)	238.0	238.0	238.0
CEM III/B 42.5 LH HS (BFS)	237.0	237.0	237.0
Water (including water in admixtures)	175.8	175.8	175.8
Liapor 9.5, 4-8 mm	538.4	538.4	538.4
Quartz sand, 0-4 mm	772.5	772.5	772.5
Lignosulphonate	0.9	0.9	0.9
Naphtalene sulphonate	7.1	7.1	7.1
Silica fume slurry (50% water)	50.0	50.0	50.0
Water in the LWA	71.0	50.4	22.7

The LWA were Liapor 9.5, 4-8 mm fraction. The grain density of the LWA was approximately 1650 kg/m<sup>3</sup>. Three different target degrees of saturation of the LWA were employed: 100, 60, and 20%. The absorption capacity of the aggregates was assumed as the weight of water absorbed after 24 hours under water at 20°C. This is only a convention, since the LWA were probably not saturated at that time, as discussed in sec. 8.2.2. Moreover, storage of the LWA for 1 day under water before concrete mixing is

an established practice in concrete technology. For Liapor 9.5, 4-8 mm fraction, the 1-day absorption was 13.5% by weight of dry LWA.

The required degree of saturation was obtained by spraying the LWA with the corresponding fraction of the 1-day absorption. To check how much of the sprayed water was actually absorbed by the LWA, wet weight and dry weight (after 24 h in the oven at 105°C) were measured on 3-kg samples taken from the aggregates just prior to mixing. The actual degree of saturation is indicated in Table 8.2 between brackets. It is noticed that the degree of saturation resulted in two cases higher than the target one. This may be due to the variability in the moisture content of different batches of the LWA, which is influenced by the storage conditions.

#### *Different particle sizes of the LWA*

In this case the LWA was Liapor 8 in two of the mixes and Liapor sand in the third mix. The grain density of the LWA was 1400-1500 kg/m<sup>3</sup> for Liapor 8 and 1100 kg/m<sup>3</sup> for Liapor sand. Details about the composition of the mixtures are reported in Table 8.3.

The water absorbed by the aggregates was the quantity required to saturate the type of aggregate with the lowest absorption capacity, Liapor 8 8-16 mm. This quantity corresponded to about 15% by weight of dry aggregates. In fact the weight of the LWA was different in the three mixes, due to the different densities; thus the quantity of absorbed water also differed. The difference was quite relevant in the case of Liapor sand (51 kg/m<sup>3</sup>) while the other two mixes were almost equivalent in this respect (72 and 77 kg/m<sup>3</sup>).

**Table 8.3 – Mixture compositions of LWAC with different particle size of the LWA**

Type of Liapor	LWAC with Liapor 8 and Liapor sand		
	Sand 0-4 mm	8 4-8mm	8 8-16 mm
w/b ratio (without entrained water)	0.35	0.35	0.35
w/b ratio (with entrained water)	0.45	0.50	0.51
	[kg/m <sup>3</sup> ]	[kg/m <sup>3</sup> ]	[kg/m <sup>3</sup> ]
CEM I 52.5 R (Portland)	238.0	238.0	238.0
CEM III/B 42.5 LH HS (BFS)	237.0	237.0	237.0
Water (including water in admixtures)	175.8	175.8	175.8
Lightweight aggregate (Liapor)	334.2	473.9	509.1
Quartz sand, 0-4 mm	772.5	772.5	772.5
Lignosulphonate	0.9	0.9	0.9
Naphtalene sulphonate	7.1	7.1	7.1
Silica fume slurry (50% water)	50.0	50.0	50.0
Water in the LWA	50.8	72.0	77.4

### **8.3.2 Methods**

The methods used for measuring autogenous deformation, self-induced stress, cube compressive strength, and elastic modulus are described in sec. 6.3.

### 8.3.3 Results

#### *Compressive strength*

Figure 8.5 shows the cube compressive strength of the LWAC with variable degree of saturation. The compressive strength of the corresponding NWC (see Mix C in Table 6.2) is also reported. All mixtures reached strengths between 75 and 85 MPa at 28 days. The mixture with 69.3% saturated aggregates shows the highest strength at all ages, even higher than the NWC. The mixture with 31.2% saturated LWA shows an early development of strength close to the mix with 69.3% saturation, but the strength at 28 days is the lowest. The mix with saturated aggregates had the lowest strength at early ages, but the 28-days value was close to the NWC.

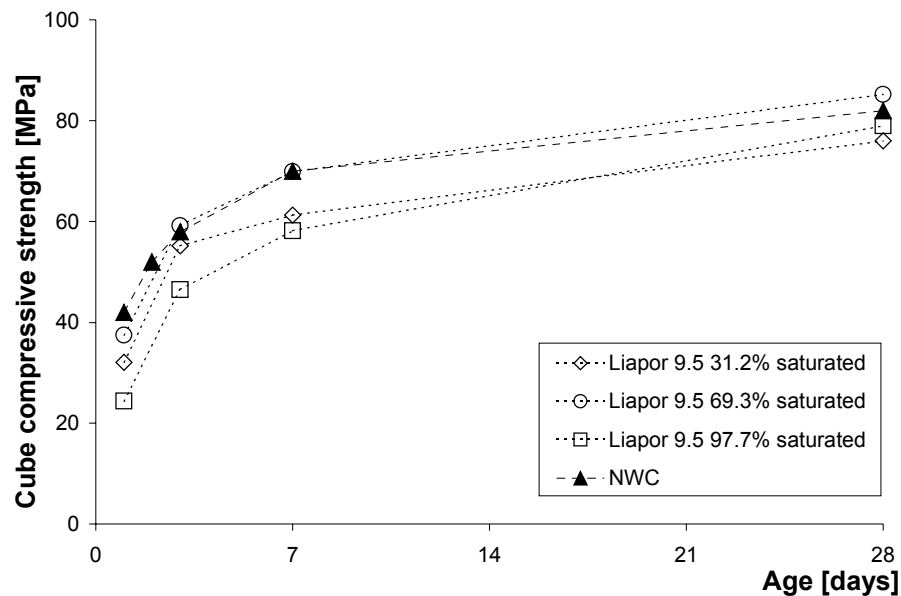


Figure 8.5 – Cube compressive strength of LWAC with different degrees of saturation of the LWA compared with the corresponding NWC

In Figure 8.6 the compressive strength of mixtures with LWA of different dimensions (Liapor 8 and Liapor sand) is presented. The strength at 28 days of the mixtures with Liapor 8 was considerably higher than the strength of the mixture with Liapor sand, 80 MPa versus 65 MPa. The three mixes, which were meant to be equivalent in every respect except for the particle size of the LWA, were in fact not totally comparable with each other. On the other hand, the two mixes with Liapor 8 4-8 mm and 8-16 mm show rather similar strength both at 3 and 28 days and can be considered almost equal as far as strength is concerned. LWAC realized with Liapor 8 reached 28-days strength similar to NWC with the same matrix.

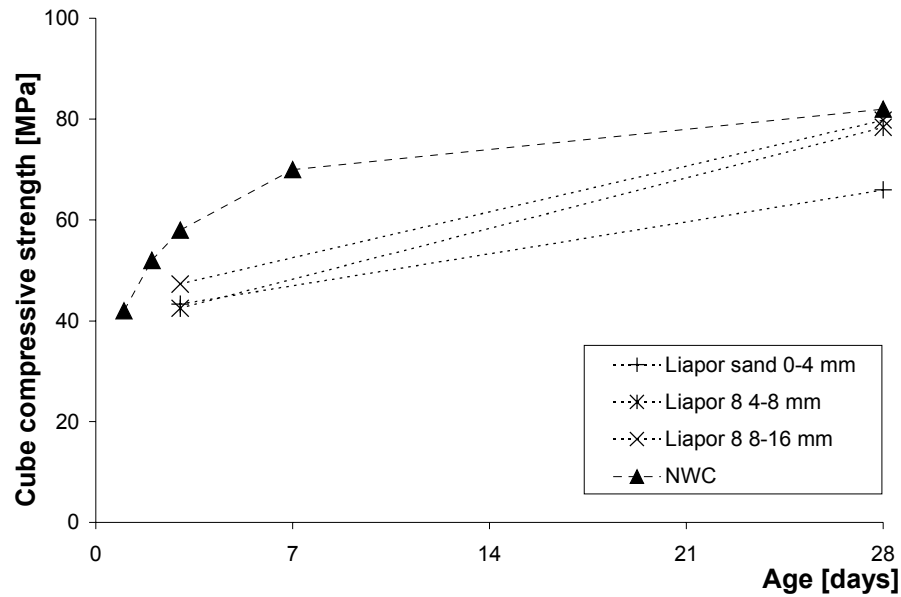


Figure 8.6 – Cube compressive strength of LWAC with different particle size of the LWA compared with the corresponding NWC

### Elastic modulus

The development of the elastic modulus is shown in Figure 8.7.

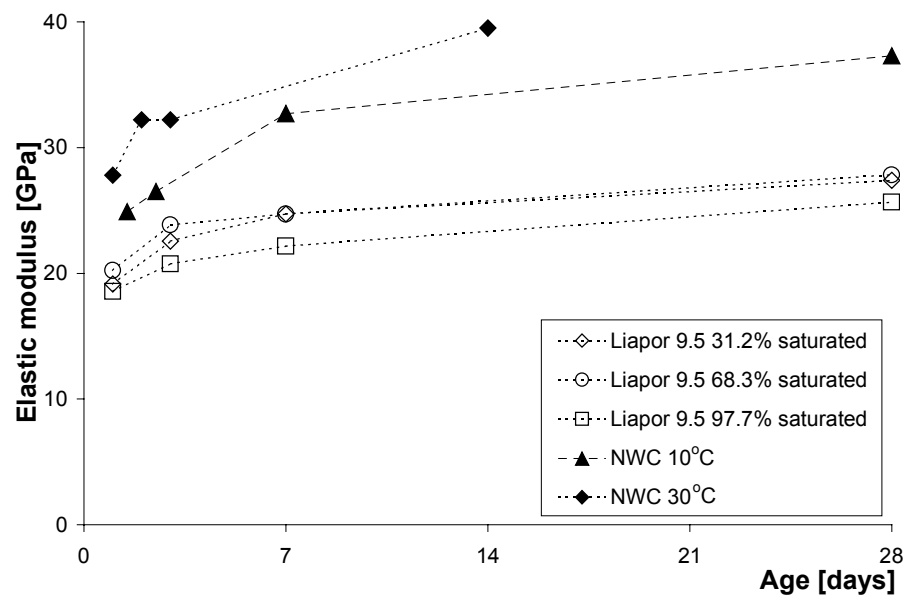


Figure 8.7 – Elastic modulus of LWAC with different degrees of saturation of the LWA compared with the corresponding NWC cured at 10 and 30 °C

Only the mixtures with variable degree of saturation of the LWA were tested. Values between 25 and 28 GPa are reached at 28 days. The two mixes with 69.3% and with 31.2% saturated LWA show the highest values. For the reference mix, the results for curing at 10 and 30°C are shown (see Table 6.3), since the elastic modulus at 20°C was not measured.

#### *Autogenous deformation and self-induced stress*

In Figure 8.8 the autogenous deformation of LWAC with different degrees of saturation of the LWA is presented. LWAC made with saturated LWA expanded from the start of the measurements, 6 hours after casting. The expansion reached a maximum of 115  $\mu$ strain at 1 day; then the deformation remained almost constant for more than 5 days. The mixture with 69.3% saturated LWA showed minor shrinkage in the very early stage of hardening. After 10 hours expansion occurred, reaching a maximum of 80  $\mu$ strain at 3 days. The mixture with 31.2% saturated LWA started with intensive shrinkage until 13 hours. The shrinkage was followed by rapid expansion between 13 and 18 hours and moderate expansion in the next 5 days. In this case the resulting deformation 6 days after casting was shrinkage.

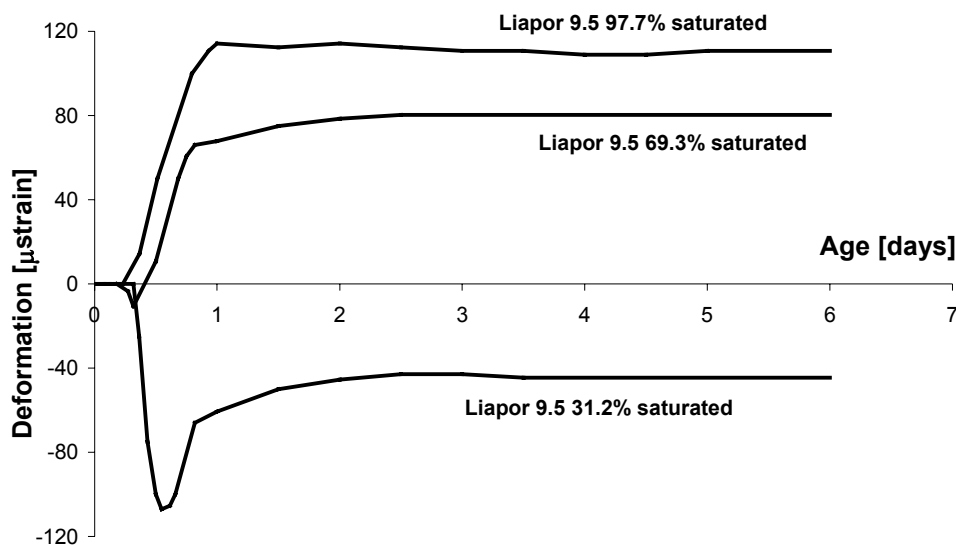


Figure 8.8 – Autogenous deformation of LWAC with different degrees of saturation of the LWA

The effect of the degree of saturation of the aggregate on the stress development is shown in Figure 8.9. For the Liapor mixtures with an actual degree of saturation of 97.7% and 69.3%, which exhibited expansion, compressive stresses were measured. The maximum stresses were between 0.6 and 0.8 MPa. After the peak, a small decrease of the stress occurred, due to relaxation. For the mixture with 31.2% saturated LWA, the shrinkage registered in the first hours did not induce any significant stress in the TSTM. The



subsequent expansion, however, resulted in compressive stresses with maximum about 0.45 MPa after 2 days of hardening.

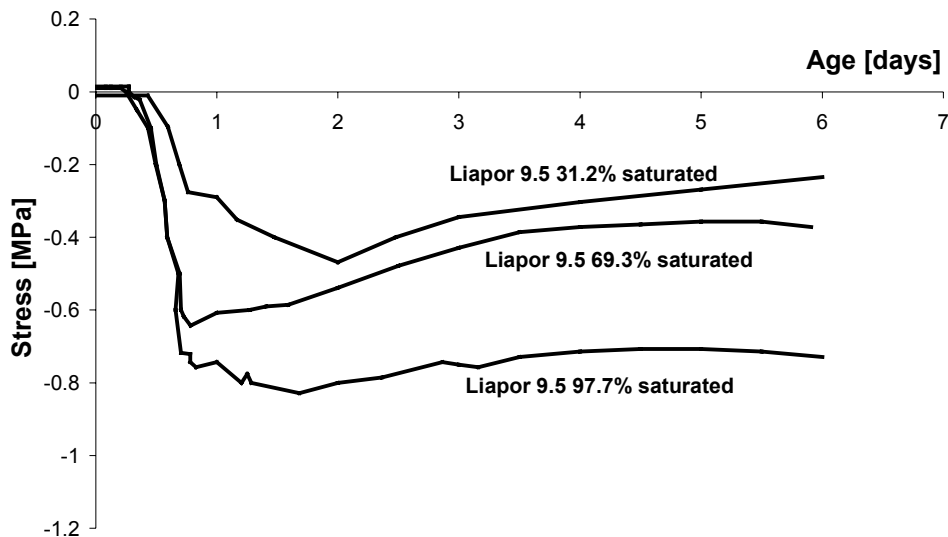


Figure 8.9 – Self-induced stress of LWAC with different degrees of saturation of the LWA

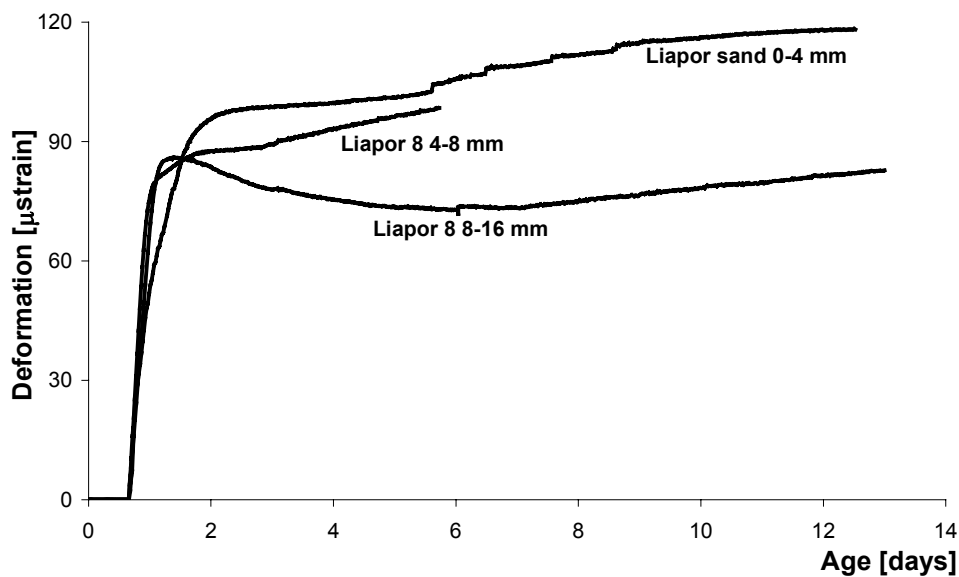


Figure 8.10 – Autogenous deformation of LWAC with different particle size of the LWA

In Figure 8.10 the autogenous deformation of LWAC mixtures with LWA of different particle size is shown. The three mixes expanded from the beginning of the measurements. The mix with Liapor sand 0-4 mm expanded rapidly until 2 days, reaching 95 μstrain. Afterwards expansion proceeded steadily but at a lower rate until a value of

120  $\mu$ strain. The expansion of the mix with Liapor 8 4-8 mm was continuous, reaching a value of 100  $\mu$ strain at 6 days. The expansion of the mixture with the Liapor 8 fraction reached a peak of 85  $\mu$ strain at 30 hours. Then a small shrinkage occurred until 6 days, followed by further expansion. At 13 days the expansion was about 80  $\mu$ strain.

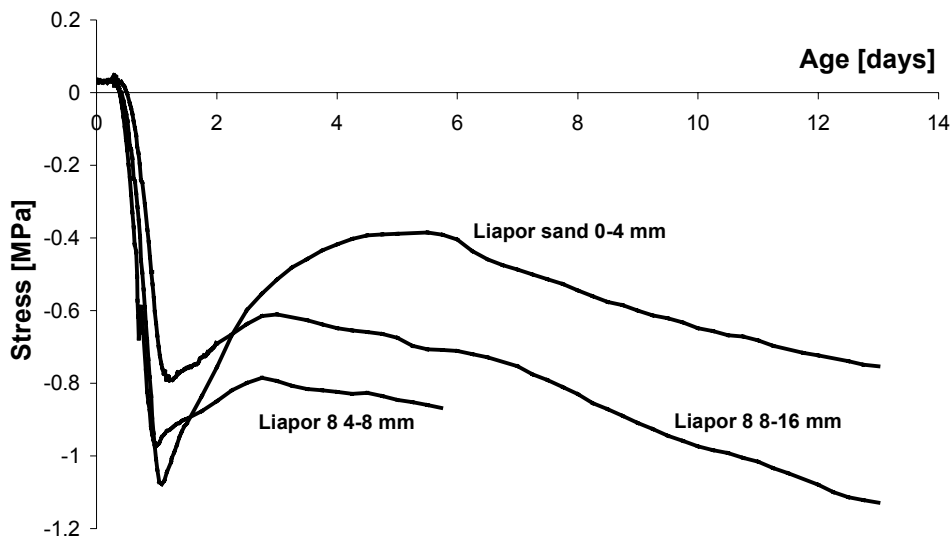


Figure 8.11 – Self-induced stress of LWAC with different particle size of the LWA

Stress development in LWAC with aggregates of different particle size is shown in Figure 8.11. The stress development of the mix with Liapor sand shows a maximum compressive stress, about 1.1 MPa, higher than the one observed for the mixture with 4-8 mm Liapor 8, 1.0 MPa, and for the mixture with 8-16 mm Liapor 8, 0.8 MPa. For all the mixes the peaks are reached within 24-30 hours from casting. The relaxation of the compressive stress after the peak is more relevant for the mixture with Liapor sand, where the stress is reduced to 0.4 MPa, than for the other two mixtures. The stress development of the two mixtures with Liapor 8 is similar, showing slight relaxation until 3 days and then an increase of the compressive stress. In the case of the mix with 8-16 mm LWA, the experiment was prolonged to 13 days showing continuous increase of the compressive stress, up to a value of more than 1.1 MPa. Also the mixture with Liapor sand, after relaxation of the stresses up to 6 days, shows an increase of the compressive stresses until the end of the experiment.

### 8.3.4 Discussion

#### *Compressive strength*

LWAC generally reached 28-days strength similar to NWC with the same matrix. In particular, the mixture with 69.3% saturated Liapor 9.5 had the highest strength at all ages,

even higher than the NWC. Possibly it combines the beneficial effects of the internal curing [Weber & Reinhardt 1997] with a relatively low w/c ratio. A fast development of strength is shown also by the mixture with 31.2% saturated Liapor 9.5, but the strength at 28 days is the lowest, possibly due to less internal curing. The opposite is shown by the mixes with saturated Liapor 9.5 and Liapor 8, where the strength at early ages was low, but the 28-days value was close to the NWC. Finally, the mixture with Liapor sand showed that the use of a LWA with lower density, and hence poorer mechanical properties, limits the strength of the LWAC.

A number of factors influence the compressive strength of LWAC:

- 1) The strength of concrete is strongly influenced by the weakest component. The mechanical properties of the LWA are generally inferior to the ones of NWA [Nilsen et al. 1995]. The strength of the aggregates provides a ceiling strength for the strength of the concrete, after which the addition of cementitious materials to the mix does not improve the strength [Holm 2001]. According to Bremner & Holm [1986], stresses occurring around the inclusions in a monoaxial compressive test, due to elastic mismatch, might cause splitting of the LWA. Crushing strength of the LWA is lower than the one of NWA and among the LWA the denser ones have generally the highest crushing strength. The strength of a particular LWA is actually the result of its porosity and of its pore size distribution as well as of the strength of the pore-free vitreous material surrounding the pores [Holm 2001]. According to these considerations, one would expect the highest compressive strength for the mixtures with NWA, followed by Liapor 9.5, Liapor 8, and Liapor sand. In reality, Liapor 9.5 and 8 performed as well as NWA and a strength decrease was noticed only for Liapor sand.
- 2) Moist concrete shows lower strength than partially dried concrete [Jensen & Hansen 2001a]. LWAC has internal RH higher than NWC due to water supply from the LWA [Bentz et al. 2002]. Accordingly, the mixes with saturated LWA should have lower strength, a fact that was not observed for the mixtures studied.
- 3) An improved quality of the interfacial transition zone and of the bond between LWA and matrix could contribute to the strength of LWAC. It has been observed [Zhang & Gjorv 1990, Wasserman & Bentur 1996], that cement paste penetrates in the outer porous layer of the LWA particles, strengthening the bond. As a matter of fact, penetration of the paste into the pores of the LWA would also partially block the transport of absorbed water to the self-desiccating paste.
- 4) Stress homogeneity in LWAC due to limited elastic mismatch between the aggregates and the cement paste [Bremner & Holm 1986] might reduce the occurrence of internal microcracking, thus increasing the strength. This fact produces also increased brittleness of LWAC, whose stress-strain curves are normally almost elastic until failure [Holm 1980, Neville 1997].
- 5) Continuous hydration of the mixture at later ages, promoted by the extra water stored in the LWA, might also contribute to the strength increase. In fact, Weber & Reinhardt [1997], using thermal gravimetry and small angle x-ray diffraction,

observed a substantial increase of the amount of hydration products in LWAC at later ages, from 180 to 360 days.

- 6) Finally, since the cement paste in the LWAC does not shrink but expands at early age (see the following sections), micro-cracks or eigenstresses in the paste [Dela 2000], due to aggregate restraint, are avoided. This fact might also contribute to increased strength at later ages of LWAC compared to NWC.

### *Elastic modulus*

The elastic modulus of NWC was much higher than the one of LWAC, essentially due to the higher elastic modulus of the NWA, about 50-75 GPa vs. 17-20 GPa of the NWA [Müller-Rocholz 1979, Nilsen et al. 1995].

Using the following equation developed by Hobbs [1974], it is possible to calculate the elastic modulus of a concrete based on the elastic modulus of matrix and aggregates:

$$E_C = \frac{(E_A - E_M) \cdot \phi_A + E_A + E_M}{E_A + E_M + \phi_A \cdot (E_M - E_A)} \cdot E_M \quad (8.1)$$

where  $E_A$  [MPa] is the elastic modulus of the aggregates,  $E_M$  [MPa] the elastic modulus of the matrix, and  $\phi_A$  [ $\text{m}^3/\text{m}^3$ ] the volume fraction of the aggregates.

To calculate the elastic modulus of the reference NWC mix (Mix C Table 6.1), the following assumptions are made:

- 1)  $E_M = E_P = 20$  GPa, as measured in [Lura & Bisschop 2003] on a 1-week old cement paste specimen cured at 30°C.
- 2)  $E_A = 60$  GPa for NWA (see Chapter 7).
- 3)  $\phi_A = 0.66$ .

Using these assumptions,  $E_C = 39.7$  GPa is obtained, whereas the measured elastic modulus varied from 37.3 to 39.5 GPa, depending on the curing temperature (Table 6.3).

To calculate the elastic modulus of a LWAC mix, a different procedure needs to be applied, since two types of aggregates with different stiffness are present. First, the elastic modulus of the mortar fraction is calculated with Eq. 8.1. Then, the obtained elastic modulus of the mortar is used as modulus of the matrix in the calculation of the elastic modulus of LWAC.

For the calculation of the elastic modulus of the mortar, the inputs are the following:

- 1)  $E_P = 20$  GPa [Lura & Bisschop 2003].
- 2)  $E_A = 60$  GPa for the sand in the mortar fraction.
- 3)  $\phi_A = 0.30/(0.30+0.34) = 0.469$  for the sand in the mortar fraction.

Using these values,  $E_{MOR} = 32.2$  GPa is obtained for the mortar. Eq. 8.1, with  $E_M = E_{MOR}$ ,  $E_A = E_{LWA} = 20$  GPa for Liapor 9.5, and  $\phi_A = \phi_{LWA} = 0.36$  yields  $E_C = E_{LWAC} = 27.2$  GPa. The measured elastic modulus varied from 25.7 to 27.8 GPa, depending on the saturation of the LWA (Figure 8.7).

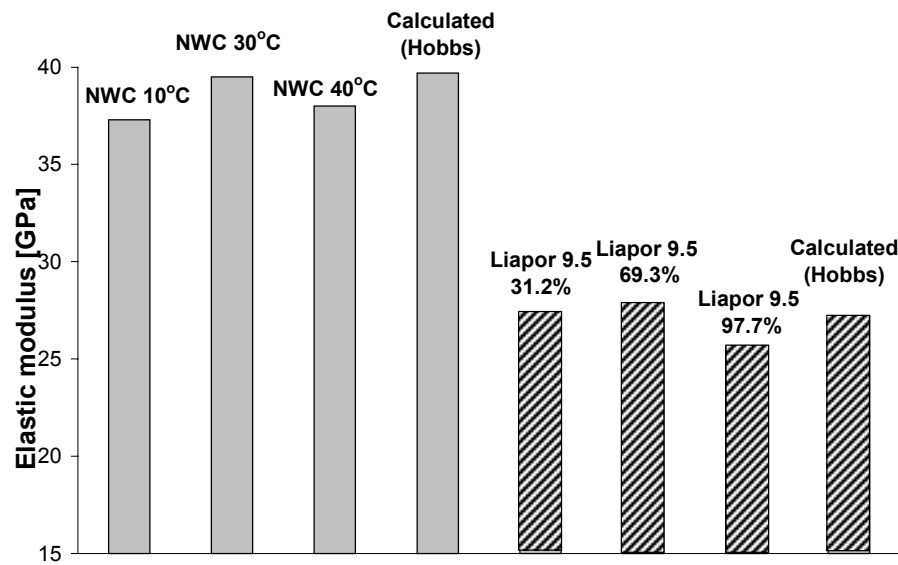


Figure 8.12 – Measured and calculated 28-days elastic modulus of NWC (left, Mix C in Table 6.1, curing temperature 10, 30 and 40°C) and LWAC (right, mixes in Table 8.2, curing temperature 20°C)

Measured and calculated elastic moduli, both for NWC and for LWAC, are reported in Figure 8.12. It is evident that Eq. 8.1 gives a good fit of experimental results and might be used both for NWC and for LWAC. The differences between the measured elastic moduli of the different LWAC mixtures (Figure 8.12) might have been caused by differences in the elastic modulus of the paste, due to internal curing, and by different moisture status [Holm 2001].

#### *Early-age expansion of LWAC*

Early-age expansion of LWAC is an intriguing phenomenon. Cement paste in sealed HPC made with regular aggregates generally shrinks due to self-desiccation. Water transport from the saturated LWA in LWAC is supposed to reduce or eliminate the shrinkage by counteracting self-desiccation, but this does not explain the origin of the expansion. In the following section, it will be shown that expansion of LWAC can be directly calculated supposing that the cement paste expands as it does when it is cured in saturated conditions.

Early-age expansion in LWAC was measured by a number of researchers [Hammer 1992, Sickert et al. 1999, Kohno et al. 1999, Bentur et al. 2001, Zhutovsky et al. 2001a]. Sickert et al. [1999] measured continuous expansion for more than 1 year, most of it occurring in the first days. The bulk expansion is due to the expansion of the cement paste, which is cured in almost saturated conditions, ensured by water from the LWA. This behavior is similar to the expansion that occurs in thin cement paste samples cured under water, which might amount to 1000-2000  $\mu$ strain [Neville 1995]. Jensen & Hansen

[2002] measured an expansion of about 800  $\mu$ strain, most of it in the first day of hydration, on a w/c ratio 0.30 cement paste with 20% silica fume addition internally cured with super-absorbent polymers (SAP).

In this section, an approximate calculation of early-age expansion of LWAC as a function of expansion of the cement paste is presented. The expansion of the mix with saturated Liapor 9.5 (Figure 8.8) will be used as an example. The main scope of this calculation is to check whether the literature values of expansion of the paste under water [Neville 1995] or in paste with SAP [Jensen & Hansen 2002] are compatible with the expansion measured on LWAC.

Most of the expansion of the LWAC occurs in the first day. To calculate expansion of LWAC, its mechanical properties need to be known. Comparing the free deformation measured with the ADTM (Figure 8.8) and the self-induced stress measured in the TSTM (Figure 8.9), the early-age effective stiffness of the mixture may be calculated. The peak of the self-induced stress of the mix with saturated Liapor 9.5 corresponds to the peak of expansion. If the peak stress,  $\sigma_{PEAK}$  [MPa], is divided by the corresponding strain,  $\varepsilon_{PEAK}$  [m/m], an effective stiffness of the LWAC during expansion is obtained:

$$E_{LWAC,EF} = \left| \frac{\sigma_{PEAK}}{\varepsilon_{PEAK}} \right| \quad (8.2)$$

The calculated stiffness probably includes also some creep and plastic deformation (see sec. 7.4.2).

According to this calculation, the average stiffness of the LWAC in the first day is 6.3 GPa. As a reference, the elastic modulus measured at 1 day was 18.6 GPa (Figure 8.7). Knowing the stiffness of the LWAC during the expansion phase, it is possible to calculate the stiffness of the mortar phase by inversion of Eq. 8.1:  $E_{MOR} = 3.83$  MPa. With the stiffness of the mortar phase, the volume fraction of the sand in the mortar,  $\phi_s = 0.469$ , and the stiffness of the sand,  $E_s = 60$  GPa, we may use Pickett's model (Chapter 7, Eqs. 7.1 & 7.2) to calculate the ratio between the expansion of the paste and the expansion of the mortar phase, obtaining  $\varepsilon_{MOR}/\varepsilon_P = 0.347$ . Expansion of the mortar is restrained by the LWA. The LWA in this calculation are supposed to be volumetrically stable since the internal RH remains high in the first hours after casting. Applying Pickett's model with  $E_{LWAC} = 6.3$  GPa (as calculated from the self-induced stresses),  $E_{LWA} = 20$  GPa, and  $\phi_{LWA} = 0.36$ ,  $\varepsilon_{LWAC}/\varepsilon_{MOR} = 0.558$  is obtained. The ratio of the deformation of the LWAC to the deformation of the paste results by multiplication of the two ratios:  $\varepsilon_{LWAC}/\varepsilon_P = 0.194$ . Since the expansion of the LWAC at one day is 120  $\mu$ strain, the expansion of the paste would be about 620  $\mu$ strain. This result, given the uncertainties of the calculation, is in fairly good agreement with the 800  $\mu$ strain measured on saturated cement paste in the first day of hydration [Jensen & Hansen 2002].

### *Self-induced stress*

The self-induced stress of all LWAC mixtures tested was always compressive in the first week of hydration. The corresponding NWC, on the other hand, developed a tensile stress of up to 2 MPa. These reduced stresses in LWAC might be an important contribution to mitigate early-age cracking risk in field conditions when external restraint is present.

More in detail, the self-induced stress and the autogenous deformation of mixtures with Liapor 9.5 were functions of the degree of saturation of the LWA. The mixtures with more entrained water expanded more and the compressive stresses were higher. It should be noticed, however, that also the mixture with 31.2% saturated aggregates showed a good performance, since the shrinkage in the first hours of hydration apparently occurred while the concrete was still plastic and did not correspond to any appreciable build up of tensile stresses. The mixtures with small and homogeneously distributed saturated LWA (Liapor 8 4-8 mm and Liapor sand 0-4 mm) showed more expansion in the first 2 weeks after casting and higher self-induced compressive stresses than the mixture with coarser aggregates (Liapor 8 8-16 mm). This behavior may be due to a better distribution of the water-reservoirs in the mixtures with finer LWA. This issue will be discussed in detail in the following sections.

## **8.4 Modeling of internal curing**

### **8.4.1 General**

In the following sections some critical issues concerning the internal-curing process will be discussed. When one designs a LWAC mixture to minimize or avoid autogenous shrinkage, some questions have to be answered:

- 1) How much water must be absorbed by the LWA in order to avoid self-desiccation and thus self-desiccation shrinkage?
- 2) How much of this water will be actually transported into the paste at high RH?
- 3) Is this entrained water well distributed in the concrete mixture? In other words, are the transport distances from the LWA to the matrix short enough to allow efficient internal curing? How far is the water absorbed in the LWA transported into the hardening cement paste?

These issues are not only fundamental in the mix design phase; they also constitute a starting point for the modeling of the internal-curing process as a whole.

### **8.4.2 Visualization of water transport from the LWA to the cement paste**

In this section an experiment devised to show the water penetration from saturated LWA into hardening cement paste is described. Knowing the effective distance of water

penetration from the rim of a LWA particle into the paste is essential for modeling the internal curing process in a LWAC mixture.

Liapor 8 grains were immersed in a thin blue-ink solution. The surface of the LWA was subsequently dried with blotting paper and fresh cement paste was poured on them. The specimens were then sealed. In this experiment, for a better contrast with the ink, a white Portland cement (CEM I 42.5) was used; w/c ratio of the paste was 0.3. At regular intervals, the cement paste was split. A blue ink corona (Figure 8.13, left) was observed around the Liapor grains. The thickness of the colored shell was growing in time, reaching 1 mm two weeks after casting.

In order to be able to follow continuously the process, the simple device shown in Figure 8.13 (right) was realized. The aggregate was fixed to a hole in a Perspex disc. The outer surface of the LWA was sealed with glue to avoid water evaporation through the aggregate. The Liapor grain was saturated with ink, the surface was dried and the cement paste was poured. The test was performed on 3 specimens at the same time. This method enabled to see the ink diffusing into the cement paste: a progression in the diffusion of the ink was noticed up to 2 weeks after casting.

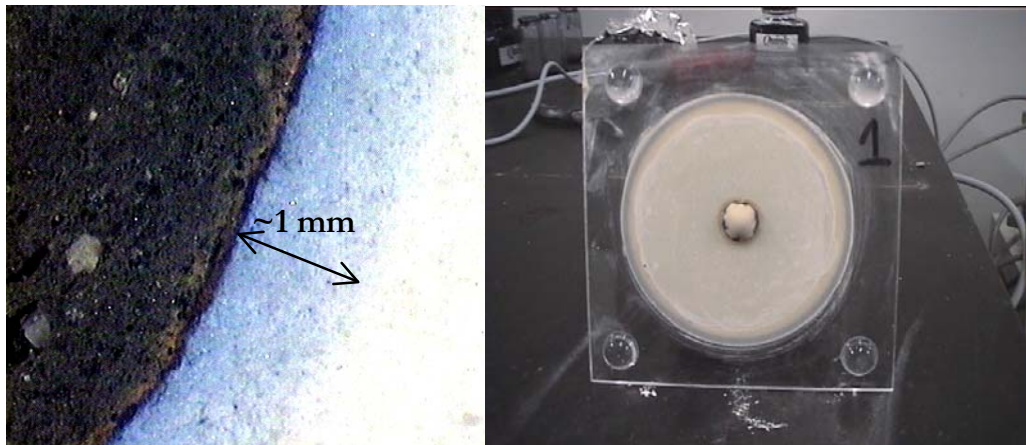


Figure 8.13 – Blue-ink corona around a Liapor aggregate (left), and setup to observe the growth of the corona around the Liapor grain (right)

It is pointed out that the fact that ink diffuses into the cement paste does not *per se* mean that also water diffuses with the same speed and depth. Nevertheless, the spreading of the ink-molecules may indicate the *possibility* of water transport in the hardening paste. In this case, transport of water from the LWA to the paste in the self-curing process might be efficient on the scale of millimeters. This fact has important consequences on the choice of the size of the LWA. If the water transport is active until at least 1 mm from the surface of the aggregate, relatively coarse LWA particles might be also efficient for internal curing. Experimental evidence (see for example Figure 8.10) supports this finding: Liapor 8 4-8 mm particles were sufficient to eliminate autogenous shrinkage in the first week. Other authors have found indirect evidence of water transport on the scale of a few



millimeters [Zhutovsky et al. 2002b]. The distance of water penetration into a hardening cement paste should in fact depend on its permeability and therefore be strongly influenced by the w/c ratio, by the cement fineness, and by the addition of silica fume.

In order to understand the internal curing process, the assessment of the distance over which water transport is effective in a concrete mixture is of fundamental importance. Observation of ink transport into the paste gives obviously only a qualitative answer to the problem. A better insight might be achieved with other more complex techniques, such as x-ray absorption [Bentz & Hansen 2000] or NMR [Bremner et al. 2002]. Both of these non-destructive techniques are able not only to follow the transport process during hardening of the cement paste, but also to quantify the flow of water from the LWA. An x-ray absorption study of water transport from LWA (pumice sand) to cement paste will be presented and discussed in Chapter 9.

### 8.4.3 Quantity of water needed for internal curing

According to Bentz & Snyder [1999], the volume of water needed to avoid self-desiccation, and thus self-desiccation shrinkage, equals the volume of chemical shrinkage of the cement paste:

$$V_e = \frac{C_f \cdot CS \cdot \alpha_{\max}}{\rho_w} \quad (8.3)$$

where  $V_e$  [m<sup>3</sup>/m<sup>3</sup>] is the volume of water entrained in the LWA,  $C_f$  [kg/m<sup>3</sup>] the cement content of the mix,  $CS$  [kg water / kg cement hydrated] the chemical shrinkage,  $\alpha_{\max}$  [-] the maximum achievable degree of hydration, and  $\rho_w = 1000$  kg/m<sup>3</sup> the density of water.

Zhutovsky et al. [2001b] designed the mix composition of LWAC on the basis of this formula. The theoretical value of the entrained water was 20 kg/m<sup>3</sup>. With this amount of water early-age autogenous shrinkage was not completely avoided. Some other authors had used a much higher amount in their mixes [Takada et al. 1999, Sickert et al. 1999], obtaining continuous expansion for days or even months.

Another approach to the problem of entrained water is given by Jensen & Hansen [2001a]. The entrained water is the quantity needed to maintain saturated conditions in a cement paste throughout hardening according to Powers' model [Powers & Brownyard 1948]. In this case hydration stops due to lack of space to accommodate the CSH gel. Thus, the hydration stops when the self-desiccation process has not yet begun. The quantity of entrained water can be calculated from the following formula [Jensen & Hansen 2001a]:

$$\left(\frac{w}{c}\right)_e = 0.18 \cdot \left(\frac{w}{c}\right) \quad \text{for} \quad \left(\frac{w}{c}\right) \leq 0.36 \quad (8.4)$$

According to Eq. 8.4, the water needed for complete curing in [Zhutovsky et al. 2001b] would be higher than the one calculated with Eq. 8.2, about 30 kg/m<sup>3</sup>.

For other LWAC mixtures [Takada et al. 1998, Sickert et al. 1999], included the ones studied in this chapter, the silica fume in the mixture could lead to additional self-desiccation [Jensen & Hansen 1996]; in this case, the quantity of water needed for internal curing is even higher. This amount can be estimated using Powers' model modified with the addition of silica fume [Jensen & Hansen 2001a], as explained in Appendices B and C. A fundamental assumption (and strong limitation) of this model is that the degree of reaction of the cement and of the silica fume is the same throughout the hydration process. According to this last approach, the water needed for complete curing in the mixes presented in this chapter (Tables 8.2 & 8.3) would be 41 kg/m<sup>3</sup>. This is still a rough approximation, since the cement used in the LWAC mixtures (see section 8.3) contains about 35% BFS, whose chemical shrinkage is different from Portland cement (Chapter 3). The entrained water calculated with this last approach is closer to the quantity actually stored in the LWA in the mixtures presented in this chapter, which was 50-80 kg/m<sup>3</sup>. It must be also considered that a significant amount of absorbed water will remain in the pores of the LWA when the RH is still high (see the desorption isotherm, Figure 8.2).

#### 8.4.4 Availability of water for internal curing – distribution of the LWA

Sufficient total water absorbed by the LWA does not mean that this water will be available for transport to the self-desiccating paste. In order to obtain this, the maximum distances of the LWA particles from any point in the paste must be compatible with the distance covered by the water transport in the hardening paste.

Lu & Torquato [1992] developed a model, based on analytical formulas, to calculate the 'nearest neighbor' functions in a collection of spheres of various sizes placed in a volume. The spheres are placed according to equilibrium statistics, i.e. as they were floating in a liquid without gravity and able to reach the desired position. This is a good approximation of the process happening during concrete mixing, if gravity forces are neglected. In the interpretation given by Bentz & Snyder [1999], Lu & Torquato's model may be used to give an estimation of the total volume of matrix that is within a certain distance from the LWA. The aggregates are simulated as spheres, following the sieve analysis. Within each sieve, the aggregates are distributed by volume [Garboczi & Bentz 1997]. A shell of given thickness, equal for all the spheres, surrounds the LWA particles. The shell represents the distance of influence of the self-curing process. According to this approach, the volume of the shells can be calculated as:

$$V_{SH} = 1 - \phi_{LWA} - (1 - \phi_{LWA}) \cdot \exp\left[-\pi \rho_{LT} (c_{LT} \cdot t_{SH} + d_{LT} \cdot t_{SH}^2 + g_{LT} \cdot t_{SH}^3)\right] \quad (8.5)$$

where  $\phi_{LWA}$  [m<sup>3</sup>/m<sup>3</sup>] is the volumetric fraction of LWA,  $t_{SH}$  [m] the thickness of the influence shell (equal for all the spheres),  $\rho_{LT}$  [-] the number of LWA per unit volume, and  $c_{LT}$ ,  $d_{LT}$ , and  $g_{LT}$  are functions of the LWA particle size distribution (PSD)

Eq. 8.5 accounts for the overlapping of the spherical shells surrounding each particle. The  $V_{SH}$  calculated in this way does not distinguish between cement paste and NWA that might be present in the proximity of the LWA. Bentz & Snyder [1999] showed, by comparison with a numerical 3D model, that the errors committed with this approach are limited when a small shell thickness, about a few hundreds of microns, is considered. If transport distances of several millimeters are considered, the differences between the two approaches become larger, as discussed in [Zhutovsky et al. 2002b].

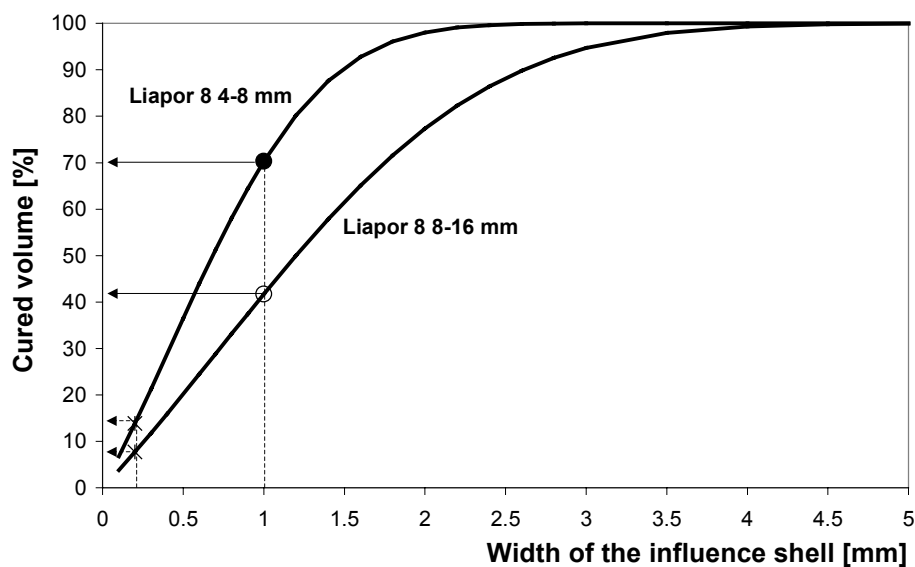


Figure 8.14 – Cured volume vs. thickness of the influence shell in two LWAC mixtures

In Figure 8.14 the calculated cured volume, as a percentage of the total volume, is plotted against the thickness of the influence shell around the aggregates for the Liapor 8 4-8 mm and Liapor 8 8-16 mm LWAC (see Table 8.3). For both mixes a shell thickness of 1 mm around the LWA particles (in agreement with results of the ink diffusion experiments, sec. 8.4.2) is assumed, as indicated by the dots in Figure 8.14. For the finer aggregates (4-8 mm) the cured volume corresponds to 70%, while for the coarser aggregates (8-16 mm) it is only about 40%. This approach clearly shows the beneficial effect of using finer LWA on the effectiveness of internal curing. It is pointed out that if we instead assume a maximum transport distance for the entrained water of 200  $\mu\text{m}$  (crosses in Figure 8.14), as proposed by Bentz and Snyder [1999], only about 10% of the paste would be cured. The effect of the saturated LWA on the curing of the concrete would in this case be negligible. But this is in contradiction with the experimental data, since the LWAC show constant expansion (Figure 8.10) and this is only possible if there exists a good communication between water in the LWA and the paste. In other words, the autogenous deformation measurements (combined with results from Eq. 8.5) show that the water transport is efficient at a distance of at least 1 mm from the rim of the LWA.

## 8.5 Conclusions

### 8.5.1 Properties of LWA

From the experiments performed on the LWA some conclusions can be drawn:

- 1) Absorption of water by Liapor 8 is very fast in the first minutes but goes on steadily for several days. In the 4-8 mm fraction 25% water by weight is absorbed after 2 weeks under water, of which about 15-17% is absorbed in the first day.
- 2) Not all the water absorbed in the LWA is available for transport to the self-desiccating paste. About 2% water by weight of the LWA remained in the LWA at 94.5% RH.
- 3) Water-saturated LWA shrunk when exposed to 50% RH, as a consequence of the moisture loss. This might influence the volume changes of LWAC and should be taken into account in a calculation.

### 8.5.2 Experiments on LWAC

Measurements on LWAC with different degrees of saturation of the LWA and with different particle size of the LWA were presented and discussed in this chapter. Main findings were:

- 1) LWAC generally reached 28-days compressive strength similar to NWC with the same matrix. For one mix with 69.3% saturated Liapor 9.5, the strength from 3 days on was even higher than for NWC. Explanations of this fact should take strength and elastic modulus of LWA, moisture conditions of the concrete, the improved ITZ in LWAC, the internal curing process, and the reduction of the eigenstresses due to absence of self-desiccation shrinkage into consideration.
- 2) The elastic modulus of the LWAC mixtures was lower than for the corresponding NWC, due to the lower stiffness of the LWA compared to NWA. Both elastic moduli of NWC and of LWAC could be calculated with good approximation using a simple composite model developed by Hobbs [1974].
- 3) Early-age expansion of LWAC was attributed to expansion of the cement paste that hydrated in almost saturated conditions due to internal curing. A calculation of the early-age expansion of the cement paste, based on the expansion of the LWAC according to Pickett's model [1956], yielded values in fair agreement with literature data on plain cement paste.
- 4) Expansion and self-induced compressive stresses were higher for the mixes with the highest amount of entrained water and for the mixes with finer LWA.

### 8.5.3 Modeling of internal curing

A combination of experiments and calculations was employed to analyze the internal curing process. The most relevant results were:

- 1) In the hardening cement paste around LWA particles saturated with a thin ink solution, an almost spherical colored shell expanding with time was detected. After 2 weeks, a shell thickness of about 1 mm was measured. This shell indicates the potential for moisture transport in the hardening paste.
- 2) For the calculation of the quantity of entrained water required to avoiding self-desiccation, Powers' model for hydration in saturated conditions may be used. An extension of Powers' model to silica-fume cement pastes is available. Other supplementary cementitious materials require further study.
- 3) Analytical calculations based on the PSD of the LWA particles show that, at least for the concrete containing the finer LWA fraction (Liapor 8 4-8 mm), most of the cement paste is influenced by the internal curing process when a penetration depth of the entrained water of about 1 mm is assumed. According to these results, gravel-size LWA might be adequate to provide uniform internal curing.



# Chapter Nine

## Pumice aggregates and lightweight mortar

---

### 9.1 Introduction

This chapter presents and discusses experiments performed on pumice aggregates, aggregate-pumice interface and lightweight mortars. The main objective of this research was the quantitative monitoring with x-ray absorption of the water release from saturated LWA to a hardening cement paste. The dynamics of the water transport and the effective distance of water penetration into the cement paste are essential for the understanding and modeling of the internal curing process.

Besides, some other issues, relevant to the comprehension of the internal curing process, have also been investigated.

The following chapter is organized in five sections:

- 1) Absorption-desorption properties of pumice grains of different sizes.
- 2) Low temperature calorimetry study of the pore structure of the LWA.
- 3) X-ray absorption study of water transport from saturated pumice to cement paste.
- 4) SEM study of the interface between saturated pumice and cement paste.
- 5) Autogenous deformation, compressive strength, and non-evaporable water content of mortars containing the same cement paste but different amounts of saturated pumice.

### 9.2 Materials

#### 9.2.1 Pumice

Different size fractions (0.6–1.18 mm, 1.18–2.36 mm, 2.36–4.75 mm, and >4.75 mm) of crushed pumice sand from the island of Yali, Greece, were used. The specific gravity

varied from about 1300 to 1200 kg/m<sup>3</sup>, the finer fractions being denser. Properties of the different size fractions will be further discussed in sec. 9.3.3.

### 9.2.2 Cement paste

The cement paste used was realized with Portland cement, CCRL Cement 135 [CCRL 2000], and had a w/c ratio of 0.3. Cement 135 was chosen because it had been the subject of an extensive study at NIST [CCRL 2000, Bentz et al. 2000] and a large amount of experimental and numerical simulation data about hydration and early age-properties was readily available.

## 9.3 Absorption-desorption isotherms of pumice aggregates

### 9.3.1 Methods

#### *IGAsorp Moisture Sorption Analyser*

The absorption-desorption isotherm at 25°C of single pumice aggregates was measured with the IGAsorp Moisture Sorption Analyser (Hiden). The system is fully automated and combines an ultra sensitive microbalance with precise measurement and control of both humidity and temperature.

The measuring range is from 0 to 95% RH and the accuracy in the RH measurements is  $\pm 1\%$  from 0 to 90% RH and  $\pm 2\%$  above. The limitation of 95% RH is a drawback of this technique when used to analyze moisture properties of LWA, where one is especially interested in their behavior in the upper RH range. Only one aggregate at a time, weighing less than 200 mg, could be tested. In the case of LWA, it would be advantageous to test a larger, more significant quantity, since different particles have different properties.

The testing procedure required starting from a dry sample. The pumice sample was dried overnight in the oven at 105°C and inserted in the moisture analyzer. The RH was then increased in steps of 5% or 10% until 95% and then decreased to about 0%. The equilibrium weight at each RH was registered. One absorption-desorption isotherm was obtained in about one week. Two pumice aggregates were measured, weighing 25.6 mg and 105 mg, respectively. For each aggregate, 3 isotherms were measured.

#### *Desiccators*

Desorption measurements at 25°C were performed on the four pumice fractions. About 10 g of each pumice fraction were dried overnight in the oven at 105°C and weighed to obtain the dry weight. The aggregates were then evacuated at high vacuum and impregnated with distilled water, over which vacuum was pulled for about 3 hours. The aggregates were left in the water for one more night. The saturated surface-dry weight was measured according to ASTM C128-97 [1997].



The pumice fractions were inserted in desiccators above saturated salt solutions. The desiccators were kept in a climate chamber at  $25 \pm 1^\circ\text{C}$  and they were provided with plugs through which the internal RH could be read at regular intervals. Three different saturated salt solutions were used:  $\text{K}_2\text{SO}_4$  (97.3% RH),  $\text{KNO}_3$  (93.7%), and  $\text{KCl}$  (84.3%). The LWA followed a decreasing RH ramp, remaining 2 weeks at every RH level. The RH in the desiccators took on average 3 days to stabilize. After the 2-week period, the LWA were weighed and moved to another desiccator. After the last step, they were oven-dried to determine the dry weight once again.

### 9.3.2 Results

#### *IGAsorp Moisture Sorption Analyser*

The absorption-desorption isotherms of two pumice grains, one weighing 25.6 mg (corresponding to fraction 1.18-2.36 mm) and one 105 mg (corresponding to fraction 2.36-4.75 mm) are shown in Figure 9.1. Every point represents the average of 3 readings.

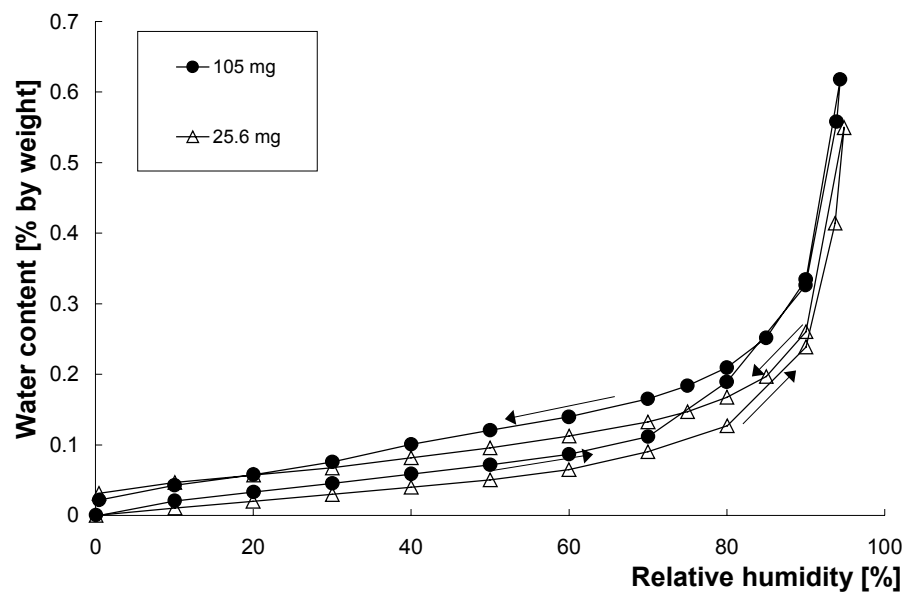


Figure 9.1 – Absorption-desorption isotherms of single pumice grains at  $25^\circ\text{C}$

#### *Desiccators*

Desorption isotherms starting from vacuum-saturated conditions are shown in Figure 9.2. In Figure 9.3 the values of absorbed water at different RH have been divided by the maximum absorption.

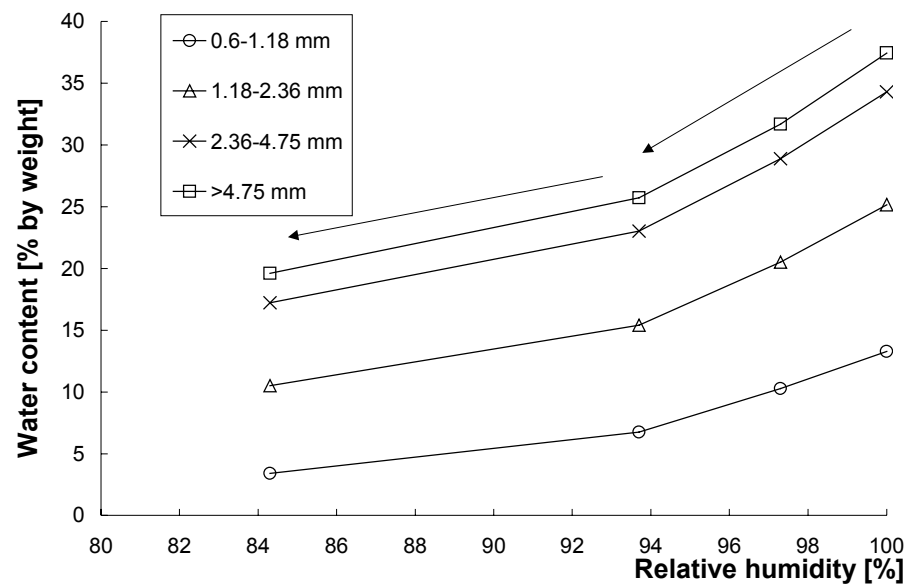


Figure 9.2 – Desorption isotherms of pumice fractions at 25 °C from vacuum-saturated conditions

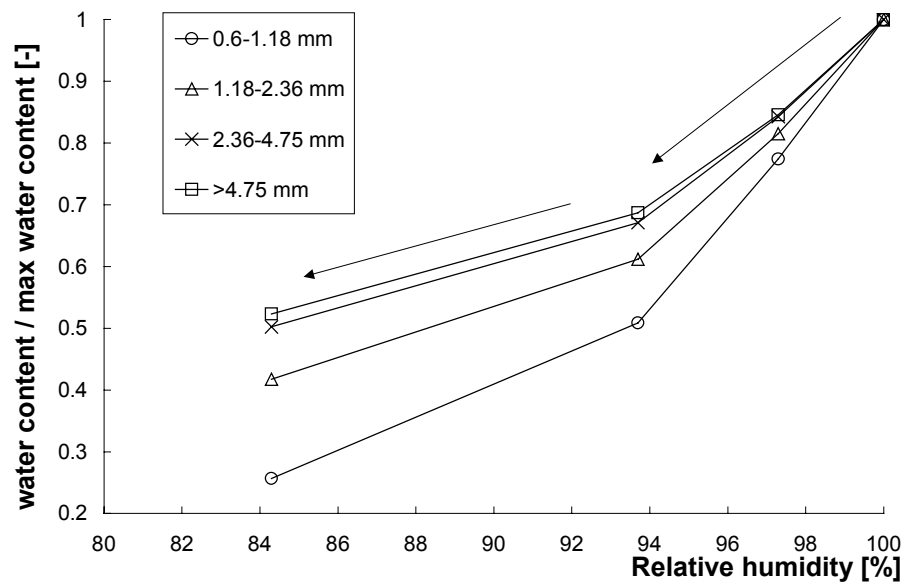


Figure 9.3 – Normalized desorption isotherms of pumice fractions at 25 °C from vacuum-saturated conditions

### 9.3.3 Discussion and conclusions

In Figure 9.1, notice the hysteresis at lower RH and the sharp increase of water content around 90%. The water content of the pumice depends on its moisture history. The water content at 95% is very low, below 1%. The behavior of the two aggregates is different, with the largest having a higher absorption at almost all RH levels.

According to the Figure 9.2, the larger the aggregates, the higher the absorption. This is in accordance with previous results on the same pumice size fractions, which were saturated in boiling water [BSF 2002]. A summary of the results of the present and previous studies is given in Table 9.1. The different absorption of particles of different sizes in the present study is even more pronounced, with the biggest fraction absorbing 38% by weight and the smallest only 13%.

A possible explanation of this fact, confirmed also from direct SEM observation [Zhutovsky et al. 2003], is that, since the aggregates are obtained by crushing, the particles break apart along the largest pores. Therefore, the largest particles have higher internal porosity and bigger pores. The lower density of the larger particles (Table 9.1) constitutes further evidence.

**Table 9.1 – Water absorption and density of pumice fractions**

Aggregate	Particle density [kg/m <sup>3</sup> ]	Particle size [mm]	Water absorption (% by weight)	
			Boiling water [Zhutovsky et al. 2001a]	Vacuum saturated
Pumice 0	Pumice 0	0.15-1.18	13.0	13.3
Pumice 1	Pumice 1	1.18-2.36	19.0	25.2
Pumice 2	Pumice 2	2.36-4.75	26.7	34.3
Pumice 3	Pumice 3	>4.75	-	37.5

In Figure 9.3, the smallest size fraction loses about 80% of the absorbed water at 84% RH, while the two largest lose only about 50%. One would expect that the largest aggregates, having supposedly the largest pores, would lose proportionately more water than the smaller ones. This apparent paradox could be due to the presence of inkbottle pores: the emptying of the larger pores would not occur until the RH dropped beyond the equilibrium value for the smaller entryways. Since a great quantity of water is in fact entrapped in the internal porosity of the larger particles, one should consider that only about half of it would be available for internal curing. In the case of the smaller fraction the opposite seems to hold: the absorption is lower, but almost 80% of the water is lost by 85% RH.

A further comment on these studies is that even if total saturation of the porosity is useful for research purposes and vacuum saturation is a very efficient way to obtain it, it is not feasible in practice. The same is true for boiling the LWA or immersing them in water for months to obtain saturation [BSF 2002]. In Chapter 8, on the other hand, it was shown that the Liapor 8 aggregates absorbed about 80% of the long-term absorption in the first day. This is a favorable property and it is in agreement with construction practice. The ideal LWA, from the point of view of the absorption properties, is the one whose porosity is almost filled in about 1 day underwater (or alternatively during mixing of concrete) and loses all absorbed water at RH higher than about 95%.

## 9.4 Low Temperature Calorimetry study of pumice aggregates

### 9.4.1 Methods

Low Temperature Calorimetry (LTC) is a technique that may be used for probing the pore structure of porous building materials. The advantage of LTC over many other techniques is that the specimen can be evaluated in the saturated state, with no pre-drying required. Pore diameters from about 4  $\mu\text{m}$  to 30 nm are detectable using LTC. Because water in a small pore freezes at a lower temperature than bulk water, the observed freezing-point depression can be related to the size of the pore. By monitoring the heat absorbed or released as a function of temperature in a Differential Scanning Calorimeter (DSC), the volume of water frozen vs. temperature (or pore size), basically equivalent to a pore-size distribution, can be determined. In the case of the pumice aggregates, performing LTC on both dry (in lab conditions  $\sim 50\%$  RH) and water-saturated particles provides information on the size of pores where the water is held. One dry and one wet aggregate particle, with dry weight about 40 mg, were tested in a DSC. The samples were first equilibrated at  $10^\circ\text{C}$  and then the temperature was lowered to  $-60^\circ\text{C}$  at a rate of  $-0.5^\circ\text{C}$  per minute. The heat flow from the sample was registered continuously as the temperature was lowered.

### 9.4.2 Results

In Figure 9.4 the freezable water, evident as heat flow from the sample, is shown for a dry and for a saturated pumice sample.

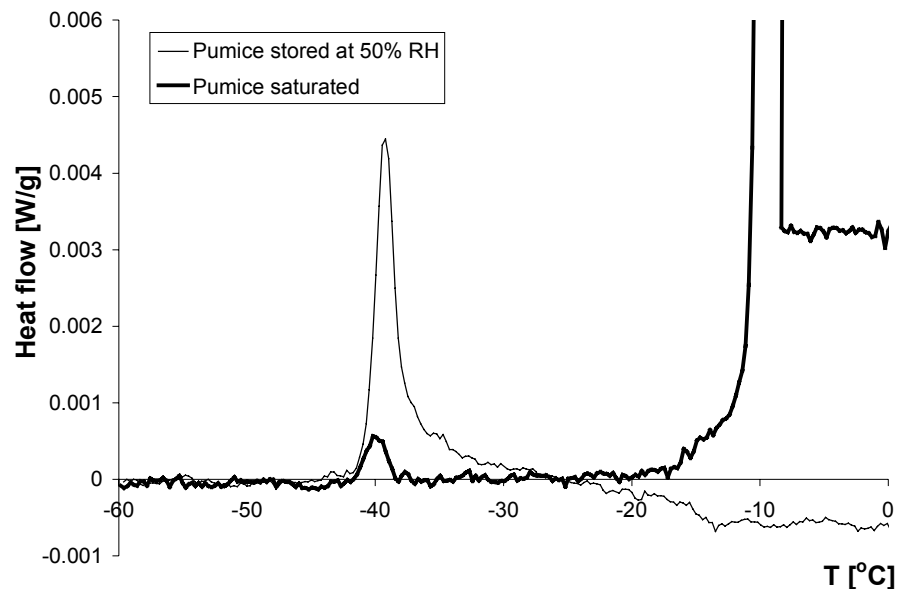


Figure 9.4 – Freezable water, evident as heat flow from the sample, for pumice particles stored at 50% RH or vacuum saturated

### 9.4.3 Discussion and conclusions

According to Figure 9.4, most of the water in the saturated LWA froze at about  $-8^{\circ}\text{C}$ , which corresponds to pores with radii around 170 nm [Fagerlund 1973]. For a comparison, capillary water in a 6-hours old cement paste with a w/c ratio 0.3 [Snyder & Bentz 1998] froze at temperatures around  $-17^{\circ}\text{C}$ , corresponding to pores with radii around 70 nm. A very small peak is visible at  $-40^{\circ}\text{C}$ , corresponding to pore sizes around 50 nm. On the other hand, even in the sample stored at 50% RH some water is actually present and it freezes at the same temperature as the second peak in the saturated specimen. This is evident because the peak of the specimen stored at 50% RH is much higher than the second peak of the saturated specimen.

An explanation of this fact is once again the presence of inkbottle pores. A possible mechanism is schematically shown in Figure 9.5. Ice formation proceeds from the outer surface of the specimen; in the saturated specimen (Figure 9.5, left) all pores are full, so that a path through larger pores connects the outside to the inside and almost all pores freeze at the same temperature  $T_1$ . In the unsaturated specimen, however, water in some large inner pores is connected to the outer surface only through smaller entries (Figure 9.5, right) and freezes at a temperature  $T_2$  lower than  $T_1$ . Therefore, the peak seen at  $-40^{\circ}\text{C}$  in the specimen stored at 50% RH (Figure 9.4) is actually also due to water-filled pores with radii larger than 50 nm. A large volume of inkbottle pores implies that a substantial part of the water held in the LWA will be released only at very low RH, as evident from the desorption isotherm shown in Figure 9.2.

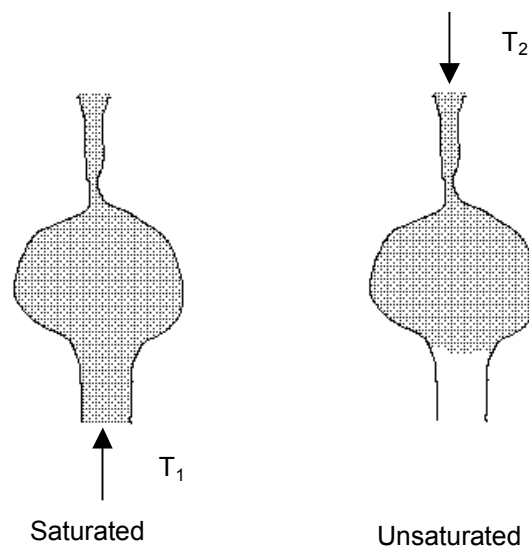


Figure 9.5 – Schematic view of the effect of inkbottle pores on the freezing of water in saturated (left) and unsaturated (right) samples. The arrows show the direction of propagation of the ice;  $T_1$  and  $T_2$  ( $T_1 > T_2$ ) are the freezing temperatures of the water in the two conditions

## 9.5 X-ray absorption test and chemical shrinkage

### 9.5.1 Methods

#### *X-ray absorption*

The x-ray profile of a sandwich specimen composed of saturated pumice and fresh cement paste was measured as a function of time with the GNI X-ray System [GNI 2002]. Changes in the x-ray counts measured by a detector are related to changes in density of the medium through which the x-rays are traveling [Hansen et al. 1999]. Higher x-ray counts are measured for lower densities. In the present case, the transport of moisture from the saturated pumice to the hardening cement paste should result in an increase of counts in the pumice (which is losing moisture) and a decrease of counts in the cement paste. The x-ray system was used successfully to measure drying profiles of cement paste at early ages [Bentz & Hansen 2000, Bentz et al. 2001a, Bentz 2002b]. Also transport of water from high to low w/c ratio cement pastes in a layered specimen could be detected [Bentz et al. 2001b]. Moreover, results have also been obtained for the transport of water from SAP to cement paste [Østergaard 2001].

The sample holder used in the test consisted of a disposable 10 mm-pathlength semi-micro cuvette. The cuvette was made of polymethyl methacrylate, with an internal cross-section 4 mm × 10 mm and wall thickness of 1 mm. It was closed with a polyethylene cap and sealed with epoxy glue. The cuvette was then placed with the 4-mm side in the direction of the x-ray beam.

Large flat pumice aggregates were selected from the largest fraction available (> 4.75 mm). To obtain a flat and smooth interface with the paste, the aggregates were polished with sandpaper to obtain prisms, 10×4×2 mm<sup>3</sup>. The LWA were cleaned by ultrasound in ultra-pure water for 1 minute to remove any dust produced by the polishing. Aggregates were then vacuum dried and weighed. Subsequently, they were evacuated under high vacuum and impregnated with distilled water over which vacuum was pulled for about 3 hours. The aggregates were left in the water overnight. The surface of the aggregates was then dried with an air stream and the saturated surface dry weight was measured. The LWA contained about 35% water by weight.

A thin slice of polished granite stone (~10×4×3 mm<sup>3</sup>) was inserted first into the cuvette, providing a support for the pumice that was inserted above. A tiny droplet of epoxy glue insured adhesion between the granite and the pumice. The cement paste was mixed by hand in a sealed plastic bag for about 3 minutes. It was then poured into the cuvette on top of the pumice. During pouring, the cuvette was kept vertical. About 180 mm<sup>3</sup> of paste were poured, corresponding to a thickness of 4.5 mm above the LWA. The thickness of the cement paste layer was calculated according to the procedure described in the Appendix C. A second slice of granite was inserted on top of the paste. A rubber cylinder was then pushed into the cuvette to ensure good sealing and the cuvette was closed with the cap and sealed with epoxy glue. A top view of the whole specimen is

shown in Figure 9.6. At this point the cuvette was turned horizontally and inserted into the x-ray chamber, kept at  $25 \pm 1$  °C. The first reading started immediately and consisted of scanning the layered specimen from end to end in 0.2 mm steps. The measured accuracy of the positioning of the x-ray beam was 0.04 mm. The collimator of the detector had a circular opening with a diameter of 0.16 mm. In the output file of the x-ray system, the target position and not the actual position is registered. This is potentially an important source of error, since slightly different points are scanned in consecutive runs.

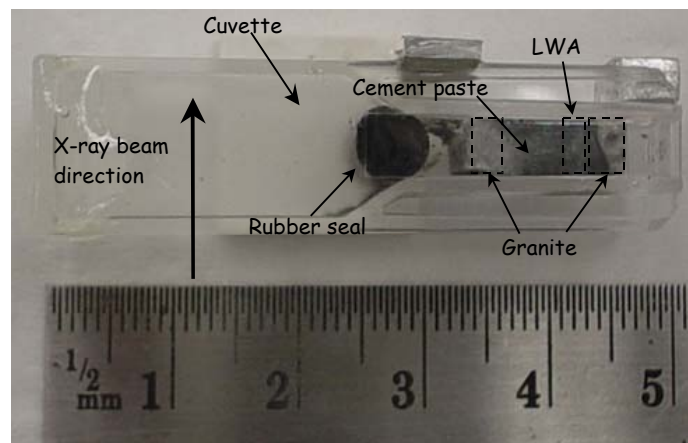


Figure 9.6 – Top view of the specimen used in the x-ray experiment

#### *Chemical shrinkage and non-evaporable water content*

Chemical shrinkage was measured on the cement paste according to the test procedure described in sec. 4.3.2. About 5 g of cement paste were cast into a glass vial, with a few drops of de-ionized water on top. The vial was then filled with paraffin oil and closed with a rubber stopper surrounding a graduated capillary tube. Changes in the level of oil in the capillary tube indicated the chemical shrinkage of the paste. The cement paste was cured at 25°C in a water bath.

The non-evaporable water content,  $W_n$ , is defined as the mass loss per gram of original cement, measured between the temperatures of 105°C and 1000°C. From the non-evaporable water content, the degree of hydration can be estimated assuming a value for the non-evaporable water of a fully hydrated sample. This value can be calculated from the phase composition of the cement ( $C_3S$  56.5%,  $C_2S$  14.3%,  $C_3A$  5.9%, and  $C_4AF$  6.6%); in the present case a value of 0.235 g  $H_2O$ /g cement was used [Bentz et al. 2000]. The specimens were stored inside the x-ray chamber ( $25 \pm 1$ °C) to realize the same conditions as in the moisture transport samples. Both saturated and sealed samples were tested. After 8 h, 1 day, 3 days, 7 days, and 28 days, one sample of each curing condition was crushed with a pestle in a mortar. The powder was flushed with methanol twice to stop hydration. Then, two crucibles were partially filled with the content of each sample and dried overnight in the oven at 105°C. The crucibles were subsequently weighed and fired in the furnace at 1000°C for about 3 hours. The difference between the two weights,

compensated for the loss on ignition of the dry cement powder, gave the non-evaporable water content of the sample.

Hydration of the cement paste was simulated with the program CEMHYD3D [Bentz 2000]. For details of the modeling, see [Bentz et al. 2000]. Chemical shrinkage and degree of hydration in saturated and in sealed curing conditions at 25°C were calculated as a function of curing age. Curing in saturated condition in CEMHYD3D is realized by guaranteeing free availability to water for hydration throughout the simulation. In the experiments, however, depercolation of the capillary pores in the low w/c paste after a few days hydration will limit access of the water, some self-desiccation will take place and further hydration will be hampered. After depercolation of the capillary porosity, the measured non-evaporable water content will therefore be lower than in the ideal case of perfect saturation, but higher than in the case of sealed hydration.

### 9.5.2 Results

#### *X-ray absorption*

The x-ray counts through the specimen measured immediately after casting and after 10 days hydration are shown in Figure 9.7. In the figure, the different materials that compose the layered specimen are also shown.

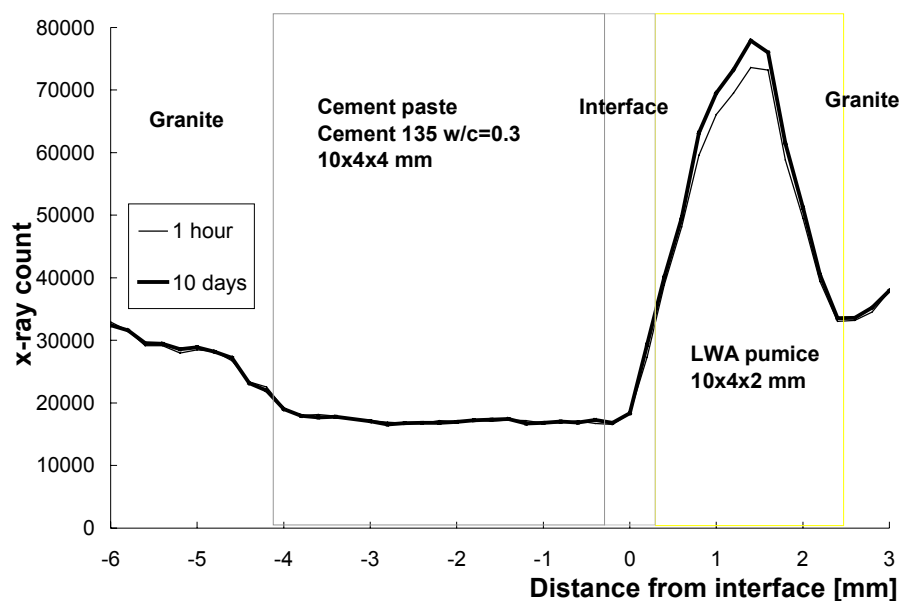


Figure 9.7 – Initial and final x-ray counts profiles

In Figure 9.8, the differential counts normalized to the initial counts (after 1 hour hydration) in each position along the profile are shown as a function of age. Figure 9.9 shows the differential counts normalized to initial counts, summed on the cement paste, on the LWA, and on the interface.



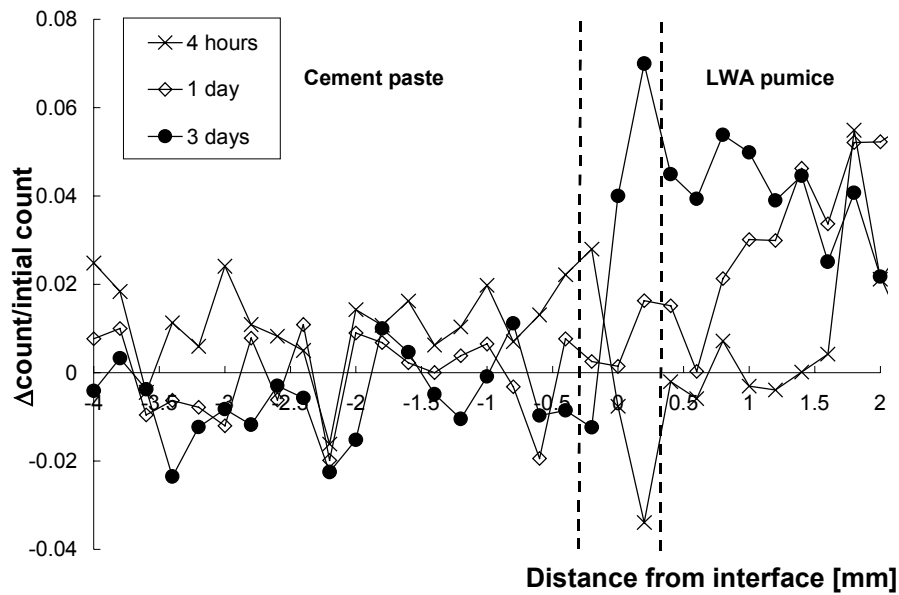


Figure 9.8 – Differential counts normalized to initial counts in cement paste and LWA at different ages

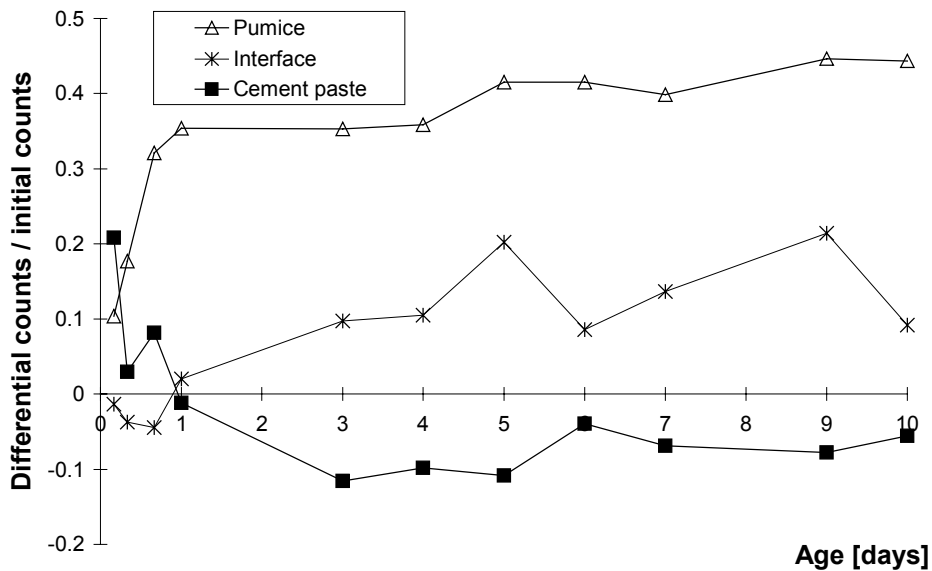


Figure 9.9 – Differential counts normalized to initial counts in cement paste, LWA, and interface as a function of age

The presence of a smooth transition between the high counts in the LWA and the low counts in the paste (Figure 9.7) is due to:

- 1) The presence of an interface at the rim of the pumice grain.
- 2) The shape of the pumice grain, which is not perfectly prismatic.

- 3) The imperfect alignment between the pumice and the cuvette and the cuvette and the x-ray beam (Figure 9.6).
- 4) The width of the x-ray beam, whose diameter is 0.16 mm.

This region has been labeled *interface* in Figure 9.7. The distances from the interface in Figures 9.7 and 9.8 are positive in the direction of the pumice and negative in the direction of the paste.

#### *Chemical shrinkage and non-evaporable water content*

Measured and simulated chemical shrinkage curves are shown in Figure 9.10. The deviation between the two curves after about 100 hours may be due to depercolation of the capillary pores. If the thickness of the chemical shrinkage sample is reduced, curves that are closer to the numerical simulation are obtained [Geiker 1983].

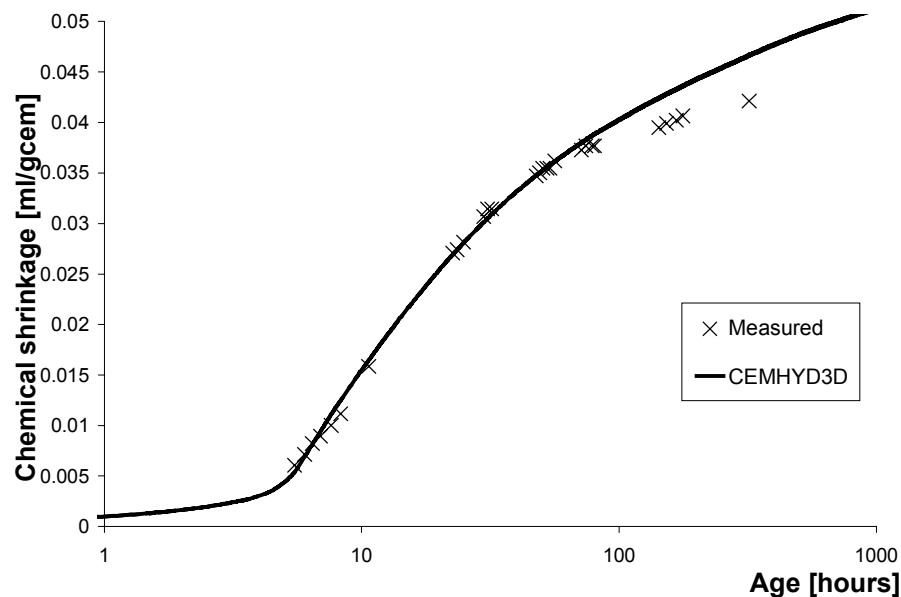


Figure 9.10 – Measured and simulated (CEMHYD3D) chemical shrinkage of cement paste in saturated conditions as a function of age

In Figure 9.11 the measured and simulated development of the degree of hydration is shown, both in sealed and in saturated conditions. The simulated curve for saturated conditions corresponds to ideal conditions of complete saturation, whereas depercolation of the capillary pores in the measured sample may have reduced the penetration of water into the sample at later ages and limited the hydration.

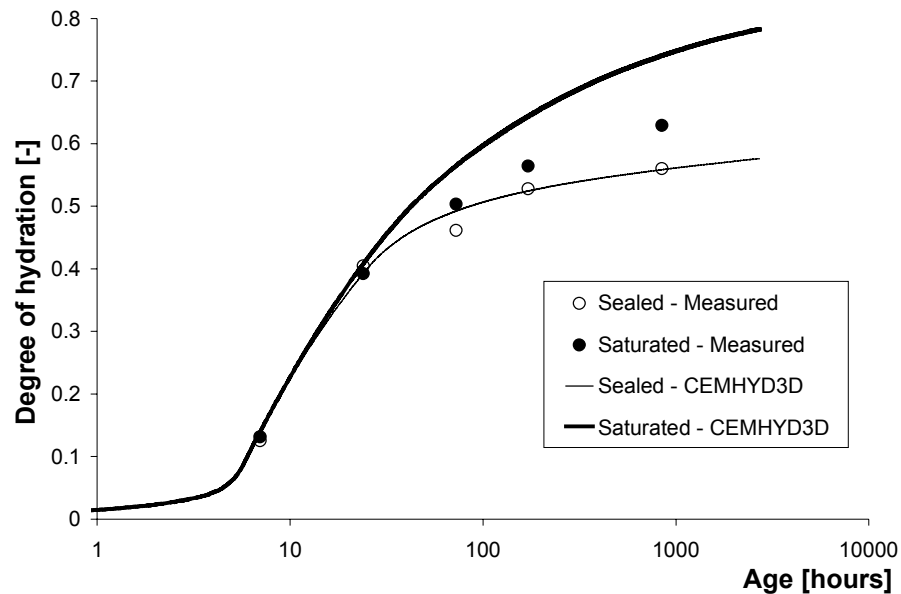


Figure 9.11 – Measured and simulated (CEMHYD3D) degree of hydration of cement as a function of age based on non-evaporable water

### 9.5.3 Discussion

From analysis of Figures 9.8 and 9.9 some clear trends emerge:

- 1) The counts in the paste increase at 4 hours almost at any point, decrease in the following readings and stabilize after 7 days (Figure 9.9). The first rise may be due to settlement of the paste between casting and the 4-hour reading. The subsequent decrease of counts, corresponding to an increase in density, is probably due to absorption of water from the LWA.
- 2) The counts in the LWA in the first hours increase at the right end and decrease at the left end (Figure 9.8), possibly indicating a moisture transport within the thickness of the pumice. Afterwards, the counts on the whole LWA increase and then become almost stable after 3 days hydration.
- 3) The interface region sees a decrease in counts in the first hours (Figures 9.8 and 9.9) and then a sudden increase. The oscillations in counts in the following days might be due to measurement error. In fact, the sudden gradient in counts in this region (from 16000 to 30000 in a few hundreds of  $\mu\text{m}$ , see Figure 9.7) amplifies the effect of the uncertainty in the positioning of the x-ray beam, which is about 0.04 mm.

As a conclusion, the global behavior observed corresponds to settlement in the paste in the first 4 hours, corresponding to the dormant period of the hydration of the paste [Bentz et al. 2000]. Once setting takes place, pores are emptied in the cement paste and water is pulled out of the LWA, passing first through the interface. Water is detected while it is passing from the right edge of the pumice to the left, through the interface and then

into the paste. From 1 day, the interface is becoming less dense, and then by 3 days the whole transport process is almost over.

The chemical shrinkage in the paste is the driving force for the moisture transport. On the other hand, the difference in counts between the LWA and the cement paste is a direct measure of the water transported. These two quantities are plotted together in Figure 9.12. The chemical shrinkage was zeroed at 1 hour to correspond to the initial x-rays reading.

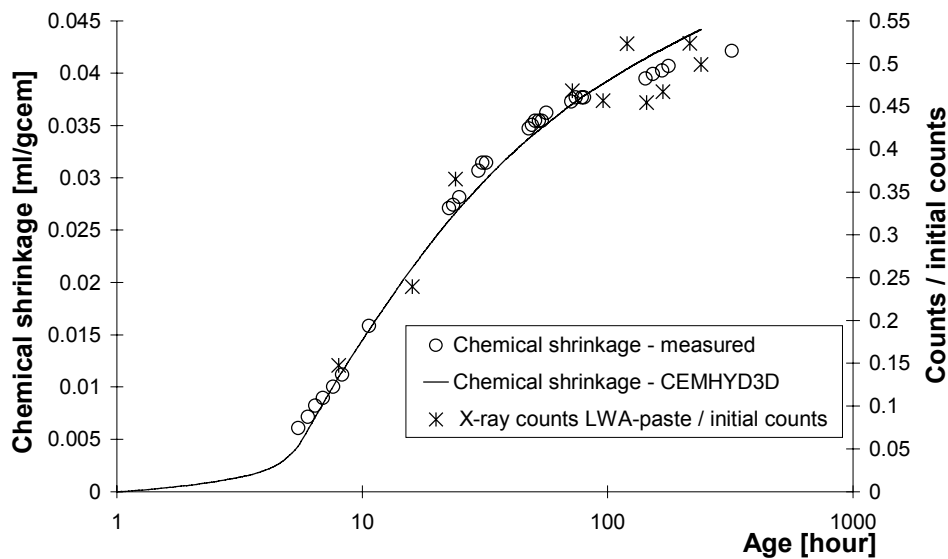


Figure 9.12 – Counts in the LWA minus counts in the paste and chemical shrinkage of the cement paste as a function of age

Figure 9.12 shows that the difference in change of counts between the pumice and the cement paste follows the same evolution as the chemical shrinkage in the paste. This fact confirms the assumption that the chemical shrinkage is the driving force that pulls water out of the LWA. Moreover, since the counts are changing in the whole cement paste (Figures 9.8 & 9.9), the transport of water seems to be effective on the whole width of the cement paste, about 4 mm.

The free transport of water may occur until depercolation of the capillary pores takes place, at about 4 days of age in this case. In fact, Figure 9.10 shows that at 100 hours the simulated and measured curves for chemical shrinkage diverge, indicating the occurrence of depercolation.

A last remark: drying of the whole specimen is probably taking place through the cap and possibly even through the walls of the cuvette. To verify this, cuvettes filled with water, one closed with a cap and one additionally sealed with epoxy, were inserted in the x-ray chamber and their weight loss was measured after 6 days. The sealed cuvette lost 0.77% of the water content, the other 1.24%. This shows that the cuvettes, as configured

for these experiments, are not totally watertight. A loss of water is expected to have occurred also in the sandwich samples: the effects of it would be superimposing a global, but not uniform, loss of counts due to drying onto the profiles created by the internal water movement.

#### 9.5.4 Conclusions

In the x-ray study, it was found that the transport of water from a saturated pumice aggregate to the hydrating cement paste follows the development of the chemical shrinkage of the paste during the first week of hydration. Moreover, the changes of x-rays counts in the specimen indicate a water penetration of about 4 mm from the rim of the LWA in the first days of hydration. This is in accordance with considerations about depercolation of capillary porosity in the cement paste, which should occur not earlier than 4 days in the present case. Before depercolation, water transport in the cement paste takes place over distances of at least several mm [Bentz & Hansen 2000, Bentz et al. 2001c]. The consequence of this fact is that supplying a sufficient quantity of entrained water for internal curing in the first days of hydration, when most of chemical shrinkage occurs (Figure 9.10), is more important than having the water reservoirs extremely well dispersed in the paste. These results confirm what was already found in Chapter 8 using ink-impregnated Liapor aggregates. Other researchers have come to the same conclusions observing the shrinkage reduction in concrete containing saturated pumice [Zhutovsky et al. 2002b].

## 9.6 SEM observation of the interface between pumice and cement paste

### 9.6.1 Methods

A prismatic specimen, with cross-section 10 mm × 10 mm, was cut from a sample that had been used in one trial run of the x-ray test. It contained a single pumice grain from the fraction > 4.75 mm and cement paste. The pumice had not been vacuum-saturated but immersed in water for 1 day. A layer of several mm of cement paste totally covered the pumice. According to calculations (Appendix C), the water contained in the pumice was in this case insufficient to compensate for the self-desiccation of the paste.

At 2 weeks of age the specimen was dried in the oven at 105°C. The specimen was vacuum impregnated with a low-viscosity epoxy resin and cured for 1 day at 60°C. The surface was cut with a diamond saw to expose the cross-section of the LWA. Saw marks were removed by grinding with 400 grit followed by 600 grit sandpaper. Final polishing was done on a lap wheel with 6, 3, 1, and 0.25 mm diamond paste for 45 s each. After each polishing, the specimen was cleaned using a clean cloth. The final polished specimen was cleaned with ultrasound and then coated with carbon to provide a conductive surface

for viewing in the SEM. Once properly prepared, the specimen was placed in the SEM viewing chamber, and signals were collected for the backscattered electrons (BE) and x-rays. Typical accelerating voltage and probe current for the backscattered electron images were 12 kV and 2 nA, respectively. For the x-ray images, the probe current was increased to about 10 nA. The contrast in the BE image is dependent on the average atomic number ( $Z$ ), with higher  $Z$  phases appearing brighter than lower  $Z$  phases. Thus, for hardened cement paste, anhydrous cement appears brightest followed by CH and CSH; porosity filled with embedding resin appears dark. The pumice grain, composed mainly of aluminosilicates, is a gray shade similar to the calcium silicate hydrate. Phase identification is made by examination of the phase shape, relative brightness, and chemical composition as determined by qualitative x-ray microanalysis. With the fairly distinct gray-level separations between anhydrous cement, CH, CSH, and the resin-filled porosity, the BE image could be processed and analyzed to obtain quantitative analysis data.

The SEM observation concentrated on the interface between the pumice grain and the cement paste. At two different points along the rim of the pumice grain, which was straight at this magnification, a series of 4 images ( $\sim 160 \mu\text{m} \times 200 \mu\text{m}$ ) was taken, proceeding from the aggregate towards the bulk cement paste. The gray levels corresponding to each phase were determined on one picture and then used to analyze all the other pictures. Phase fractions were measured as a function of distance from the aggregate surface for both sets of pictures. The degree of hydration  $\alpha$  [-] as a function of the distance from the interface was calculated according to:

$$\alpha = \frac{\frac{CSH + CH}{C_{anhyd} + \frac{\nu}{\nu}}}{\nu} \quad (9.1)$$

where  $CSH$  [-] is the number of pixels of calcium silicates hydrated in the area of interest,  $CH$  [-] of calcium hydroxide,  $C_{anhyd}$  [-] of anhydrous cement, and  $\nu = 2.15$  is the volume ratio between the reaction products and the anhydrous cement [van Breugel 1991].

### 9.6.2 Results

In Figure 9.13 a BE image of the interface between the aggregate and the cement paste is shown. The dark gray porous region at the top is the rim of the LWA. Notice the high porosity region at the interface and the absence of outer-product CSH gel. In Figures 9.14-16, porosity, anhydrous cement, and degree of hydration are plotted as a function of the distance from the interface. Two independent sets of BE images were analyzed.

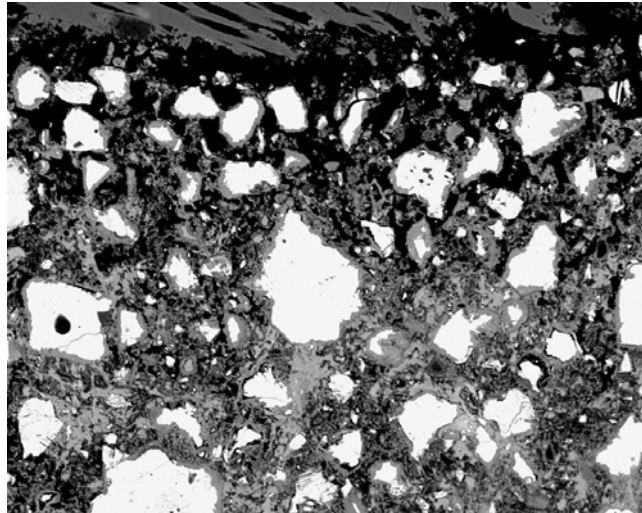


Figure 9.13 – BE image of the interface between pumice and cement paste ( $160\ \mu\text{m} \times 200\ \mu\text{m}$ )

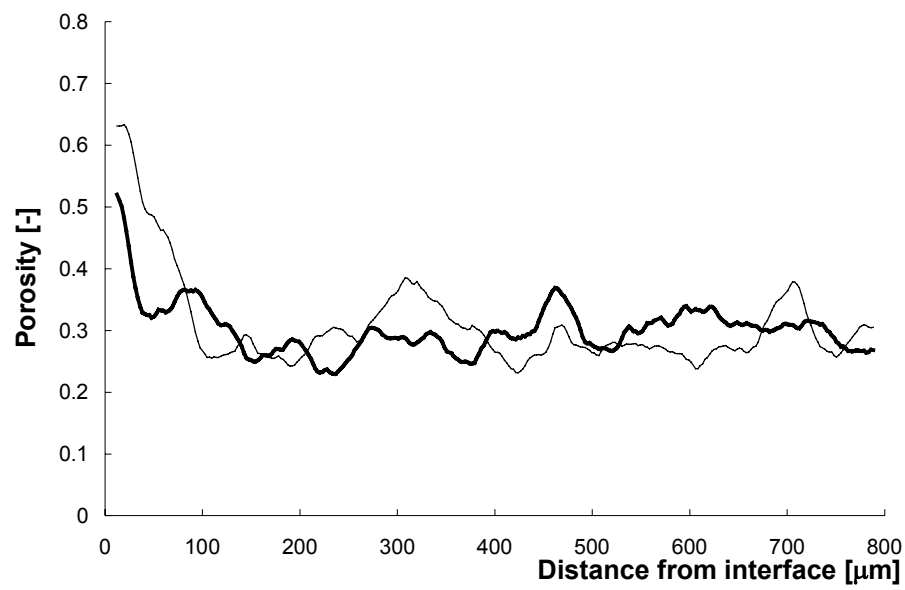


Figure 9.14 – Porosity as a function of the distance from the interface, measured on two different sets of BE images

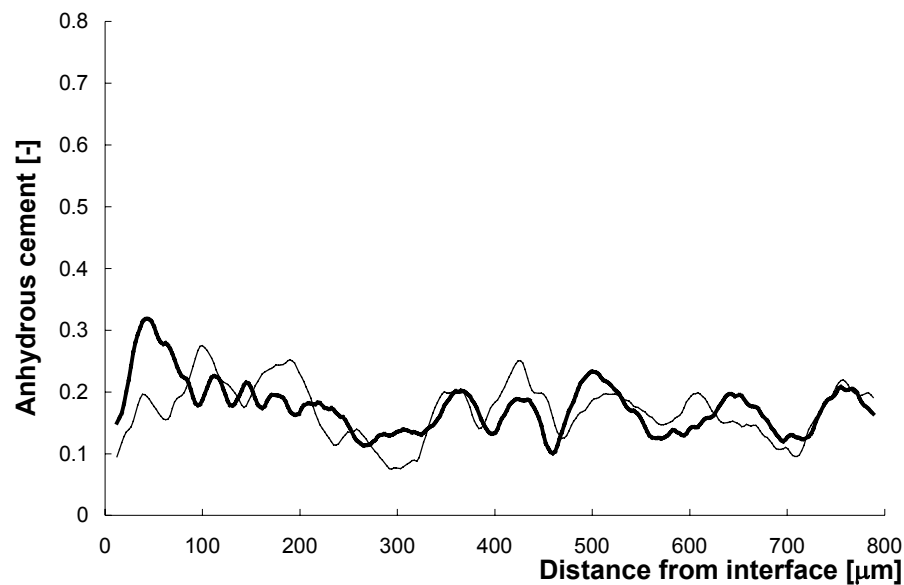


Figure 9.15 – Anhydrous cement as a function of the distance from the interface, measured on two different sets of BE images

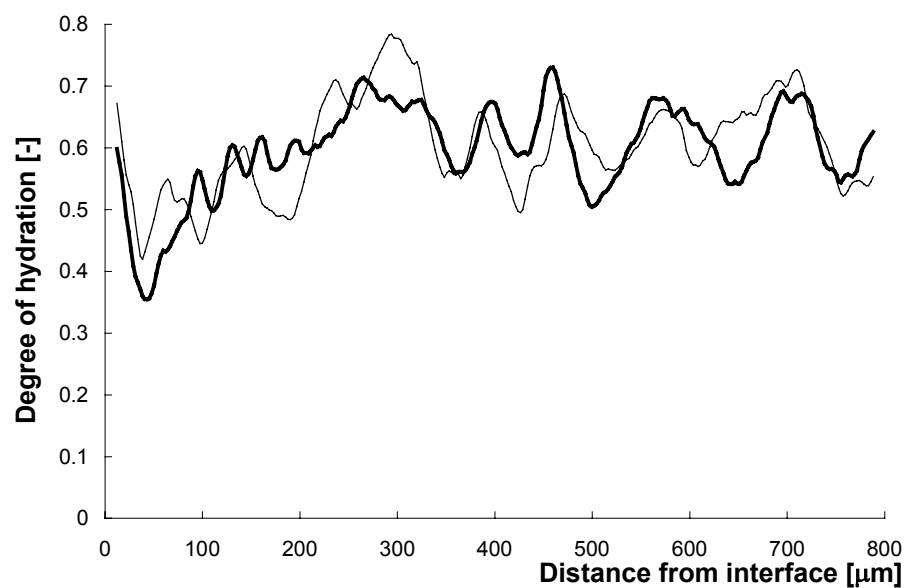


Figure 9.16 – Degree of hydration (calculated with Eq. 9.1) as a function of the distance from the interface on the basis of two different sets of BE images

### 9.6.3 Discussion and conclusions

Both the BE image (Figure 9.13) and the plots in Figure 9.14 show that there is a region, about 40  $\mu\text{m}$  wide, with very high porosity at the interface with the pumice grain. This was



observed before in the case of saturated synthetic LWA [Helland & Maage 1993]. A possible explanation is that water and air came out of the LWA, creating a high porosity zone at its outer rim. At other points along the interface (not shown in Figure 9.13) large circular air voids,  $\sim 50 \mu\text{m}$  diameter, were present right at the interface. Air may have escaped from the pumice grain that was certainly not saturated after 1 day under water [BSF 2002].

The degree of hydration plotted in Figure 9.16 was calculated with Eq. 9.1 on the basis of the BE images; it is evident that the degree of hydration at the interface is very low. In fact, a relatively high amount of anhydrous cement is present at the interface (Figure 9.15), especially if one considers that very little cement is present there at all (notice the local high porosity in Figure 9.14). One would expect the degree of hydration of the cement at the interface to be very high, because of the high local w/c ratio and the supply of water from the pumice. In fact, the low degree of hydration measured at the interface could be explained by water having been pulled out of the interface porosity. This explanation is confirmed by two observations:

- 1) From  $200 \mu\text{m}$  to  $350 \mu\text{m}$  from the interface, all around the LWA a denser region of paste is observed, where the degree of hydration is higher than average and very little anhydrous cement is found (Figures 9.15-9.17). This region, that had dense initial packing because of being far from the interface, has probably taken advantage of the water coming from the pumice grain to reach a higher degree of hydration.
- 2) The pores observed at the interface are larger than the ones in the paste, and the largest pores are emptied first in a self-desiccating system (see sec. 9.5).

Thus, a possible explanation of what observed is that, because the water in the LWA is insufficient to cure the whole cement paste, water was sucked into the cement paste not only from the aggregate but also from the interface. A rim around the pumice that had a high porosity and little hydrated cement was created this way. The effect of the curing water was seen in a small area from  $200 \mu\text{m}$  until about  $350 \mu\text{m}$  from the LWA (Figure 9.16). Probably, the increased hydration in this area would not compensate, in the global properties of the composite, the fact that a very bad interface was created. The principal reason for this phenomenon to occur is the insufficient amount of curing water provided to the hydrating system.

## 9.7 Mortars with different pumice content

### 9.7.1 Materials

Three mortar mixtures with the same cement paste but different contents of saturated pumice were mixed: reference mix without LWA,  $\sim 4\%$ , and  $\sim 8\%$  LWA by volume. Mix compositions are shown in Figure 9.17 and Table 9.2. The two LWA mixes were obtained

by replacing a fraction of the normal weight aggregates with the same volume of saturated pumice. The pumice was vacuum saturated according to the procedure described in sec. 9.3 and contained 38% water by weight. In this case the pumice was not in surface dried conditions, but excess water was removed mechanically.

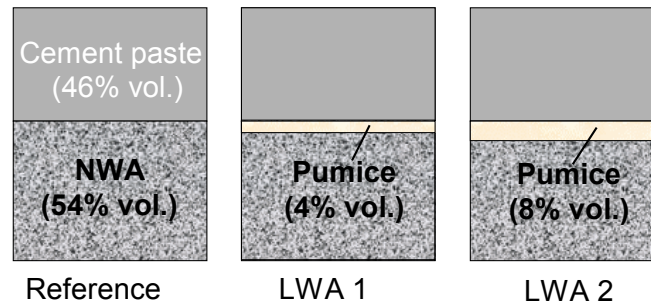


Figure 9.17 – Schematic representation of the volume fractions of the mortar mixes (Table 9.2)

The cement paste used was described in sec. 9.2.2. About 1.5 l of each mortar were mixed in a Hobart mixer. The water was inserted first into the mixer, then the cement was added and finally the aggregate, ending with the pumice fraction. Total mixing time was approximately 5 minutes.

Table 9.2 – Mixture compositions of LWAC with different particle size of the LWAs

Mixture	Reference	LWA 1	LWA 2
w/b ratio (without entrained water)	0.30	0.30	0.30
w/b ratio (with entrained water)	0.30	0.33	0.35
	[kg/m <sup>3</sup> ]	[kg/m <sup>3</sup> ]	[kg/m <sup>3</sup> ]
Cement 135 (Portland)	775	775	775
Water	225	225	225
Pumice 1 1.18-2.36 mm (dry)	-	54	108
Quartz sand, 0-4 mm	1409	1281	1171
Superplasticizer WRDA-19	9	9	9
Water in pumice	-	21	42

## 9.7.2 Methods

### *Autogenous deformation*

The cement paste was cast into corrugated, tight, low-density polyethylene plastic moulds and vibrated on a vibrating table. Length of the samples was approximately 300 mm. The moulds were specially designed to minimize restraint on the paste and were watertight [Jensen & Hansen 1995]. The moulds were similar to the ones used for the measurements of autogenous deformation of cement paste (Chapter 3). The CT1 digital dilatometer allowed measuring linear autogenous deformation of the mortars from the moment of setting. The device consisted of a measuring bench of stainless steel in which the specimen was longitudinally supported by two parallel cylindrical 20 mm-diameter rods. A

Mitutoyo ID-C digital gauge recorded length changes to the nearest 1  $\mu\text{m}$ . The specimens were kept in a room at  $23\pm 1^\circ\text{C}$ . They were supported by special racks during hardening and manually transferred to the dilatometer only for measuring. Measurements started about 4 hours after casting.

### *Compressive strength*

Compressive strength was measured on 2-inch cubes at 3 days, 7 days, and 28 days. For each mixture, age and curing condition, two cubes were tested. Cubes were cast into steel molds and demolded after 1 day. The cubes were kept at  $23\pm 1^\circ\text{C}$ . After demolding, the two LWA mixes were cured in sealed conditions. For the reference mix two different curing regimes, sealed and underwater, were employed.

### *Non-evaporable water content*

Pieces of mortar were collected from the inner core of the 2 inch-cubes crushed in the compressive strength test. Non-evaporable water was measured for all mixes and curing conditions at 3 days, 7 days, and 28 days of age. The procedure for measuring the non-evaporable water content was the same as the one used for cement paste (sec. 9.5). A further correction had to be made for the loss on ignition of the normal sand and the pumice, which were previously measured. About 10 g of crushed mortar were weighed in each crucible; this quantity was greater than for cement paste to ensure homogeneity of the sample.

### *Modeling of internal curing with the Hard Core Soft Shell model*

The mixtures were simulated with the Hard-Core Soft-Shell (HCSS) model [Bentz et al. 1999] to calculate the fraction of paste within a certain distance from the LWA. The input of the model is the particle size distribution of the NWA and of the LWA. Assuming a transport distance of the curing water from the saturated LWA (the same for all LWA), the corresponding volume of cured paste is calculated. The HCSS model is more accurate than the equations developed by Lu & Torquato [1992], since it takes into account the presence of the NWA in the mortars [Bentz & Snyder 1999].

## **9.7.3 Results**

Figure 9.18 shows the autogenous deformation of the three mortars measured from the moment of setting. In Figure 9.19 the compressive strength of the mortars, measured on 2-inch cubes, is shown. In Figure 9.20 the degree of hydration, calculated from non-evaporable water content, is represented.

In Figures 9.21 and 9.22, some results of the numerical simulation of the two LWA mixtures with the HCSS model are presented. Figure 9.21 shows the fraction of paste within a certain distance from the rim of the LWA. In Figure 9.22, 2D plots from the 3D models of the two LWA mixtures are shown, where different tonalities of gray indicate the internally cured volume.

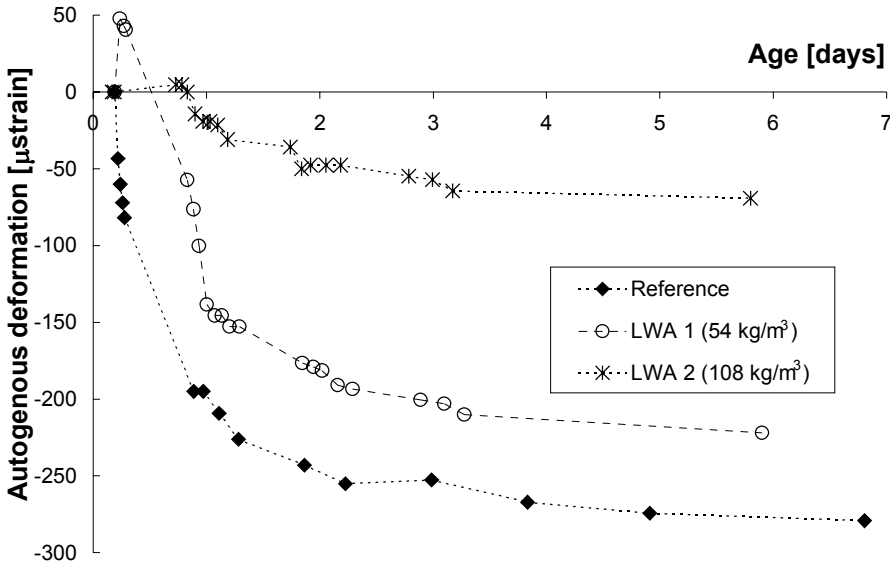


Figure 9.18 – Autogenous deformation of mortars (Table 9.2)

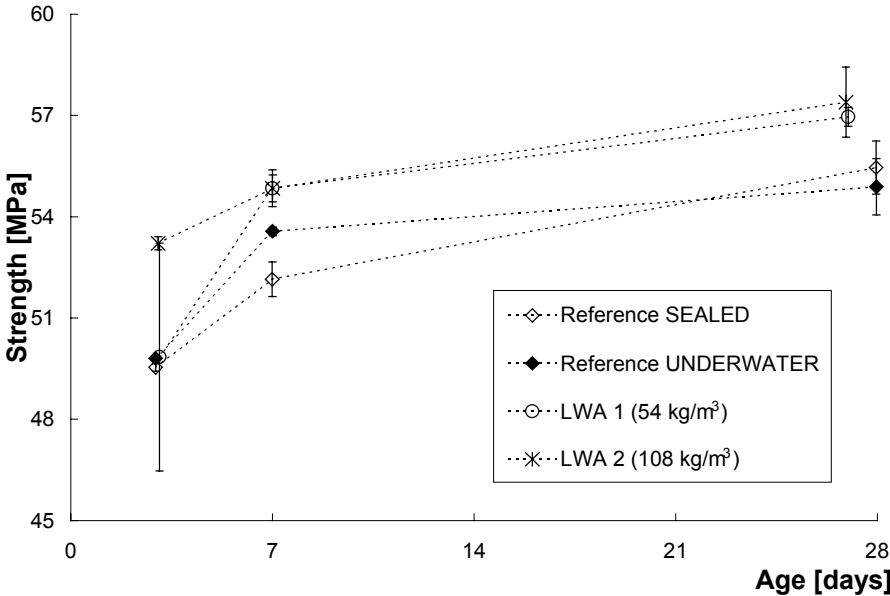


Figure 9.19 – Compressive strength of mortars (Table 9.2) measured on 2 inch-cubes. The average and the standard deviation of two cubes are indicated

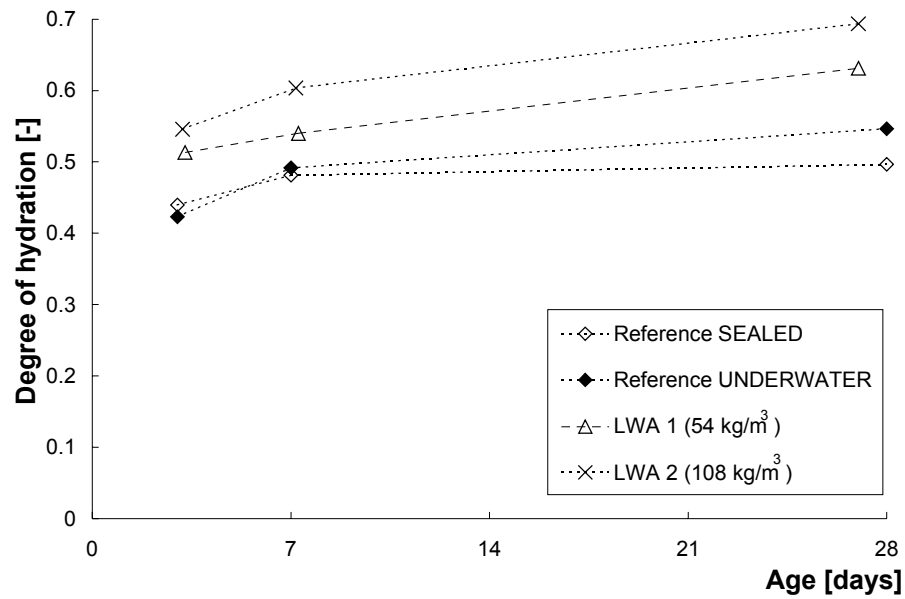


Figure 9.20 – Degree of hydration of mortars (Table 9.2) calculated on the basis of non-evaporable water measurements. The average value of two samples is indicated

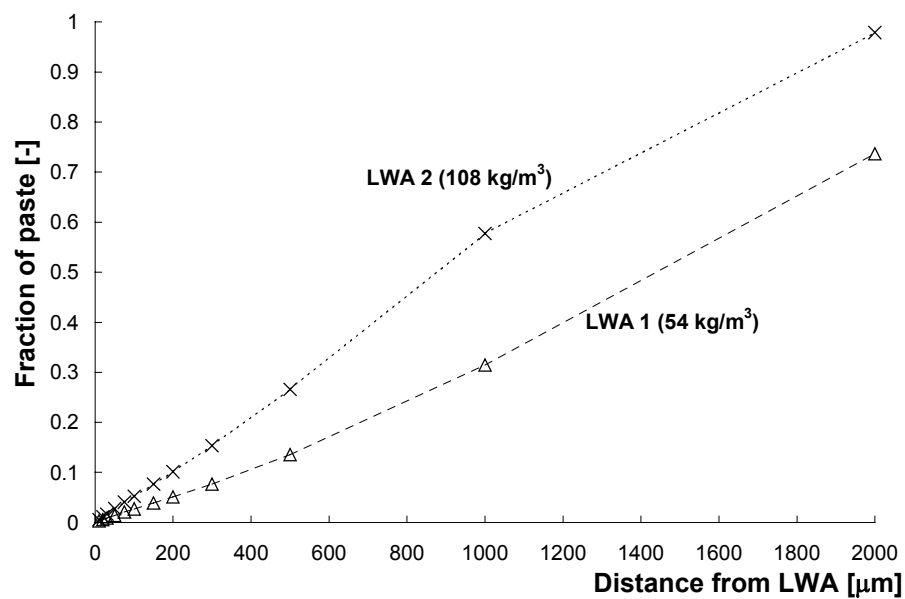


Figure 9.21 – Fraction of paste within a fixed distance from the LWA, calculated with the HCSS model

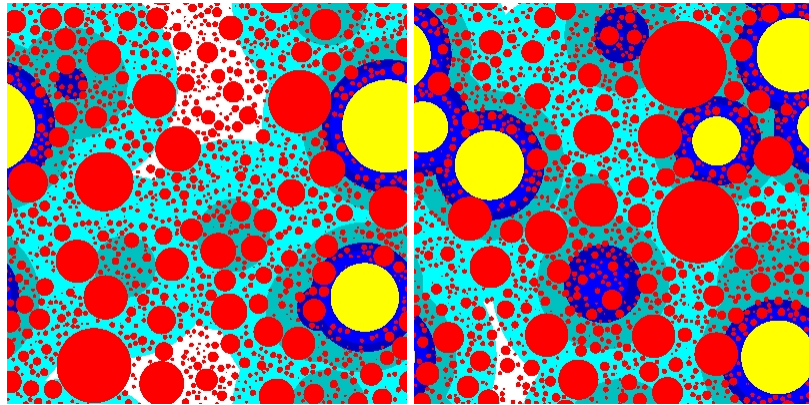


Figure 9.22 – 2D plots of the HCSS model of the LWA mixtures 1 (left) and 2 (right). LWA are white. Lighter shades of gray indicate the regions of the paste progressively farther away from the LWA

#### 9.7.4 Discussion and conclusions

The two LWA mixtures studied were designed having in mind the theoretical quantity of entrained water needed to avoid self-desiccation (see Appendix C). LWA 2 contained a sufficient quantity to avoid it, LWA 1 about half of that amount. Since internal RH was not measured on these mixtures, no direct proof of the success of this approach is available. Nevertheless, both the available experimental results and the numerical simulation show clear trends.

Autogenous shrinkage of mixture LWA 2 was about 1/4 of the reference and 1/3 of mixture LWA 1 (Figure 9.18). Compressive strength of the two LWA mixtures was higher than for the reference mixtures and LWA 2 had the highest strength (Figure 9.19). The same is valid for the degree of hydration, where the two mixtures with LWA performed better than the cubes cured underwater (Figure 9.20), clearly showing the advantages of internal curing over water ponding in the case of HPC. All these data confirm that at least a part of the water absorbed in the LWA was available for transport to the cement paste.

The shrinkage of mixture LWA 1 also confirms that the water in the LWA was insufficient to avoid self-desiccation, in agreement with the calculations (Appendix C). It must be noticed that most of the shrinkage occurred in the first 3 days, and took place after an initial expansion. Also mixture LWA 2, which was designed to avoid self-desiccation, showed some minor shrinkage, most of it in the first 3 days. The causes of this fact could be:

- 1) The quantity of entrained water was insufficient to totally compensate for self-desiccation of the paste. This means that the amount calculated in Appendix C was underestimated. This might be the case, since the coefficients used should vary according to the type of cement. However, there is good agreement between the final calculated value and the measured chemical shrinkage of the cement paste (see Figure 9.10 and Appendix C).
- 2) The transport distance the entrained water had to cover was too long (Figure 9.21). However, it was observed that shrinkage occurred mostly in the

first 3 days, when no depercolation of the capillary pores had taken place and transport of water should be very rapid. This indication is also confirmed by the x-ray experiments (sec. 9.5).

- 3) Some of the entrained water, and some water present on the surface of the LWA, might have come out during mixing. According to the calculations in Appendix C, at low w/c ratio (below 0.36) an increase of the initial w/c ratio leads to a higher amount of entrained water needed to totally avoid self-desiccation.
- 4) In the first days, when shrinkage occurred, the RH drop in the cement paste was very small and possibly not sufficient to pull the water out of the LWA. It was shown in sec. 9.3 that a relatively high amount of absorbed water remains in the pumice at high RH. The same situation might have occurred in the LWA mortars in the first days: the paste was self-desiccating but the capillary depression in the pore water was not sufficient to pull out sufficient water from the LWA.
- 5) Another possibility is that the force that drove water from the LWA was very small, so that the transport was not quick enough to avoid some self-desiccation of the paste. It is pointed out that most of the curing water for the cement paste is needed in the first days, since most of the chemical shrinkage occurs at this stage (Figure 9.10). Nevertheless, the degree of hydration of the LWA mortars (Figure 9.20) was higher than the one of the reference at all ages, indicating that some internal curing took place at least from 3 days of age.

Simulation results of the HCSS model (Figures 9.21-22) show that, because of the small amount of LWA in the mixes (4% and 8% by volume), a transport distance of 2 mm was needed to cure the whole cement paste in mix LWA 2, while it cured only 70% in mix LWA 1 (Figure 9.21). Since most of the autogenous deformation takes place in the first 3 days, transport of water is not hampered by depercolation of the cement paste and may occur on large distances. Nevertheless, the transport through the capillary pores might be very slow, since the driving force, a small drop of the RH, is also very small.

As a conclusion of the experiments and numerical simulations on mortars, it was observed that mortars with improved strength, enhanced degree of hydration and reduced autogenous shrinkage could be obtained by addition of saturated pumice aggregates. Internal curing of 2-inch cubes was, for strength and degree of hydration, more efficient than curing underwater. The LWA mortar with higher pumice and entrained water content (calculated in order to avoid self-desiccation) had slightly higher strength, higher degree of hydration and much less shrinkage than the mortar with half the amount of LWA. Most of the shrinkage occurred in the first 3 days, when depercolation of the capillary porosity was not an issue.

## 9.8 Conclusions

X-ray absorption showed that most of the transport of water from saturated LWA to hydrating cement paste occurs in the first days after casting. This is also the period when the greatest part of the chemical shrinkage takes place. On the other hand, most of the autogenous shrinkage is also concentrated in the first days. In this period, transport of water within cement paste should be a relatively fast process (as shown indeed by the x-ray study), since the capillary pores are not depercolated yet. As a consequence, to avoid self-desiccation shrinkage in the first days after casting, entraining a large amount of water in the LWA is more important than having the LWA well dispersed in the mix, with very short transport distances.

An additional issue that emerged in this study is the importance of the pore structure of the pumice in the internal curing process. The different pumice fractions show different porosity, absorption, and desorption. The smaller fractions have lower absorption, but they release a greater percentage of the absorbed water at the RH of practical interest. Absorption-desorption isotherms and Low Temperature Calorimetry indicated the presence of inkbottle pores in the pumice aggregates. To design a LWA mixture, one should also take into account the amount of entrained water that will actually remain inside the LWA, basically useless for internal curing.

Finally, the study of an interface between pumice and cement paste showed a worst-case scenario: Due to insufficient water entrained into the pumice, the hydrating cement paste pulled water out of the interface, preventing further hydration and leaving a very porous and weak region around the LWA. To avoid this inconvenience, sufficient water must be entrained in the LWA.



# Epilogue

---



# Chapter Ten

## Conclusions and further research

---

### 10.1 Conclusions

In this thesis, autogenous deformation of Portland and BFS cement pastes were measured at different temperatures. Portland cement paste showed high shrinkage around setting, followed by a sudden reduction of the shrinkage rate. BFS cement paste expanded around setting, but the subsequent shrinkage was greater than for Portland cement pastes. Shrinkage of Portland cement pastes was a function of the degree of hydration, while pastes containing BFS did not show a systematic dependence of the autogenous deformation on the curing temperature. Self-desiccation shrinkage was related to self-desiccation using the capillary tension approach. The tensile stresses in the pore water were calculated from the measured internal RH of the cement pastes, once compensated for the influence of dissolved salts. Only a part of the measured shrinkage could be explained with this approach, which assumed linear elastic behavior of the cement pastes. Additional shrinkage may have been caused by plastic deformation and creep of the cement paste under internal stress, conversion of ettringite into monosulphate, and consumption of calcium hydroxide crystals in the pozzolanic reaction.

Autogenous deformation of concrete realized with the same cement pastes was measured at different temperatures. Portland cement concrete showed a bilinear shrinkage behavior similar to the cement paste. Concrete containing BFS showed later development of shrinkage, preceded by expansion, but the shrinkage after one week was higher than for Portland cement concrete. Higher temperatures accelerated the occurrence of shrinkage, but did not significantly influence its magnitude. Composite models based on the deformation and the early-age mechanical properties of the cement paste and on the mechanical properties of the aggregates allowed calculating the autogenous shrinkage of Portland cement concrete with fair accuracy.

In LWAC, incorporation of wet LWA in the mix produced early-age expansion in place of shrinkage. The cause of the bulk expansion was the expansion of the cement paste hardening in saturated conditions due to internal curing, as was confirmed by

analytical calculations. Early-age expansion was strongly dependent on the degree of saturation of the LWA and to a lesser extent on their particle size, being larger for smaller LWA. These facts showed the impact on the internal curing process of the quantity of entrained water and of the distance of water penetration into the hardening cement paste. Transport of water from the LWA to the hardening cement paste was measured by x-ray absorption. This transport occurred mostly in the first days after casting and was active until a few mm from the rim of the LWA. The development in time of the amount of water transported from the LWA closely followed the development of chemical shrinkage in the paste. Properties of the LWA favorable for internal curing, such as a high porosity and an open pore structure, were pointed out and measured. Models to calculate the amount of entrained water necessary to avoid self-desiccation were derived taking into account the influence of supplementary cementitious materials. LWAC mixtures designed with these models showed negligible autogenous shrinkage and slightly increased strength and degree of hydration.

## **10.2 Recommendations**

Some practical recommendations about internal curing and LWAC:

- LWA do not necessarily have a detrimental effect on strength, if they possess good mechanical properties. In this thesis, almost no effect was measured on 28-day strength on concretes with water/binder ratio 0.35, where about 35% by volume of the NWA was substituted with Liapor 9.5 or Liapor 8. However, the elastic modulus had a 30% reduction, which is advantageous for the reduction of the early-age stress but might increase the deformations of the structure.
- Since some of the water absorbed by the LWA will not be released to the hardening cement paste, an amount of water more than sufficient to counteract self-desiccation must be entrained in the LWA.
- LWA with an open pore structure must be used. This ensures quick absorption underwater and release of the water in the concrete mix at high internal RH.

## **10.3 Future research**

The following are indications about possible future research in the field of autogenous deformation:

- The reliability of the different methods used to measure autogenous deformation of paste and concrete must be assessed and a standard method should be developed. A RILEM committee (TC-DTD) about test methods for autogenous deformation is working in this direction.

- A closer examination of setting and straightforward methods to measure it must be adopted. Confusion between deformations happening before and after setting can lead to significant differences in the measured values.
- Plastic deformations and creep on early-age deformations must be the object of further study. Nanoindentation techniques [Acker 2001] might help defining mechanical properties and creep of CSH gel, CH crystals and anhydrous cement.
- The relationships between hydration, microstructure formation, pore structure evolution, and self-desiccation could be studied with simulated cementitious materials [Ye et al. 2003]. The aim of this study would be calculating self-desiccation shrinkage directly from the mix composition of the cement paste. However, a problem of resolution of the computer-simulated microstructures (which is at the moment about tenths of  $\mu\text{m}$ ) does not allow resolving the smallest capillary pores, which are the relevant ones for the self-desiccation process. A possible solution could be a multiscale approach that incorporates a model for the pore structure of the smallest capillary pores together with the pore structure of the CSH gel.



# References

---

- ACI 233R-95 (1995), Ground granulated blast-furnace slag as a cementitious constituent in concrete, 18 pp., ACI, Farmington Hills, Michigan.
- P. Acker (2001), 'Micromechanical analysis of creep and shrinkage mechanisms', Proc. 6<sup>th</sup> Int. Conf. Creep, Shrinkage and Durability Mechanics of Concrete and Other Quasi-Brittle materials, eds. F.-J. Ulm, Z.P. Bazant & F.H. Wittmann, Cambridge, MA, August 20-22, Elsevier Science Ltd, pp. 15-26.
- P.-C. Aïtcin (1998), High-Performance Concrete, E&F SPON, London.
- P.-C. Aïtcin, G. Haddad & R. Morin (2002), 'Controlling Plastic and Autogenous Shrinkage in High-Performance Concrete Structures by Early Water Curing', Presented at ACI Fall 2002 Convention, Session Autogenous deformation of concrete, Phoenix, AZ.
- S. Aroni & M. Polivka (1967), 'Effect of expanded shale aggregate on properties of expansive-cement concrete', Proc. RILEM Symp. On Testing and Design Methods of Lightweight Aggregate Concretes, Ed. J. Ujhelyi, Budapest, Hungary.
- ASTM C128-97 (1997), Standard Test Method for Specific Gravity and Absorption of Fine Aggregate, ASTM International.
- R. Badmann, N. Stockhausen & M.J. Setzer (1981), The Statistical Thickness and the Chemical Potential of Adsorbed Water Films, Journal of Colloid and Interface Science, 82(2) 534-42.
- R.F.M. Bakker (1983), 'Permeability of blended cement concretes', ACI SP79, Detroit, pp. 589-605.
- D. H. Bangham & N. Fakhoury (1931), The swelling of charcoal, Royal Society of London, CXXX (Series A) 81-89.
- L. Barcelo (1997), 'Béton au jeune âge, mesure en continu des déformations endogènes de la phase liante, dès le coulage du matériau', Mémoire de D.E.A., INSA Lyon, LAFARGE LCR.
- L. Barcelo (2002), 'Chemical shrinkage', Early age cracking in cementitious systems, ed. A. Bentur, RILEM TC 181-EAS Committee, RILEM, Cachan, pp. 22-28.
- L. Barcelo, S. Boivin, S. Rigaud, P. Acker, B. Clavaud & C. Boulay (1999), 'Linear vs. volumetric autogenous shrinkage measurement: Material behaviour or experimental artefact?', Proc. 2<sup>nd</sup> Int. Res. Sem. on Self-desiccation and its Importance in Concrete Technology, Lund, Sweden, pp. 109-125.
- V. Baroghel-Bouny, M. Mainguy, T. Lassabatere & O. Coussy (1999), Characterization and identification of equilibrium and transfer moisture properties for ordinary and high-performance cementitious materials, Cem Concr Res 29(8) 1225-1238.

- 
- J. Baron & M. Buil (1979), Comments on the paper “Mechanical features of chemical shrinkage of cement pastes” by N. Setter & D.M. Roy, *Cem Concr Res* 9(4) 545-547.
  - Z. P. Bažant & F. H. Wittmann (1982), *Creep and shrinkage in concrete structures*, John Wiley & Sons, New York.
  - F. Beltzung, F.H. Wittmann & L. Holzer (2001), ‘Influence of composition of pore solution on drying shrinkage’, *Proc. 6<sup>th</sup> Int. Conf. Creep, Shrinkage and Durability Mechanics of Concrete and Other Quasi-Brittle materials*, eds. F.-J. Ulm, Z.P. Bazant & F.H. Wittmann, Cambridge, MA, August 20-22, Elsevier Science Ltd, pp. 39-48.
  - A. Bentur & K. van Breugel (2002), ‘Internally cured concretes’, *Early age cracking in cementitious systems*, ed. A. Bentur, RILEM TC 181-EAS Committee, RILEM, Cachan, pp. 339-353.
  - A. Bentur, R.L. Berger, J.H. Kung, N.B. Milestone & J.F. Young (1979), *Structural Properties of Calcium Silicate Pastes: II, Effect of Curing Temperature*, *J Amer Ceram Soc* 62(7-8) 362-366.
  - A. Bentur, S. Igarashi & K. Kovler (1999), ‘Control of autogenous shrinkage stresses and cracking in high strength concretes’, *Proc. 5th Int. Symp. on Utilization of High Strength/High Performance Concrete*, Sandefjord, Norway, pp. 1017-1026.
  - A. Bentur, S. Igarashi & K. Kovler (2001), *Prevention of autogenous shrinkage in high-strength concrete by internal curing using wet lightweight aggregates*, *Cem Concr Res* 31(11) 1587-1591.
  - D.P. Bentz (2000), *CEMHYD3D: A Three-Dimensional Cement Hydration and Microstructure development Modelling Package. Version 2.0*, NIST Internal Report 6485, Gaithersburg, MD.
  - D.P. Bentz (2002a), private communication.
  - D.P. Bentz (2002b), *Influence of Curing Conditions on Water Loss and Hydration in Cement Pastes with and without Fly Ash Substitution*, NIST Internal Report 6886, Gaithersburg, MD.
  - D.P. Bentz & E.J. Garboczi (1991), *Simulation Studies of the Effects of Mineral Admixtures on the Cement Paste-Aggregate Interfacial Zone*, *ACI Mater J* 88(5) 518-529.
  - D.P. Bentz & K.K. Hansen (2000), *Preliminary observations of water movement in cement pastes during curing using X-ray absorption*, *Cem Concr Res* 30(7) 1157-1168.
  - D.P. Bentz & K.A. Snyder (1999), *Protected paste volume in concrete: extension to internal curing using saturated lightweight fine aggregate*, *Cem Concr Res* 29(11) 1863-1867.
  - D.P. Bentz, E.J. Garboczi & D.A. Quenard (1998), *Modelling drying shrinkage in reconstructed porous materials: application to porous Vycor glass*, *Modelling Simul Mater Sci Eng* 6 211-236.
  - D.P. Bentz, E.J. Garboczi & K. A. Snyder (1999), *A hard core/soft shell microstructural model for studying percolation and transport in three-dimensional composite media*, NIST Internal Report 6265, Gaithersburg, MD.
  - D.P. Bentz, X. Feng, C.J. Haecker & P. Stutzman (2000), *Analysis of CCRL Proficiency Cements 135 and 136 Using CEMHYD3D*, NIST Internal Report 6545, Gaithersburg, MD.
  - D.P. Bentz, M.R. Geiker & K.K. Hansen (2001a), *Shrinkage-reducing admixtures and early-age desiccation in cement pastes and mortars*, *Cem Concr Res* 31(7) 1075-1085.
  - D.P. Bentz, K.K. Hansen, H.D. Madsen, F. Vallee & E.J. Griesel (2001b), *Drying/hydration in cement pastes during curing*, *Mater Struct* 34(243) 557-565.
  - D.P. Bentz, O.M. Jensen, K.K. Hansen, J.F. Olesen, H. Stang, & C.J. Haecker (2001c), *Influence of Cement Particle Size Distribution on Early Age Autogenous Strains and Stresses in Cement-Based Materials*, *J Amer Ceram Soc* 84(1) 129-135.



- D.P. Bentz, M. Geiker & O.M. Jensen (2002), On the mitigation of early age cracking, Proc. 3<sup>rd</sup> Int. Sem. on Self-desiccation and Its Importance in Concrete Technology, Lund, Sweden, pp. 195-204.
- S. Bernander (1982), 'Temperature stresses in early-age concrete due to hydration', Proc. Int. Conf. on Concrete at Early Ages, RILEM, Paris, Vol. II, pp. 218-221.
- J. Bijen (1996), Blast furnace slag cement for durable marine structures, CIP Royal Library Den Haag, Stichting Betonprisma, 's-Hertogenbosch, The Netherlands.
- J. Bisschop (2002), Drying shrinkage microcracking in cement-based materials, Ph.D. thesis. Delft University of Technology, Delft, The Netherlands.
- J. Bisschop, P. Lura & J.G.M. van Mier (2001), Shrinkage microcracking in cement-based materials with low water-cement ratio, Concrete Science and Engineering 3 151-156.
- Ø. Bjontegaard (1999), Thermal dilation and autogenous deformation as driving forces to self-induced stresses in high performance concrete, Ph.D. thesis, NTNU Division of Structural Engineering, Trondheim, Norway.
- T.W. Bremner & T.A. Holm (1986), Elastic Compatibility and the Behavior of Concrete, ACI Journal 83(2) 244-250.
- T.W. Bremner, J. Cano, B. Balcom & T.A. Holm (2002), 'Use of Magnetic Imaging to Study Moist Curing', Presented at ACI Fall 2002 Convention, Session High-Performance Structural Lightweight Concrete, Phoenix, AZ.
- K. van Breugel (1991), Simulation of hydration and formation of structure in hardening cement-based materials, Ph.D. thesis, Delft University of Technology, Delft, The Netherlands.
- K. van Breugel (2001), Numerical modelling of volume changes at early ages - Potential, pitfalls and challenges, Mater Struct 34(239) 293-301.
- K. van Breugel & J. de Vries (1999), 'Mixture optimization of HPC in view of autogenous shrinkage', Proc. 5<sup>th</sup> Int. Symp. on Utilization of High Strength/High Performance Concrete, Sandefjord, Norway, 20-24 June 1999, Vol. II, pp. 1041-1050.
- BSF (2002), Autogenous Curing of High Strength Cementitious Materials, United States-Israel Binational Science Foundation (BSF), Report of First Year Study, Technion, Israel.
- CCRL (2000), Final Report Portland Cement proficiency Samples Number 135 and 136, Cement and Concrete Reference Laboratory at NIST, Gaithersburg MD.
- P.P. Budnikov & M.I. Strelkov (1966), 'Some recent concepts on Portland cement hydration and hardening, Proc. Symp. on Structure of Portland cement paste and concrete', ACI Special report 90, pp. 447-464.
- M. Buil (1979), Contribution à l'étude du retrait de la pâte Studies of the shrinkage of hardening cement paste (in French), Ph.D. thesis, Rapport de recherche LPC No. 92, Laboratoire Central des Ponts et Chaussées, Paris, France.
- J.P. Charron, J. Marchand & B. Bissonette (2001), 'Early-age deformations of hydrating cement systems: comparison of linear and volumetric shrinkage measurements', Proc. RILEM Int. Conf. on Early Age Cracking in Cementitious Systems (EAC'01), 12-14 March 2001, Haifa, Israel, pp. 245-257.
- I. Chartschenko, V. Rudert & H.D. Wihler (1996), Factors affecting the hydration process and properties of expansive cement .1., Zement Kalk Gips Int 49(8) 432-&.
- C.W. Correns (1949), Growth and dissolution of crystal under linear pressure, Discussions of the Faraday Society 5 267-271.

- 
- H.E. Davis (1940), 'Autogenous volume changes of concrete', Proc. Am. Soc. Test. Mater., Vol. 40, pp. 1103-1112.
  - B.F. Dela (2000), Eigenstresses in hardening concrete, Ph.D. thesis. Department of Structural Engineering and Materials, The Technical University of Denmark, Lyngby, Denmark.
  - R.K. Dhir, P.C. Hewlett, J.S. Lota & T.D. Dyer (1994), An Investigation into the Feasibility of Formulating Self-Cure Concrete, *Mat Struc* 27(174) 606-615.
  - S. Diamond (2000), Mercury porosimetry - An inappropriate method for the measurement of pore size distributions in cement-based materials, *Cem Concr Res* 30(10) 1517-1525.
  - G. Fagerlund (1973), Determination of pore-size distribution from freezing-point depression, *Materiaux et Constructions* 6(33) 215-225.
  - Q.L. Feng & F.P. Glasser (1990), 'Microstructure, mass transport and densification of slag cement pastes', *Mat. Res. Soc. Symp. Proc.*, Vol. 178, pp. 57-65.
  - C. Ferraris & F.H. Wittmann (1987), Shrinkage mechanisms of hardened cement paste, *Cem Concr Res* 17(3) 453-464.
  - E.J. Garboczi (2002), Three-dimensional mathematical analysis of particle shape using X-ray tomography and spherical harmonics: Application to aggregates used in concrete, *Cem Concr Res* 32(10) 1621-1638.
  - E.J. Garboczi & D.P. Bentz (1997), Analytical formulas for interfacial transition zone properties, *Adv Cem Based Mater* 6(3-4) 99-108.
  - S. Garcia Boivin (2001), Retrait au jeune âge du béton - Développement d'une méthode expérimentale et contribution à l'analyse physique du retrait endogène (in French), Ph.D thesis, Etudes et Recherches des LPC, OA 37, Paris, France.
  - M.R. Geiker (1983), Studies of Portland Cement Hydration, Ph.D. thesis, Institute of Mineral Industry, The Technical University of Denmark, Lyngby, Denmark.
  - GNI (2002), GNI X-ray System, <http://www.gni.dk/>.
  - P. Goltermann (1994), Mechanical predictions on concrete deterioration. Part 1: eigenstresses in concrete, *ACI Mater J* 91(6) 543-550.
  - A.-W. Gutsch (1998), Stoffeigenschaften jungen Betons – Versuche und Modelle (in German), Ph.D. Thesis, Technical University of Braunschweig, Germany.
  - J. Hagymassy, J.R. Brunauer & R.S. Mikhail (1969), Pore structure analysis by water vapor adsorption, *Journal of Colloid and Interface Science* 29(3) 485-491.
  - T.A. Hammer (1992), 'High strength LWA concrete with silica fume - Effect of water content in the LWA on mechanical properties', Supplementary Papers in the 4<sup>th</sup> CANMET/ACI Int. Conf. On Fly Ash, Silica Fume, Slag and natural Pozzolans in Concrete, Turkey, pp. 314-330.
  - T.A. Hammer (1993), 'The maturation of mechanical properties of high strength concrete exposed to different moisture conditions', *Utilization of High Strength Concrete*, eds. I. Holand & E. Sellevold, Proc. Int. Symp., Lillehammer, Norway, pp. 1084-1091.
  - T.A. Hammer (2002), 'Is there a relationship between pore water pressure and autogenous shrinkage before and during setting?', Proc. 3<sup>rd</sup> Int. Sem. on Self-desiccation and Its Importance in Concrete Technology, Lund, Sweden, 15 June 2002, pp. 27-38.
  - T.A. Hammer, Ø. Bjøntegaard & E.J. Sellevold (2002a), 'Measurement methods for testing of early age autogenous strain', *Early age cracking in cementitious systems*, ed. A. Bentur, RILEM TC 181-EAS Committee, RILEM, Cachan, France, pp. 234-245.

- T.A. Hammer, Ø. Bjøntegaard & E.J. Sellevold (2002b), 'Internal curing – Role of Absorbed Water in Aggregates', Presented at ACI Fall 2002 Convention, Session High-Performance Structural Lightweight Concrete, Phoenix, AZ.
- S. Hanehara, H. Hirao & H. Uchikawa (1999), 'Relationship between autogenous shrinkage and the microstructure and humidity changes at inner part of hardened cement pastes at early ages', Proc. Int. Workshop Autoshrink'98, ed. E.-I. Tazawa, Hiroshima, Japan, E & FN SPON, London, pp. 89-100.
- K.K. Hansen & O.M. Jensen (1997), 'Equipment for Measuring Autogenous RH-Change and Autogenous Deformation in Cement Paste and Concrete', Proc. Int. Res. Sem. on Self-desiccation and its Importance in Concrete Technology, Lund, Sweden, pp. 27-30.
- K.K. Hansen, S.K. Jensen, L. Gerward & K. Singh (1999), 'Dual-energy X-ray absorptiometry for the simultaneous determination of density and moisture content in porous structural materials', Proc. 5<sup>th</sup> Symp. Build. Phys. Nordic Countries, Gothenburg, Sweden, pp. 281-288.
- T.C. Hansen & K.E.C. Nielsen (1965), Influence of aggregate properties on concrete shrinkage, ACI Journal 62(7) 783-794.
- P.F. Hansen & E.J. Pedersen (1977), Measuring instrument for the control of concrete hardening (in Danish), Nordisk Betong 21-25.
- A.M. Harrison, N.B. Winter & H.F.W. Taylor (1987), 'Microstructure and microchemistry of slag cement pastes', Mat. Res. Soc. Symp. Proc., Vol. 85, pp. 213-222.
- H. Hedlund & J.-E. Jonasson (2000), 'Effect on stress development of restrained thermal and moisture deformation', Proc. Shrinkage 2000 – Int. RILEM Workshop on Shrinkage of Concrete, Paris, France, pp. 355-375.
- S. Helland & M. Maage (1993), 'Strength loss in Un-remixed LWA Concrete, Proc. Int. Symp. Utilization of High Strength Concrete, eds. I. Holand & E. Sellevold, Lillehammer, Norway, pp. 744-751.
- R. L'Hermite (1960), 'Volume changes of concrete', Proc. 4<sup>th</sup> Int. Symp. On the Chemistry of Cement, Washington DC, Vol. II, pp. 659-694.
- J. Hill & J.H. Sharp (2002), The mineralogy and microstructure of three composite cements with high replacement levels, Cem Concr Comp 24(2) 191-199.
- K.H. Hiller (1964), Strength reduction and length changes in porous glasses caused by water vapour adsorption, J. Applied Physics 35 1622-1628.
- G.C. Hoff (2002), The use of lightweight fines for the internal curing of concrete, Report for Northeast Solite Corporation, Richmond, VA.
- D.W. Hobbs (1969), Bulk Modulus Shrinkage and Thermal Expansion of a Two Phase Material, Nature 222 849-851.
- D.W. Hobbs (1974), Influence of aggregate restraint on the shrinkage of concrete, ACI Journal 71 445-450.
- T.A. Holm (1980), 'Performance of Structural Lightweight Concrete in a Marine Environment', ACI SP65, ed. V.M. Malhotra, Proc. Int. Symp. St. Andrew By-The-Sea, Canada.
- T.A. Holm (2001), Lightweight Concrete and Aggregates, ASTM Standard Technical Publication 169C, 48 522-532.
- E.E. Holt & M.T. Leivo (1999), 'Autogenous shrinkage at very early ages', Proc. Int. Workshop Autoshrink'98, ed. E.-I. Tazawa, Hiroshima, Japan, E & FN SPON, London, pp. 133-140.
- C. Hua, P. Acker & A. Erlacher (1995), Analyses and models of the autogenous shrinkage of hardening cement paste: I. Modelling at macroscopic scale, Cem Concr Res 25(7) 1457-1468.

Japan Concrete Institute Committee on Autogenous Shrinkage (1999), Report on Autogenous Shrinkage of Concrete, Proc. Int. Workshop Autoshrink '98, ed. E.-I. Tazawa, Hiroshima, Japan, E & FN SPON, London, pp. 1-67.

- H.M. Jennings, B.J. Dagleish & P.L. Pratt (1981), Morphological development of hydrating tricalcium silicate as examined by electron microscopy techniques, *J Am Ceram Soc* 64 567–572.

- O.M. Jensen (1993a), Autogenous deformation and RH-change – self-desiccation and self-desiccation shrinkage (in Danish), TR 284/93, Building Materials Laboratory, The Technical University of Denmark, Lyngby, Denmark.

- O.M. Jensen (1993b), Autogenous deformation and RH-change – self-desiccation and self-desiccation shrinkage. Appendix - measurements and notes (in Danish), TR 285/93, Building Materials Laboratory, The Technical University of Denmark, Lyngby, Denmark.

- O.M. Jensen (1995), Thermodynamic limitation of self-desiccation, *Cem Concr Res* 25(1) 157-164.

- O.M. Jensen (1996), Dilatometer – further development, Building Materials Laboratory, The Technical University of Denmark, Lyngby, Denmark.

- O.M. Jensen (1997), HETEK – Control of early age cracking in concrete – Phase 2: Shrinkage of mortar and concrete, Report No. 110, Danish Road Directorate, Denmark.

- O.M. Jensen & P.F. Hansen (1995), A dilatometer for measuring autogenous deformation in hardening Portland cement paste, *Mater Struct* 28(181) 406-409.

- O.M. Jensen & P.F. Hansen (1996), 'Autogenous deformation and change of the relative humidity in silica fume-modified cement paste', *ACI Materials Journal* 93 (6) 539-543.

- O. M. Jensen & P. F. Hansen (1999), Influence of temperature on autogenous deformation and relative humidity change in hardening cement paste, *Cem Concr Res* 29(4) 567-575.

- O.M. Jensen & P.F. Hansen (2001a), Water-entrained cement-based materials. I. Principles and theoretical background, *Cem Concr Res* 31(5) 647-654.

- O.M. Jensen & P.F. Hansen (2001b), Autogenous deformation and RH-change in perspective, *Cem. Con. Res.* 31(12) 1859-1865.

- O.M. Jensen & P.F. Hansen (2002), Water-entrained cement-based materials II. Experimental observations, *Cem Concr Res* 32(6) 973-978.

- M.I. Khan, C.J. Lynsdale & P. Waldron (2000), Porosity and strength of PFA/SF/OPC ternary blended paste, *Cem Concr Res* 30(8) 1225-1229.

- E.A.B. Koenders (1997), Simulation of volume changes in hardening cement-based materials, Delft University of Technology, Ph.D. thesis, Delft, The Netherlands.

- K. Kohno, T. Okamoto, Y. Isikawa, T. Sibata & H. Mori (1999), Effects of artificial lightweight aggregate on autogenous shrinkage of concrete, *Cem Concr Res* 29(4) 611-614.

- H. Le Chatelier (1900), 'Sur les changements de volume qui accompagnent le durcissement des ciments', *Bull. Soc. Encour. Ind. Natl.* V, 5<sup>th</sup> series, pp. 54–57.

- Y. Li, B.W. Langan & M.A. Ward (1996), The strength and microstructure of high-strength paste containing silica fume, *Cem Concr Aggr* 18(2) 112-117

- F.W. Locher, W. Richartz & S. Sprung (1976), Erstarren von Zement (in German), *Zement Kalk Gips* 29(10) 435-442.

- S.J. Lokhorst (1998), Deformational behaviour of concrete influenced by hydration related changes of the microstructure, Research Report, Delft University of Technology, Delft, The Netherlands.

- P. Longuet, L. Burglen & A. Zelwer (1973), La phase liquide du ciment hydrate, *Revue Materiaux et Constructions* 676 35-41.
- B.L. Lu & S. Torquato (1992), Nearest-surface distribution-functions for polydispersed particle-systems, *Physical Review A* 45(8) 5530-5544.
- P. Lura & D.P. Bentz (2002), unpublished results.
- P. Lura & J. Bisschop (2003), On the origin of eigenstresses in Lightweight Aggregate Concrete, accepted for publication in *Cem Concr Comp*.
- P. Lura, O.M. Jensen & K. van Breugel (2002), 'Autogenous deformation and RH change in portland and Blast Furnace Slag cement pastes', *Proc. 3<sup>rd</sup> Int. Sem. on Self-desiccation and Its Importance in Concrete Technology*, 15 June, Lund, Sweden, pp. 127-137.
- P. Lura, K. van Breugel & H. de Vries (2002b), 'Experimental research about early-age creep of B65 and B85 concrete mixtures', *Proc. Int. Workshop on Control of Cracking in Early-Age Concrete*, eds. H. Mihashi & F.H. Wittmann, 23-24 August 2000, Sendai, Japan, Balkema, Lisse, pp.275-286.
- M.P. Lutz & R.W. Zimmerman (1996), Effect of the interphase zone on the bulk modulus of a particulate composite, *J Appl Mech-T ASME* 63(4) 855-861.
- C.G. Lynam (1934), 'Growth and Movement in Portland Cement Concrete', Oxford Univ. Press, London, pp. 26–27.
- S. Marciniak (2002), Autogenous deformations and relative humidity change: experimental studies, M.Sc. thesis, Department of Building Technology and Structural Engineering, Aalborg University, Aalborg.
- P. Morabito, Ø. Bjontegaard, K. van Breugel, P. Dalmagioni, H.-E. Gram, A.-W. Gutsch, H. Hedlund, J.-E. Jonasson, T. Kanstad, P. Lura, R. Pellegrini, F. Rostásy & E. Sellevold (2001), Round Robin Testing Programme. Equipments, testing methods, test results, Int. BriteEuram project IPACS (Improved Production of Advanced Concrete Structures), Luleå, <http://cassiopeia.anl.luth.se/>.
- M. Morioka, A. Hori, H. Hagiwara, E. Sakai & M. Daimon (1999), 'Measurement of autogenous length changes by laser sensors equipped with digital computer systems', *Proc. Int. Workshop Autoshrink'98*, ed. E.-I. Tazawa, Hiroshima, Japan, E & FN SPON, London, pp. 191-200.
- J. Müller-Rochholz (1979), Investigation of the absorption of water by Lightweight Aggregate from Cement Paste, *Journal of Lightweight Concrete* 1(1) 39-41.
- J.C. Nadeau (2002), Water-cement ratio gradients in mortars and corresponding effective elastic properties, *Cem Concr Res* 32(3) 481-490.
- S. Nagataki & H. Gomi (1998), Expansive admixtures (mainly ettringite), *Cem Concr Comp* 20(2-3) 163-170.
- C.M. Neubauer, H.M. Jennings & E.J. Garboczi (1996), A three-phase model of the elastic and shrinkage properties of mortar, *Adv Cem Based Mater* 4(1) 6-20.
- A.M. Neville (1995), *Properties of concrete*, John Wiley & Sons, New York (4th edition).
- A.M. Neville (1997), Aggregate bond and modulus of elasticity of concrete, *ACI Mater J* 94(1) 71-74.
- H.A. Neville & H.C. Jones (1928), 'The study of hydration changes by a volume-change method', *Colloid Symp. Monogr. VI*, pp. 309–318.
- L.F. Nielsen (1991), A research note on sorption, pore size distribution, and shrinkage of porous materials, TR 245/91, Building Materials Laboratory, The Technical University of Denmark, Lyngby, Denmark.

- 
- A.U. Nilsen & P.J.M. Monteiro (1993), Concrete - A 3 phase material, *Cem Concr Res* 23(1) 147-151.
  - A.U. Nilsen, P.J.M. Monteiro & O.E. Gjrv (1995), Estimation of the elastic moduli of lightweight aggregate, *Cem Concr Res* 25(2) 276-280.
  - C.L. Page & Ø. Vennesland (1983), Pore solution composition and chloride binding capacity of silica-fume cement pastes, *Mater Struct* 16(91) 19-25.
  - A.M. Paillere, M. Buil & J.J. Serrano (1989), Effect of Fiber Addition on the Autogenous Shrinkage of Silica Fume Concrete, *ACI Mater. J.* 86(2) 139-144.
  - L.J. Parrot, M. Geiker, W.A. Gutteridge & D. Killoh (1990), Monitoring Portland cement hydration – Comparison of methods, *Cem Concr Res* 20(6) 919-926
  - R. Philleo (1991), ‘Concrete Science and Reality’, *Materials Science of Concrete II*, eds. J.P. Skalny & S. Mindess, American Ceramic Society, Westerville, Ohio, pp. 1-8.
  - G. Pickett (1956), Effect of aggregate on shrinkage of concrete and a hypothesis concerning shrinkage, *ACI Journal* 52(5) 581-590.
  - T.C. Powers (1935), Absorption of water by Portland cement paste during the hardening process, *Industrial and Engineering Chemistry* 27(7) 790-794.
  - T.C. Powers (1965), ‘Mechanisms of shrinkage and reversible creep of hardening cement paste’, in *Proc. Int. Symp. Structure of Concrete and its behaviour under load*, Cem. & Concr. Ass., London, pp. 319-344.
  - T.C. Powers & T. L. Brownyard (1948), Studies of the physical properties of hardened Portland cement paste (9 parts), *J Amer Concr Inst* 43 (Oct. 1946 to April 1947), Bulletin 22, Research Laboratories of the Portland Cement Association, Chicago.
  - K. Rakel (1965), *Beitrag zur Bestimmung der Hydrationswrme von Zement* (in German), Ph.D. thesis, Aachen, Germany.
  - G. Ramesh, E.D. Sotelino & W.F. Chen (1996), Effect of transition zone on elastic moduli of concrete materials, *Cem Concr Res* 26(4) 611-622.
  - RILEM Technical Committee “Early Age Cracking in Cementitious Systems” TC 181-EAS (2002), ed. A. Bentur, *Early age cracking in cementitious systems*, RILEM, Cachan, pp. 388.
  - RILEM Technical Committee “Internal Curing of Concrete” TC-ICC (2002), Statement of work.
  - RILEM Technical Committee “Internal Curing of Concrete” TC-ICC (2003), Internal curing – definitions, in preparation.
  - P.E. Roelfstra, H. Sadouki & F.H. Wittmann (1985), *Le beton numerique*, *Mater Struct* 18 327–335.
  - F. Rosts, A.-W. Gutsch & M. Laube (1993), ‘Creep and relaxation of concrete at early ages – experiments and mathematical modelling’, *Proc. 5<sup>th</sup> Int. RILEM Symp. Creep and Shrinkage of Concrete*, Barcelona, pp. 453-458.
  - D.M. Roy & G.M. Idorn (1982), Hydration, Structure and properties of Blast Furnace Slag Cements, Mortars, and Concrete, *ACI Journal* 79(6) 444-457.
  - D.M. Roy, W. Jiang & M.R. Silsbee (2000), Chloride diffusion in ordinary, blended, and alkali-activated cement pastes and its relation to other properties, *Cem Concr Res* 30(12) 1879-1884.
  - H. Sadouki & F.H. Wittmann (2000), ‘Shrinkage and internal damage induced by drying and endogenous drying’, *Proc. Shrinkage 2000 – Int. RILEM Workshop on Shrinkage of Concrete*, Paris, pp. 299-314.

- I. Schackinger (2002), 'Early-Age Cracking Risk and Relaxation by Restrained Autogenous Deformation of Ultra High Performance Concrete', Bauingenieur Sonderpublikation, 4<sup>th</sup> Int. PhD Symposium, September 2002, Munich, Germany, Vol. 2, pp 203-210.
- G.W. Scherer (1999), Crystallization in pores, *Cem Concr Res* 29(8) 1347-1358.
- F. Schmidt-Döhl & F. Rostásy (1995), Crystallization and hydration pressure or formation pressure of solid phases, *Cem Concr Res* 25(2) 255-256.
- F. Schmidt-Döhl & K-Ch. Thienel (2000), 'Measurement of Swelling and Shrinkage of Lightweight Aggregate', Proc. 2<sup>nd</sup> Int. Symp. On Structural Lightweight Aggregate Concrete, Kristiansand, Norway, 18-22 June 2000, pp. 737-746.
- G. de Schutter, Fundamental and practical study of thermal stresses in hardening massive concrete elements (in Dutch), Ph.D. thesis, University of Gent, Gent, Belgium.
- K.L. Scrivener, A. Bentur & P.L. Pratt (1988), Quantitative Characterization of the Transition Zone in High Strength Concretes, *Advances in Cement Research* 1(4) 230-237.
- E.J. Sellevold & C.W. Richards (1972), Short-Time Creep Transition for Hardened Cement paste, *J Am Ceramic Soc* 55(6) 284-289.
- N. Setter & D.M. Roy (1978), Mechanical features of chemical shrinkage of cement paste, *Cem Concr Res* 8(5) 623-634.
- M.J. Setzer (1977), Einfluss des Wassergehals auf die Eigenschaften des erhärteten Betons (in German), *Deutscher Ausschuss für Stahlbeton* 280 (1977) 43-79.
- G. Sickert, P. Schwesinger & G. v. Haza-Radlitz (1999), 'Creep, shrinkage and creep recovery of HPLWA-Concrete', Proc. Int. Symposium on Utilization of High Strength / High Performance Concrete, Sandefjord, Norway, 20-24 June 1999, Vol. 2, pp.1301-1310.
- J. Skalný & J.F. Young (1980), Mechanisms of Portland cement hydration, 7<sup>th</sup> international Congress on the Chemistry of cement, Vol. I, Sub-theme II-1, Paris, pp.1/3-1/45.
- K. Snyder & D.P. Bentz (1998), Early age cement paste hydration at 90% relative humidity and the loss of freezable water, unpublished results.
- S.J. Song & H.M. Jennings (1999), Pore solution chemistry of alkali-activated ground granulated blast-furnace slag, *Cem Concr Res* 29(2) 159-170.
- I. Soroka (1979), Portland cement paste and concrete, Macmillan Press, London.
- M. Stroeven (1999), Discrete Numerical Modeling of Composite Materials, Ph.D. thesis, Delft University of Technology, Delft, The Netherlands.
- M.S. Sule (2003), Effect of Reinforcement on Early-Age Cracking in High Strength Concrete, Ph.D. Thesis, Delft University of Technology, Delft, The Netherlands.
- K. Takada, K. van Breugel, E.A.B. Koenders & N. Kaptijn (1999), 'Experimental Evaluation of Autogenous Shrinkage of Lightweight Aggregate Concrete', Proc. Int. Workshop Autoshrink'98, ed. E.-I. Tazawa, Hiroshima, Japan, E & FN SPON, London, pp. 221-230.
- E. Tazawa & S. Miyazawa (1995), Influence of cement and admixture on autogenous shrinkage of cement paste, *Cem Concr Res* 25 (2) 281-287.
- E. Tazawa, Y. Matsuoka, S. Miyazawa & S. Okamoto (1995), 'Effect of autogenous shrinkage on self stress in hardening concrete', Proc. Int. RILEM Symp. Thermal Cracking in Concrete at Early Ages, Munich, pp. 221-228.
- E. Tazawa, R. Sato, E Sakai & S. Miyazawa (2000), 'Work of JCI committee on autogenous shrinkage', Proc. Shrinkage 2000 – Int. RILEM Workshop on Shrinkage of Concrete, Paris, pp. 21-40.

- 
- Y. Tezuka, J.G. Djanikan, H. Uchikawa & S. Uchida (1986), 'Hydration characteristics and properties of mixtures of cement and high content of calcium', Proc. Symp. on Chemistry of Cement, Rio de Janeiro, Brazil, Vol. II, pp. 323–329
  - J.J. Thomas & H.M. Jennings (2001), 'Chemical aging and the colloidal structure of the C-S-H gel: implications for creep and shrinkage', Proc. 6<sup>th</sup> Int. Conf. Creep, Shrinkage and Durability Mechanics of Concrete and Other Quasi-Brittle materials, eds. F.-J. Ulm, Z.P. Bazant & F.H. Wittmann, Cambridge, MA, August 20-22, Elsevier Science Ltd, pp. 33-38.
  - A.M. Vaysburd (1996), Durability of Lightweight Concrete Bridges in Severe Environments, Concrete International 18 33-38.
  - C. Vernet & G. Cadoret (1992), Suivi en continu de l'évolution chimique et mécanique des BHP pendant les premiers jours (in French), Les Bétons à Hautes Performances – Caractérisation, durabilité applications, Presses de l'Ecole Nationale des Ponts et Chaussées, Paris, France.
  - R. Wasserman & A. Bentur (1996), Interfacial Interactions in Lightweight Aggregate Concretes and their Influence on the Concrete Strength, Cem Concr Comp 18(1) 67-76.
  - S. Weber & H.W. Reinhardt (1996), 'A Blend of Aggregates to Support Curing of Concrete', Proc. Int. Symp. on Structural Lightweight Concrete, eds. I. Holand, T.A. Hammer & F. Fluge, Sandefjord, Norway, pp. 662-671.
  - S. Weber & H.W. Reinhardt (1997), A New Generation of High Performance Concrete: Concrete with Autogenous Curing, Adv Cem Based Mater 6(2) 59-68.
  - S. Weber & H.W. Reinhardt (1999), 'Manipulating the water content and microstructure of high performance concrete using autogeneous curing', Modern concrete materials: binders, additions and admixtures, eds. R. Dhir & T. D. Dyer, Thomas Thelford, London, pp. 568-577.
  - E.J.W. Wensink, A.C. Hoffmann, M.E.F. Apol & H.J.C. Berendsen (2000), Properties of adsorbed water layers and the effect of adsorbed layers on interparticle forces by liquid bridging, Langmuir 16(19) 7392-7400.
  - E.M. Winkler (1973), 'Stone: Properties, Durability in Man's Environment', Applied Mineralogy 4, Springer-Verlag 1973, pp.113-125.
  - F.H. Wittmann (1976), 'The structure of hardened cement paste - A basis for a better understanding of the material properties', Proc. Conf. on Hydraulic cement paste: Their structure and properties, Sheffield, England, pp. 96-117.
  - F.H. Wittmann (1977), Grundlagen eines Modells zur Beschreibung charakteristischer Eigenschaften des Betons (in German), Deutscher Ausschuss für Stahlbeton 290 (1977) 42-101.
  - F.H. Wittmann (1992), 'On the interaction of gel particles in hydrating Portland cement', Hydration and Setting of Cements, ed. A. Nonat & J.C. Mutin, RILEM, E&FN Spon, London.
  - F.H. Wittmann (2001), 'Mechanisms and mechanics of shrinkage', Proc. 6<sup>th</sup> Int. Conf. Creep, Shrinkage and Durability Mechanics of Concrete and Other Quasi-Brittle materials, eds. F.-J. Ulm, Z.P. Bazant & F.H. Wittmann, Cambridge, MA, August 20-22, Elsevier Science Ltd, pp. 3-12.
  - C.E. Wuerpel (1946), Laboratory studies of concrete containing air-entraining admixtures, ACI Journal 42(4) 305-359.
  - X. Xu, L. Lohaus & M.J. Setzer (2001) 'Damping Behaviour of Hardened Cement Paste (hcp) in a Temperature Range between 20°C and 80°C: Effect of the Disjoining Pressure', Proc. 6<sup>th</sup> Int. Conf. Creep, Shrinkage and Durability Mechanics of Concrete and Other Quasi-Brittle materials, eds. F.-J. Ulm, Z.P. Bazant & F.H. Wittmann, Cambridge, MA, August 20-22, Elsevier Science Ltd, pp. 49-54.



- Y. Yamazaki, T. Monji & K. Sugiura (1976), 'Early age expanding behaviour of mortars and concretes using expansive additives of CaO-CaSO<sub>4</sub>-4CaO·3Al<sub>2</sub>O<sub>3</sub>·SO<sub>3</sub> system', 6<sup>th</sup> Int. Cong. on the Chemistry of Cement, Moscow, September 1974, Stroyizdat, Moscow III-5 pp. 192-195.
- C.C. Yang (1998), Effect of the transition zone on the elastic moduli of mortar, *Cem Concr Res* 28(5) 727-736.
- G. Ye, K. van Breugel and A. L. A. Fraaij (2003), Three-dimensional microstructure analysis of numerically simulated cementitious materials, *Cem Concr Res* 33(2) 215-222.
- M.H. Zhang & O.E. Gjörv (1990), Microstructure of the interfacial zone between lightweight aggregate and cement paste, *Cem Concr Res* 20(4) 610-618.
- M.H. Zhang and O.E. Gjörv (1991), Characteristics of Lightweight Aggregates for High-Strength Concrete, *ACI Mater J* 88(2) 150-158.
- X. Zhang, Y. Li & K. Wu (2000), 'Study on autogenous shrinkage and AC impedance of paste with additive's, *Proc. Shrinkage 2000 – Int. RILEM Workshop on Shrinkage of Concrete*, Paris, pp. 547-557.
- S. Zhutovsky, K. Kovler & A. Bentur (2001a), 'Efficiency of lightweight aggregates for internal curing of high strength concrete to eliminate autogenous shrinkage', *Proc. RILEM Int. Conf. on Early Age Cracking in Cementitious Systems (EAC'01)*, 12-14 March 2001, Haifa, Israel, pp. 365-373.
- S. Zhutovsky, K. Kovler & A. Bentur (2001b), 'Influence of Wet Lightweight Aggregate on Autogenous Shrinkage of Concrete at Early Ages', *Proc. 6<sup>th</sup> Int. Conf. Creep, Shrinkage and Durability Mechanics of Concrete and Other Quasi-Brittle materials*, eds. F.-J. Ulm, Z.P. Bazant & F.H. Wittmann, Cambridge, MA, August 20-22, Elsevier Science Ltd, pp. 697-702.
- S. Zhutovsky, K. Kovler & A. Bentur (2002a), 'Autogenous curing of High-Strength Concrete using pre-soaked pumice and perlite sand', *Proc. 3<sup>rd</sup> Int. Res. Sem. Self-desiccation and its importance in concrete technology*, 15 June, 2002, Lund, Sweden, pp. 161-173.
- S. Zhutovsky, K. Kovler & A. Bentur (2002b), 'Assessment of Distance of Water Migration in Internal Curing of High-Strength Concrete', Presented at ACI Fall 2002 Convention, Session Autogenous deformation of concrete, Phoenix, AZ.
- S. Zhutovsky, K. Kovler & A. Bentur (2003), Influence of cement paste matrix properties on the autogenous curing of High-Performance Concrete, submitted to *Cem Concr Comp*.
- T. Østergaard (2001), Measurements on water-entrained cement paste, Research report, Department of Building Technology and Structural Engineering, Aalborg University, Aalborg, Denmark.



# Appendix A

## Derivation of Raoult and Kelvin laws

---

### Introduction

The derivations of Raoult's law, Kelvin's law, and the combination of Kelvin's law and Raoult's law have been taken from Jensen [1993a]. The formulas in Chapter 6 used to separate different contributions to the internal RH are based on the following analysis.

### Raoult's law

The Gibbs free energy for a system may be written as:

$$G_i = G_i^0 + RT \cdot \ln a_i \quad (\text{A.1})$$

where  $G_i$  is the Gibbs free energy of component  $i$ ,  $G_i^0$  the Gibbs free energy of component  $i$  in standard conditions ( $p = 1 \text{ atm}$ ,  $c = 1 \text{ mol/l}$ ,  $m = 1 \text{ mol/kg}$ ),  $R$  the ideal gas constant,  $T$  the temperature,  $a_i$  the activity of component  $i$ .

For an ideal gas:  $a_g = \frac{p_g}{p^0}$ ; for an ideal liquid:  $a_l = \frac{X_l}{X^0} = X_l$

where  $p^0$  is the atmospheric pressure,  $X_0 = 1$  is the molar fraction of pure water and  $X_l$  is the molar fraction of water in the solution.

At equilibrium:  $G_l = G_g$

$$\Rightarrow G_l^0 + RT \cdot \ln X_l = G_g^0 + RT \cdot \ln p_g - RT \cdot \ln p^0 \quad (\text{A.2})$$

For pure water,  $X_l = 1$  and  $p_g = p_{sat}$ , where  $p_{sat}$  is the saturation pressure. Therefore (A.2) can be rewritten as:

$$G_l^0 + RT \cdot \ln 1 = G_g^0 + RT \cdot \ln p_{sat} - RT \cdot \ln p^0 \quad (\text{A.3})$$

Subtracting (A.3) from (A.2):

$$RT \cdot \ln X_l = RT \cdot \ln \frac{p_g}{p_{sat}} \quad (\text{A.4})$$

and finally:

$$X_l = \frac{p_g}{p_{sat}} = RH \quad \text{Raoult's law} \quad (\text{A.5})$$

## Kelvin's law

For thermodynamic equilibrium between water and vapor:  $G_l = G_g$ .

Stability of thermodynamic equilibrium requires that:

$$dG_l = dG_g \quad (\text{A.6})$$

The infinitesimal work for a variation of pressure at constant temperature can be written as:

$$dG_i = V_i dp_i \quad \text{Gibbs-Duhem equation} \quad (\text{A.7})$$

where  $V_i$  is the volume of phase  $i$  and  $dp_i$  is the infinitesimal change of pressure acting on phase  $i$ .

Inserting the Gibbs-Duhem into (A.6):

$$V_g dp_g = V_l dp_l \quad (\text{A.8})$$

For an ideal gas  $V_g = \frac{RT}{p_g}$ ; for an incompressible liquid  $V_l = \frac{M_l}{\rho_l}$

$$RT \frac{dp_g}{p_g} = \frac{M_l}{\rho_l} dp_l \Rightarrow RT \cdot d \ln p_g = \frac{M_l}{\rho_l} dp_l \quad (\text{A.9})$$

Integrating with boundary conditions  $p_l = p^0$  for  $p_g = p_{sat}$ :

$$\int_{p_{sat}}^{p_g} RT \cdot d \ln p_g = \int_{p^0}^{p_l} \frac{M_l}{\rho_l} dp_l \Rightarrow \quad (\text{A.10})$$

$$RT \cdot \ln \frac{p_g}{p_{sat}} = \frac{M_l}{\rho_l} (p_l - p^0) \quad (\text{A.11})$$

Even for very small changes in vapor pressure,  $|p_l| \gg |p^0|$ . Therefore (A.11) is reduced to:

$$\ln \frac{p_g}{p_{sat}} = \frac{M_l}{\rho_l RT} p_l \quad (\text{A.12})$$

The force balance for a circular cylindrical pore is written as:

$$\gamma 2\pi r \cos \vartheta = -p_l \pi r^2 \Rightarrow p_l = -\frac{2\gamma \cos \vartheta}{r} \quad \text{Laplace law} \quad (\text{A.13})$$

where  $\gamma$  is the surface tension of the pore fluid and  $\theta$  the contact angle between fluids and solids.

Inserting the Laplace law into (A.12):

$$RH = \frac{p_g}{p_{sat}} = \exp\left(-\frac{2\gamma M_l \cos \vartheta}{r \rho_l RT}\right) \quad \text{Kelvin's law} \quad (\text{A.14})$$

## Combination of Raoult's law and Kelvin's law

If the liquid contains dissolved salts, the boundary conditions for integration of (A.9) have to be changed. Using Raoult's law (Eq. A.5), the boundary conditions become:

$$p_l = p^0 \quad \text{for} \quad p_g = p_{sat} \cdot X_l$$

Considering the partial molar volume of water,  $V_l$ , independent of the dissolved salts, (A.10) becomes:

$$\int_{p_{sat} \cdot X_l}^{p_g} RT \cdot d \ln p_g = \int_{p^0}^{p_l} \frac{M_l}{\rho_l} dp_l \quad (\text{A.15})$$

$$RT \cdot \ln \frac{p_g}{p_{sat} \cdot X_l} = \frac{M_l}{\rho_l} (p_l - p^0) \quad (\text{A.16})$$

$$RH = \frac{p_g}{p_{sat}} = X_l \cdot \exp\left(-\frac{2\gamma M_l \cos \vartheta}{r \rho_l RT}\right) \quad (\text{A.17})$$

With Eq. A.17 it is possible to calculate the relative humidity of a porous system that has Kelvin radius  $r$  and contains dissolved salts in the pore solution.



# Appendix B

## Powers' model

---

### Powers' volumetric model for cement paste and silica fume modified cement paste

The models described on this appendix are based on [Jensen & Hansen 2001a] and [Jensen 1993b].

#### Phase composition of hardening Portland cement paste

The following set of formulas describes Powers' model for the phase composition of a hardening Portland cement paste.

$$\begin{aligned}\text{Chemical shrinkage:} \quad V_{cs} &= 0.20 \cdot (1-p) \cdot \alpha \\ \text{Capillary water:} \quad V_{cw} &= p - 1.32 \cdot (1-p) \cdot \alpha \\ \text{Gel water:} \quad V_{gw} &= 0.60 \cdot (1-p) \cdot \alpha \\ \text{Gel solid:} \quad V_{gs} &= 1.52 \cdot (1-p) \cdot \alpha \\ \text{Cement:} \quad V_c &= (1-p) \cdot (1-\alpha)\end{aligned}$$

$$\text{where} \quad \sum_i V_i = 1 \quad \text{and} \quad p = \frac{w/c}{(w/c) + (\rho_w / \rho_c)}$$

$w$  and  $c$  refer to masses of water and cement:  $\rho_c \cong 3150 \text{ kg} / \text{m}^3$        $\rho_w \cong 1000 \text{ kg} / \text{m}^3$

The constants in Powers' volumetric model are derived from the following data:

$$\begin{aligned}\text{Non-evaporable water:} \quad W_n &= 0.23 \text{ g} / \text{g cement reacted} \\ \text{Gel water:} \quad W_{gw} &= 0.19 \text{ g} / \text{g cement reacted} \\ \text{Chemical shrinkage:} \quad \Delta V &= 6.4 \text{ ml} / 100 \text{ g cement reacted}\end{aligned}$$

#### Phase composition of hardening Portland cement paste with silica-fume addition

The following set of formulas describes Powers' volumetric model for the phase composition of a hardening Portland cement paste with silica-fume addition. N.B.: In the formulas it is assumed that the silica fume reacts proportionally to the cement.

$$\begin{aligned}
\text{Chemical shrinkage:} & \quad V_{cs} = k \cdot (0.20 + 0.69 \cdot (s/c)) \cdot (1-p) \cdot \alpha \\
\text{Capillary water:} & \quad V_{cw} = p - k \cdot (1.32 + 1.57 \cdot (s/c)) \cdot (1-p) \cdot \alpha \\
\text{Gel water:} & \quad V_{gw} = k \cdot (0.60 + 1.57 \cdot (s/c)) \cdot (1-p) \cdot \alpha \\
\text{Gel solid:} & \quad V_{gs} = k \cdot (1.52 + 0.74 \cdot (s/c)) \cdot (1-p) \cdot \alpha \\
\text{Cement:} & \quad V_c = k \cdot (1-p) \cdot (1-\alpha) \\
\text{Silica fume:} & \quad V_s = k \cdot (1.43 \cdot (s/c)) \cdot (1-p) \cdot (1-\alpha)
\end{aligned}$$

$$\text{where } \sum_i V_i = 1 \quad p = \frac{w/c}{(w/c) + (\rho_w / \rho_c) + (\rho_w / \rho_s) \cdot (s/c)} \quad k = \frac{1}{1 + \frac{\rho_c}{\rho_s} \cdot (s/c)}$$

$w$ ,  $c$  and  $s$  refer to masses of water, cement and silica fume:

$$\rho_c \cong 3150 \text{ kg} / \text{m}^3 \quad \rho_s \cong 2200 \text{ kg} / \text{m}^3 \quad \rho_w \cong 1000 \text{ kg} / \text{m}^3$$

The constants in the model are derived from the data shown in the previous paragraph, with the addition of similar data for the silica-fume pozzolanic reaction:

$$\begin{aligned}
\text{Non-evaporable water:} & \quad W_n = 0 \text{ g} / \text{g silica fume reacted} \\
\text{Gel water:} & \quad W_{gw} = 0.5 \text{ g} / \text{g silica fume reacted} \\
\text{Chemical shrinkage:} & \quad \Delta V = 22 \text{ ml} / 100 \text{ g silica fume reacted}
\end{aligned}$$



# Appendix C

## Amount of entrained water

---

### Model to calculate the quantity of entrained water necessary to avoid self-desiccation

#### Entrained water in a plain cement paste (derivation of Eq. 8.4)

The amount of entrained water needed to avoid self-desiccation equals the chemical shrinkage of a cement paste in saturated conditions. It is assumed that hydration at low w/c ratios stops when all capillary water is consumed and the available space is occupied by gel water, gel solid and anhydrous cement. For a Portland cement paste, using Powers' model (see Appendix B), one has [Jensen & Hansen 2001a]:

$$\alpha = \alpha_{max} \quad \text{for} \quad V_{gw} + V_{gs} + V_c = 1 \quad (\text{C.1})$$

$$0.60 \cdot (1-p) \cdot \alpha_{max} + 1.52 \cdot (1-p) \cdot \alpha_{max} + (1-p) \cdot (1-\alpha_{max}) = 1 \quad (\text{C.2})$$

Hence, in an open system with a low w/c ratio:

$$\alpha_{max} = \frac{p}{1.12 \cdot (1-p)} \quad (\text{C.3})$$

The relative volume of initially entrained water,  $V_{en,0}$ , equals the chemical shrinkage developed at the maximum degree of hydration, given by (C.3). Since  $p = V_{en,0}$ , it results in:

$$V_{en,0} = 0.20 \cdot (1-p) \cdot \alpha_{max} = 0.18 \cdot p = 0.18 \cdot V_{en,0} \quad (\text{C.4})$$

On a w/c ratio basis (kg water / kg cement), entrained water and initial capillary water can be expressed as:

$$(w/c)_e = \frac{V_{en,0} \cdot \rho_W}{V_{c,0} \cdot \rho_C}; \quad (w/c) = \frac{V_{en,0} \cdot \rho_W}{V_{c,0} \cdot \rho_C} \quad (\text{C.5})$$

Therefore, from (C.4) and (C.5), the quantity of entrained water necessary to obtain  $\alpha_{max}$  as in (C.3) is:

$$(w/c)_e = 0.18 \cdot (w/c) \quad \text{for } (w/c) < 0.36 \quad (C.6)$$

Eq. C.6 is only relevant for  $w/c < 0.36$ . Above this  $w/c$  ratio, complete hydration can be achieved with less entrained water than stated in (C.6). According to Powers' model, complete hydration in an open system is possible in the range  $0.36 \leq (w/c) \leq 0.42$  if:

$$(w/c) + (w/c)_e = 0.42$$

The necessary condition to obtain  $\alpha_{max} = 1$  in this  $w/c$  range is:

$$(w/c)_e = 0.42 - (w/c) \quad \text{for } 0.36 \leq (w/c) \leq 0.42 \quad (C.7)$$

### Entrained water in a silica-fume modified cement paste

Eq. C.1 is rewritten according to Powers' model for silica-fume modified cement paste (see Appendix B):

$$\alpha = \alpha_{max} \quad \text{for } V_{gw} + V_{gs} + V_c + V_s = 1 \quad (C.8)$$

$$k \cdot (0.6 + 1.57 \cdot (s/c)) \cdot (1-p) \cdot \alpha_{max} + k \cdot (1.52 + 0.74 \cdot (s/c)) \cdot (1-p) \cdot \alpha_{max} + k \cdot (1-p) \cdot (1 - \alpha_{max}) + k \cdot (1.43 \cdot (s/c)) \cdot (1-p) \cdot (1 - \alpha_{max}) = 1 \quad (C.9)$$

$$\alpha_{max} = \frac{1 - k \cdot (1 + 1.43 \cdot (s/c)) \cdot (1-p)}{k \cdot (1.12 + 0.9 \cdot (s/c)) \cdot (1-p)} = \frac{p}{k \cdot (1.12 + 0.88 \cdot (s/c)) \cdot (1-p)} \quad (C.10)$$

By comparison with (C.3), it is evident that the maximum degree of hydration achievable in saturated conditions for a given  $w/c$  ratio is reduced by the addition of silica fume.

The relative volume of initially entrained water,  $V_{ew,0}$ , which equals the chemical shrinkage developed at the maximum degree of hydration, is rewritten as:

$$V_{ew,0} = k \cdot (0.2 + 0.69 \cdot (s/c)) \cdot (1-p) \cdot \alpha_{max}$$

$$V_{ew,0} = k \cdot (0.2 + 0.69 \cdot (s/c)) \cdot (1-p) \cdot \frac{p}{k \cdot (1.12 + 0.88 \cdot (s/c)) \cdot (1-p)}$$

$$V_{ew,0} = \frac{(0.2 + 0.69 \cdot (s/c)) \cdot p}{(1.12 + 0.88 \cdot (s/c))} \quad (C.11)$$

Also in this case,  $p = V_{ew,0}$ . By further application of Eq. C.5, the quantity of entrained water for a silica-fume modified cement paste with low  $w/c$  ratio can be written as:

$$(w/c)_e = \frac{0.2 + 0.69 \cdot (s/c)}{1.12 + 0.88 \cdot (s/c)} \cdot (w/c) \quad \text{for} \quad (w/c) \leq (0.36 + 0.28 \cdot (s/c)) \quad (C.12)$$

Eq. C12 is only relevant for w/c ratio lower than the one sufficient to obtain full hydration in saturated condition, which was found by imposing  $\alpha_{max} = 1$  in (C.10).

For a silica-fume modified cement paste, the w/c ratio necessary for complete hydration in sealed conditions may be obtained by imposing that all the capillary water is consumed at a degree of hydration  $\alpha = 1$ . The resulting minimum w/c ratio in sealed conditions,  $(w/c)_{min, sea}$ , is:

$$(w/c)_{min, sea} = (0.42 + 0.73 \cdot (s/c)) \quad (C.13)$$

Above this w/c ratio, complete hydration can be achieved with less entrained water than stated in (C.12). According to Powers' model, complete hydration in an open system is possible in the range  $(0.36 + 0.28 \cdot (s/c)) \leq (w/c) \leq (0.42 + 0.73 \cdot (s/c))$  if:

$$(w/c) + (w/c)_e = (0.42 + 0.73 \cdot (s/c)) \quad (C.14)$$

Hence, the necessary condition to obtain  $\alpha_{max} = 1$  in this w/c range is:

$$(w/c)_e = (0.42 + 0.73 \cdot (s/c)) - (w/c) \quad (C.15)$$

Figure C.1 shows the entrained w/c ratio necessary to avoid self-desiccation as a function of w/c ratio in cement pastes with different s/c ratio. This plot can be used to design the quantity of water to be entrained in a LWAC mixture.

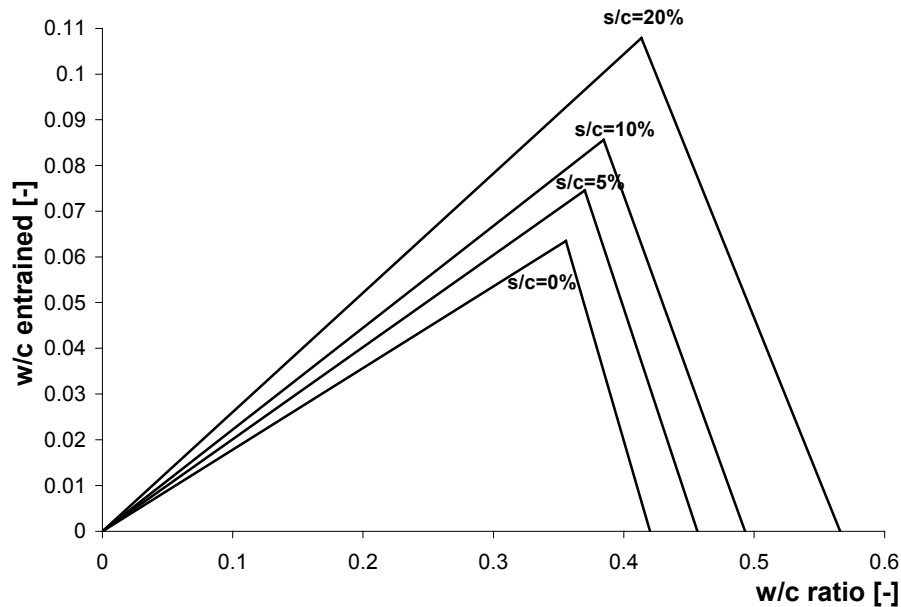


Figure C.1 – Entrained w/c ratio necessary to avoid self-desiccation as a function of w/c ratio for different s/c ratios

It is noticed that, according to the model, the maximum achievable degree of hydration is decreased by the addition of silica fume at each w/c ratio, due to absorption of a part of the capillary water on the surface of the pozzolanic CSH gel. The absorbed water becomes unavailable for hydration of cement. However, since the pozzolanic reaction produces a great chemical shrinkage (about 3 times the chemical shrinkage of Portland cement, see Chapter 2), the quantity of necessary entrained water is significantly increased by the addition of silica fume, as shown in Figure C.1.

## **Applications of the entrained water calculations**

The following applications refer to experiments and calculations reported in Chapter 9 of this thesis.

### **Comparison with chemical shrinkage – a verification**

For w/c ratio 0.3, Eq. C.6 yields  $(w/c)_e = 0.054$ . The asymptotic value of chemical shrinkage in saturated conditions for the cement paste studied in Chapter 9, according to the CEMHYD3D simulation (Figure 9.10, thick line), is 0.054 ml / g cement. Since this is exactly the volume that needs to be filled by entrained water, the agreement of the two methods is perfect. However, if one considers the chemical shrinkage measurements instead (Figure 9.9, crosses), which diverge from the simulations probably due to depercolation of the capillary porosity, one would conclude that only about 0.043 ml / g cement is needed. It is noticed that using different values for the parameters of Powers' model (non-evaporable water, gel water, and chemical shrinkage, see Appendix B) leads to a different coefficient in Eq. C.6.

### **X-ray experiment**

In the x-ray experiment (sec. 9.5), the amount of water in the pumice was measured first. Then the maximum volume of cement paste that would be internally cured was calculated on the basis of Eq. C.6 and of the w/c ratio of the cement paste (0.3). This corresponded to a thickness of 6 mm above the pumice. However, due to imprecision in the sample configuration, the thickness of the cement paste turned out to be about 4.5 mm (sec. 9.5). Therefore, the water entrained in the pumice must be considered to have been more than sufficient to avoid self-desiccation of the cement paste, if all of it was available to be transported into the cement paste.

### **LWA mortars**

The amount of water entrained in mortar LWA 2 (sec. 9.7) was calculated with Eq. C.6. Mortar LWA 1 had half of the pumice and therefore half of this amount. The very little autogenous shrinkage and high non-evaporable water content of mortar LWA 2 is an indirect proof of the applicability of Eq. C.6.

# Summary

---

## Scope of this thesis

High-performance concrete (HPC) is generally characterized by a low water/binder ratio and by silica-fume addition, which guarantee a low porosity and a discontinuous capillary pore structure of the cement paste. Modern concretes possess some highly advantageous properties compared to traditional concrete, such as good workability in the fresh state, high strength, and low permeability. However, they have also shown to be more sensitive to early-age cracking than traditional concrete. Early-age cracking mainly occurs due to the fact that the deformations of the concrete member are restrained by adjoining structures. In addition, internal microcracking may occur, due to restraint offered to the shrinking paste by the non-shrinking aggregates. A main source of early-age deformations in HPC is autogenous deformation.

Autogenous deformation is the self-created deformation of a cement paste, mortar or concrete during hardening. In traditional concretes it is negligible compared to drying shrinkage. However, the low water/binder ratio and the addition of silica fume in HPC cause a significant drop of the internal relative humidity (RH) in the cement paste during sealed hydration and the occurrence of autogenous shrinkage. Despite the growing interest in autogenous shrinkage, no consensus has been reached in the scientific community about its mechanisms neither about measuring methods. Moreover, different strategies aimed at limiting the autogenous shrinkage are debated at the moment.

In this thesis, autogenous deformation of cement pastes, Normal Weight Concrete (NWC), and Lightweight Aggregate Concrete (LWAC) were measured. Both Portland and Blast Furnace Slag (BFS) cement were studied. A model for calculating self-desiccation shrinkage of cement paste was proposed and validated with experiments. Shrinkage of NWC was derived with a composite model and early-age expansion of LWAC, a puzzling phenomenon up to now, was explained. Finally, transport of water from saturated lightweight aggregates (LWA) to hardening cement paste was measured with x-ray absorption.

---

## Summary of the results

### Portland cement pastes and concrete

Most of the autogenous deformation of the Portland cement paste occurred before and around setting and did not correspond to a RH drop, but was due to chemical shrinkage. Only a little part of the very early-age shrinkage of the paste resulted in shrinkage of the concrete. Both shrinkage of the paste and shrinkage of the concrete showed a bilinear behavior: high shrinkage rate in the first hours of hydration followed by a sudden reduction of the rate. The knee point corresponded to the beginning of self-desiccation in the paste, as shown by the measurements of internal RH. The internal RH dropped after setting, mainly due to salt dissolution in the pore fluid, and then stabilized after a couple of days of hydration. The slope of the RH vs. shrinkage curve decreased in the first days, corresponding to a stiffness gain of the paste. A further increase in the deformation rate followed, which was attributed to creep.

Measurements of autogenous deformations of cement pastes performed at different temperatures (10-40°C) showed that high curing temperatures accelerated the autogenous shrinkage but did not substantially modify its value after one week of hydration. When autogenous shrinkage after setting was normalized to the isothermal heat of hydration, a single master curve was found, showing the dependence of the development of the shrinkage on the degree of hydration in the temperature range studied. The effect of temperature on the autogenous deformation in concrete was more unsystematic. Generally, higher temperatures accelerated the deformations but did not lead to higher deformations in the tested period (1 week). On the other hand, the effect on the self-induced stress, measured with a Temperature Stress Testing Machine (TSTM), was more systematic, perhaps also due to a better reproducibility of the results: higher temperatures caused faster development of self-induced stresses.

### Blast furnace slag cement pastes and concrete

On BFS cement pastes and concrete, expansion was measured after setting, inducing for the concrete mixes a compressive stress in the TSTM. Expansion was even measured on cement pastes that were rotated until setting and was attributed to crystallization pressure of ettringite or other hydrates. The initial expansion did not show a clear dependence on the curing temperature and was also very variable among duplicate samples.

A higher shrinkage than for the Portland cement followed both in BFS cement pastes and BFS concrete. At the same time, the internal RH dropped: at 1-week hydration it was lower than for the Portland cement pastes. The significant self-desiccation (i.e. RH drop) and autogenous shrinkage of BFS cement paste and concrete was attributed to the pozzolanic reaction of the slag with the calcium hydroxide (CH) crystals. In fact, the pozzolanic reaction refines the pore structure of the paste and possesses a high chemical shrinkage, factors that both increase self-desiccation. Moreover, consumption of CH

crystals, acting as internal restraints, leads to additional shrinkage. At all curing temperatures (10-40°C), concrete containing BFS cement showed higher shrinkage and higher self-induced stresses than Portland cement concrete.

### **Modeling of self-desiccation shrinkage**

Self-desiccation shrinkage of a Portland and a BFS cement paste were calculated from the measured internal RH using a model based on the capillary tension in the pore fluid. The measured internal RH was divided into a contribution due to formation of menisci and one due to salts dissolved in the pore fluid. Measurements of non-evaporable water content, chemical shrinkage, elastic modulus, surface tension and composition of the pore fluid, and internal RH were used to calculate the self-desiccation shrinkage.

Only a part of the measured shrinkage could be explained with this approach, which assumes linear elastic behavior of the cement pastes. Additional shrinkage may have been caused by plastic deformation and creep of the cement paste under internal stress, conversion of ettringite into monosulphate, and consumption of CH crystals.

### **Calculation of shrinkage of Normal Weight Concrete**

Shrinkage of NWC was calculated based on the shrinkage of the cement paste according to 2-phase composite models. The calculated shrinkage agreed fairly well with the measurements, especially if one considers that microcracking and creep of the cement paste were not included in the models, nor was the presence of the interfacial transition zone (ITZ).

### **Lightweight Aggregate Concrete**

LWAC generally reached 28-days compressive strength similar or even higher than NWC. To explain this fact, the elastic modulus of the LWA, the moisture conditions of the concrete, the improved ITZ, the internal curing process, and the reduction of the eigenstresses due to absence of self-desiccation shrinkage should be taken into consideration. The elastic modulus of LWAC was more than 30% lower than the one of NWC.

Internal curing provided by saturated LWA was effective in offsetting self-desiccation and turning the early-age shrinkage into expansion. Early-age expansion of LWAC is due to expansion of the cement paste cured in almost saturated conditions, thanks to water from the LWA. Calculations with composite models showed that the expansion of LWAC is compatible with early-age expansion of cement pastes cured under water. Early-age expansion significantly depended on the degree of saturation of the LWA ( $L_{iapor}$ ) and to a lesser extent on their particle size, being larger for smaller LWA. These facts showed the impact on the internal curing process of the quantity of entrained water and of the distance of water penetration into the hardening cement paste.

The quantity of entrained water needed to avoid self-desiccation was calculated based on Powers' model. An extension to silica-fume modified cement pastes was discussed and

---

results found in the literature were explained with help of the model. Mortar mixes with saturated pumice aggregates that were designed according to this model showed negligible autogenous shrinkage.

### **Moisture transport and properties of Lightweight Aggregates**

X-ray absorption showed that most of the transport of water from saturated LWA to hydrating cement paste occurs in the first days after casting. This is also the period when most of the chemical shrinkage takes place. On the other hand, also most of the autogenous shrinkage occurs in the first days. In this period, transport of water within the hardening cement paste is a relatively fast process and water travels for at least some millimeters, since the capillary pores are not depercolated yet. Analytical calculations and numerical simulations, based on the particle size distribution of the LWA particles, showed that, for all the LWAC mixtures studied, most of the cement paste is influenced by the internal curing process when one assumes a penetration depth of the entrained water of 1-2 mm. According to these results, gravel-size LWA might be adequate to provide uniform internal curing of the composite. As a consequence, to avoid self-desiccation shrinkage in the first days after casting in the concrete mixtures studied, the amount of water absorbed in the LWA resulted more important than the effective transport distance of the adsorbed water.

Properties of LWA that facilitate the internal curing process are essentially a high porosity, a fast water uptake when underwater, and an open pore structure that allows releasing water in the concrete at high internal RH. Adsorption underwater and desorption isotherms at high RH were measured for expanded shale (Liapor) aggregates and pumice sand from Yali island (Greece). It was found that the Liapor aggregates had a quicker absorption and released the absorbed water at higher RH, which are both favorable qualities for internal curing.



# Samenvatting

---

## Doel van dit proefschrift

Hoge sterkte beton (HSB) heeft een lage water/bindmiddelfactor en bevat microsilica. Deze factoren staan garant voor een lage porositeit en een onderbroken capillaire poriënsysteem in de cementpasta. Moderne betonmengsels hebben grote voordelen ten opzichte van traditionele betonmengsels, zoals een goede verwerkbaarheid, hoge sterkte en lage permeabiliteit. HSB is in de vroege verhardingsfase gevoeliger voor scheurvorming dan normaal beton. Scheurvorming treedt dan op, omdat de vervormingen van het jonge beton worden verhinderd door andere, aangrenzende constructiedelen. Ook kunnen interne microscheuren optreden door verhindering van de vervorming van de krimpende cementpasta door het niet-krimpde toeslagmateriaal. Een belangrijke oorzaak van het vervormen van de cementpasta van jong HSB is de autogene krimp.

Autogene krimp is de zelf-gecreëerde vervorming van cementpasta, mortel of beton tijdens het verharden. In traditioneel beton is de autogene krimp klein vergeleken met de uitdrogingskrimp. Echter, een lage water/bindmiddelfactor en de toevoeging van microsilica in HSB veroorzaken een belangrijke daling van de interne relatieve vochtigheid (RV) van de cementpasta tijdens het verharden in gesloten omstandigheden. Dit resulteert in het optreden van autogene krimp.

Ondanks de groeiende interesse in autogene krimp heeft de wetenschappelijke wereld geen consensus bereikt over de mechanismen en de meetmethoden. Bovendien worden nu verschillende strategieën voor het beperken van autogene krimp bediscussieerd.

In dit proefschrift is de autogene krimp van cementpasta, van beton met toeslagmateriaal van normale dichtheid (NTB) en van beton met licht toeslagmateriaal (LTB) gemeten. Zowel Portland- als hoogovencement is toegepast. Een model voor het berekenen van de zelf-drogingskrimp van cementpasta is ontwikkeld. De krimp van NTB is berekend met een composiet model en de zwelling van LTB in de vroege fase, een tot op heden niet doorgrond fenomeen, is verklaard. Ook is het transport van water uit

---

verzadigde lichte toeslagkorrels (LWA) naar verhardende cement pasta met röntgenstraling absorptie zichtbaar gemaakt.

## **Samenvatting van de resultaten**

### **Portlandcementpasta's en beton**

Een groot deel van de autogene krimp van Portlandcementpasta trad vóór en tijdens het 'zetten' van het materiaal op. Deze krimp was niet gerelateerd aan een daling van de RV, maar werd veroorzaakt door de chemische krimp. Slechts een klein deel van de krimp in de vroege fase van de pasta resulteerde in krimp van het beton. Zowel de krimp van pasta als van het beton vertoonde een bilineaire relatie: een hoge krimpsnelheid in de eerste uren van hydratatie gevolgd door een plotselinge afname van de snelheid. Het knikpunt was gerelateerd aan het begin van zelfdroging in de pasta. Dit werd aangetoond met interne RV-metingen. De interne RV daalde na het 'zetten' van het materiaal, grotendeels vanwege het oplossen van zouten in het poriewater, en stabiliseerde na een paar dagen hydrateren. De helling van de RV-krimprelatie nam af in de eerste dagen als gevolg van de toenemende stijfheid van de pasta. Een verdere toename van de vervormingssnelheid volgde. Dit is door kruip van de pasta veroorzaakt.

Het meten van de autogene krimp van cementpasta bij verschillende temperaturen (10-40°C) toonde aan dat hoge temperaturen de autogene krimp versnellen, maar bijna geen invloed hebben op de waarden die werden bereikt na een week hydratatie. Als autogene krimp na het 'zetten' aan de isotherme hydratatie-warmteontwikkeling is gerelateerd, is een enkele 'basiscurve' gevonden. Dit toonde aan dat in het onderzochte temperatuurbereik de autogene krimp afhankelijk was van de hydratatiegraad. De invloed van de temperatuur op de autogene krimp van beton was minder systematisch. In het algemeen versnellen hogere temperaturen het optreden van vervormingen maar leiden zij niet tot grotere vervormingen binnen de onderzochte tijdspanne (1 week). Anderzijds was het effect op de zelf-creëerde spanningen, gemeten met een Temperature-Stress Testing Machine (TSTM) meer systematisch, mogelijk vanwege een betere herhaalbaarheid van de resultaten: hogere temperaturen leiden tot een snellere ontwikkeling van zelf-gecreëerde spanningen.

### **Hoogovencementpasta's en beton**

In hoogovencementpasta's en hoogovencementbeton werd na het 'zetten' zwelling gemeten, hetgeen in de TSTM leidde tot drukspanningen in het beton. Zwelling werd ook gemeten aan cementpasta die tijdens het beproeven continu werden 'rondgedraaid'. Deze zwelling werd veroorzaakt door de kristallisatiedruk van ettringiet en andere hydratatieproducten. De initiële zwelling was niet duidelijk temperatuurafhankelijk en was ook niet reproduceerbaar.

Een grotere krimp dan bij het Portlandcement werd gevonden voor beide hoogovencementpasta's en in het hoogovencementbeton. De interne RV na een week hydratatie was lager dan in de Portlandcementpasta's. De aanzienlijke zelfdroging (d.w.z. RV-daling) en autogene krimp van hoogovencement werd veroorzaakt door de puzzolane reactie van slak met calciumhydroxide (CH) kristallen. In feite leidde de puzzolane reactie ertoe dat de poriën in de pasta kleiner werden en nam de chemische krimp toe; twee factoren die tot een toename van de zelfdroging leidden. Bovendien leidde het verwijderen van CH-kristallen, die interne vervormingsverhindering veroorzaken, tot extra krimp. Bij alle onderzochte temperaturen (10-40°C) vertoonde beton met hoogovencement een grotere krimp en hogere zelf-gecreëerde spanningen dan het Portlandcementbeton.

### **Het modelleren van zelfdrogingkrimp**

Zelfdrogingkrimp van Portland- en hoogovencementpasta's werd berekend op basis van de interne RV met een model dat is gebaseerd op capillaire trekspanningen in het poriewater. De verandering in de interne RV werd voor een deel veroorzaakt door de vorming van menisci en voor een deel door zouten opgelost in het poriewater. Metingen aan het niet-verdampbare water, de chemische krimp, de elasticiteitsmodulus, de oppervlaktespanning en samenstelling van het poriewater en de interne RV werden gebruikt voor het berekenen van de zelfdrogingkrimp.

Slechts een deel van de gemeten krimp werd met deze benadering, die elastisch gedrag van de cementpasta veronderstelt, verklaard. De rest van de krimp zou door plastische vervormingen en kruip van de cementpasta onder interne spanningen, door omzetting van ettringiet in monosulfaat en door het verwijderen van CH-kristallen veroorzaakt kunnen zijn.

### **De berekening van de krimp van traditioneel beton**

De krimp van NTB werd met een 2-fasen composiet model berekend op basis van de krimp van de cementpasta. De berekende krimp was een vrij goede benadering van de metingen, vooral omdat microscheurvorming, kruip en de grenszone niet in het model waren opgenomen.

### **Lichtbeton**

LTB bereikte na 28 dagen een druksterkte die gelijk aan of hoger was dan die van NTB. Om dit te verklaren, kunnen de volgende factoren in gedachten worden gehouden: de elasticiteitsmodulus van het LWA, het vochtgehalte van het beton, de kwalitatief betere grenszone, de interne nabehandeling en de reductie van eigenspanningen door de afwezigheid van zelfdrogingskrimp. De elasticiteitsmodulus van LTB was meer dan 30% lager dan die van NTB.

Interne nabehandeling door verzadigde toeslagkorrels was effectief tegen zelfdroging en leidde ertoe, dat in de vroege fase geen krimp maar zwelling optrad. Zwelling van LTB

---

werd veroorzaakt door zwelling van de cementpasta die, vanwege het water dat uit de LWA vrijkwam, in nagenoeg verzadigde omstandigheden verhardde. Berekeningen met composietmodellen wezen uit dat zwelling van LTB vergeleken kan worden met de vroege fase zwelling van cementpasta die zich onder water bevindt. De zwelling van LTB in de vroege fase was sterk afhankelijk van de verzadigingsgraad van de LWA (Liapor) en minder afhankelijk van de afmetingen ervan; de zwelling was groter naarmate de korrels kleiner waren. Deze factoren toonden de invloed op de interne nabehandeling van de hoeveelheid water in de LWA en van de afstand van penetratie van water in de verhardende cementpasta.

De hoeveelheid water benodigd om zelfdroging te voorkomen werd berekend op basis van het model van Powers. Een uitbreiding voor pasta's met microsilica werd ontwikkeld. Mortels met verzadigde puimsteentoeslagmateriaal die met het model werden ontworpen, vertoonden een zeer geringe autogene krimp.

### **Vochttransport en eigenschappen van lichte toeslagmaterialen**

Röntgenstralingabsorptie wees uit dat het grootste deel van het watertransport vanaf de verzadigde LWA naar de verhardende cementpasta in de eerste dagen na het storten plaatsvond. Dit is ook de periode waarin het merendeel van de chemische krimp werd gemeten. Ook vond het grootste deel van de autogene krimp in de eerste dagen plaats. In deze periode was transport van water binnen de verhardende cementpasta een proces dat relatief snel plaatsvond; het water legde afstanden van enkele millimeters, omdat de capillaire poriën nog niet gedepercoleerd waren. Analytische berekeningen en numerieke simulaties toonden aan, dat voor alle bestudeerde LTB-mengsels het grootste deel van de cementpasta door de interne nabehandeling werd beïnvloed als werd aangenomen dat het geabsorbeerde water over een afstand van 1-2 mm vanaf de LWA kan worden getransporteerd. Volgens deze resultaten is LWA met dezelfde afmetingen als grind voldoende fijn om een uniforme interne nabehandeling te bereiken. Het gevolg is dat, om zelfdroging gedurende de eerste dagen in de onderzochte mengsels te voorkomen, de hoeveelheid water in de LWA belangrijker is dan de afstand waarover het water moet worden getransporteerd.

Eigenschappen van de LWA die gunstig zijn voor interne nabehandeling zijn: een hoge porositeit, een snelle absorptie onder water en een open poriestructuur die geabsorbeerd water beschikbaar maakt in het beton bij een hoge interne RV. Absorptie onder water en desorptieisothermen bij hoge RV werden gemeten aan geëxpandeerde lei (Liapor) toeslagmateriaal en puimsteenzand van het eiland Yali (Griekenland). Het Liapor-toeslagmateriaal vertoonde een snellere absorptie en liet het geabsorbeerde water vrij bij een hogere RV; twee eigenschappen die gunstig zijn uit het oogpunt van interne nabehandeling.

# Acknowledgements

---

Most of the research described in this thesis was conducted within the Concrete Structures group of the Faculty of Civil Engineering and Geosciences at Delft University of Technology. The BriteEuram project IPACS (Improved Production of Advanced Concrete Structures) and the Delft Cluster Project 01.02.06 'Durability of underground concrete structures' founded this study.

I would like to thank my supervisor Prof.dr.ir. K. van Breugel for supporting me during these years. Albert, Arjen, Erik en Ron: bedankt voor jullie ideeën, hulp en gezelligheid. Thanks also to all the staff in the lab and visitors at TUDelft for the friendly environment. In particular, thanks to Ye Guang, Maya, Jan, Ippei, Antonio, Angelo and Alberto for the nice and fruitful collaboration.

I also would like to thank Prof.dr. O.M. Jensen for the experiments performed during my visit at the Department of Building Technology and Structural Engineering of Aalborg University (Denmark) and for the cooperation that followed and is to follow.

Chapter 9 was written during a summer stay at the Building and Fire Research Laboratory of the National Institute of Standards and Technologies (NIST), Gaithersburg (MD), USA, founded by the United States-Israel Binational Science Foundation (BSF), project: 'Autogenous Curing of High Strength Cementitious Materials by Means of Lightweight Micro-Aggregates Acting as Internal Water Reservoirs'. I would like to thank Prof. D. Lange (University of Illinois at Urbana-Champaign, USA) and Dr. K. Kovler (Technion, Israel) for choosing me for this job and constantly supporting me. Mr. D.P. Bentz, with his human sympathy and vast knowledge, was determinant for the success of this research. I would also like to thank Dr. C. Ferraris, Dr. P. Stutzman, Dr. Xiuping Feng and Mr. K. Snyder for assistance with the experiments and useful discussion, and Mr. N. Muzzatti and Mr. S. Larrea for performing measurements.

Last but not least, grazie ai due sciapulini per la presenza, l'aiuto e l'infinita pazienza...



# Curriculum vitae

---

Name: Pietro Lura

Born: February 23, 1973 at Desenzano del Garda (Brescia), Italy

1992 Maturità' Classica (60/60)

1998 Laurea in Ingegneria Civile (110/110 cum laude), Università degli Studi di Brescia, Brescia, Italy

Dec. 1998 – Jan. 2003 Ph.D. student at Technical University Delft, Faculty of Civil Engineering and Earth Sciences, Concrete Structures group

